Seismic soil amplification in alpine valleys: a case study : the Rhône valley, Valais, Switzerland

Frischknecht, Corine

This publication URL: https://archive-ouverte.unige.ch/unige:26879
Publication DOI: 10.13097/archive-ouverte/unige:26879

UNIVERSITÉ DE GENÈVE
Département de minéralogie

FACULTÉ DES SCIENCES
Professeur J.-J. Wagner

Seismic Soil Amplification in Alpine Valleys.
A Case Study : the Rhône Valley, Valais, Switzerland.

THÈSE

présentée à la Faculté des sciences de l'Université de Genève
pour obtenir le grade de Docteur ès sciences, mention sciences de la Terre

par

Corine FRISCHKNECHT
de
Rehetobel (AR)

Thèse N° 3154

GENÈVE

Atelier de reproduction de la Section de Physique

2000

La Faculté des sciences, sur le préavis de Monsieur J.-J. WAGNER, professeur ordinaire et directeur de thèse (Section des sciences de la Terre - Département de minéralogie), Madame A.S. KIREMIDJIAN, professeur (Stanford University, John A. Blume Earthquake Engineering Center - California, U.S.A.), Messieurs M. CAMPILLO, professeur (Université Joseph Fourier, Laboratoire de géophysique et de tectonophysique interne - Grenoble, France) et D. MAYER-ROSA, docteur (Section des sciences de la Terre - Département de minéralogie), autorise l'impression de la présente thèse, sans exprimer d'opinion sur les propositions qui y sont énoncées.

Genève, le 31 mars 2000

Thèse - 3154 -

Le Doyen, Jacques WEBER

Frischknecht C.: Seismic soil amplification in Alpine valleys. A case study : The Rhône valley, Valais, Switzerland
Terre & Environnement, vol.21, XXV, + 144p. +13pp. annexes (2000)

ISBN 2-940153-20-5

Section des Sciences de la Terre, Université de Genève, 13, rue des Maraîchers, CH-1205 Genève, Suisse
Téléphone ++41-22-379.61.11 – Fax ++41-22-379.31.10
Email: miner@terre.unige.ch

TABLE OF CONTENTS

* This chapter “executive summary” is written in French in accordance with the instructions for publications of PhD theses of the “Faculté des Sciences, Université de Genève”.

3. ANALYSIS OF THE INFLUENCE OF SUBSURFACE GEOMETRY ON SOIL AMPLIFICATION USING 2D MODELING

4. MICROZONATION OF THE SION AREA

ABSTRACT

Earthquakes have a damaging potential that can be strongly amplified by local soil conditions. This research focuses on the influence of the Rhône valley, an Alpine sedimentary and narrow structure, on the seismic response.

The Rhône valley (Valais, Switzerland) belongs to one of the most seismically active zones in Switzerland. The last major earthquake in Switzerland during the 20th century (magnitude ML=6.1) occurred in 1946 in this zone, in the Rawil area, causing about 150 millions of Swiss francs of direct damages (today's value). Since then the Rhône valley has seen the development of its infrastructure (major lifelines, hospitals, chemical industries, etc.) and the consistent growth of its number of inhabitants, which may lead to a higher vulnerability than in 1946. It is therefore necessary to assess the seismic hazard.

Documents on historical events show that damage distribution was not uniform and varied with local soil conditions. Recent instrumental data from the Swiss strong motion network indicate that the valley can amplify the ground motion in the frequency domain up to 8 times at specific frequencies in comparison with the ground motion recorded on outcropping rock.

Alpine valleys are characterized by peculiar conditions, such as thick and young quaternary unconsolidated deposits (several hundred meters deep), steep slopes, rapid lateral variation of surficial deposit and a shallow water-table. In order to better appreciate the role of these elements on the seismic response, two areas were studied using different methodological approaches depending on the available data.

In the Sion region, the soil amplification was evaluated in the frequency domain. Two-dimensional (2D) modeling and horizontal to vertical component (H/V) ratio on ambient seismic noise were independently used in order to cross-check their reliability and usefulness. Microzonation maps of the relative maximum amplification and its associated frequency were established. Both techniques are consistent with the general trend, i.e. low frequency value where the deposit is thicker and higher values towards the edges where the sediment is thinning out. 2D modeling makes possible to demonstrate the influence of the asymmetry of the valley geometry, the importance of the slope gradient and the role of structure like shoulders on the amplification distribution. The H/V ratio on ambient seismic noise shows to be more sensitive to very local soil conditions.

In the upper part of the Rhône valley, in the Susten-Brig area, the influence of local geologic conditions on soil amplification has been examined through a qualitative rating scheme. This approach not only integrates data on the surficial geology, depth to the water table, and thickness, but also on the slope gradient of the quaternary deposit because its influence on the amplification distribution has been demonstrated in the Sion region. The resulting relative maximum amplification map shows that the amplification distribution is mainly controlled by the steep slopes, although the level of amplification at a site depends on all of the present conditions.

These results demonstrate the importance of considering not only the surficial characteristics but also the hidden morphological structure of a valley for a seismic hazard assessment in Alpine regions since both elements contribute to modify the seismic response of a site.

The seismic microzonation maps produced in this study are drawn based on the present knowledge and the available data and techniques. They can therefore be changed at any time as

data are acquired and new methods are developed. Nevertheless such maps are an useful tool. They display areas in function of their capability to alter the ground motion. They cannot obviously be used immediately in a building code, but they can be useful in defining steps to improve such codes. These maps also contribute to raise awareness among policy maker, land-use planers and politicians on the capacity of Alpine valleys to amplify the seismic ground motion. They can serve as guidance for a preventive management.

RESUME EXECUTIF

Introduction

Lorsqu'un tremblement de terre se manifeste en un site donné, il provoque, selon les conditions géologiques locales préexistantes, des phénomènes tels que des amplifications du mouvement du sol, des fractures, de la liquéfaction et peut également déclencher des glissements de terrain. Ce sont les effets de site.

De nombreux tremblements de terre (par ex. Michoacan, Mexique 1985; Loma Prieta, Californie, 1989; Meythet, France, 1994; Izmit, Turquie, 1999) ont montré que les dégâts aux bâtiments n'étaient pas seulement à imputer à l'état des bâtiments, mais également au phénomène d'amplification du mouvement du sol. Ce phénomène peut être induit par différentes conditions de site, telle la présence d'un sommet (colline, crête, montagne) ou celle d'un matériau non consolidé déposé sur un soubassement rocheux. Cette recherche se focalise sur le deuxième cas.

L'amplification du mouvement du sol par du matériau non consolidé est générée par plusieurs processus. Si on considère le cas de couches planes, le fait qu'un matériau meuble surmonte un matériau plus rigide entraîne un contraste d'impédance sismique (rapport des vitesses des ondes sismiques et des masses volumiques). Ce contraste a pour effet d'une part d'augmenter l'amplitude de l'onde incidente, augmentation qui sera d'autant plus importante que le contraste sera élevé et d'autre part de piéger l'onde à l'intérieur de la couche plus meuble. Cela génère des interférences, qui, si elles sont constructives, vont provoquer également une amplification, mais à des fréquences bien déterminées, et c'est l'effet de résonance. Dans le cas d'une vallée ou d'un bassin sédimentaire, d'autres causes d'amplification s'ajoutent. En effet, la présence d'un interface irrégulier entre le matériau meuble et celui de l'encaissant induit une focalisation des ondes en certains points et une génération d'ondes de surface en raison des variations latérales. Cela a pour conséquence d'augmenter l'amplitude et la durée des signaux sismiques.

Dans l'analyse de l'amplification sismique, la pratique utilisée est généralement basée sur l'approche unidimensionelle (1D). Dans ce cas-là les calculs montrent que la fréquence fondamentale de résonance du sol change en fonction de l'épaisseur pour une vitesse sismique de propagation identique. Cependant des enregistrements sismiques effectués dans la vallée de Chusal (Tajikistan) ont montré que la fréquence fondamentale de résonance sur un profil transversal ne changeait pas de valeur quelque soit la variation d'épaisseur sous-jacente. King & Tucker (1984) en concluent que cette stabilité de la fréquence fondamentale est dû à un phénomène de résonance qui met en mouvement l'ensemble de la vallée. Des simulations numériques bidimensionnelles (2D) ont montré que l'apparition de cette résonance globale est principalement contrôlée par le rapport de forme, définit par le rapport entre l'épaisseur maximale du dépôt sédimentaire et la demi-largeur de la vallée, ainsi que par le contraste de vitesse sismique entre la roche encaissante et la couche sédimentaire (Bard & Bouchon, 1985).

Dans cette recherche, l'étude de cas est situé dans la vallée du Rhône, une structure née de la tectonique alpine et des glaciations de la période Quaternaire. Le résultat est une vallée profonde et encaissée qui présente des spécificités, à savoir :

- un fort gradient de pente de l'encaissant,
- des sédiments quaternaires jeunes et épais,
- des variations latérales rapides des dépôts superficiels.

D’autre part, cette vallée est également caractérisée par la présence d’une nappe phréatique proche de la surface.

Des études récentes sur des enregistrements sismiques dans les Appenins en Italie (Pessina et al. 1997) et dans les Alpes françaises (Le Brun, 1997) ont montré que les vallées alpines peuvent induire une amplification du mouvement du sol supérieure à un facteur 10 à certaines fréquences.

Etudes des effets de site en Suisse

Les premières études consacrées à l’influence des variations géologiques locales sur la réponse sismique en Suisse datent du milieu des années 80 avec le travail de Fäh (1985). Dans le contexte de la décennie internationale pour la réduction des catastrophes naturelles (IDNDR) proclamée pour la période 1990-2000 par l’assemblée générale des Nations Unies, le comité suisse IDNDR a encouragé les recherches dans le domaine de l’évaluation de l’aléa sismique par deux projets. Le projet OBWALD (Schindler et al. 1996) a été dédié à l’analyse de l’influence des conditions géologiques locales sur l’aléa sismique régionale en utilisant l’approche des anomalies d’intensité sismique. Cette approche a été également appliquée dans le canton de Niedwald et de Soleure (Beer, 1997). Le projet OBWALD a été suivi par le projet SISVAL (Wagner et al. 2000). Cette étude a été menée dans le canton du Valais, plus précisément dans la vallée du Rhône où deux zones d’études ont été choisies et dans lesquelles différents approches ont été utilisées afin d’évaluer l’effet des conditions géologiques locales. Ce travail fait partie de ce projet.

En parallèle, dans le cadre du PNR31, un programme de recherche national sur les changements climatiques et les catastrophes naturelles, trois études régionales ont été menées dans des contextes géologiques différents (Mayer-Rosa et al. 1997). Il s’agit de la ville de Bâle, dans le graben du Rhin, où les dépôts quaternaires montrent une variation d’épaisseur jusqu’à 40m; la région de Buchs-Seewald, dans les Préalpes, où la vallée du Rhin est remplie par 200 m de dépôts quaternaires, voire par endroits jusqu’à 500 m et finalement la région de Sion, dans les Alpes, dont les dépôts atteignent dans cette partie de la vallée du Rhône une épaisseur d’environ 900 m.

Le but de cette recherche sectorielle a été d’analyser l’influence des conditions locales sur les variations de mouvements sismiques en utilisant différentes approches étant donné qu’il n’existe pas une méthode idéale et unique pour l’estimation des effets de site et que les données à disposition sont de différents types.

Dans ces diverses études, l’accent a été mis sur l’identification de paramètres permettant de caractériser l’amplification du sol afin d’établir des cartes de microzonage délimitant les zones en fonction de leur capacité à modifier le mouvement sismique.

Contexte de la vallée du Rhône

La partie de la vallée du Rhône concernée dans cette recherche se situe dans le canton du Valais, en Suisse. Elle a la forme d’une structure allongée d’environ 113 km de long et est caractérisée par une largeur variant entre 0 et 6 km.

Cette vallée est située dans une des zones les plus sismiquement actives de Suisse où s’est produit le dernier tremblement de terre majeur de ce 20^{e} siècle dans ce pays, d’une magnitude ML = 6.1. Les dégâts directs causés à cette époque correspondent à une somme de 150 millions de francs suisses actuels. Depuis lors, la vallée du Rhône est devenu le centre socio-économique de la région; elle a vu sa population résidente s'accroître régulièrement et son infrastructure se développer (hôpitaux, autoroutes, conduites de gaz, industries chimiques, chemins de fer, etc.). Par conséquent, si un tel événement devait se reproduire, les dommages seraient plutôt de l'ordre de 0.4 à 1.9 mia de francs suisses. Cela démontre l'importance d'évaluer le danger sismique de la région.

La sismicité de cette région de la Suisse est induite par la tectonique des plaques qui voit interagir la plaque africaine et la plaque Eurasienne dans un mouvement de compression de direction NW-SE à NNW-SE et à une vitesse d'environ 1mm/an (Roeder, 1992). Cette interaction provoque une poussée verticale, à laquelle s'ajoute les forces isostasiques, ce qui a pour conséquence l'élévation de certaines zones des Alpes suisses de quelques 1.5 mm/an (Geiger et al. 1986; Balling & Banda, 1992; Kahle et al. 1997). Cette géodynamique est responsable des tremblements de terre de la région.

Le premier tremblement de terre répertorié pour le canton du Valais date du 14^{e} siècle (1394). Depuis, en se basant sur les données historiques et sur les données instrumentales (depuis les années 70), la région a subit plus de 150 tremblements de terre de ML $\geq$ 3.0. Elle a également été touchée durant ces 250 dernières années par trois événements majeurs d'intensité sismique MSK entre VIII-IX (5.0<ML$\geq$6.0). Cette connaissance de l'histoire sismique d'une région est indispensable pour l'analyse de l'aléa sismique régional puisque l'hypothèse de base stipule que l'activité passée se reproduira. En Valais, l'aléa sismique régional a été évalué sur la base d'une analyse probabilistique en considérant une période d'exposition de 100 ans avec une probabilité de 90% que la valeur estimée ne sera pas dépassée. Cela signifie également qu'un tremblement de terre d'une valeur donnée à 0.01% par année de se produire. Ce choix d'une période de 100 ans et de cette probabilité implique une période de retour des événements sismiques de 950 ans. Etant donné que la majeure partie du catalogue contient des événements sismiques historiques, le paramètre utilisé est l'intensité sismique MSK. Le résultat est une carte dont les isoséistes varient entre VII et IX, de Sion à Brig. Il s'avère que dans cette approche régionale la spécificité de la vallée du Rhône n'est pas prise en compte.

Cependant les documents historiques montrent sans ambiguïté l'influence des conditions géologiques de la vallée du Rhône sur la réponse sismique. Lors des tremblements de terre de Viège (1855) et de Rawil (1946), les levés de terrain (Volger, 1858; Montandon, 1942-43; Mariétan, 1945-46) font état de l'apparition de fissures, de structures d'échappement d'eau dans les alluvions (indice probable de liquéfaction), de glissements de terrain, d'affaissement de sol. Il est également fait mention de variations d'intensité jusqu'à deux unités d'intensité sismique sur de très courte distance dans la vallée et que la plupart des bâtiments endommagés de la ville de Sierre étaient localisé sur des cônes d'alluvions récents (Wanner & Grütter, 1950) et que ceux atteints de la ville de Viège étaient établis sur les alluvions du Rhône (Montandon, 1946).

Les données instrumentales obtenues par le réseau suisse d'accéléromètres, mis en place à partir de 1992, confirment que la vallée du Rhône, comme par exemple dans la région de Brig, peut amplifier le mouvement du sol à certaines fréquences jusqu'à 10 fois par rapport à la roche environnante (Wagner et al. 2000).

Objectifs de cette recherche

Etant donné que les données historiques et instrumentales démontrent que les caractéristiques de la vallée du Rhône modifient la réponse sismique, il s'agit de déterminer d'une part quels pourraient être les éléments contrôlant le phénomène d'amplification dans les vallées alpines et d'autre part d'établir des cartes de microzonage. Ces documents, en mettant spécifiquement en évidence les différentes capacités d'amplification, permettent de sensibiliser les autorités, décideurs, ingénieurs civils, etc. à l'influence des conditions géologiques spécifiques sur le mouvement du sol. Ces cartes sont un outil d'aide à la décision concernant l'aménagement du territoire et le développement de mesures à appliquer pour la réduction des risques sismiques.

L'étude s'est faite sur deux zones, la ville de Sion et la zone de Susten-Brig, en utilisant des approches différentes d'évaluation des effets de site et de zonage. Dans le premier cas, l'analyse a été faite dans le domaine fréquentiel en utilisant d'une part la modélisation numérique bidimensionnelle et d'autre part les mesures du bruit de fond sismique. Un réseau temporaire d'accéléromètres en complément des stations du Service suisse de sismologie a également été installé dans le but d'obtenir des données de tremblements de terre. Dans le second cas un schéma qualitatif de classification a été appliqué en prenant en compte certaines caractéristiques géologiques des dépôts et ensuite comparé aux résultats obtenus par l'approche des anomalies d'intensité sismique. L'application de différentes techniques pour l'analyse des effets de site résulte du contexte géologique variable, des données sismiques et géotechniques disponibles et également du fait qu'en l'état actuel des choses, il n'existe pas une méthode idéale et unique d'évaluation.

La cartographie exige la manipulation et l'analyse de nombreuses informations définies dans un contexte spatial. Pour faciliter la production et la gestion de ces données, le système d'information géographique s'est avéré l'outil indispensable.

Modélisation bidimensionnelle (2D)

Etant donné que le site étudié est une vallée alpine encaissée, il est nécessaire lors de l'analyse des effets de site de tenir compte de sa géométrie, à savoir un interface irrégulier entre le soubassement et le remplissage quaternaire, du fort gradient de pente du soubassement rocheux ainsi qu'une fermeture latérale du dépôt. L'utilisation d'un modèle 2D permet de tenir compte de ces éléments.

Le programme, développé et mis à disposition par Pedersen et al. (1995), permet de calculer la réponse sismique d'une structure soumise à une onde incidente déterminée.

La réponse est donnée dans le domaine fréquentiel pour des points à la surface régulièrement espacés le long du profil. Elle est exprimée en terme d'amplitude de déplacement, sur trois axes, deux horizontaux et le troisième vertical. Il s'agit là de la réponse globale de la structure soumise à une onde spécifique. Pour obtenir la réponse générée par la vallée uniquement, on effectue un rapport entre l'amplitude du mouvement obtenue à la surface de la vallée sédimentaire et celle qui serait obtenue en l'absence du remplissage sédimentaire. On obtient ainsi une fonction d'amplification.

La vallée est assimilée à une inclusion encastrée dans un demi-espace, celui-ci représentant le soubassement rocheux. Les deux éléments du modèle suivent une loi de comportement élastique et linéaire et ils sont également considérés comme isotropes et homogènes, ce qui réduit le nombre de constantes élastiques nécessaires pour caractériser les milieux. Les informations principales nécessaires sont la géométrie de la vallée, le type d'onde incidente et son angle d'incidence, les caractéristiques physiques moyennes de la vallée et de la roche encaissante, comme les vitesses sismiques, la masse volumique, le facteur de qualité qui est une information sur l'atténuation induite par les roches sur la trajectoire des ondes, l'intervalle de fréquence étudié, le nombre de stations, le taux d'échantillonnage du signal.

La recherche a été centrée sur la réponse sismique induite par des ondes cisaillantes, étant donné qu'elles sont les plus aptes à provoquer des dommages aux infrastructures et aux bâtiments, ceux-ci n'étant à priori pas construits pour résister à des mouvements horizontaux cisaillants importants.

Des calculs 2D préliminaires ont été effectués sur deux profils de sismique réflexion levés dans la vallée du Rhône, à proximité de Sion. Des comparaisons ont été faites avec un modèle 1D. Il ressort qu'au niveau de l'amplification la modélisation 2D donne une amplification au moins deux fois plus importante et qu'en ce qui concerne les fréquences, celles-ci se déplacent vers des valeurs supérieure pour la modélisation 2D. De tels résultats ont une implication directe sur l'interaction sol-structure.

Ces calculs 2D montrent également que la vallée présente un rapport de forme et un contraste de vitesse sismique suffisamment élevés pour induire une résonance impliquant l'ensemble du dépôt et qui se traduit, comme noté par King & Tucker (1984) et modélisé par Bard & Bouchon (1985), par une fréquence fondamentale de résonance qui ne varie pas quelque soit l'emplacement le long du profil.

Les signaux temporels modélisés, obtenus par la convolution avec une ondelette de Ricker, montrent que la durée de vibration et l'amplitude sont les plus importantes à la verticale des flancs de la morphologie cachée de la vallée.

Des tests de sensibilité de la réponse bidimensionnelle aux paramètres physiques et à l'incertitude liée au traitement des données géophysiques ont été menés sur les deux profils issus de la sismique réflexion. Les variations des paramètres ont été effectuées dans la fourchette de valeur donnée par les différentes études de géophysiques menées dans la vallée du Rhône ou dans d'autres régions alpines. La sensibilité se joue sur plusieurs niveaux, à savoir la position de la fréquence fondamentale, le niveau d'amplification maximale et la valeur de la fréquence associée ainsi que sur la distribution spatiale des amplifications. Dans le cas de ces deux profils et pour une onde SH, il s'avère que le niveau d'amplification maximale et la fréquence associée sont particulièrement sensibles au contraste de vitesse de l'onde cisaillante entre le soubassement et la vallée sédimentaire ainsi qu'à l'angle d'incidence. Ce dernier peut également modifier la distribution spatiale des valeurs d'amplification. Par contre, la position de la fréquence fondamentale n'est pas influencée par l'angle d'incidence, ni par une variation de masse volumique raisonnable, cette dernière devant être trop faible pour modifier le contraste d'impédance de manière significative.

L'incertitude liée au traitement des données géophysiques montre surtout la sensibilité de la réponse sismique à la géométrie de la vallée.

Microzonage de Sion

La microzonation par modélisation de la zone de Sion, qui couvre une surface d'environ 10 km^2, nécessite de connaître la morphologie cachée de la vallée. L'existence de plusieurs profils de sismique réflexion dans la vallée, dont celui de Vétroz et de Bramois dans la région de Sion, ont permis l'élaboration par interpolation d'une carte d'altitude du soubassement rocheux (Besson et al. 1993). A partir de cette carte et des données numériques d'altitude (OFT, 1993), il est possible d'obtenir une carte d'épaisseur des sédiments quaternaires. Sur cette base, 15 profils ont été tracés, espacés de 250 m entre chacun et perpendiculairement à l'axe principal de la vallée, afin de respecter les conditions de la modélisation.

La faible variation de l'épaisseur maximale (~590 m) de ces profils (moins de 2%) ainsi que la présence de sismofaciés similaires, tels que montrés par l'interprétation des deux profils Vétroz et Bramois, permet d'utiliser les mêmes paramètres physiques pour chaque profil. La roche encaissante, relativement dure, est définie par un coefficient de Poisson de 0.22, une masse volumique de 2670 kg/m^3, et un facteur de qualité de 100. Quant au remplissage sédimentaire, le coefficient de Poisson est égal à 0.41, la masse volumique à 2100 kg/m^3 et le facteur de qualité à 50. Il s'avère que le contraste d'impédance sismique est égal à 4.8, ce qui est relativement élevé et influence la réponse sismique de la vallée. Ces paramètres ont été sélectionnés dans la fourchette de valeurs compilées à partir des différentes recherches géophysiques effectuées dans la vallée du Rhône ou dans des vallées alpines françaises.

La modélisation a été lancée pour les deux types d'ondes cisaillantes, c'est-à-dire l'onde SH et l'onde SV. Les informations utilisées pour le microzonage sont l'amplification relative maximale et la fréquence associée. En d'autres termes, cela donne la fréquence prédominante dans la zone et son niveau d'amplification. Sur chaque profil, l'espacement entre les stations est de 50 m, cela donne ainsi une bonne information sur l'évolution de l'amplification maximale relative et de sa fréquence le long de ce profil.

Ces deux éléments ont été extraits à chaque station, sur chaque profil et géoréférencé. Un krigeage linéaire a ensuite été appliqué afin d'interpoler les données pour obtenir une carte d'amplification relative maximale et une carte de fréquence associée pour chacune des ondes cisaillantes incidentes. Puis pour une question de clarté de lecture, les données ont été réparties par classe. Dans le cas de la carte des fréquences, la classification est non linéaire afin de faire ressortir la zone contenant la fréquence de résonance de la structure. Dans le cas de la carte d'amplification, la classification est linéaire.

Les cartes d'amplification montrent que dans le cas de l'onde SH le niveau atteint de l'amplification est plus élevé et que cela est limité à certaines zones bien spécifiques. Quant aux cartes de fréquence, elles présentent une même tendance générale, c'est-à-dire de très basses fréquences (< 1Hz) au centre de la vallée et une augmentation des valeurs vers les flancs. Cela coïncide avec l'évolution de l'épaisseur du dépôt sédimentaire, les basses fréquences correspondent à la partie la plus profonde, alors que les valeurs augmentent avec l'amincissement du dépôt vers les flancs. On peut également noter que dans le cas de l'onde SH la fréquence de résonance est plus basse que dans le cas de l'onde SV. Il est à noter que l'approche 1D, généralement utilisée, ne donne qu'une valeur de fréquence fondamentale pour le cas d'une onde cisaillante à incidence verticale. Par conséquent, le fait que la fréquence fondamentale peut varier en fonction de l'axe considéré est de première importance dans l'analyse de la réponse sismique des infrastructures.

La variation du rapport de forme joue un rôle fondamental sur la distribution de l'amplification relative maximale. Ce rapport est directement lié à la variation d'épaisseur et de gradient de pente du soubassement rocheux. Une analyse croisée entre les classes d'amplification maximale et de la distribution de l'épaisseur des sédiments ainsi que du gradient de pente de l'encaissant a permis de montrer que l'amplification maximale pour une onde SH se produisait pour la classe d'épaisseur 500-600 m et pour une catégorie de gradient de pente 20-30°, tandis que dans le cas de l'onde SV, elle se produisait pour une classe d'épaisseur de 300-400 m et de pente 40-50°.

Ces résultats fournissent des éléments pour le développement d'un schéma qualitatif pour évaluer le niveau d'amplification de la zone de Susten-Brig.

En sus des tests de sensibilité de la réponse bidimensionnelle déjà réalisés sur les profils de Vétroz et Bramois, des paramètres comme l'angle d'incidence de l'onde SV, la masse volumique, le coefficient de Poisson, et le facteur de qualité ont été testés sur les profils de Sion. Il s'avère que le paramètre le plus influant est l'angle d'incidence, son impact étant à la fois sur le niveau d'amplification maximale et la fréquence d'occurrence ainsi que sur la répartition spatiale. Les autres éléments ne modifient que le niveau d'amplification et les valeurs de fréquence. Les modifications induites par une onde à incidence non verticale dépendent fortement de l'asymétrie du profil et du type d'onde. Si l'asymétrie est prononcée, le niveau d'amplification va dépasser celui d'une onde à incidence verticale. Dans la région de Sion, au vu des différents profils, on peut estimer que cet effet sera très local et effacé dans la tendance générale du zonage. Par contre, cela signifie que dans des zones où l'asymétrie de la morphologie est plus prononcée, l'angle d'incidence de l'onde peut jouer un rôle non négligeable et modifier un zonage établit pour une onde à incidence verticale.

Rapport H/V sur le bruit de fond sismique

La modélisation 2D est une approche prédictive basée sur certaines simplifications des conditions réelles du milieu. Pour conforter ces résultats, il est utile de pouvoir les comparer à des mesures sur le site. Cependant dans des régions à sismicité modérée, l'acquisition de données sismiques peut exiger un laps de temps assez long de l'ordre de plusieurs années avant d'obtenir une base de données permettant de caractériser les réponses locales. C'est pourquoi des méthodes alternatives, dont la méthode du rapport entre les composantes horizontales et verticale (H/V) calculé sur le bruit de fond, ont été appliquées.

Le bruit de fond est généré par des forces naturelles (vent, orages, vagues océaniques) et/ou par des sources de surface artificielles (industries, automobiles, train, etc.). Dans l'analyse classique des signaux sismiques, ce bruit est généralement considéré comme une perturbation du signal que l'on doit filtrer. Cependant, de nombreux auteurs ont utilisé ce bruit pour tenter de caractériser la réponse sismique locale. Parmi eux, Nakamura (1989) a développé la technique du rapport H/V sur le bruit de fond en utilisant des sites urbains au Japon. Cette technique est basée sur l'hypothèse que le bruit de fond est composée d'ondes de volumes (onde P et S) et d'ondes de surface de type Rayleigh, ces dernières étant produites par l'activité urbaine (industrie, automobile, etc.) située à proximité du point de mesure. Ces ondes sont donc considérées comme des perturbations et doivent être enlevées. Nakamura (1989) propose donc le rapport H/V afin de supprimer l'effet des ondes de surface. Cette mesure s'effectue sur un seul site avec un sismomètre trois composantes. Selon Nakamura (1989), ce rapport permet d'obtenir la fréquence prédominante et le facteur d'amplification de la structure sédimentaire en un point donné. De nombreux travaux ont été effectués afin de tester la méthode (ex. Lermo & Chávez-García, 1993; Lachet & Bard, 1994; Seekins et al. 1996) non seulement sur le bruit de fond, mais également sur les données de tremblement de terre. En général, la méthode donne une bonne indication de la résonance fondamentale de la structure sédimentaire, également dans des régions où l'épaisseur sédimentaire est de plusieurs centaines de mètres, mais sous-estime le plus souvent le niveau d'amplification.

Cette méthode a donc été appliquée dans la région de Sion. La première campagne d'acquisition et de traitement des données a été effectuée par Gonzenbach (1997), suivies par deux complémentaires afin de vérifier certains points et d'en acquérir de nouveaux. Les points ont été mesurés sur ou à proximité des profils de modélisation 2D. Le bruit de fond a été enregistré en chaque site pendant 5 minutes, par un sismomètre à trois composantes caractérisé par une fréquence propre de 1Hz. Le signal de chaque composante est divisé en fenêtre de 33 secondes qui sont filtrées, adoucies dans le domaine fréquentiel avant d'être utilisées pour le rapport H/V. Le résultat final est donné par la moyenne des rapports H/V de chaque fenêtre. La dernière étape consiste à extraire la fréquence dominante et le facteur d'amplification du rapport H/V moyen. Les données de fréquence ont pu être utilisées pour établir une carte de la fréquence dominante de la zone de Sion, au contraire des données d'amplification, dont la distribution ne présente pas de dépendance face à la variation d'épaisseur du remplissage ni au gradient de pente du soubassement rocheux.

La comparaison entre les cartes de fréquence obtenues par modélisation 2D et par méthode H/V montre une même tendance, à savoir des valeurs de basse fréquence pour les zones caractérisées par une grande épaisseur sédimentaire et une augmentation des fréquence lorsque la zone s'amincit. Cependant le niveau de fréquence obtenu par la méthode H/V est plus bas que celui obtenu par modélisation. Ce résultat montrerait que la méthode H/V ne donne que la réponse unidimensionnelle du site, c'est-à-dire à la verticale du point de mesure. D'autre part, la méthode H/V montre une sensibilité aux variations très locales dont la modélisation 2D ne peut pas tenir compte.

Réseau temporaire d'accéléromètres

Pour obtenir des données sismiques, trois accéléromètres temporaires ont été installés, en 1997, en complément du réseau national déjà existant dans la région. Le choix des sites a été effectué en fonction des réponses modélisées. C'est ainsi qu'une station a été installée au centre de la vallée et les deux autres de part et d'autre du Rhône, en bordure de la vallée. Au total, cela fait un réseau composé de 6 stations, deux stations sur le rocher et 4 sur le remplissage sédimentaire.

Une année après la mise en route du réseau temporaire, un tremblement de terre de magnitude ML = 3.1 s'est produit dans la zone du barrage de la Grande Dixence à une profondeur de 5.9 km et à une distance épicentrale des stations d'une douzaine de kilomètres. Toutes les stations en place ont enregistré le séisme, excepté celle de Valère, localisée sur le rocher entre les deux collines Valère et Tourbillon.

En raison du seuil de déclenchement, activé sur les stations afin d'éviter l'enregistrement de l'activité urbaine, c'est le seul tremblement de terre enregistré en 3 ans d'activité du réseau temporaire. Cela ne constitue donc pas un échantillonnage représentatif. Cependant, cela permet de faire des observations préliminaires qui devront être confirmées par d'autres événements sismiques.

Tout d'abord, les signaux temporels montrent que l'amplitude et la durée est plus importante pour les stations situées dans la vallée que pour la station au rocher et que d'autre part pour les stations dans la vallée, les signaux sont plus amplifiés et plus longs à la verticale des flancs cachés de la vallée qu'au centre de la vallée, confirmant par là les résultats de la modélisation 2D.

La comparaison entre le signal sismique et le bruit de fond s'est effectuée sur la base d'un rapport H/V utilisant la sommation des deux composantes horizontales. Le rapport H/V sur le signal sismique présente des fréquences dominantes dans les hautes fréquences (≥ 5 Hz) alors que dans le cas du bruit de fond, deux stations sur trois présentent une fréquence dominante dans les basses fréquences (< 1 Hz). La présence de hautes fréquences peut être due à la présence de la nappe phréatique, de profondeur variable, dont l'influence se fait sentir au niveau de l'épaisseur de la couche non saturée et du coefficient de Poisson; deux paramètres intervenant sur la fréquence et l'amplitude.

Pour la station située au centre de la vallée, la fréquence fondamentale donnée par le rapport H/V sur le bruit de fond est inférieure à celle donnée par le rapport H/V sur le signal sismique, ce qui pourrait indiquer que le bruit de fond ne contient pas assez énergique pour mettre en résonance l'ensemble du dépôt mais uniquement l'épaisseur de la couche située à la verticale du point de mesure.

En ce qui concerne la confrontation avec la modélisation 2D, les composantes horizontales ont été considérées séparément pour le rapport H/V et ont de plus subies une rotation de manière à être défini dans le même système d'axes que la modélisation. Pour la composante horizontale NS, il y a une bonne concordance sur la position de la fréquence fondamentale de résonance, alors que pour la composante EW, la modélisation 2D donne une fréquence plus basse que le signal sismique.

Microzonage de la zone de Susten - Brig

Dans cette région, l'approche suivie est basée sur une approche qualitative utilisant les données géologiques, géotechniques et morphologiques connues. Dans un récent travail (Wagner et al. 2000) la zone de Susten-Brig a été cartographiée amenant ainsi de nouvelles connaissances dans cette région sur la distribution et composition des dépôts superficiels, la profondeur de la nappe phréatique ainsi que l'épaisseur des sédiments quaternaires. Sur la base de ces éléments une carte des facteurs de correction de l'intensité sismique avait été obtenue suivant la méthode de l'anomalie d'intensité sismique. Cependant dans cette approche, le gradient de pente du soubassement rocheux n'a pas été pris en considération. Etant donné que la région de Sion a montré que ce gradient de pente joue également un rôle et qu'aucun facteur de correction de l'intensité sismique n'est disponible pour ce paramètre, un schéma d'attribution de facteur d'amplification qualitatif a donc été développé considérant toutes les informations disponibles et ayant un rôle prépondérant sur l'amplification du mouvement du sol.

Les facteurs qualitatifs ont été attribué de façon linéaire au sein de chaque paramètre (épaisseur du quaternaire, type de dépôt superficiel, etc). Chaque paramètre étant subdivisé en plusieurs catégories, un facteur d'amplification a été attribué à chacune d'entre elles. Les facteurs d'amplification varient entre 1 et 5, la valeur 1 étant attribuée à la catégorie considérée comme produisant une amplification minimale et la valeur 5 à la catégorie induisant l'amplification maximale. Le résultat est présenté sous forme de carte d'amplification sismique qualitative.

La comparaison entre la carte d'amplification qualitative et celle issue de l'approche par anomalie de l'intensité sismique confirme que, quelque soit l'approche, la partie supérieure de la vallée du Rhône présente également les conditions générant un phénomène d'amplification. Les zones d'amplification maximale ne sont pas mis en relief exactement de la même manière entre les deux cartes. Cela tient à l'intégration du paramètre de gradient de pente dans la carte qualitative.

La carte qualitative aussi bien que la carte d'anomalie de l'intensité sismique prennent en considération des éléments dont l'impact se situe à une échelle différente. En effet, les éléments tels que l'épaisseur du Quaternaire et le gradient de pente du soubassement rocheux jouent de l'encaissant non seulement un rôle local mais influent également sur la distribution spatiale à l'échelle de la zone étant donné qu'ils caractérisent la morphologie cachée de la vallée et que c'est celle-ci qui régit la réponse sismique à basse fréquence, comme le montre l'analyse faite sur la zone de Sion. Quant aux dépôts superficiels et à la nappe phréatique, leur influence se situe surtout à une échelle locale étant donné leur variation latérale extrêmement rapide dans une vallée Quaternaire.

Conclusions

Cette recherche confirme que les vallées alpines ont une capacité élevée d'amplification du mouvement du sol et démontrent également la complexité du phénomène.

Le fait d'aborder l'analyse des effets de site par une approche bidimensionnelle permet de prendre en considération le rôle joué par la géométrie de la vallée ainsi que sa variation, et d'identifier les autres paramètres influant sur la réponse sismique. En effet, son application dans la région de Sion montre que la vallée est suffisamment encaissée et est caractérisée par un contraste d'impédance sismique suffisamment élevé pour induire une résonance mettant en mouvement l'ensemble du dépôt ce qui prolonge la durée et augment l'amplitude des signaux sismiques.

La modélisation 2D a également montré que l'amplification maximale et la fréquence associée formaient une association paramétrique variant en fonction de la position dans la vallée. Cela a permis d'atteindre l'objectif de la définition de paramètres pour l'élaboration des cartes de microzonage pour la région de Sion. Dans cette zone, le microzonage établi par la modélisation 2D a été comparé aux résultats obtenus par la méthode du rapport H/V sur le bruit de fond. En terme de distribution des fréquences, les deux méthodes sont en accord sur la tendance générale, à savoir de basses fréquences lorsque le remplissage sédimentaire est profond et de plus hautes fréquences lorsque le dépôt s'amincit. Mais elles montrent également des différences qui sont vraisemblablement liés à des variations géologiques très locales qui ne sont pas prises en considération dans l'approche 2D.

Les tests de sensibilité de la réponse bidimensionnelle à différents paramètres (par ex. angle d'incidence, coefficient de Poisson, rapport de vitesse, etc.) permettent de circonscrire les incertitudes paramétriques et spatiales. Ces tests montrent que le paramètre critique est l'association angle d'incidence et forte asymétrie de la vallée. En effet, cela affecte la distribution spatiale de l'amplification maximale ainsi que sa fréquence associée par comparaison aux résultats obtenus pour une onde à incidence verticale. La variation des paramètres physiques (par ex. vitesse, facteur de qualité, etc.), comprise dans un intervalle de valeurs plausibles, n'altère que la valeur de l'amplification maximale et la fréquence associée, sans en déplacer les zones correspondant à la réponse sismique maximale.

Dans la région de Susten-Brig, l'analyse du phénomène d'amplification s'est faite en utilisant un schéma qualitatif permettant de considérer d'une part les éléments géologiques et géotechniques reconnus pour leur influence sur ce phénomène et d'autre part d'intégrer les résultats obtenus sur la zone de Sion. La comparaison de la carte de microzonage résultante à celle déjà existante et obtenue par l'approche de l'anomalie de l'intensité sismique met en relief les paramètres en fonction de leur impact spatial. Les paramètres comme le gradient de pente du soubassement rocheux et l'épaisseur du remplissage montrent un rôle global, alors que la géologie des couches superficielles modifient localement la réponse. Le rôle de la nappe phréatique joue ici un rôle non négligeable sur le niveau de l'amplification et a une influence également locale.

Les cartes établies sont un premier échelon dans la connaissance du danger sismique. Elles peuvent aider à la mise à jour des codes de construction et également servir de guide pour une gestion préventive du territoire.

Dans une région à sismicité modérée, les événements majeurs sont plutôt rares. Cela a pour conséquence de biaiser la perception du risque sismique. De telles recherches sur les effets de site sont donc nécessaires également pour sensibiliser les opinions et devraient être systématisées, particulièrement dans les régions sensibles du pays.

ACKNOWLEDGMENTS - REMERCIEMENTS

I thank the Professor Jean-Jacques WAGNER for having given me the opportunity to work on this fascinating subject as well as, in parallel, to work in the Multifaculty Programme in Humanitarian action (ppAH) and later on to be part of a research group on “Management des Risques Majeurs” (MRM) at the University of Geneva.

I am grateful to Professor Anne S. KIREMIDJIAN for having accepted to be part of the board of examiners as well as for having offered me the chance and the finance to do an internship at the John A. Blume Earthquake Engineering Center.

I give also thanks to Professor Michel CAMPILLO for his acceptance of being part of the board of examiners as well as having received me at the Laboratoire de Géophysique Interne et Tectonophysique (LGIT). This internship was financed by the Communauté de Travail des Alpes Occidentales, Région Rhône-Alpes (COTRAO) to which I also express my gratitude. I am also indebted to Prof. Michel CAMPILLO and Dr. Helle PEDERSEN for having given me access to the modeling programs (1D and 2D).

I acknowledge Dr. Dieter MAYER-ROSA, former chief of the Swiss Seismological Service, for having been part of the board of examiners as well as for his support.

This work took place in a very beautiful canton, the Valais, and is part of the project SISVAL, sponsored by the Swiss national committee for the International Decade for Natural Disaster Reduction (IDNDR) as well as of a project financed by the Swiss National Research Program 31 (PNR31) on climatic changes and natural disasters. Special thanks to Olivier LATELTIN, former secretary of the Swiss national committee of IDNDR, for his understanding and to Pierre KUNZ, former scientific adjunct of the PNR31, for our numerous discussions and his friendship.

Un travail ne dépend pas seulement du terrain mais également des gens rencontrés.

Je remercie M. Jean-Daniel ROUILLER, géologue cantonal du Valais, pour m’avoir facilité la recherche documentaire. Ma reconnaissance va également aux collaborateurs du CREALP, plus particulièrement à Pascal ORNSTEIN et à Jean-Marc REY pour leur aide dans ma recherche d’information géologique, lithologique et hydrologique. Je tiens également à exprimer ma gratitude à M. Marc-Antoine ROBYR du Service des routes et cours d’eau, à Sion, pour son accueil et sa disponibilité dans ma quête de forages. Je remercie le responsable des archives de la bibliothèque cantonale à Sion pour son appui dans ma recherche de documents historiques.

M. Yves DESSIMOZ, commandant du Centre d’intervention de la police cantonale, M. GENOUD, directeur du Service environnement et M. Charles RIVA, directeur de l’institut de recherche en ophtalmologie de Sion ont toute ma gratitude pour avoir accepté l’installation de stations accélérométriques dans leur bâtiment. MM. TISSIERES et MAX (Centre d’intervention de la police), Mme Nicole MICHELLOD (Institut d’ophtalmologie) et M. François COQUOZ (Service environnement) ont toute ma reconnaissance pour leur aide bénévole dans leur maintien en fonctionnement.

Que soit aussi remercié l’Office fédéral de topographie, et son directeur Monsieur F. JEANRICHARD, pour la mise à disposition des modèles numériques de terrain, éléments indispensables, couvrant la zone de Sion à Brig.

Cette recherche n'aurait pu se faire sans informatique et sans stations accéléromètriques. Je remercie donc tout particulièrement Stephane JORDI, pour son aide précieuse grâce à laquelle j'ai pu naviguer entre les divers environnements et programmes informatiques, et pour nos nombreuses et joyeuses conversations électroniques. Je remercie également M. Bob MATTHEWS (Université de Genève) pour l'accès à la station de travail, qui a permis les calculs de modélisation, et pour son aide dans la résolution des problèmes techniques. Je dois une fière chandelle à Patrick SMIT pour m'avoir introduit dans le monde des accéléromètres, de leurs mécanismes à leurs installations, et je lui adresse un tout grand merci pour les précieuses discussions thématiques, pour ses encouragements et sa disponibilité.

La section des Sciences de la Terre recèle de personnes ressources. Merci à Jacqueline BERTHOUD pour son aide logistique, sa gentillesse (et son succulent gâteau revigorant), à Gilbert OVERNEY pour son art de résoudre les problèmes techniques, et à Jacques METZGER pour ses magnifiques posters et ses astuces graphiques.

Au gré des années passées, des personnes précieuses m'ont aidé d'une manière ou d'une autre. Un grand merci à André PUGIN, Mario SARTORI, Donat FAEH, Erik RÜTTENER, Helle PEDERSEN, Jean-Michel JAQUET, Steeve EBENER, Fabio HEER, Carlos MUÑOZ, Markus KESSELER, Hy DAO pour les discussions et/ou leur apport dans le traitement des données. Un remerciement tout particulier à Philippe ROSSET et à Martin GONZENBACH pour leur travail d'investigation sur le bruit de fond.

Je remercie mes collègues Jean-Dominique LAPORTE, Diane ROTH, Marie-Claire CALOZ-TSCHOPP, Caroline MEIER, Isabelle PORCHET, Catherine RITTER, Claire GRIMBERT PETTERSEN, Isse BOKATOLA ainsi que le Professeur T.-W. HARDING, du programme plurifacultaire en Action humanitaire (ppAH), ainsi que Sébastien BERTRAND, Franco ROMERIO et Jean ROSSIAUD, du projet de recherche “Management des Risques Majeurs” (MRM) pour leur compréhension lors des moments de “haute tension”.

Dans la vie, les amis sont précieux. Merci à Thierry BASSET, Valérie STÄHLI et Téo, Katrien, Vincent et Amélie BERNARD-BEECKMAN, Henry GAUDRU, Catherine ANNEN, Alain DROUX et Lucie, Philippe, Florence et Flora ROSSET, Pierre, Carmen, Michaël et Sabine KUNZ, Catia MOSCHELLA, Regula et Peter BIESERT, Valérie, Thierry et Marie PLATTET, Catherine, Yvan et Gaétan GAGNAUX-LOVO, Claudine MARTIN, Valérie MARTIN et Anthony EBENER, Margrit ZELLER, Mireille et Jean-Pierre PEIGNEUX pour leur chaleureuse présence et pour leurs encouragements.

Finalement j'adresse toute ma reconnaissance à mes parents Doris et Hans FRISCHKNECHT pour m'avoir offert la chance d'étudier. Je terminerais sur une pensée toute particulière à mon fiancé Boris PEIGNEUX, dont j'ai pu apprécier le calme olympien lors de la dernière boucle de ce marathon qu'est une thèse.

LIST OF FIGURES

Chapter 1

Chapter 2

Chapter 3

Chapter 4

Chapter 5

1 INTRODUCTION

1.1 Background

When an earthquake strikes, the observed impacts on the natural environment at a particular site can be soil amplification, soil rupture, liquefaction or landslides. The occurrence of such phenomena is controlled by the local geologic conditions. All mentioned phenomena are called site effects.

This work will focus on soil amplification phenomenon as it is responsible of most of the observed damages to the built environment. This phenomenon is particularly sensitive to the local site conditions. Indeed it has been noticed for a long time that the seismic response can vary in a large scale over a short distance depending on the type of deposits, rocks or unconsolidated sediments, natural or man-made. The seismic response variation can be observed in form of intensity anomalies and/or on seismic records. The analysis of seismic records has shown that local site conditions can modify the amplitude, the frequency content and the duration of the ground motion.

The local soil conditions can induce two main effects (figure 1.1) :

- topographical effects, due to the presence of hills, mountains, ridges,
- sediment effects, soft sediment deposits above bedrock in form of a plain layers, closed basins or alluvial valleys.

The influence of surface topography is not the target of this work, but as the study area is surrounded by mountains, it must be taken into account that observations often made after earthquakes show that buildings located on top of hills or at the crest of a ridge suffer more damages than those located on the flat ground. It seems that amplification is more important on top of a topographic structure and deamplification is connected to at the base (Bard, 1994). This phenomenon depends on the ratio between the height and the half length of the structure, and on how the lateral dimensions are related to the wavelengths of the ground motion. Indeed if dimensions of the structure are in the range of the wavelengths, there is a potential of significant effect on ground motion (Finn, 1991). Other elements can also intervene by mainly modifying the amplification level, such as the internal layering and the three-dimensional shape of the surface topography (Spudich et al. 1996; Bouchon & Barker, 1996).

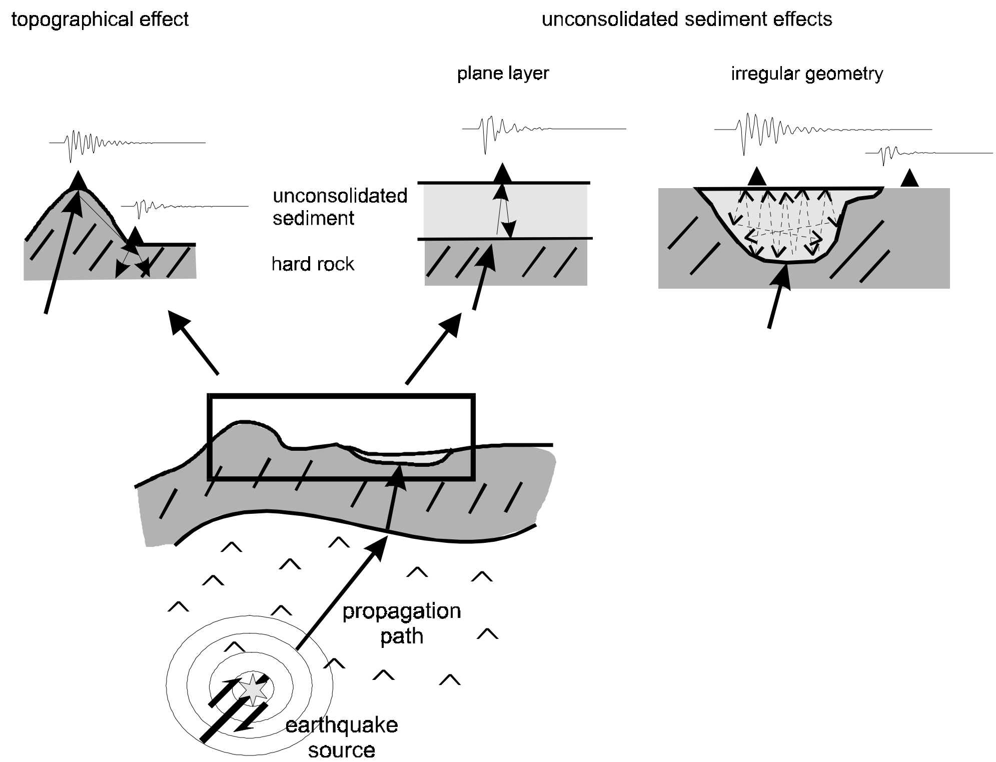

Figure 1.1. From the seismic source to the site (modified from Riepl-Thomas & Cotton, 1999).
Figure 1.1. De la source sismique au site (modifié de Riepl-Thomas & Cotton, 1999).

Effects induced by unconsolidated sediments are of concern for a long time. Numerous earthquakes have shown that intensities were higher for sites on alluvial material compared to rock site. First analysis was done by approximating the seismic response of a site through the vertical column of soil submitted to seismic waves. Generally the shear wave velocity is considered the most influential to produce damages on the built environment. In such an approximation by flat layers, the amplification phenomenon is only due to :

- impedance contrast,
- resonance effect.

Impedance contrast (I_c) depends on the physical characteristics of the material (density and seismic velocity) which are related to the history of the deposit. Considering unconsolidated sediments, the younger the deposit, the less consolidated is the material, thus the higher will be the impedance contrast. This contrast can be expressed as :

$$I_c = \frac{\rho_b * V_b}{\rho_s * V_s} \quad \text{with } V_b >> V_s$$

with ρ_b = density and V_b the seismic velocity of the bedrock
ρ_s = density and V_s the seismic velocity of the unconsolidated layer

The impedance contrast is responsible for trapping the seismic waves inside layer with lower impedance and therefore provoking amplification for characteristic frequencies.

Resonance effect is caused by the constructive interference of waves at a specific frequency having for consequence an amplification at these defined frequencies. For a simple structure with horizontally plane layers and a vertical incident seismic wave, these resonant frequencies are dependent on the thickness and the seismic velocity as given by the formula :

$$f_n = \frac{V}{4H}(2n+1) \qquad n=0,1,2,3,\ldots,\infty$$

with H being the thickness in meter, V the seismic velocity in m/s and f_n the resonant frequencies of the soil deposit. For n=0, the resonant frequency is called the fundamental frequency as it is the lowest frequency at which an amplification occurs and for n>0, the frequencies are the harmonics of the fundamental frequency.

Unconsolidated sediments can be found very frequently. However the spatial arrangement can strongly differ as a consequence of the local geologic history. It can be deposited in valleys or in basins of various size and shapes having non planar subsurface geometry.

Numerical studies (Bard & Bouchon, 1980 a,b; 1985) showed that the valley edges can generate local surface waves (Rayleigh and Love waves) which are trapped inside a sedimentary valley, whereas irregular geometry induces focusing of waves at specific places. The result is seen as increase of the signal duration, variation of its amplitude and modification of the frequency content. For symmetric two-dimensional valleys the generation of lateral surface waves is controlled by the velocity contrast. If this contrast is high, the waves can be reflected at the edges several times (Bard & Bouchon, 1980 a,b).

However symmetry is not always the rule in nature. Asymmetric valleys can display abrupt as well as gentle edges. Such an asymmetric geometry will influence the valley response in terms of amplitude and duration; abrupt edges being a more efficient reflector of surface waves. All that also depends on the angle of the incident wave (Papageorgiou & Kim, 1991).

Among different valley types, Alpine valleys are a rather peculiar case. The action of glaciers and rivers in the Quaternary period have often deepened and embanked these valleys. As a result they exhibit specific characteristics such as :

- steep slopes,
- thick and young Quaternary sediments,
- rapid lateral variations of surficial deposits.

Recent studies on seismic records in the Appenins (Pessina et al., 1997) and in the French Alps (Le Brun, 1997) have shown that Alpine alluvial valleys can amplify the ground motion more than 10 times at specific frequencies.

1.2 Previous work in Switzerland on soil amplification

Switzerland is located in the Alpine context with moderate seismic activity on the average. However due to its high density of population and vulnerable infrastructures (highways, gasolines, nuclear power plants, high dams etc.), the risk in Switzerland is considered rather high in some areas.

It is therefore necessary to assess the seismic hazard. This has to be done at different levels, national, regional and local. At the national level, pioneer work was done by Sägesser & Mayer-Rosa (1978) with the first zoning map of Switzerland based on a probabilistic approach. Since that time, the Swiss national seismic network, in operation since the mid-seventies, allowed to accurately locate earthquakes, improving the understanding of the earthquake distribution in the country. These instrumental data serve in addition the historical data in seismic hazard assessment, specially at regional and local level. Still local site effects are not yet integrated in these local studies (Rüttener, 1995).

Systematic investigation on site effects appeared in Switzerland in the middle of the eighties (Fäh, 1985). In the context of the International Decade for Natural Disaster Reduction (IDNDR) declared by the General Assembly of the United Nations for the period of 1990-2000, the Swiss national IDNDR committee sponsored two projects for investigations on the seismic hazard field. The first project OBWALD (Schindler et al, 1996) was dedicated to study the influence of the local geologic conditions on the regional seismic hazard by investigating the seismic intensity anomalies. Further applications of this approach were carried out in the cantons of Niedwald and Solothurn (Beer, 1997). The OBWALD project was followed by the SISVAL project (Wagner et al. 2000), in which this work is integrated. The SISVAL study was carried out in the the Rhône valley, canton of Valais, where two study areas were chosen. Different methodologies were applied in order to consider the effects of local geologic conditions, as it will be described in this work.

Besides the OBWALD and SISVAL projects, in the frame of the national research program PNR31 on climatic changes and natural disasters, three studies (figure 1.2) were performed in different geologic settings (Mayer-Rosa et al., 1997). These areas are :

- the city of Basel, in the Rhinegraben which is characterized by Quaternary deposits of varying depths up to 40 m;
- the Buchs-Seenwald area in the St-Gall Rhine valley. This valley was overdeepened by glacier erosion and then filled by about 200m of Quaternary deposits and in some places up to 500m;
- the Sion area (Valais) in the Swiss Alps. In this area, the Quaternary deposit of the Rhône valley reach a maximum depth of about 900 m.

The goal of this research was to analyze influence of the local site conditions on ground motion variation using different methodologies, depending on the available data and techniques.

Special care was taken to identify parameters that can characterize the soil amplification in order to establish microzonation maps. The spatial variation of the ground motion due to local site conditions is considered important to raise awareness of land-use planners, civil engineers, and decision-makers concern by seismic risk mitigation.

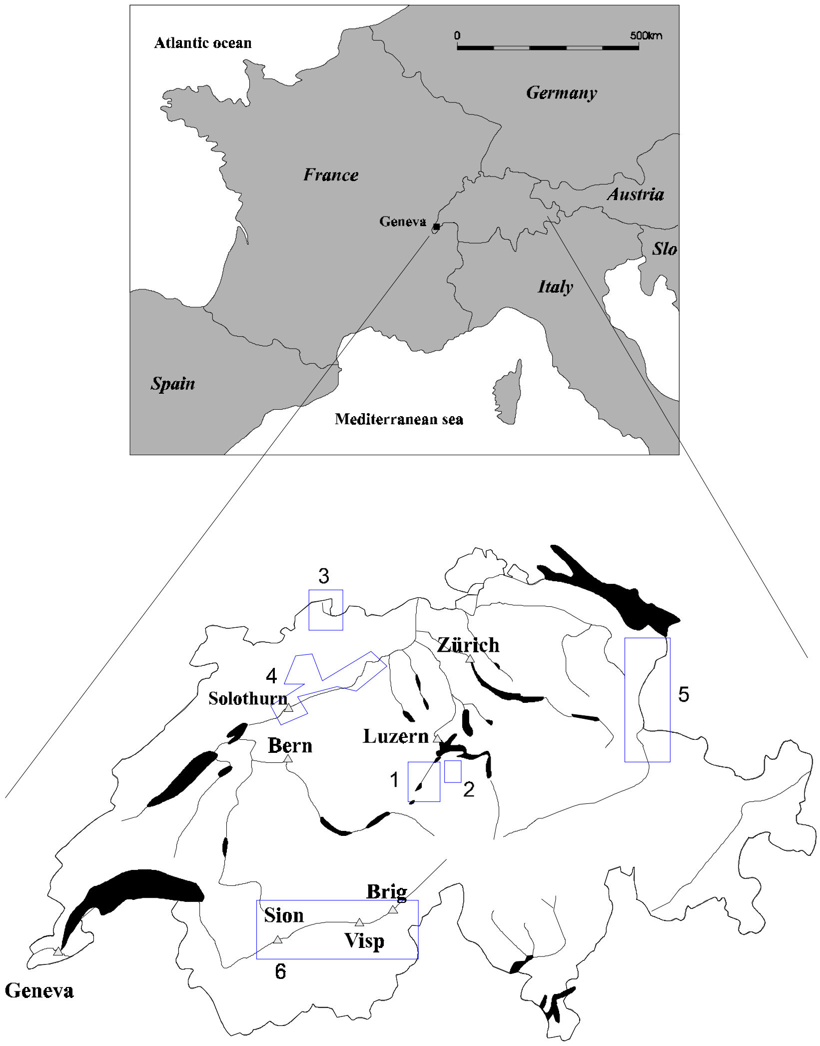

Table 1.2. Location of the different microzonation studies in Switzerland. 1. Obwald; 2. Niedwald; 3. Basel, 4. Solothurn, 5. Buchs-Seenwald; 6. Valais region.
Figue 1.2. Situation des différentes études de microzonage effectuées en Suisse. 1. Obwald, 2. Niedwald, 3. Bâle, 4. Soleure, 5. Buchs-Seenwald, 6. La région du Valais.

1.3 Context of the Rhone Valley

1.3.1 Introduction

The Swiss part of the Rhône valley is an elongated structure, approximately 110 km long and up to 6 km wide. The Quaternary deposits start at Brig and end at the Geneva lake. Most of the territory is located in the canton of Valais.

This valley is a sedimentary structure resulting from the combined action of tectonics and Quaternary glacier erosion. Tectonics is the initiator of the structure, whereas the action of glaciers modifies the shape and usually overdeepens the valley incised initially by rivers. The accumulated sediment thickness reaches a maximum around 1000 m near Martigny (Pfiffner et al. 1997).

The canton of Valais is one of the most active seismic zones in Switzerland. The first reference of an earthquake in this region is dated from the 14^{th} century (1394). Based on the earthquake catalog of historical and instrumental seismic events, the study area experienced over 150 earthquakes with ML ≥ 3.0 and was struck by three major earthquakes of MSK intensity VIII-IX (5.0 < ML ≥ 6.0) in the past 250 years. The most recent one occurred on the 25.01.1946. Since then, the Rhône valley has become an important socio-economic center with chemical industries, pipelines, hospitals and major lifelines. The number of inhabitants in the entire canton has also increased, from 154'204[1] to 273'362 in 1997 (Office fédéral de la statistique, 1999), which indicates a 77 % increase in about 50 years. Most of the population is concentrated in the Rhône valley. Therefore, seismic hazard assessment is a main topic for the area.

1.3.2 Seismic activity

1.3.2.1 Seismotectonics

Earthquakes are the result of stress release along fracture zones. In the Valais region, the stress is accumulated due to the fact that this area belongs to the Alpine belt, a structure formed by the collision of the Adriatic promontory and the Eurasian plate in the Tertiary age. This tectonic process is still going on with a convergence rate between the African and Eurasian plates in the order of 1mm/year (Roeder, 1992). Since the Miocene, the tectonic stress in much of the Western part of Europe shows a compression component in the NW-SE to NNW-SE direction, and a NE-SW to ENE-WSW extension component (Balling & Banda, 1992). This regional stress regime is modified by local components, such as galcial isostasic rebound and tectonic uplift. In the Swiss Alps, the vertical movement, resulting from the horizontal compression as well as the glacial and tectonic isostasic rebounds, is around 1.5 mm/year relative to a station near Aarburg in the Prealps, in the northern Switzerland (Geiger et al. 1986; Balling & Banda, 1992; Kahle et al. 1997). The maximum strain energy obtained from the uplift data shows a fairly good coincidence with the seismic active zone (Geiger et al. 1986, Kahle et al. 1997).

Several geological fault systems are mapped in the Valais region, as shown in figure 1.3 (Wagner et al. 2000). The major ones are (Maurer et al. 1997) :

- the Simplon fault, a low-angle normal fault with a SW oriented dip,
- the Rhône fault, predominantly a dextral strike-slip fault,
- the faults of the Rawil depression, dextral strike-slip fault.

Evidences of their recent seismic activities are rather difficult to find at the surface (Wagner et al. 2000). Two main causes can be advanced, either earthquakes are too weak to rupture the surface or traces are hidden by flank settlements and human activities or covered by vegetation (Wagner et al. 2000).

[1] Interpolation based on the data for the resident population between 1920-1950 of the canton Valais (source : Statistical office of the Canton Valais)

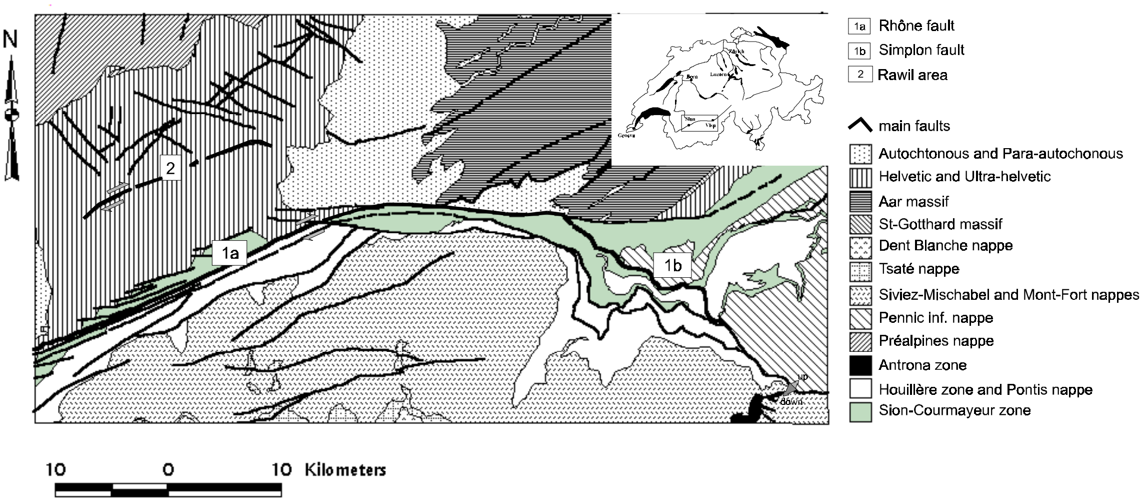

Table 1.3.Tectonic sketch of the central and upper part of the Valais region presenting the main tectonic units and faults (Wagner et al. 2000).
Figure 1.3. Esquisse tectonique de la région du Valais central et du Haut-Valais présentant les unités tectoniques principales ainsi que les failles (Wagner et al. 2000).

Studies of microearthquakes (Maurer, 1993; Pavoni et al. 1997; Maurer et al. 1997) show that the Rhône-Simplon fault zone separates two stress regimes in the Valais region :

- in the North (right side of the Rhône river), in the Helvetic Nappes, earthquakes are characterized by dominant strike-slip mechanisms and hypocenters are clustered along near-vertical faults. These mechanisms are a consequence of regional NW-SE compression and NE-SW extension;
- in the South, earthquake hypocenters are scattered throughout the Penninic Nappes above the gently S-dipping basal Penninic trust and normal faulting is predominant. This is the result of a vertical maximum stress and N-S extension. The reason of such a movement might be due to the collapse of the Penninic Nappes and/or continued uplift and relative northward displacements of the underlying Alpine massifs (Maurer et al. 1997).

Table1.4 (part B). This figure displays an epicenter map and the hypocenters projection on a structural model of the crust obtained from the interpretation of the NRP20 seismic reflection profiles. It can also be seen in the figure 1.4 (part A) that the earthquake distribution patterns differ on both sides of the Rhône valley, showing clustering of earthquakes in the North (Wildhorn area) and diffuse seismicity in the South.

The 1946 earthquake occurred on the Rawil depression (in the North), the strongest event in Switzerland in the 20th century. Based on the aftershocks and detailed microearthquake surveys, a fault system could be traced, which trends WSW-ENE (Pavoni et al., 1997). This zone is called the Wildhorn seismic zone and is actually the most seismically active region in the Swiss Alps (Pavoni et al. 1997). Comparison between the historical seismicity and the instrumental data (figure 1.5) confirms this fact and also allows to see that the seismic activity has a tendency to move toward the Northwest (Wagner et al. 2000).

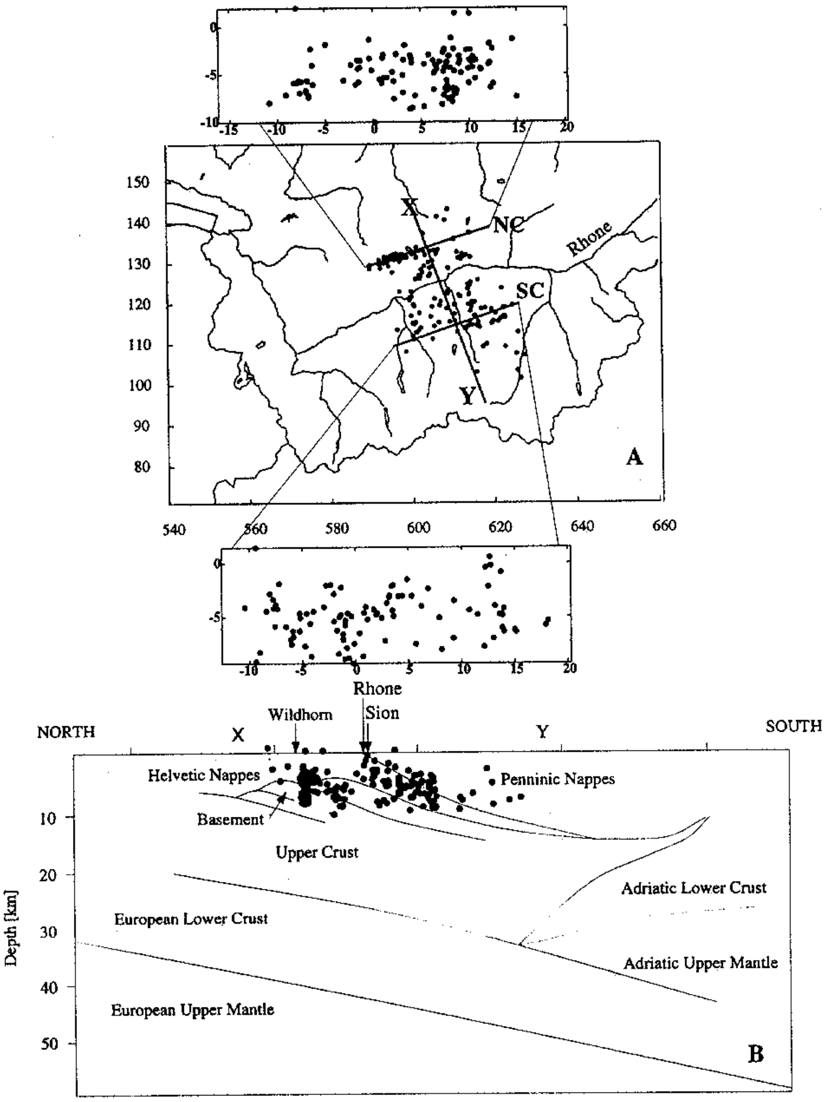

Figure 1.4. Part A shows epicenters with reliable focal depth on two cross section, the NC in the North part and the SC in the South. Part B shows a projection of the hypocenters on a crustal model obtained from the NRP20 high reflection seismic profiles (Pavoni et al. 1997).

Figure 1.4. La partie A présente les épicentres de tremblement de terre et la projection de leur hypocentre sur deux coupes, NC au Nord et SC au Sud. La partie B montre une projection des hypocentres sur un modèle crustal dérivé des profiles de sismique haute réflexion du PNR20 (Pavoni et al. 1997).

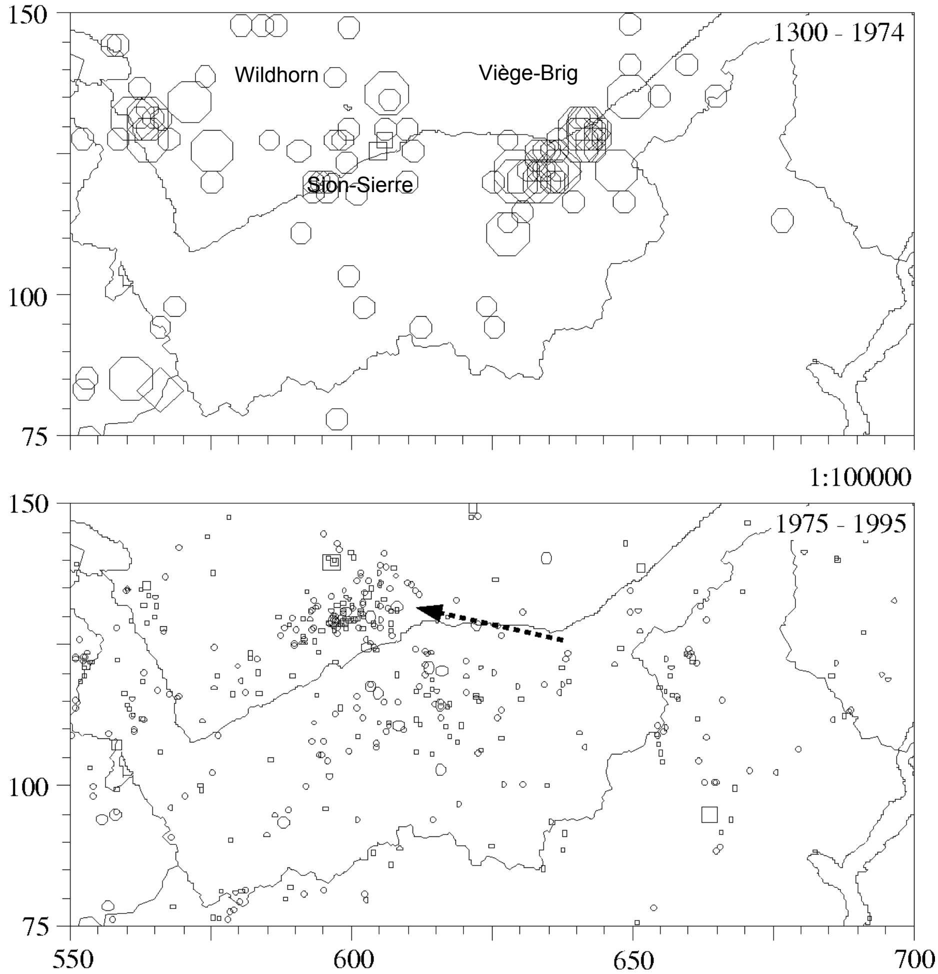

Table 1.5. Historical (1300-1974) and instrumental (1975-1995) seismicity in the Valais region. For the historical data, only MSK intensities $I_0 \geq V$ are represented. Regarding the instrumental data, earthquakes with magnitude $M \geq 2.0$ are shown. The arrow shows the displacement of the seismic activity to the Northwest (Wagner et al. 2000).
Figure 1.5. Sismicité historique (1300-1974) et instrumentale (1975-1995) du Valais. Les données historiques sont représentées à partir de l'intensité MSK $I_0 \geq V$. Quant aux données instrumentales, elles figurent à partir d'une magnitude $M \geq 2.0$. La flèche indique le déplacement de l'activité sismique vers le nord-ouest (Wagner et al. 2000).

1.3.2.2 Regional seismic hazard

The regional seismic hazard assessment for the Valais region was carried out applying a probabilistic scheme, based on Cornell 's deductive or seismic source approach (Rüttener, 1995). Since the major part of the earthquake catalog (SED, 1995) is composed of historical events expressed in terms of MSK intensities, the probabilistic regional seismic hazard is represented in this unit.

Usually the intensity is a scalar value ascribed to characterize the observed and felt effects of an earthquake (see Appendix A) and is represented by roman numbers. For calculation purposes the assumption is made that these intensity values are continuous.

The main steps to achieve the deductive analysis of the seismic hazard are (Cornell, 1968; Shah et al. 1975; Sägesser & Mayer-Rosa, 1978; Rüttener, 1995) :

- compilation of an earthquake catalog,
- delineation of seismic sources,
- intensity-frequency distribution,
- ground motion attenuation model using the selected ground motion parameter (e.g. acceleration, intensity),
- probabilistic analysis, taking into account uncertainties.

Such analysis is based on the assumption that the past activity will repeat in the future in the same way.

For the central and upper part of the Valais area, the seismic hazard has been estimated, for a given exposure time window of 100 years, that a certain intensity will not be exceeded with a probability of 90% during this period. It is also equivalent to a 10% probability of exceedance. The considered return period can be calculated using the following formula :

$$Pn = 1 - \left(1 - \frac{1}{Tr}\right)^n$$

with n= a given exposure time window, Pn = probability of exceedance of at least one occurrence of n successive years, Tr = the return period in years for an event of a particular magnitude.

Using the mentioned parameters, the return period is then equal to 950 years. This formula is based on a binomial distribution of the events assuming one or more independent occurrences in n years. Therefore only the main shocks are considered.

Table1.6. Obviously, the strong 1755 and 1855 events, in the Viège-Brig area (figure 1.5), have a dominant influence on the MSK intensity distribution. It can also be seen that no differences in seismic response occur between the Rhône valley and the surrounding areas. This is certainly due to the fact, that average attenuation functions have been used, which do not exhibit different ground conditions.

1.3.3 Site effect observation

Site effects have been noticed in the Valais region through historical and recent events. Instrumental records of the Swiss national strong motion networks do confirm soil amplification due to unconsolidated sediments.

1.3.3.1 Historical seismic events

The three major documented seismic events which struck the Valais region in the past 250 years and were felt through out Switzerland and also in the neighboring countries (France, Italy, Austria, Germany) are the following :

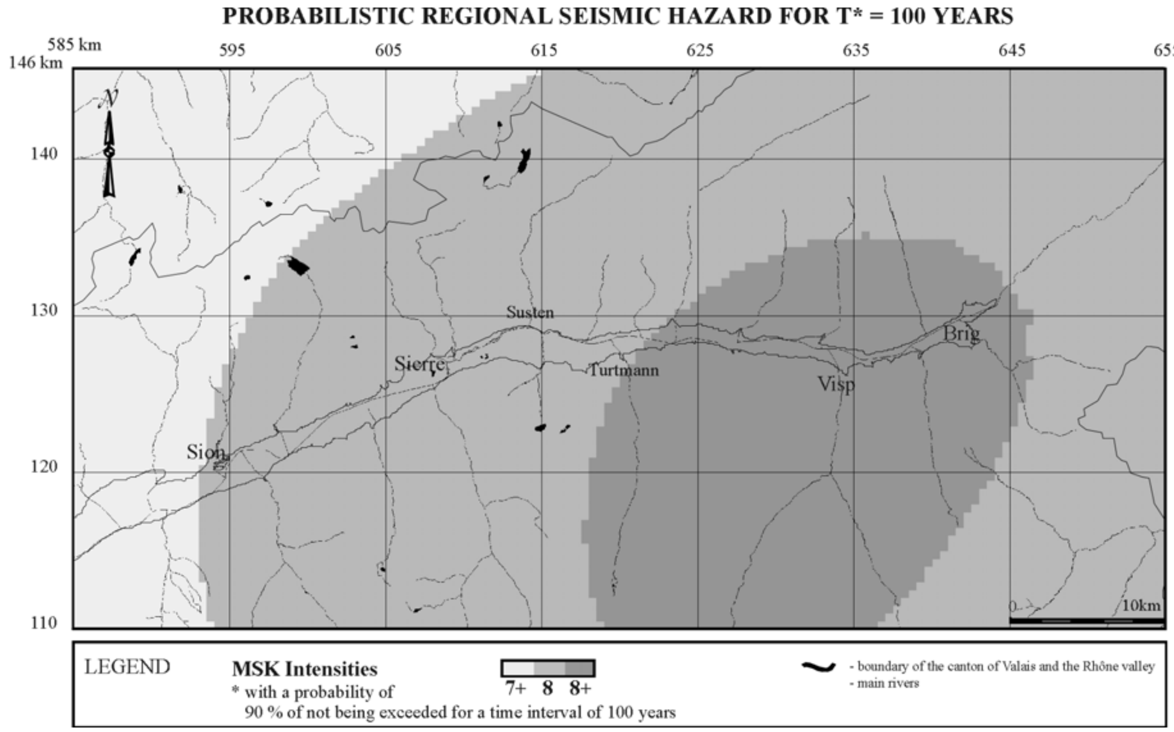

Figure 1.6. Probabilistic regional seismic hazard for the Valais region for a given exposure time window of T=100 years (Wagner et al. 2000).*
Figure 1.6. Aléa sismique probabilistique régional pour le Valais pour une fenêtre d'exposition de T=100 ans (Wagner et al. 2000).*

- Brig earthquake - 9th of December 1755 (Intensity VIII),
- Visp earthquake - 25th of July1855 (Intensity IX),
- Rawil earthquake - 25th of January 1946 (Intensity VIII).

The names of the earthquakes indicate the epicentral area where the events originated.

Their locations are displayed on figure 1.7 as well as those of smaller events. Moreover major faults are also shown.

The figure 1.8 displays a historical document of the isoseismals of the 1855 Visp event (Montandon & Staub, 1946). It is interesting to notice their extension. The isoseismal A (Rossi-Forel intensity X, see Appendix A) is following the Visp and the Matter valleys whereas the isoseismal B (Rossi-Forel intensity IX) extend into to the Rhône valley. Such distribution of intensity values might be considered as a certain indication of alluvial valley amplification phenomenon. However, they also follow the main populated area from which the observations were collected.

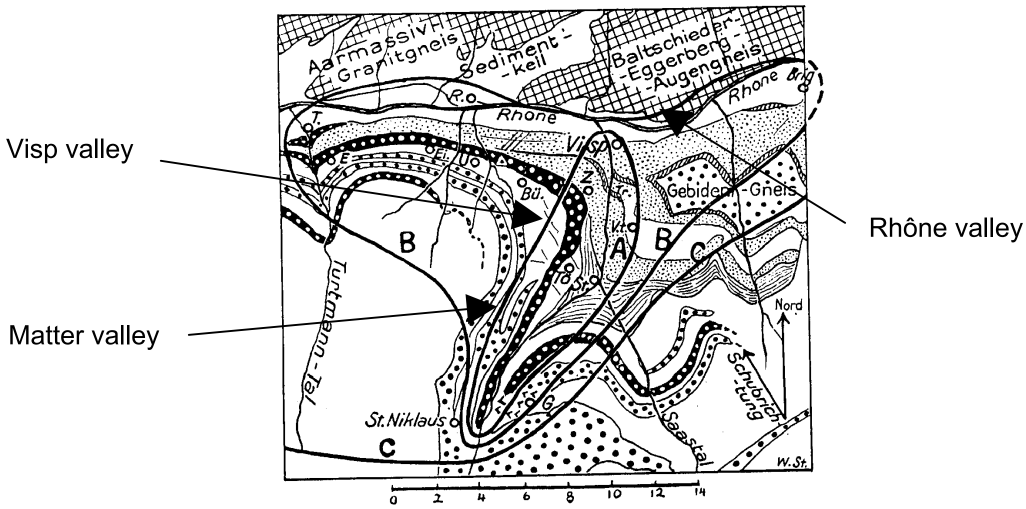

Figure 1.8. Isoseismals of the 1855 Visp event. A=Rossi-Forel intensity X (MSK intensity IX). B=Rossi-Forel intensity IX. C=Rossi-Forel intensity VIII (Montandon & Staub, 1946).
Figure 1.8. Isoséistes du tremblement de terre de Viège en 1855. A=intensité Rossi-Forel X (intensité MSK attribuée IX). B=intensité Rossi-Forel IX. C=intensité Rossi-Forel VIII (Montandon & Staub, 1946).

For the 1946 Rawil event, Wanner & Grütter (1950) noticed that the distribution of the damage was very likely related to the different soils present in the valley. As an example they cited the town of Sierre where most of the damaged buildings were located on a recent alluvial fan or on ancient marshes. They also mention seismic intensity variations up to two units over very short distance.

Damaged buildings were also observed in other towns in the Rhône valley like in Visp and Sion (figure 1.9). In Visp, the modern part (at that time) established on the Rhône alluvium was more affected than the old town, partly built on schists (Montandon, 1946).

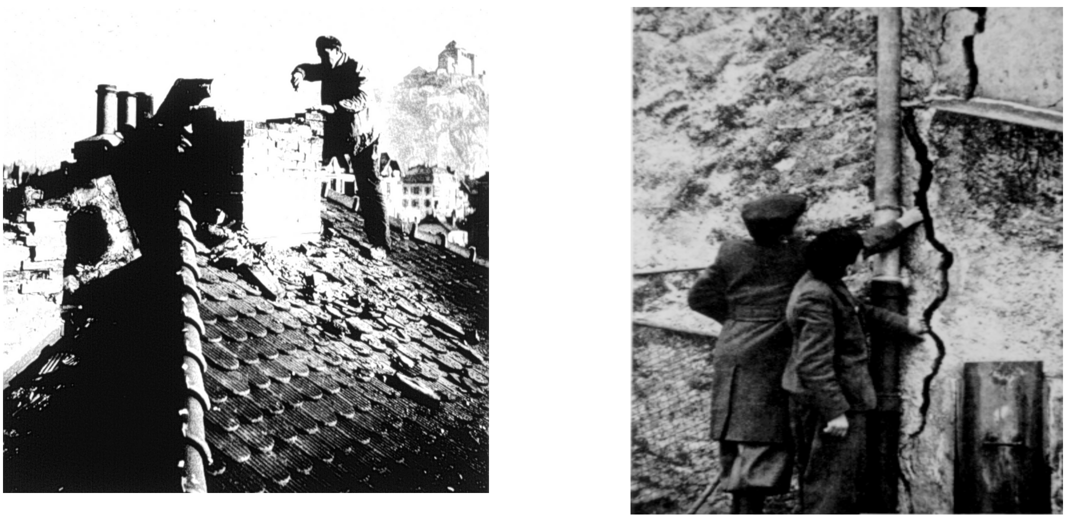

Figure 1.9. Damages on buildings. Left side, a chimney was partially destroyed (Sion area; Mr J.-D. Rouiller's collection). Right side, fissure on a wall (revue L'illustré, 1946).
Figure 1.9. Dommages aux bâtiments. A gauche : une cheminée partiellement détruite (zone de Sion; collection de M. J.-D. Rouiller). A droite : fissuration (revue L'illustré, 1946).

Additional types of local site effects have also been observed (Volger, 1858; Montandon, 1942-43; Mariétan, 1945-46), such as :

- appearance or interruption of water sources,
- opening of cracks,
- water escape structures in the alluvium (if they correspond to sand boils, they are an indication of the occurrence of liquefaction phenomenon),
- rock falls, landslides,
- soil collapse.

The most impressive rock fall was triggered by one of the Rawil aftershocks, on May 30^{th}, 1946. 4-5 mio^3 of rocks fell from "Six des Eaux Froides" (or Rawilhorn - figure 1.10) around 10 km northeast from the city of Sion and filled up the Luchet lake located on the small valley below (figure 1.10). As the initial location of this rock mass was not far from the top of the crest, one of the reasons of this rock fall might be found in the surface topography effect.

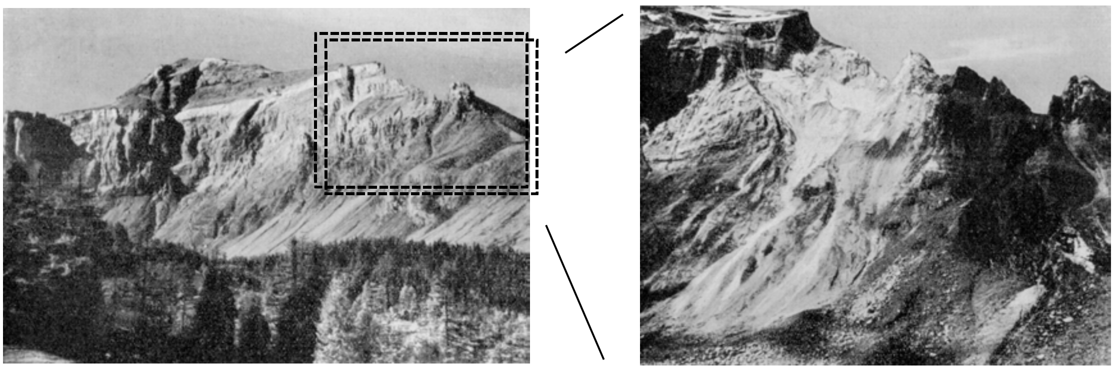

Figure 1.10. Rawilhorn before (left side) and after the rock fall of May 1946 (right side) (Mariétan, 1945-46).
Figure 1.10. Rawilhorn avant (à gauche) et après l'éboulement de mai 1946 (à droite) (Mariétan, 1945-46).

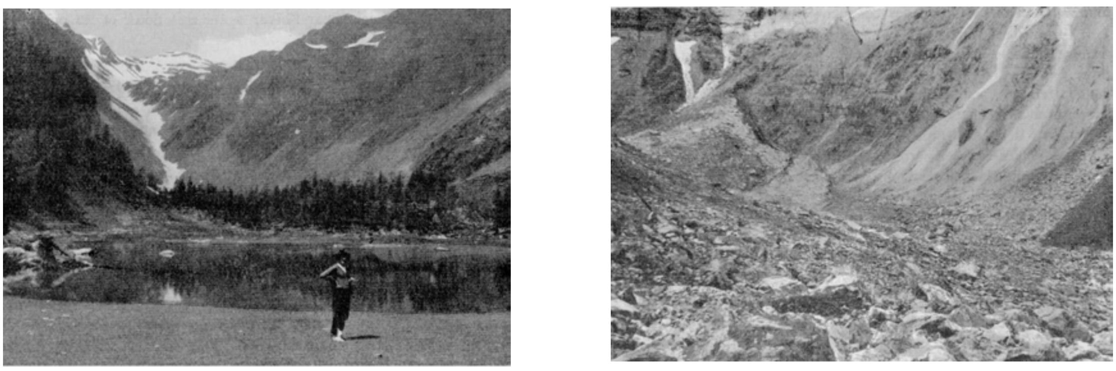

Figure 1.11. Luchet lake before (left side) and after the rock fall (right side) (Mariétan, 1945-46).
Figure 1.11. Le lac du Luchet avant (à gauche) et après l'éboulement (à droite) (Mariétan, 1945-46).

1.3.3.2 Instrumental data

Since 1992, the Swiss Seismological Service is operationg a national strong motion accelerograph network of which one of the tasks is to investigate site effects due to different local geology (SED, 1998). It is entirely composed of three component seismic instruments.

An example of recorded site effects in the Rhône valley is shown in figure 1.12, recording of the Domodossola earthquake (ML=4.4) which occurred in June 1993 around 40 km away with a focal depth of 16km and was registered among others by the stations located in Brig-Glis-Dorf (SBRG) on unconsolidated soils and Stalden-Merjen (STAM) on rock.

Accelerograms and the spectral ratios are displayed in figure 1.12. On the time series, it can be noticed that the Brig-Glis-Dorf station produced records characterized by a longer duration of ground motion and a lower frequency content. The spectral ratio, i.e. the ratio between the station on soil and the station on rock, clearly shows the amplification phenomenon, especially on the horizontal (EW) and the vertical (V) components. The amplification factor goes up to 8. It means that the alluvial cover of the Rhône valley amplified 8 times the initial ground motion at this specific frequency of 3.3 Hz.

1.4 Objective of this research

It could be shown that the Rhône valley has the capability to amplify the ground motion. Therefore, this research has a twofold objective :

- determining elements which control the amplification phenomenon in Alpine valleys,
- identifying parameters for microzonation purpose, i.e. to delineate zones in function of their capability to amplify the ground motion.

1.4.1 Study areas

This research contains two case studies, the city of Sion and the Susten-Brig area (figure 1.13) where different techniques for site effect evaluation and zoning have been used. In the first case, 2D modeling as well as field measurements based on ambient seismic noise is applied, whereas in the latter case, a qualitative rating scheme is developed, applied and compared with the results obtained in earlier seismic intensity anomaly approaches. One reason of applying more than one zonation procedure is the availability of geologic, geotechnical and seismic data, which varies from region to region. It is also due to the fact that currently there are no ideal and unique method to analyze soil amplification.

1.4.2 Application of Geographical information system (GIS)

Microzonation implies that various elements are geographically defined and are interpreted in order to produce new maps. Thus, the Geographical information system is the key tool as it allows to acquire, analyze, process data, handle database, display the result and produce documents defined in a specific coordinate referencing system. GIS is also characterized by its relative rapidity and flexibility.

To be integrated into a GIS, data have to be transformed either in raster images or in vector representation. The raster image is composed of uniform cells having a specific size and arranged in a grid defined by *x* columns and *y* rows. The term "vector" refers to the fact that lines can be described by small segment having magnitude (length) and direction.

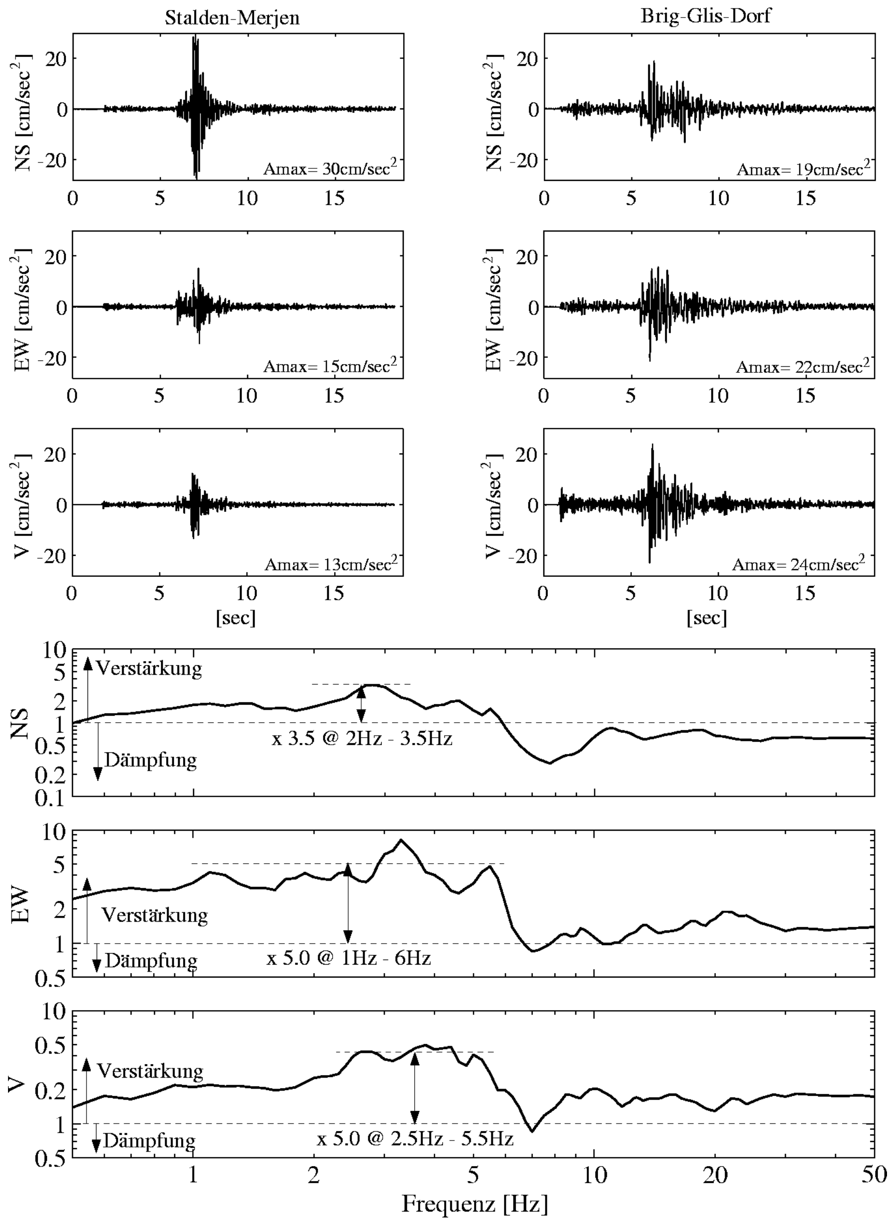

Figure 1.12. Accelerograms (up) of the Domodossola earthquake (June 1994) on the two horizontal components (NS and EW) and the vertical component (V) for the Stalden-Merjen (on rock) and Brig-Glis-Dorf station (on unconsolidated soil) and the spectral ratio for each component (damping = 5%) (Wagner et al. 2000).

Figure 1.12. Accélérogrammes enregistrés lors du tremblement de terre de Domodossola (juin 1994) par les stations de Stalden-Merjen (sur le rocher) et Brig-Glis-Dorf (sur un sol non consolidé) à trois composantes, NS et EW, les horizontales et V, la verticale. En bas figurent le rapport spectral pour chaque composante (amortissement = 5%) (Wagner et al. 2000).

Figure 1.13. Location of the study area. a) the Sion area, b) the Susten-Brig area. The thin black line delimits the canton, the thick black line outlines the Rhône valley with the alluvial fans. The background image is a shaded relief derived from the digital elevation model of the Swiss federal office of Topography (1993).
Figure 1.13. Situation des études de cas. a) la zone de Sion, b) la région de Susten-Brig. La limite du canton est donnée par la fine ligne noire, et le contour de la vallée y inclus les cônes de déjection est souligné d'un trait noir épais. L'image de fond est un relief ombré dérivé du modèle numérique d'altitude de l'Office fédéral de topographie (1993).

Data integrated into a GIS also need to be clearly described in terms of data content, its acquisition, its quality and format. Therefore the concept of metadata, initially developed for handling books (Milstead & Felman, 1999), has been extended into the GIS domain. Metadata are like an identity card giving the necessary information on the data. Several norms have been developed in order to facilitate the sharing of data. They usually contain categories (Dao, 1998) such as identification (e.g. name, purpose), quality of data (e.g. attribute accuracy, positional accuracy), spatial data representation (vector, raster) and spatial reference system, objects and attributes description, distribution of the data, etc.

As the use of GIS is particularly extended in the chapter 5, special attention will be given in this chapter to describe the purpose, the date of acquisition, accuracy of data and its spatial representation, the spatial reference system and the attributes description.

The set of softwares used to acquire and process the data in order to integrated them into a GIS and to produce maps are described in table 1.14.

Software	version	Domain of use	Application area

IDRISI™	v. 2.00 for windows Clark University, 1987-1997	GIS raster	Sion and Susten - Brig
ILWIS™	v. 1.3, ITC, 1992	GIS raster, specifically for interpolation	Sion and Susten - Brig
PC ARCINFO™	v. 3.4.2. Environmental systems Research Institute, 1994	GIS vector, used for digitalization	Sion and Susten - Brig
SURFER™	v. 6.01 Golden software Inc., 1993-1995	Interpolation	Sion
ADOBE PHOTOSHOP™	v. 3.05 Adobe systems Inc., 1989-1996	Images treatment, specifically transparent effect	Sion
CORELDRAW™	v. 6.0 Corel Corporation, 1988-1995	Map presentation	Sion and Susten - Brig

Table 1.14. Description of the main softwares used to process the basic data for microzonation.
Tableau 1.14. Description des principaux logiciels utilisés pour le traitement des données utiles au microzonage.

2 METHODS OF INVESTIGATION ON SOIL RESPONSE

Seismic zonation is a fastidious task
As soil conditions can wear so different masks
cf, 1999

2.1 Introduction

As the built environment is influenced by the ground motion variation, its characterization is a fundamental task to achieve. Depending on the available data and techniques, the method of investigation will differ.

This part introduces the different approaches that have been developed in the past years to analyze the ground motion variation in function of the local site conditions. They can be classified into three main categories :

- analysis of observed seismic intensity anomalies,
- seismic measurements and analysis,
- numerical simulations.

These categories also reflect the level of zonation as defined by the Technical Committee on Earthquake Geotechnical Engineering (TC4) of the International Society of Soil Mechanics and Foundation Engineering (1993). A zonation map is a document on which zones with different levels of ground motion potential are identified. This committee has defined three levels of zonation depending on the data used and the scale of mapping. The grade 1 is attributed to zonation using historical earthquakes and existing information, usually done on a large scale (1:1’000’000 - 1:50’000), grade 2 contains microtremor analysis and simplified geotechnical study (1:100’000 - 1:10’000) and grade 3 is assigned to zonation based on geotechnical investigation and ground response analysis which is applied on a local scale (1:25’000 - 1:5’000). This classification is going from the lowest to the most expensive in terms of cost and time.

2.2 Seismic intensity anomaly approach

When an earthquake occurs, one of the fastest ways to characterize the severity of ground shaking is to attribute at each site an intensity value which is defined by the observation of impacts on humans, buildings and natural environment. Several macroseismic scales have been developed through the world, such as the Rossi-Forel (1883), the MSK (1964) mainly used in Europe, with some improvements (European Macroseismic Scale, Grünthal, 1998), the modified Mercalli, mostly used in USA and the Japan Meteorological Agency Scale (JMA scale), the only one with 7 degrees, applied in Japan.

As differences in intensity have been observed over a short distance, the idea has been to correlate these variations with the surface geology. As a consequence, empirical correlations between the observed macroseismic intensity variation and the local soil conditions have been developed with the purpose to produce seismic zonation maps in areas presenting the same geologic characteristics. Such maps thus permit to delineate areas in function of their different capability to modify the ground motion.

For example, Medvedev (1965) established intensity increments from macroseismic observations in the former USSR for different categories of local geology (such as granites, limestones, sandy ground, etc), choosing the granite as a reference rock. Then using the impedance of the material (defined by the bulk density and the seismic velocity) and the depth to the groundwater level, he obtained the following equation allowing him to derive an intensity increment for various ground (table 2.1).

$$\Delta I = 1.67\ [\log(v_0\rho_0)-\log(v_n\rho_n)] + e^{-0.04h^2}$$

v_0, ρ_0 : propagation of seismic waves (m/s) and density (kg/m^3) in granite
v_n, ρ_n : propagation of seismic waves (m/s) and density (kg/m^3) in investigated ground
h : depth to the ground water table (m)

Ground	**ΔI range in MSK intensity**
Granites	0
Limestones, sandstones, shales	0.2-1.3
Gypsum, marl	0.6-1.4
Coarse-fragmental ground	1.0-1.6
Sandy ground	1.2-1.8
Clayey ground	1.2-2.1
Fill	2.3-3.0
Moist ground (gravel, sand, clay)	1.7-2.8
Moist fill and soil ground (marsh)	3.3-3.9

Table 2.1. MSK seismic intensity increment for various grounds (Medvedev, 1965)
Tableau 2.1. Augmentation de l'intensité sismique MSK en fonction de différentes lithologies (Medvedev, 1965).

It can be noticed that the higher ΔI is attributed to categories representing loose water filled deposits (e.g. moist ground, moist fill).

In California, USA, Borcherdt & Gibbs (1976) derived intensity increments for various geological units from the 1906 earthquake intensity data determined on the 1906 San Francisco intensity scale[2] (0 to 4) using the following procedure :

- definition of an intensity attenuation law in function of distance from the zone of surface faulting for sites on the Franciscan formation (Greenstone or sandstone over shale), based on the macroseismic observations of the 1906 San Francisco earthquake,
- definition of intensity increments based on the difference between observed intensity and predicted intensity obtained with the attenuation law at a specific site, therefore obtaining intensity increments for various geological units with respect to the Franciscan formation.

Then, they compared the calculated intensity increments with the average spectral horizontal amplification (ASHA) obtained from the nuclear explosions normalized by the average value of

[2] Grades of the 1906 San Francisco intensity scale go from "very violent" to "weak" which correspond to letters A to E and numbers 4 to 0 (Borcherdt & Gibbs, 1976).

Franciscan formation. The mean ASHA derives from all the spectral amplification values obtained for each geologic unit on both horizontal components. These values and the corresponding mean intensity increments are given in table 2.2 and it can be seen that both parameters exhibit the same variation in function of the geological units : less consolidated grounds give higher values.

Integrating these intensity increments, a predicted maximum earthquake intensity map was produced for the San Francisco area (Borcherdt & Gibbs, 1976).

Geological unit	**mean value of AHSA**	**mean ∆I in San Francisco intensity**
Granite	0.63	-0.29
Greenstone or sandstone over shale	1.00	0.19
Indurated sandstone and siltstone	1.42	0.64
Stiff clay and conglomerate	1.70	0.82
Alluvium	2.44	1.34
Bay mud	7.08	2.43

Table 2.2. Mean value of average horizontal spectral amplification (AHSA) and mean intensity increments with respect to Franciscan formation for different geological units. Summarized from Borcherdt & Gibbs (1976).
Tableau 2.2. Valeur moyenne de l'amplification spectrale horizontale moyenne et valeurs de variations moyennes de l'intensité en fonction de la formation "Franciscan" pour différentes unités géologiques. Résumé de Borcherdt et Gibbs (1976).

In Switzerland, in the framework of a pilot project in the canton of Obwald, the MSK intensity increment for various lithological units was obtained with the following procedure (Rüttener, 1995, Schindler et al. 1996) :

- an intensity value was calculated following the Sponheuer attenuation law (1960) for each site where macroseismic observation was available. The Sponheuer law is of the form :

$$I_s = I_0 - 3\log\left(\frac{\sqrt{r^2+h^2}}{h}\right) - \alpha\left(\sqrt{r^2+h^2} - h\right)$$

with I_s *= intensity at a particular site*
I_0 *= epicentral intensity*
r *= distance between the epicenter and the site*
h *= hypocentral depth*
α *= attenuation coefficient varying in function of the tectonic environment*

- each site was classified depending on its geotechnical characteristics, according to the simplified geotechnical map of Switzerland in the scale 1:200'000 (Rösli, 1990),
- an intensity variation (e.g. figure 2.3) was obtained for each unit based on all differences between the observed macroseismic intensity and the calculated one available for the unit. It is assumed that the intensity distribution follows a normal distribution.

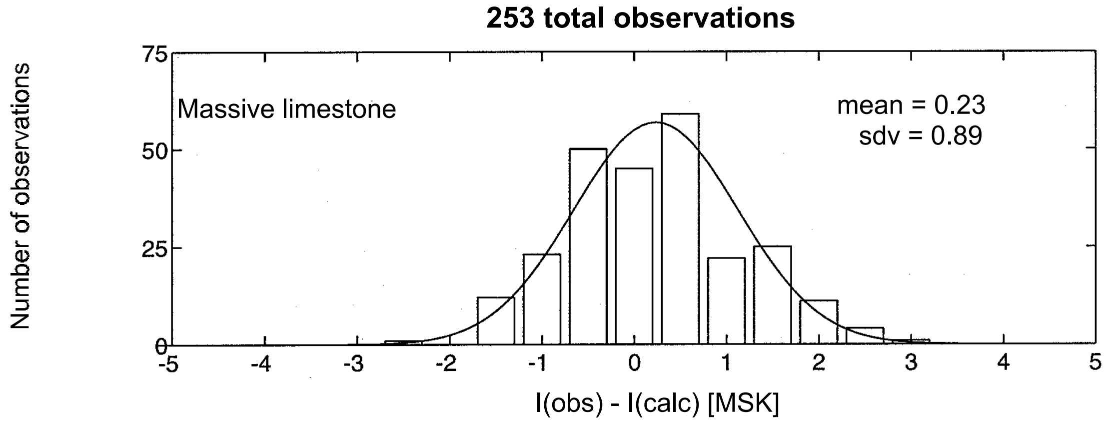

Figure 2.3. Differences between the observed and calculcated seismic intensity MSK for the geotechnical unit of massive limestone. Modified from Schindler et al. 1996.
Figure 2.3. Différences entre l'intensité MSK observée et calculée pour l'unité géotechnique "Calcaires massifs". Modifié de Schindler et al. 1996.

The intensity increment for each geotechnical unit is given in table 2.4. It can be noticed that the depth to the water table has been considered in the case of the unconsolidated sediments. Based on these increment values, a MSK seismic intensity correction map was produced for the canton of Obwald. The result showed that the higher seismic intensity increments (up to 1.5 MSK unit) were observed inside the valley characterized by unconsolidated deposit and a shallow water table (Schindler et al. 1996).

Geotechnical unit based on the Swiss geotechnical map at a scale 1:200'000	**mean ΔI in MSK intensity**
marly limestones	0.4
massive limestones	0.2
dolomite and gypsum	0
marly schists with intercalations of sandstone	0.4
various conglomerates	0.2
unconsolidated sediments and depth to groundwater level	
0-9m	1.5
9-30m	0.5
> 30 m	0

Table 2.4. MSK intensity increment for geotechnical units in Switzerland (Rüttener, 1995; Schindler et al. 1996).
Tableau 2.4. Augmentation de l'intensité sismique MSK pour les unités géotechniques en Suisse (Rüttener, 1995; Schindler et al. 1996).

Such maps are an useful tool as they delineate the areas in function of their potential to amplify the seismic hazard. It therefore allows to raise awareness on the influence of the local conditions on the seismic response. However for earthquake engineers the intensity value is not a parameter which they can use straightforward. Indeed this parameter does not give any indication related to the infrastructure-soil interaction. Infrastructure (buildings, lifelines, bridges, etc.) carries a natural resonant frequency. If this frequency is close or equal to the resonant frequency of the soil, the building will enter into resonance, thus increasing the potentiality of damages. Therefore the identification of the predominant frequency of the soil and the quantification of the related amplification are of primary interest. This goal can only be achieved by seismic analysis or numerical simulation.

2.3 Seismic measurements and analysis

Seismic measurements deal with several categories of ground motions, such as ambient seismic noise, weak or strong ground motions.

Ambient seismic noise is usually called microseisms for motions having periods larger than > 2 sec and are induced for example by ocean waves along the coast or change of atmospheric pressure variations over the ocean (Dravinski et al., 1996). Microtremors refer to short period ambient seismic noise (< 2 sec) and is produced by natural local forces (wind, storm, etc) and artificial surface sources such as industries, automobiles, trains (Nakamura, 1989).

On the opposite, weak and strong ground motions refer to earthquake data, weak referring to event with magnitude between 1 and 5 whereas strong ground motion designates seismic event with magnitude > 5.

Whatever the source, ground motion can be characterized by amplitude and frequency content and in case of an earthquake by duration. Therefore methodologies have been developed to extract this information. In this part, we will only focus on the standard spectral ratio and the H/V ratio techniques which are applied for all types of ground motion (noise to strong motion). The choice of ground motion type depends on the available data as some regions are located in areas of high seismicity whereas others are situated in moderate to low seismic area.

2.3.1 Standard spectral ratio (SSR)

The standard spectral ratio technique consists in comparing records at nearby sites in the frequency domain, one on soil, the second on rock. It is assumed that the site on rock is free of site effects, i.e. showing no amplification, at least in the frequency range of interest. Spectral ratio is the ratio between the Fourier spectra of the signal recorded on soil and the signal recorded on rock. This ratio, also called empirical transfer function or reference site technique, has been used by Borcherdt (1970) for the first time.

In the time domain, the content of a seismogram can be described as follows (Borcherdt, 1970) :

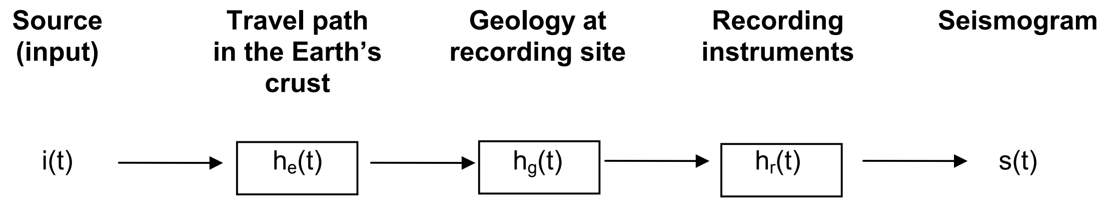

In the frequency domain, it can be considered as the result of the multiplication of the different components, i.e. (Borcherdt, 1970) :

$$S(f) = I(f)H_e(f)H_g(f)H_r(f)$$

Therefore Borcherdt (1970) considers that the spectral ratio between a record on sediments and rocks will allow the elimination of source effects, travel path and instruments recording effects. As a result only the response characteristic of the local geology is obtained. The spectral ratio can thus be described as follows :

$$\frac{S_s(f)}{S_b\ (f)} = \frac{H_{gs}\ (f)}{H_{gb}\ (f)}$$

with $S_s(f)$ a record on sediments and $S_b(f)$, a record on rock
with H_{gs} (f) = geology of soil and H_{bg} (f) = geology of rock.

This hypothesis is valid if *I(f), $H_e(f)$ and $H_r(f)$* are identical in both cases. The path effect *$H_e(f)$* is considered to be site independent when the distance to the reference site is small compared to the source-to-site distance (Bard, 1994).

However the application of the spectral ratio technique is limited by (Lermo & Chávez-García, 1993; Theodulidis et al. 1996) :

- the difficulty to find bedrock sites near the unconsolidated ones,
- the quality of the outcrops rock sites which might be weathered. In this case, the reference site response is also modified,
- the level of background noise which can be different at both sites, so that the records are not comparable.

Other techniques have been developed in order to overcome these limitations. They are called non-reference site techniques among which is the H/V ratio technique, the most common.

2.3.2 H/V ratio technique

The H/V ratio technique calculates site effects in terms of predominant frequency and amplification factor for surface layers by only using the ratio between the horizontal components and the vertical component at the same site. This technique has been applied on microtremors by Nakamura (1989) at the end of the eighties in urban areas in Japan. His assumption is that the H/V ratio corresponds to the transfer function of surface layers submitted to horizontal motions.

Nakamura (1989) based his work on the hypothesis that a microtremor is composed of body waves and Rayleigh waves, the latter being mainly induced by artificial sources (train, traffic, etc.) located near the point of measurement. These surface waves are considered as disturbance and which have be removed. To achieve this goal, Nakamura (1989) postulated several assumptions :

1. Rayleigh waves affect only the top of the surface layer and not the base,
2. the effect of Rayleigh waves is mainly visible on the vertical motion, therefore the ratio

$$E_s = {S_{V_S}}/{S_{V_B}}$$

with S_{VS} *and* S_{VB} corresponding to the Fourier amplitude spectra of the vertical component of motion at the surface ($_S$) and at the base ($_B$) of the surface layer, represents the effect of the Rayleigh wave. This ratio is 1 if there is no effect and becomes larger with an increase of the presence of Rayleigh wave.

3. the effect of Rayleigh wave is equal on surface for both vertical and horizontal motions.

Based on these assumptions, Nakamura proposed a modified transfer function, corrected for Rayleigh waves. Considering the classical definition of the transfer function :

$$S_T = S_{H_S} / S_{H_B}$$

with S_{HS} and S_{HB} being the Fourier amplitude spectra of the horizontal component of motion at the surface ($_S$) and at the base ($_B$) of the soil layer, respectively, the modified transfer function is defined as follows :

$$S_M = S_T / E_S = \left(\frac{S_{H_S}}{S_{H_B}}\right) \Big/ \left(\frac{S_{V_S}}{S_{V_B}}\right) = \left(\frac{S_{H_S}}{S_{V_S}}\right) \Big/ \left(\frac{S_{H_B}}{S_{V_B}}\right)$$

Nakamura still simplified this equation, assuming, on the basis of results obtained in three urban sites in Japan, that for a frequency range between 0.1-20 Hz, the ratio

$$S_{H_B} / S_{V_B} \cong 1 .$$

Therefore the modified transfer function becomes :

$$S_M = S_{H_S} / S_{V_S}$$

Consequently the transfer function of a site can be obtained by a unique measurement on surface with a 3 component sensor.

From a theoretical point of view, some reserve has been mentioned regarding at least for two of the Nakamura's assumptions. The first concerns the role of the S_T/E_S ratio which is dependent on the nature of the microtremors. If the microtremor is composed of body and surface waves, it is usually considered that these waves are summed and not convoluted. Therefore the ratio does not compensate really for Rayleigh waves (Kudo, 1995; Lachet, 1996; Le Brun, 1998).

The suggestion has been made that microtremors may mainly consist of Rayleigh waves as the peak of the H/V ratio corresponds to the fundamental mode of the Rayleigh waves (Lermo & Chávez-García, 1994; Lachet & Bard, 1994). However if the peak of the H/V ratio corresponds to the horizontal polarization curve, the amplitude would theoretically be infinite which has not been observed (Duval et al. 1996). Moreover the ratio S_T/E_S will in this case not remove the effect of the Rayleigh waves but rather the source effects (Lermo & Chávez-García, 1994).

Second, the assumption that $H_B/V_B \cong 1$ is function of the ellipticity of the Rayleigh waves. Lermo & Chávez-García (1994) compared the 1D vertical S-wave transfer function of a site in Mexico with the ellipticity for the fundamental mode of Rayleigh waves. They showed that at the interface sediments/half-space the ellipticity for the fundamental mode of the Rayleigh waves was near one at the fundamental resonant frequency of the structure which is in agreement with the assumption. However this ellipticity depends on the impedance contrast between the sedimentary layer and the bedrock, the Poisson's ratio of the sediments, the mode of Rayleigh waves and the frequency (Kudo, 1995).

Despite these limitations, this technique has been applied successfully in various contexts, if the following points are kept in mind.

First of all, considering the use of microtremors to identify the predominant frequency and its associated amplification factor, studies in Mexico city and San Francisco have compared the H/V ratio on microtremors with standard spectral ratio on the S-wave part of weak and strong motions and shown that the H/V ratio permits to identify the fundamental resonant frequency (Lermo & Chávez-García,1994; Seekins et al. 1996). In case of deep sedimentary valleys, the remaining question is whether the surface sources of microtremors are able to excite the very low resonant frequency (< 0.5 Hz) expected in such structure (Lachet & Bard, 1994). A study made in the city of Grenoble, located at the junction of three alpine valleys (Grésivaudan, Isère and Drac valleys) and characterized by a deep sedimentary deposit (>400 m), compared the H/V ratio on microtremors with the standard spectral ratio on weak motions. Results showed that the H/V ratio on microtremors is able to reliably predict the fundamental resonant frequency of the deep alpine valley.

Regarding the amplification level studies differ on whether the H/V ratio technique can estimate the amplification level. The Nakamura's assumption is that the maximum spectral amplitude of the H/V ratio can give an estimate of the seismic motion amplification resulting from the resonance of surface layers. In some cases, comparisons between standard spectral ratio on S-wave weak or strong motion and the H/V ratio on microtremor display similarity on amplification level (Lermo & Chávez-García,1994; Seekins et al. 1996), whereas in other cases, the comparison failed, especially in context of alpine valleys (Malagnini et al. 1996; Le Brun, 1997).

The H/V ratio technique has also been applied on weak and strong motion records. Studies in Mexico (Lermo & Chávez-García, 1993) and in Greece (Theodulidis & Bard, 1995) have compared results obtained from this technique and the standard spectral ratio. The conclusion is that there is a good agreement between the two methods to determine the first resonant frequency and the amplitude level with less dispersion for the H/V ratio's one.

Another field of application of this ratio is to determine the suitability of site located on an outcropping rock to be used as a reference in the standard spectral ratio. Indeed one of the assumption of the H/V ratio technique is that the ratio on the interface sediment-basement H_B/V_B is more or less equal to 1. As one assumed that the outcropping rock is representative of the basement, the H/V ratio of microtremors recorded on an outcropping rock chosen as a reference site should therefore be more or less equal to 1 if this site is free from site effects or not weathered. Some studies (Lermo & Chávez-García, 1994; Field & Jacob, 1995) have shown that measurement of microtremors on reference sites gives a relatively flat H/V ratio over the frequency range of interest. On the opposite a reference station installed on the top of a hill in Oaxaca (Mexico) showed an amplification phenomenon at specific frequency. Modeling confirmed that this site was subject to topographical effect (Lermo & Chávez-García, 1993).

In summary the H/V ratio on microtremors as well as on weak and strong ground motion gives a reliable indication on the fundamental resonant frequency of the sedimentary structure, but not on the higher-resonant frequencies (Lachet & Bard, 1994; Lermo & Chávez-García, 1993; Dravinski et al. 1996). Regarding the amplification level, there is still some debates on considering the value given by the H/V ratio as a reliable prognostic. In the best case, this value could be considered as the low boundary of the linear amplification at a site (Wenk et al. 1998).

2.3.3 Seismic measurements and microzonation

The use of weak or strong ground motion for microzonation purpose not only requires a dense array of recorders on the chosen study area but also a high seismic activity which allows to obtain a representative dataset. California is one of those active seismic areas and a first generation of map based on ground motions has been established for the Los Angeles area (Hartzell et al. 1996). Amplification maps have been drawn for three different frequency bands. Zones with higher amplification factors (scaled up to 5) are coincident with the deeper part of the basin and also with the presence of a shallow water-level table (Hartzell et al. 1996). In zones of low to moderate seismic activity, the H/V ratio on microtremors is an useful alternative. This latter method does not request a reference site and is using microtremors, thus data acquisition is relatively simple and low-cost. Therefore measurements can be rapidly done over a wide area. Usually the microzonation is based on the predominant frequency. Examples are given by Duval et al. (1996) for the Nice region in France and Le Brun (1997) in an French alpine valley. They found that the predominant frequency is dependent on the thickness variation, lower the value, thicker is the deposit.

2.4 Numerical simulation

Numerical simulation has been developed in order to identify the controlling parameters of wave propagation at the different levels, source mechanism, propagation and site effect. In the latter case, the numerical simulation of the seismic response can be dedicated to several purposes, such as :

- theoretical studies to point out wave propagation phenomena,
- parameter sensitivity studies for idealized models of surface topography, subsurface topography (valley, basins),
- comparison with recorded seismic data in order to analyze the controlling parameter on the seismic response at a specific site,
- evaluation of the potential seismic response in absence of seismic data, but in case of available geologic data.

2.4.1 1D / 2D / 3D approaches

The 1D approach is based on the assumption that the ground is composed of a superposition of homogeneous horizontal layers of infinite lateral extent. Therefore the seismic response is calculated only considering the vertical column of soil below the observation point. The plane wave propagation through such vertically heterogeneous structure can be resolved either using the propagation matrix (Thomson, 1950; Haskell, 1953) or the Kennett (1983) transmission-reflection matrix (see chapter 4). Such calculations are carried out in the frequency domain.

The 1D approach can be considered suitable for area characterized by mainly horizontal layers over a long area.

In a valley- or basin-region, field observations after earthquake often show that damages are concentrated in some specific places leading to the conclusion that not only vertical but also lateral heterogeneities are responsible for amplification. Based on this hypothesis, the 2D numerical simulation method has been developed in order to take into account complex subsurface geometry. It starts from an incident horizontally shear wave incident on a simple geometry (semi-elliptical or triangular shape) for theoretical studies. Then with the development of computer capacities and mathematical approaches, models get more complex.

Therefore depending on the purposes of the two dimensional numerical simulation and the chosen medium configuration (irregular interfaces, heterogeneous medium) different numerical approaches have been developed to describe the wave propagation through the structure and the structure itself. The main used methodologies are shortly described in table 2.5 :

Some 2D comparative studies in sedimentary valleys (e.g. Jongmans & Campillo, 1993) showed discrepancies between observed and simulated amplifications. They were associated with the limitation of the 2D approach. Consideration of 3D propagation problem, i.e. taking into account the azimuth of the incoming wave, has therefore been given weight (e.g. Pedersen et al. 1994, 1995).

However closed basins require a third geometrical dimension, therefore dealing with a real 3D structure. Pure 3D model methods have also been developed (Olsen et al. 1995; Riepl & Bard,1998; Cotton et al.1998).

Including two or three dimensions has a direct influence on the amplification level and on the frequency value at which it occurs. This can be illustrated by the figure 2.6 which displays the comparison between the 1D, 2D and 3D response for an elliptic basin, an idealized case. It can be seen that the fundamental frequency shifts toward higher frequencies and the amplification increases from 1D to 3D.

Therefore the choice of a 1D, 2D or 3D numerical approach depends on the specific local geological conditions. In some cases, an 1D approach would be sufficient to investigate the site effects whereas in other cases a 3D approach would be necessary. In this research, the part of the Rhône valley under study is a rather elongated structure. Its length is large enough to consider that the energy of seismic waves will be sufficiently attenuated in this direction to not influence the seismic motion in the study area. Therefore the seismic response of this structure can be investigated with the 2D approach, assuming a structure of infinite extension but of closed lateral extent.

Numerical approach	Domain of utilization	Limitations
Geometrical method (e.g. Jongmans, 1991)	For simple geometrical configuration. The structure is schematized in layer elements (dipping or flat). In each layer the wave field is decomposed into ray families. The displacement is obtained by the superposition of the wave field obtained for each layer	• no limitation towards high frequencies
Discrete wavenumber method (Aki-Larner method) (e.g. Bard et al. 1992)	For irregular surface or subsurface topographies, having one or several layers. The method is based on the representation of the diffracted wave field as a superposition of plane waves and the total displacement is obtained by integration on every possible horizontal wavenumber	• slopes should not be more than 40°. • Small incidence angles are requested (< 30°).
Indirect Boundary Element Method (e.g. Sanchez et al. 1993; Pedersen, 1994)	For irregular surface or subsurface topographies, with one or several layers This method is based on the integral equation representation of elastic wave fields. For computation, the structure as well as the wave field are discretized into segments.	• high computation time and large memory would be requested if the medium becomes complex as a great number of segments would be requested to describe the interfaces
Finite differences (e.g. Riepl, 1997)	For complex geometry and rheology. This approach is based on the transformation of the wave equation with partial derivative into an equation with finite differences.	• High computation time needed to minimize the numerical dispersion as it is based on a fine discretization scheme in time and space
Finite elements (e.g. Riepl, 1997)	For complex geometry and rheology. In this case, the structure is discretized in small elements. All elements are relied with a finite number of nodes.	• High computation time requested for calculation in the high frequency domain as the mesh elements have to be much more smaller than the wavelength

Table 2.5. Description of main numerical approaches for 2D or 3D calculation.
Tableau 2.5. Description des principales approches numériques employées dans les calculs 2D ou 3D.

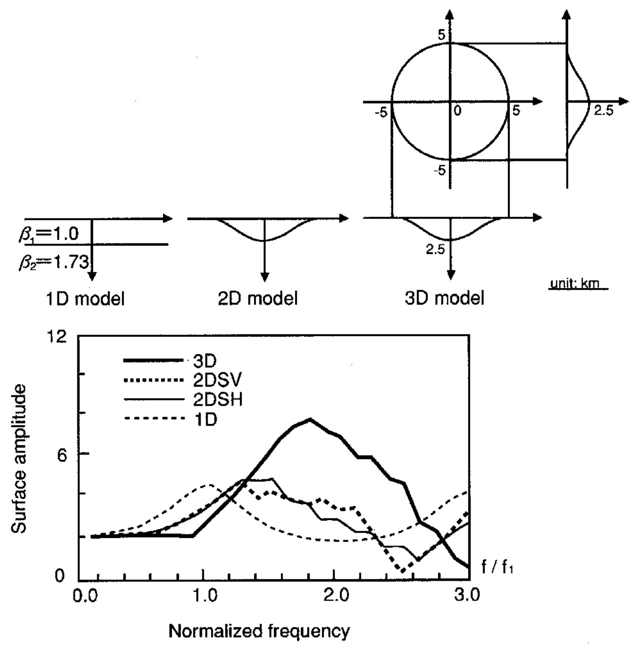

Figure 2.6. Comparison of spectral responses of 1D, 2D and 3D models for an elliptic basin (extract from TC4, 1993).
Figure 2.6. Comparaison des réponses spectrales entre des modèles 1D, 2D et 3D pour un bassin de forme elliptique (tiré de TC4, 1993).

3 ANALYSIS OF THE INFLUENCE OF SUBSURFACE GEOMETRY ON SOIL AMPLIFICATION USING 2D MODELING

Ce qui est simple est toujours faux
Ce qui ne l'est pas est inutilisable
Paul Valéry

3.1 Introduction

Numerous theoretical studies have shown the role of the finite lateral extent of a sedimentary deposit on seismic signal, as it can extend the duration, increase the amplification level and modify the frequency content of the incident waves. Specially in mountain environments field observations (King & Tucker, 1984; Yegian et al. 1994) showed that 1D modeling is insufficient to explain all the observed amplification.

In this part on the analysis of the influence of subsurface geometry on the soil amplification, focus is put on two transverse profiles (figure 3.10), located in the west and east of Sion. They will be submitted to a vertical incident shear wave, type SH (horizontally polarized shear wave). This type of shear wave is usually considered to be the most important source of damages on buildings. 1D and 2D modeling will be carried out in parallel for comparison.

Both modeling approaches are based on several assumptions regarding the medium (elastic, visco-elastic) and the wave propagation (plane waves). 1D modeling uses a transmission-reflection matrix and the 2D model, developed by Pedersen et al. (1995) is based on the Indirect Boundary Element Method (IBEM) which allows to include various subsurface geometries. These programs do not require a definition of the seismic source in terms of fault mechanisms and location nor a specific propagation path as some other programs do (e.g. Fäh et al. 1994). The seismic wave is generated at the interface of the sediment layer and the bedrock and propagated throughout the sedimentary structure.

3.2 Modeling

3.2.1 Unidimensional approach

In this approach, local geological conditions are approximated by a system of plane, horizontal, isotropic and homogeneous layers of infinite lateral extension overlaying the substratum, defined as a half space. The seismic response of this system subjected to a plane wave can be resolved using Kennett's work (1983) on transmission-reflection matrix in stratified media.

The wave propagation is controlled by a reflection-transmission matrix defined at layers interface in function of their physical characteristics (velocities (V_p, V_s), densities (ρ), quality factor (Q_p and Q_s), thickness (h)) and the incidence angle of the wave (γ) as illustrated in figure 3.1. The Q factor is a measurement of the seismic attenuation due to rocks and soils. Depending on the incident wave (P or S), it also accounts for the converted waves.

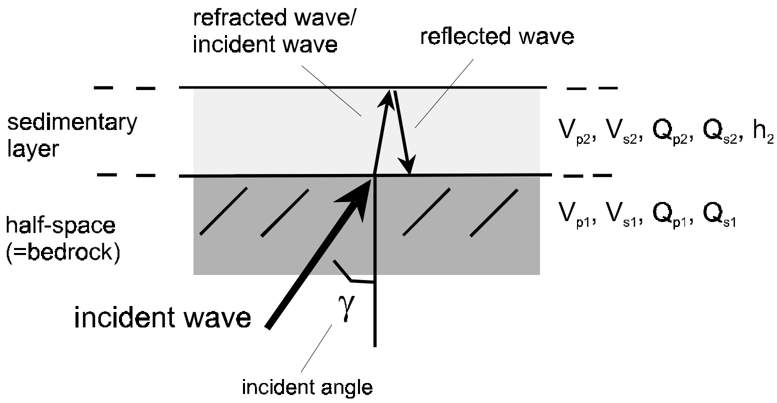

Figure 3.1. Illustration of the 1D model, with V_{p1}, V_{s1}, Q_{p1}, Q_{s1} >> V_{p2}, V_{s2}, Q_{p2}, Q_{s2}.
Figure 3.1. Illustration du modèle 1D, avec V_{p1}, V_{s1}, Q_{p1}, Q_{s1} >> V_{p2}, V_{s2}, Q_{p2}, Q_{s2}.

The medium is following a linear, homogeneous, isotropic, visco-elastic behavior law.

The boundary conditions to resolve are :

- zero-traction at the surface,
- continuity of displacement and traction across the interface between each layer

The ground motion is calculated on one point at the surface and results from the interference between the incident wave and the reflected one. The response is given in terms of amplitude of the displacement versus the frequency.

3.2.2 Bidimensional approach

In this case, the behavior of the local soil conditions is simulated through a transverse section of infinite extension (figure 3.2).

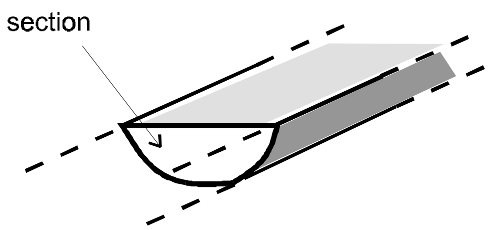

Figure 3.2. Illustration of the transverse of infinite extension used to define the local soil conditions in the 2D approach.
Figure. 3.2. Illustration de la section transversale d'extension infinie utilisée pour définir les conditions de sol locale dans le cas d'une approche 2D.

The program used in this work has been developed by Pedersen et al. (1995). It allows to calculate the seismic response of a two-dimensional alluvial valley submitted to a specific incident plane wave (P, SH, SV and Rayleigh).

The valley is approximated by an “inclusion” embedded into a half space with an irregular interface, which represents the bedrock (figure 3.3). Both elements are following a linear elastic behavior law and are also considered as isotropic and homogeneous, which reduces the number of the needed elastic constants.

The seismic response is computed for different locations regularly spaced along the profile, in the frequency domain. The response is given in terms of displacement amplitude, calculated on the three components, two horizontal and one vertical.

The wave-fields are calculated by the indirect boundary element method based on an integral representation of these fields. It allows to consider the displacements and traction in terms of surface forces (Pedersen, 1994).

The total motion u_i at the surface is assumed to result from the superposition of the diffracted waves and the free-field, i.e. the field in absence of the irregularity (Pedersen, 1994) :

$$u_i = u_i^{(o)} + u_i^{(d)}$$

with $u_i^{(o)}$ representing the response of the half space in absence of the irregularity, i.e. the superposition of the incident and reflected wave-fields

with $u_i^{(d)}$ representing the response of the inclusion, i.e. the refracted and diffracted wave-fields

The basic formulas to describe the displacement (u) and traction (t) for a wavefield in an elastic medium, neglecting body forces are (Pedersen, 1994) :

$$u_i(x) = \int_s \psi_j(\varsigma) G_{ij}(x,\varsigma) dS\varsigma$$

$$t_i(x) = c\psi_i(x) + \int_s \psi_j(\varsigma) T_{ij}(x,\varsigma) dS_\varsigma$$

G_{ij}, T_{ij} are Green functions. These mathematical functions represent the displacement in space, i.e. the displacement (or traction) in the direction i at point x, due to the application of a unit force applied in the direction j at point ζ. ψ_j is a force density in the direction j and $\psi_j(\zeta)dS_\zeta$ is a force distribution at the boundary.

The numerical implementation of the integrals requires a discretization scheme. The structure as well as the wavelength have to be discretized. This operation can be done if the following conditions are respected (Pedersen, 1994) :

- the length of each segment of the structure has to be smaller than the wavelength,
- the number of the segments has to be sufficient to correctly represent the structure,
- the surface has to be truncated far enough to avoid edge effects.

The main difficulty consists in the computation of the displacement induced by the diffracted waves. The method developed by Sánchez-Sesma et al. (1993) and Pedersen et al. (1995) permits to create the diffracted wave-field from secondary sources localized on the irregular interface between the sedimentary filling and the half space. In order to facilitate the computation of the different wave-fields, the structure is divided in two parts. On one hand, one consider the half-space E delineated by an irregular interface δ and on the other hand the sedimentary filling defined as an inclusion R (figure 3.3). The two geometries are joined by their common border δ in such a way that displacement and traction induced by the seismic motion are continuous in between (Pedersen, 1994).

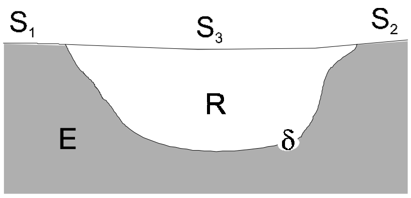

Figure 3.3. Model of an alluvial valley following the IBEM approach. S1, S2, S3 being the free surfaces, S1 and S2 being the lateral flat parts, E is the half-space, R the inclusion and δ the irregular interface between R and E.
Figure 3.3. Modèle de vallée alluviale suivant l'approche IBEM. S1, S2, S3 représentent les surfaces libres, avec S1 et S2 étant les parties latérales planes. E représente le demi-espace et R l'inclusion. δ est l'interface irrégulier entre R et E.

The boundary conditions are (Pedersen, 1994) :

- zero-traction at the surface,
- continuity of displacement and traction across the interface between the inclusion and the half space,
- zero field at infinity.

The resulting motion "observed" on surface depends not only from the interference of incoming waves with refracted, reflected but also with the ones diffracted by the irregular geometry of the subsurface (Sánchez-Sesma et al. 1993).

The number of sources for the diffracted waves relies on the number of discretized segments used for the structure which depends itself on the wavelength, the number of segments per wavelength and the size of the structure. Consequently the number of sources varies with the frequency.

3.2.3 Main required parameters for 2D modeling

The main required parameters needed in the 2D modeling approach to process the numerical simulation of the seismic response of a geological structure are described and compared with the 1D case in table 3.4.

1D model (J.-C. Gariel, 1990)	**2D model** (Pedersen et al. 1995)
• number of the horizontal layers • type of plane wave (P or S wave) • incidence angle of the upcoming wave • characteristics of the layers ⇒ thickness of the layer ⇒ seismic velocities (P and S) ⇒ bulk density ⇒ Quality factor (Qp and Qs) • maximum frequency value • number of samples in frequency ⇒ indication of the sampling rate	• geometry of the two-dimensional section • type of plane wave (SH, SV, P, Rayleigh) • incident angle of the upcoming wave • azimuth of the incident wave • mean characteristics of the layers ⇒ seismic velocities (P and S) ⇒ bulk density ⇒ Quality factor Q • total discretization length • segment per wavelength • frequency range • sampling rate in frequency • length of the signal in time • number of samples in time • number of stations

Table 3.4. Description of the main required parameters for modeling.
Tableau 3.4. Description des principaux paramètres nécessaires à la modélisation.

3.2.3.1 Incidence angle and azimuth

The geometrical parameters are displayed in figure 3.5. The angle of incidence can vary between 0 and 90°, with 0° being defined as the vertical incidence. The azimuth is defined between 0 and 180°. In this study 0° corresponds to the northwest side and 180° the southeast side.

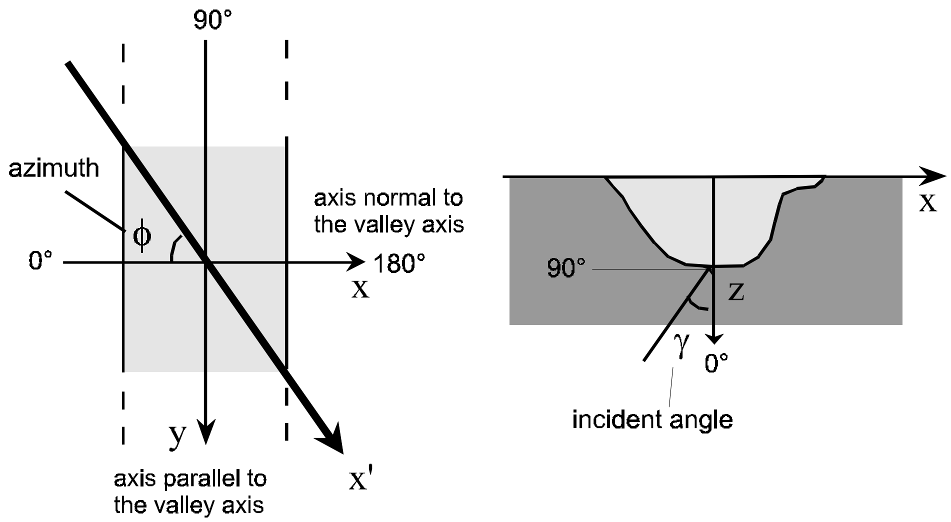

Figure 3.5. Geometrical parameters for the 2D modeling. Modified from Pedersen (1994).
Figure 3.5. Paramètres géométriques de la modélisation 2D. Modifié de Pedersen (1994).

3.2.3.2 P and S waves velocities

P wave is a compressional (or dilatational) wave travelling at a speed defined in isotropic solid materials as :

$$V_p = \sqrt{\frac{\lambda + \mu}{\rho}}$$

with λ and μ being the Lamé's constants and ρ being the density. The constant μ is the modulus of rigidity of the material, also called the shear modulus.

The S wave is a rotational wave which speed can be described in isotropic solid materials as :

$$V_s = \sqrt{\frac{\mu}{\rho}}$$

These velocities can be used to characterize the elastic behavior of the medium through the Poisson's ratio. This ratio can be defined as

$$\sigma = \frac{\lambda}{2(\lambda + \mu)}$$

or as

$$\sigma = \frac{\theta - 2}{2(\theta - 1)}$$

with θ being defined as $(V_p/V_s)^2$.

Values of the Poisson's ratio can theoretically vary from 0 to 0.5 (liquid). In practice values vary from 0.05 to 0.45, the lowest value characterizing very hard, rigid rocks whereas the highest one is for soft, poorly consolidated materials (Sheriff & Geldart, 1995). For rocks, a standard value of 0.25 is generally assumed.

3.2.3.3 Q factor

The quality factor (Q) is a measurement of the seismic wave attenuation due to the inelastic behavior of rocks and soils. It has a direct impact on wave amplitude and signal duration.

It can be written as :

$$Q = 2\pi \left(E / \Delta E \right)$$

with E the energy, and ΔE the energy loss (Sheriff & Geldart, 1995) or as :

$$Q = \frac{1}{2\zeta}$$

ζ being the damping factor.

The quality factor has an important effect on duration and amplitude of ground motions during earthquakes, especially regarding the surficial layers. Lower the quality factor, higher is the attenuation and consequently duration and amplitude are decreasing.

The attenuation is stronger in unconsolidated sediments than in rock. For example, a limestone can have a quality factor around 200 whereas a saturated sand has one around 20 (Schön, 1996).

3.2.3.4 Total discretization length

For modeling purpose, the sedimentary structure is approximated through a model which will be truncated. These truncation points are susceptible to generate diffracted waves which will affect the seismic response of stations located close to them. Therefore, in order to limit such influence, the truncation has to be positioned relatively far away from the structure. Thus the diffracted wave will be attenuated before arriving at the sedimentary structure (Pedersen, 1994). This can be done by enlarging the model in considering two or three times the length of the sedimentary structure (figure 3.6). But the consequence is an increase of the computation time as the size of discretization increases.

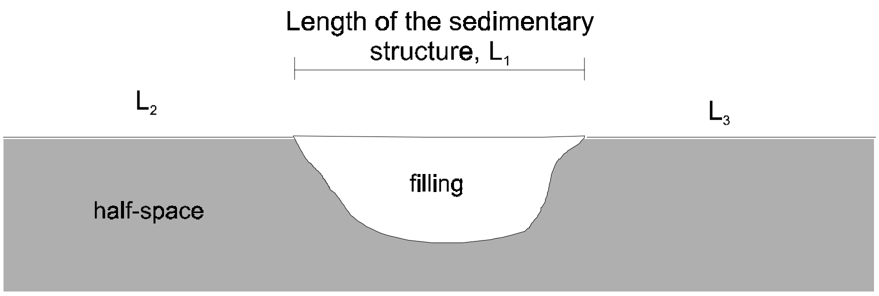

Figure 3.6. The total discretization length ($L_1 + L_2 + L_3$) considering two times the length L_1 of the sedimentary structure.
Figure 3.6. La longueur totale de discrétisation ($L_1 + L_2 + L_3$) prenant en compte deux fois la longueur L_1 de la structure sédimentaire.

3.2.3.5 Segment per wavelength

As well as the structure, wavelength has to be discretized. The choice of the number of segments will have an impact on the accuracy of the result and on the computation time.

3.2.3.6 Length of observation in time, frequency range, sampling rate

In the present modeling approach, the observation in time and the frequency range are two variables fixed by the user. Then the other parameters, such as the number of points, the sampling rate can be deduced from these values. Table 3.7 provides the main equations that characterize the signal in the frequency and time domain.

	Frequency domain [**Hz**]	**Time domain** [**sec**]
Sampling rate	$\Delta f = \frac{1}{Lt}$	$\Delta t = \frac{1}{Fe}$
Number of points	$Nf = \frac{F\max}{\Delta f}$	$Nt = \frac{Lt}{\Delta t}$
Limit	$F\max = \frac{Fe}{2}$	$Lt = Nt*\Delta t$

with *Lt* the limit in time; *Fmax* the maximum frequency; *Fe* the sampling frequency; *Δt* the sampling interval in frequency, *Δf* the sampling interval in time.

Table 3.7. Basic equations in the frequency and time domains to characterize the signal.
Tableau 3.7. Equations de base pour caractériser le signal dans le domaine fréquentiel et temporel.

The time of observation in the 2D modeling approach plays an important role. Time window has to be chosen long enough in order to let all phenomena (refraction, reflection and diffraction) to occur. The choice of the time window depends on the size of the sedimentary structure, the type of wave and its velocity. For example, a time window of 40 seconds for the Vétroz profile submitted to an incident shear wave of 800 m/s is sufficient.

3.2.3.7 Number of stations

The choice of the number of stations has to be done in order to obtain a realistic representation of the ground motion variation along the profile. More stations calculated, better can the variation of the seismic response be followed along the profile. However an increase of stations will expand the computer time. Therefore an appropriate compromise has to be chosen in function of the chosen objective, precise study or general tendency.

3.2.4 Results representation

The raw results are given in terms of displacement amplitude versus frequency for the 1D as well as for the 2D approach. The general name for such representation is the transfer function. It designates the modification of the incident wave by its passage through rocks and/or sediments having different characteristics.

In the frequency domain, one is also interested in the effect of the sedimentary filling itself. This can be express through an amplification function. Such function is obtained by the ratio of the amplitude of steady-state motion at a considered site (free surface of the soil) to the amplitude of motion that would be recorded in absence of the sedimentary filling (figure 3.8). It is called elastic rock amplification (Roësset, 1970).

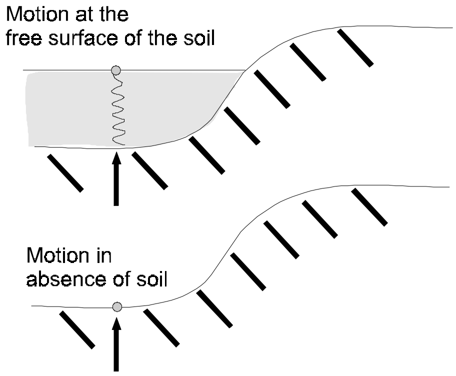

Figure 3.8. Location of the two amplitude motions considered in an amplification function.
Figure 3.8. Positionnement des deux mouvements sismiques considérés dans une fonction d'amplification.

Another way of presentation is to create synthetic seismograms that represent the result in the time domain. The principle is based on the convolution of the transfer function with an input motion, as the transfer function can be regarded as a filter which determines how each frequency in the input motion is modified by the soil deposit. Ricker (1940) has shown that seismograms are constituted by a succession of a defined wavelet. The shape depends on the nature of the earth's characteristics. As a result the common used input motion is the Ricker pulse (Ricker, 1945) as illustrated in figure 3.9. Such representation in time domain allows to follow the evolution of the displacement at different location along the profile. It permits to see the variation of the signal in terms of duration and amplitude.

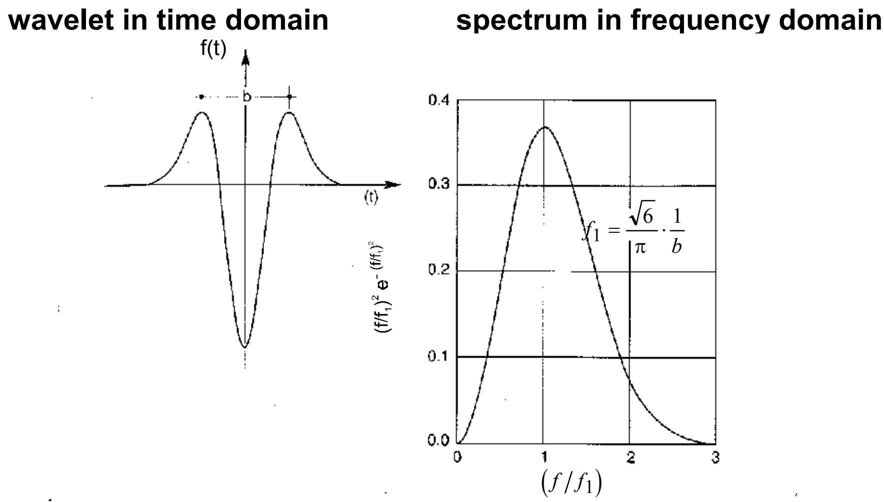

Figure 3.9. Form of the Ricker wavelet expressed in time domain and frequency domain. b represents the width of the wavelet in seconds, t is the time measured from the wavelet center and f, f_1 indicates the frequency.
Figure 3.9. Forme de l'ondelette de Ricker dans le domaine temporel et fréquentiel. La lettre b désigne la largeur de l'ondelette en seconde; le t est le temps mesuré depuis le centre de l'ondelette et le f, f_1 désigne la fréquence.

3.2.5 Computation requirements

Both 1D and 2D modeling programs have been implemented on a workstation. The 1D modeling program is running on a SUN station having 64 MB of Random Access Memory (RAM) and requires only a few seconds to produce results. The 2D modeling requires higher capabilities in terms of memory. Therefore it has been implemented on a IBM RISC 6000 whose capacity is divided into several nodes each of them having at disposition at least 192 MB of RAM (Matthews, 1995). The computation time length will vary in function of total discretization length (irregularity size plus the enlargement choice), the velocity contrast, especially regarding the shear waves, and the number of segments per wavelength. The longer the profile, the more important is the time requirement. Each numerical simulation required a minimum of 4 hours for the Bramois profile (81 stations) and 7 hours for the Vétroz profile (91 stations), the two profiles investigated in the Sion area.

3.3 Seismic response of the Rhône Valley's subsurface geometry

3.3.1 Presentation

In the Rhône valley, the sedimentary deposit is the result of the glaciers, lakes and rivers action. All the deposit was accumulated during the late Quaternary, i.e. Superior Pleistocene to Holocene (Finger & Weidman, 1987), after the last maximum glacial period (25000 - 15000 BP[3]; Pugin & Marchant, 1992) in the Würm stage. The common action of glacial erosion as well as isostasic and tectonic uplift lead to the accumulation of several hundreds meters of sediments (more than 900 m in some places; Besson et al. 1993). Most of sediment accumulation during and after the glacial retreat period was estimated to be achieved in a maximum of 5000 years (Pugin & Marchant, 1992) inducing a sedimentation rate over 100 mm/year. This rate reduced to a mean rate of 4-5 mm/year in the last 12000 years, without considering the modern period in which the natural sedimentation process has been modified by the embankment of the Rhône river and the installation of dams in lateral valleys (Finger & Weidman, 1987).

This deposit is a subject of interest for a long time. Various studies, gravimetric or seismic (e.g Gonet, 1965; Wagner, 1970; Bernauer & Geiger, 1986; Finckh & Klingelé, 1991) have been carried out in the Rhône valley in order to investigate the characteristics of the Quaternary deposit, such as the subsurface geometry and the thickness of the deposit based on density and P velocity.

One of the most recent seismic study was carried out during the GEOTHERMOVAL project (Besson et al. 1993) and the PNR20 (Pfiffner et al. 1997). High resolution seismic profiles were investigated between St-Maurice and Sion, as displayed in figure 3.10.

Two of them, the Vétroz and the Bramois profiles, have been selected as test profiles for the 2D modeling. The Vétroz profile reaches an estimated depth of 893 m whereas the maximum depth of the Bramois profile is 560 m. Their respective geological interpretation are displayed in figure 3.11.

[3] Before Present, the term "Present" being fixed at the year 1956

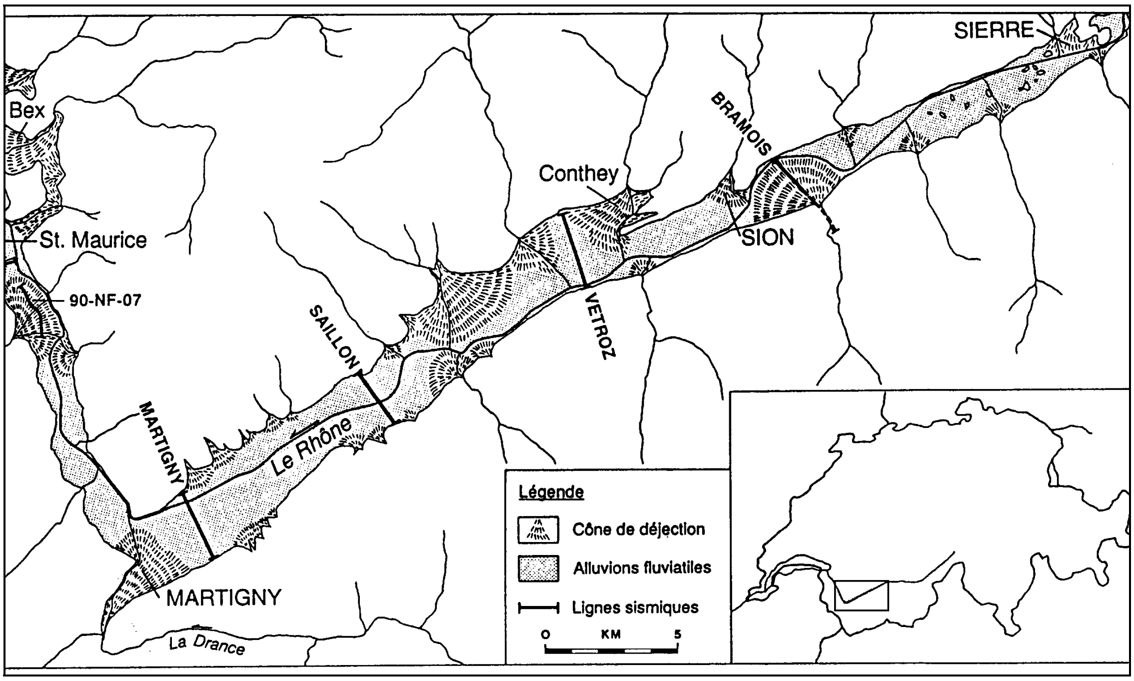

Figure 3.10. Positions of the high resolution seismic profiles carried out during the PNR20 and GEOTHERMOVAL. Modified from Besson et al. 1993.
Figure 3.10. Localisation des profils de sismique réflexion levés dans le cadre du PNR20 et de GEOTHERMOVAL. Modifié de Besson et al. 1993.

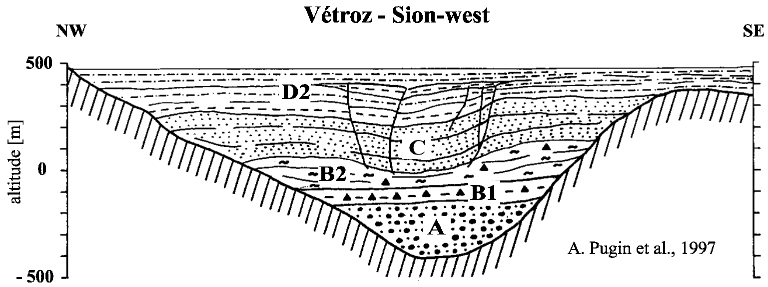

Units	Geological interpretation
D2	deltaic sediments
D1	lacustrine deposits
C	glaciolacustre deposits
B2	meltout and reworked till
B1	lodgement till
A	subglacial deposits

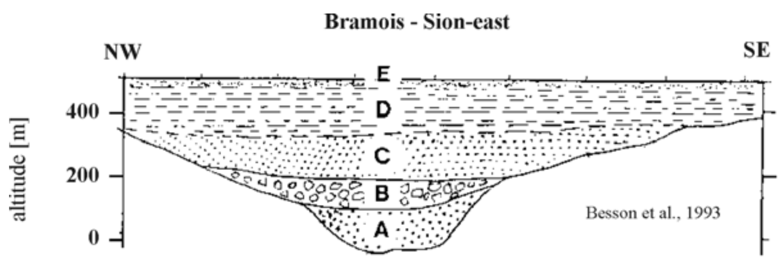

Units	Geological interpretation
E	post-lacustrine deposits
D	lacustrine deposits
C	glaciolacustre deposits
B	meltout and reworked till
A	subglacial deposits

Figure 3.11. Geological interpretation of the high resolution seismic profiles of Vétroz and Bramois.
Figure 3.11. Interprétation géologiques des profils sismique réflexion de Vétroz et Bramois.

3.3.2 Physical parameters

Parameters such as density and P-wave velocities have been investigated through the several studies in geophysics which have been carried out in the Rhône valley. Principal researches and the obtained values are indicated in the appendix B. In summary, the mean density is varying between 1900 and 2200 kg/m^3 for the Quaternary sedimentary deposit and between 2400 and 2720 kg/m^3 for rocks. Regarding the P velocity, values range from 500 to 2800 m/s for Quaternary deposit and from 4000 to 5000 m/s for rocks.

Recent shear-wave velocities data are available for surficial deposits (up to 30-50 m) in Bâle (Fäh et al. 1997). But no data are available for thick Quaternary deposit (> 100 m). The difficulty is to obtain a source which can trigger shear waves with enough energy to travel through all the sediment thickness. It was planned to study the propagation of the shear wave on the entire depth of the Vétroz profile. But the appropriate shear-wave generator was not accessible. Therefore measurements were made using seismic reflection and refraction using a less energetic source through a contract given to Burri (1995).

The shear-waves were generated by a Buffalo gun in a hole 40 to 60 cm deep with an angle of 60° from the vertical and the shots were done perpendicularly to the direction of the profile using two cartridges per shot. Figure 3.12 shows the different positions of the gun in respect to the wave choice.

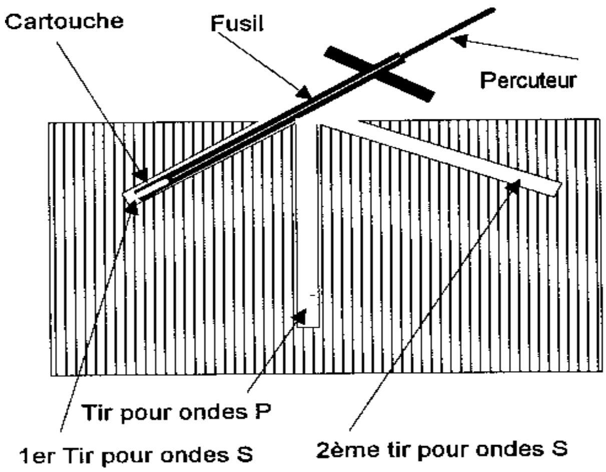

Figure 3.12. Positions of the gun shot in respect to the wave to trigger (Burri, 1995).
Figure 3.12. Position de tir du fusil en fonction du type d'onde à générer (Burri, 1995).

The main results are summarized in the table 3.13.

	S wave		***P wave***	
Acquisition technique	**depth [m]**	**velocity [m/s]**	**depth [m]**	**velocity [m/s]**
Seismic refraction	2.3 2.6 8.5 16 ?	130 160 250 270 456	2.2 3.7 ?	300 400 2000
Seismic reflection	32.5 49 71 176	260 280 340 420	18 301 357 677	1200 2100 2800 4000

Table 3.13. Seismic velocities in function of seismic acquisition technique (Burri, 1995).
Tableau 3.13. Vitesses sismiques en fonction de la technique sismique d'acquisition (Burri, 1995).

It can be seen that in the surficial layers the shear-wave velocities are quite low. Regarding the P wave, the seismic refraction shows that for the first 4 meters, the velocity is also low but then the value increases to 2000 m/s. This transition is likely due to the fact that sediments become water saturated. It has been found that the velocity of the P waves varies from 200-500 m/s to about 1600 - 2000 m/s when the sediments are water saturated (Schön, 1996). Piezometers located near the Vétroz profile show a water-table at a depth around 2m below the surface.

3.3.3 2D modeling

The lateral borders of the subsurface geometry given by the geological interpretation of the high seismic resolution profiles were adjusted to the topographical surface in order to be suitable for modeling purpose. The Vétroz profile is therefore 3 km long and Bramois 2.5 km long. The resulting profiles are shown in figure 3.14.

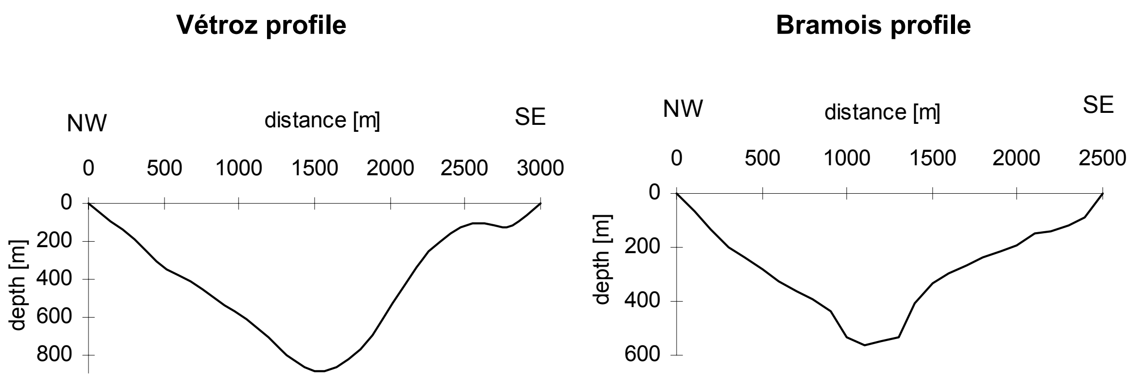

Figure 3.14. Subsurface geometry of Vétroz and Bramois profiles adjusted for 2D modeling.
Figure 3.14. Géométrie de subsurface des profils de Vétroz et Bramois ajustée pour la modélisation 2D.

These profiles exhibit different geometric elements, causing different seismic responses. The Vétroz profile shows a shoulder on its right side and the Bramois profile displays gentler slopes and a center part which is more accentuated.

The physical characteristics used in the modeling are described in table 3.15. They represents a compromise on the value ranges given by the various studies done in the Rhône valley.

Concerning the Q factor for sedimentary deposit, its mean value is usually chosen in the range 40-50 (e.g Bard & Chávez-García, 1993; Pedersen, 1994). For the bedrock, the value is based on the work of Pedersen (1994) on the Ubaye valley (French Alps). Regarding the shear-wave velocity, a mean value of 800 m/s is used to characterized the sedimentary filling. This value seems to be reasonable in an alpine context. Pedersen (1994) is using a mean value of 900 m/s for the Ubaye valley (French Alps) and Le Brun (1997) is considering a mean velocity of 700 m/s for the Grésivaudan valley (French Alps).

	Vp [**m/s**]	**Vs** [**m/s**]	**Poisson's ratio**	ρ [**kg/m³**]	**Q**
sedimentary deposit	2050	800	0.41	2100	50
bedrock	4000	2200	0.28	2670	100

Table 3.15. Parameters used for the 2D modeling of Vétroz and Bramois profiles.
Tableau 3.15. Paramètres employés dans la modélisation 2D pour les profils Vétroz et Bramois.

All numerical simulations on the Vétroz and Bramois profiles have been processed for a frequency range between 0 and 5Hz with a sampling rate of 0.025 Hz. Stations are regularly spaced by 50 m. The incident wave is a SH wave.

The total discretization length represents three times the length of the irregularity and the wavelength is divided into 5 segments.

3.3.3.1 Results

All displacement amplitudes calculated on surface of the sedimentary valley have been normalized by the displacement amplitude obtained in absence of the structure in order to obtain the amplification induced by the valley alone (see § 3.2.4). As the incident wave is a vertically incident SH wave, the displacement amplitude at the surface, in absence of the structure, is equal to 2.

This value results from the free-surface boundary condition. On the surface of the earth a solid-air interface (figure 3.16) is present.

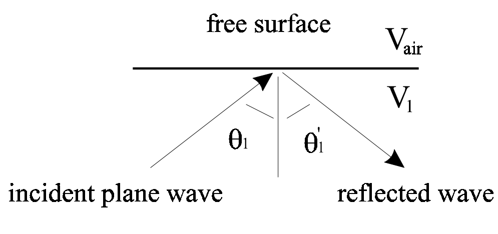

Figure 3.16. An incident plane wave at a free surface. With V_1>>>V_{air}
Figure 3.16. Onde plane incidente sur une surface libre. Avec V_1>>>V_{air}

In this case, the elastic constants of the atmosphere are several orders of magnitude smaller than the elastic constants of the rock. Therefore no stress can be transmitted and all stress components are equal to zero at the interface (Aki & Richards, 1980). To satisfy this zero stress boundary condition, the displacement amplitude at this boundary (which corresponds to the amplitude of the refracted wave) must be twice the amplitude of the incident wave (Kramer, 1996). The displacement amplitude of a refracted SH wave can be written as :

$$A_{SHr} = \left(1 + \frac{1 - \dfrac{\rho_r \beta_r \cos\theta_r}{\rho_i \beta_i \cos\theta_i}}{1 + \dfrac{\rho_r \beta_r \cos\theta_r}{\rho_i \beta_i \cos\theta_i}} \right) A_{inc} \qquad \text{(Kramer, 1996)}$$

with ρ_r ,β_r ,θ_r = density, shear-wave velocity and angle of refraction of the medium in which the wave is refracted and ρ_i ,β_I ,θ_i = density, shear-wave velocity and incidence angle of the medium from which the wave is coming.

In presence of a free surface, the impedance $\rho_r\beta_r$ is equal to zero, thus A_{SHr} is equal to $2A_{inc}$. As the amplitude of the incident wave is equal to 1, the displacement amplitude is thus equal to 2.

Looking at the amplification functions all together on both profiles (figure 3.17), three major features can be observed :

- the maximum amplification does not occur specifically at the fundamental resonant frequency;
- the amplification value of the fundamental predominant frequency is increasing toward the center (gray color);
- the fundamental resonant frequency stays unchanged whatever the location on the profile. The value is equal to 0.35 Hz for the Vétroz profile and 0.5 Hz for the Bramois profile. The difference is due to the change in global thickness of the sedimentary deposit, Vétroz being thicker than Bramois.

The unchanged location of the fundamental resonant frequency was an expected result as the profiles describe an embanked valley and as the sedimentary deposit and the bedrock are characterized by a high velocity contrast, two elements necessary to induce a resonance involving the entire valley as a whole as theoretically demonstrated by Bard & Bouchon (1985). For symmetric valley they described the valley embankment by a shape ratio that they defined as the ratio of the maximum sediment thickness (*h*) to the valley half-width (*l*).

Regarding asymmetric valley the shape ratio is modified as follows (Bard & Bouchon, 1985) :

$$\text{shape ratio} : \frac{h}{2w}$$

with *2w* the total width over which the sediment thickness is more than half its maximum value (h).

The necessary conditions for the existence of a global resonance in the SH case are given in figure 3.18. The curve delimits the type of phenomenon which can occur in a valley in function of its shape ratio and velocity contrast. The velocity contrast C_v is defined by the ratio between the seismic velocities of the bedrock and the unconsolidated sediments. The shape ratio is given as *h/l* but the curve may also be valid for asymetric valley considering that the shape ratio is obtained with *h/2w* (Bard & Bouchon, 1985).

Using the shape ratio formula for asymmetric valley, Vétroz has a shape ratio equal to 0.72 (893m/1243m) and to 0.54 (560m/1040m) for Bramois. With a shear-wave velocity contrast of 2.75, both profiles meet the conditions for generating a 2D resonance as displayed in figure 3.18.

Looking now at the distribution of the maximal amplification along the profile, figure 3.19 displays both profiles in the case of a SH wave with vertical incidence. The slope gradient calculated on the thickness data has also been plotted in order to underline the subsurface geometry variation.

Three distinct features occur :

- a steeper slope, characterized by a strong slope gradient, induces a stronger amplification than a gentle slope (Vétroz case). The reason is that an abrupt edge can strongly reflect the energy therefore inducing amplification;
- an asymmetric profile, such as Bramois, induces an asymmetric distribution of the amplification. The asymmetry is defined by the slope gradient and the thickness variation;
- a presence of a well-marked shoulder (Vétroz) induces its specific amplification pattern. This structure is long and deep enough so that waves can be trapped inside and generate specific seismic amplification.

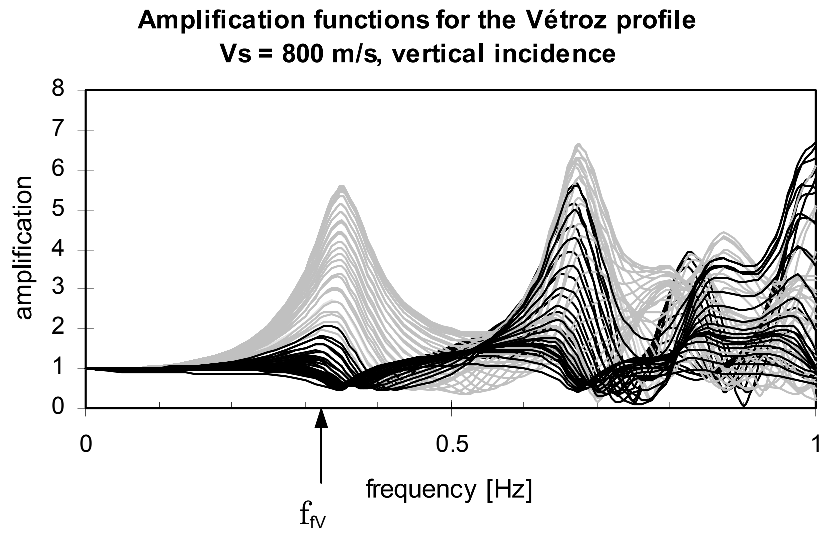

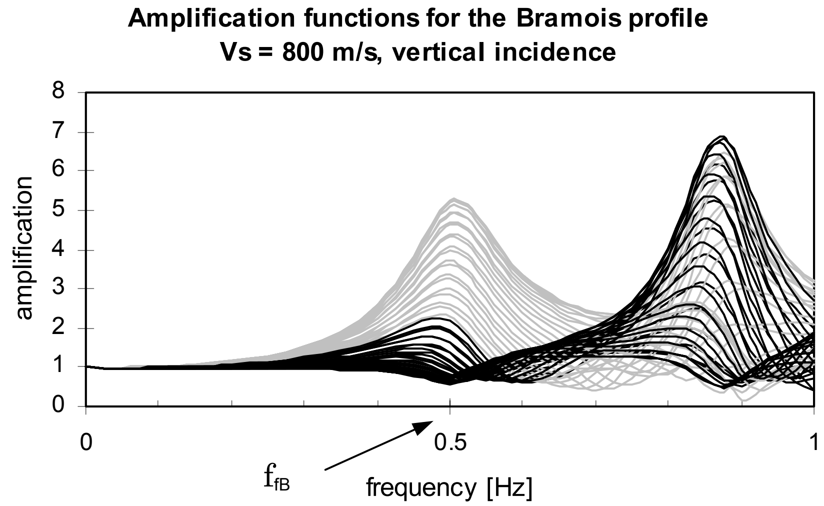

Figure 3.17. All amplification functions along the Vétroz and Bramois profiles; 61 for Vétroz and 51 for Bramois. The black color is used for the amplification functions located on the edges of the profiles whereas the gray designates those in the middle. f_{fV} = fundamental frequency for the Vétroz profile and f_{fB} = fundamental frequency for the Bramois profile. Display only up to 1 Hz for better reading.

Figure 3.17. Toutes les fonctions de transfert des profils de Vétroz et de Bramois, soit 61 pour Vétroz et 51 pour Bramois. La couleur noire désigne les fonctions de transfert situées en bordure, la grise est utilisée pour celles situées au centre. f_{fV} = fréquence fondamentale pour le profil Vétroz et f_{fB} = fréquence fondamentale du profil Bramois. Affichage seulement jusqu'à 1Hz pour faciliter la lecture.

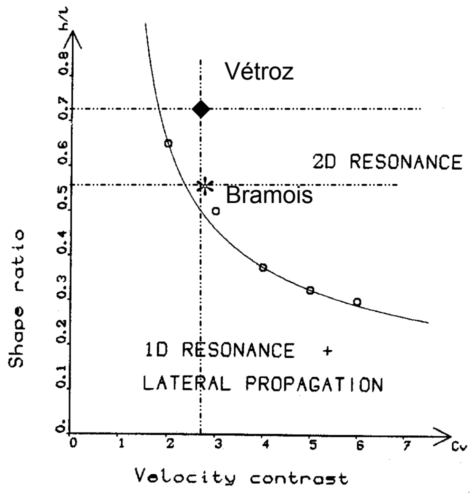

Figure 3.18. Relationship between the shape ratio and velocity contrast for the existence of a 2D resonance in the SH case (modified from Bard & Bouchon, 1985).
Figure 3.18. Relation entre le rapport de forme et le contraste de vitesse pour l'existence d'une résonance bidimensionnelle dans le cas d'une onde SH (modifié de Bard & Bouchon, 1985).

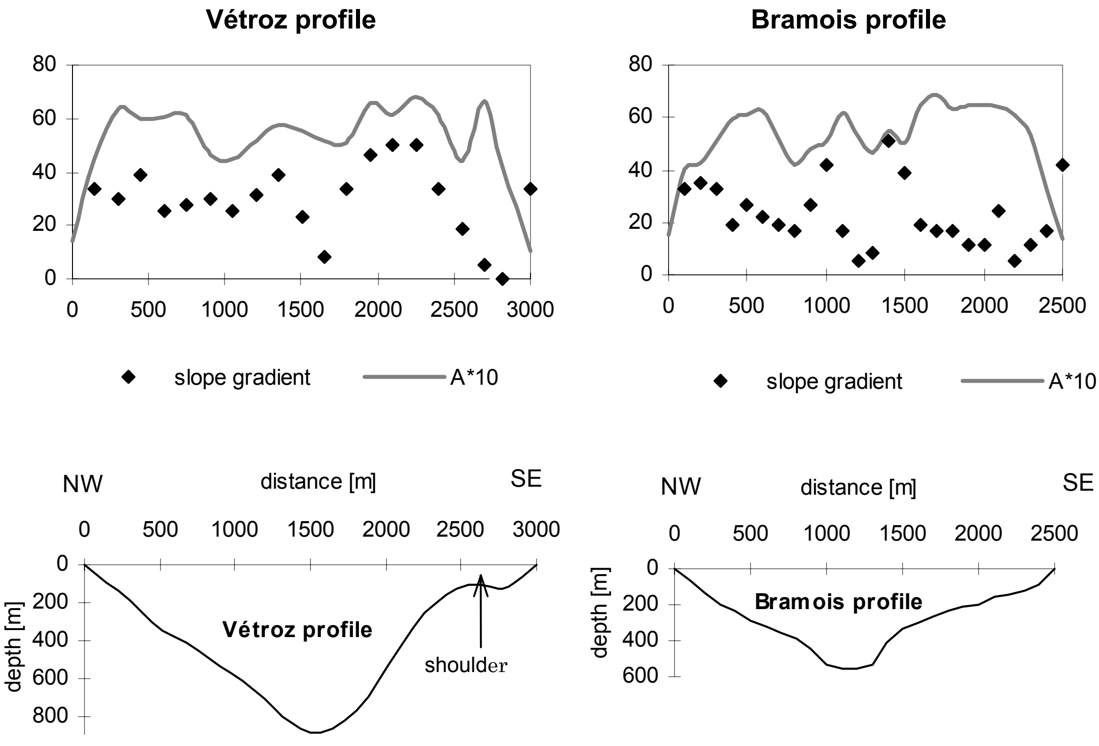

Figure 3.19. Amplification versus the subsurface geometry and the slope gradient. SH case with vertical incidence. In order to ameliorate the reading, amplification values have been multiplied by a factor of 10.
Figure 3.19. Représentation de l'amplification en fonction de la géométrie de subsurface et des gradients de pente. Cas de l'onde SH à incidence verticale. Pour faciliter la lecture, les valeurs d'amplification ont été multipliées par un facteur de 10.

Considering the time domain, synthetic seismograms have been calculated using a Ricker wavelet with a central period T_p of 2 seconds. Specific seismograms as functions of their location along the profiles are displayed in figure 3.20. It can be seen that the seismic response is changing in terms of amplitude, duration and frequency content depending on the location along the profiles. Stations located on a steep slope, which exhibit the higher value of maximum amplification in the frequency domain (figure 3.18) show higher amplitude and longer signal in the time domain.

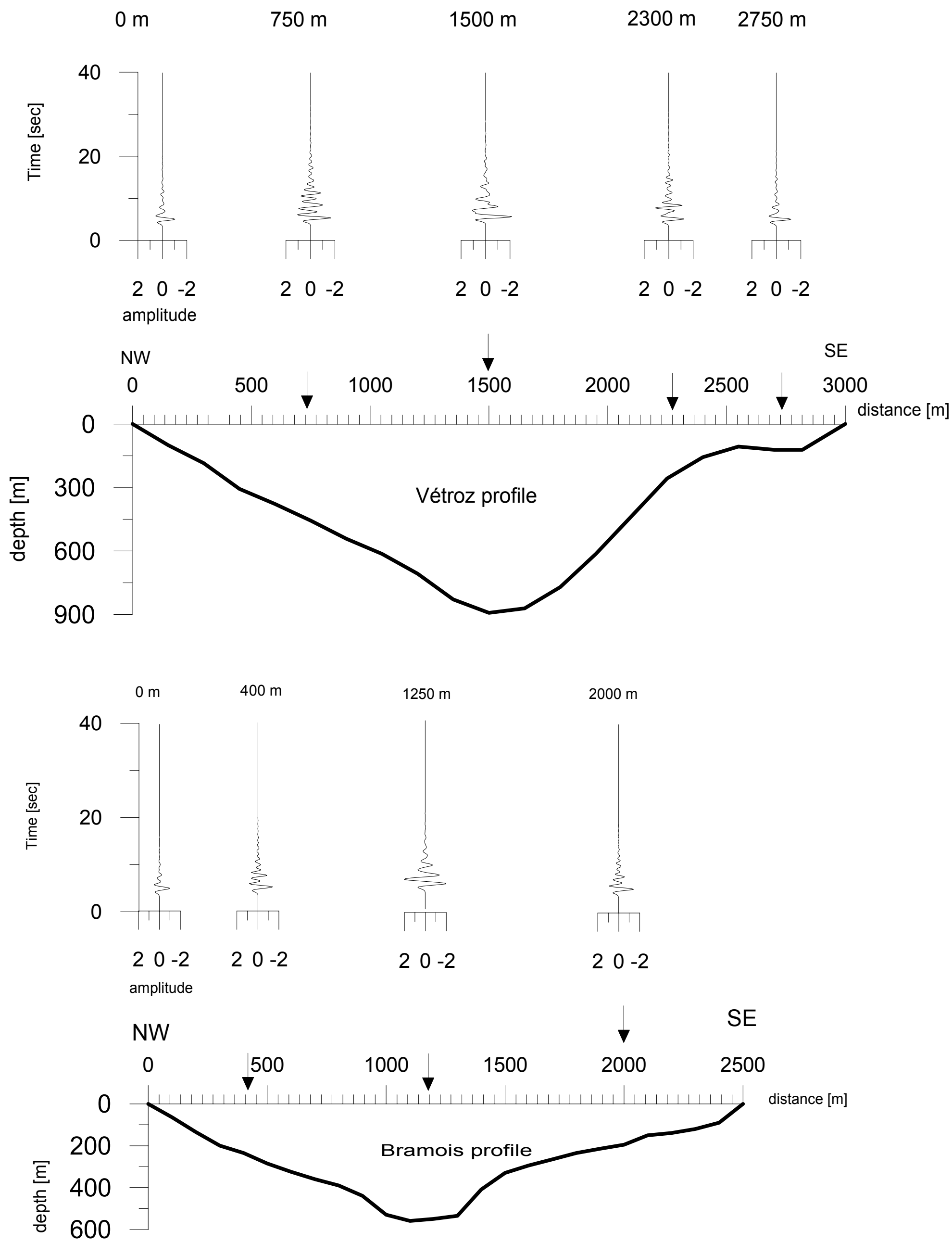

Figure 3.20. Synthetic seismograms on different locations of the Vétroz and Bramois profiles. The incident wavelet is a Ricker wavelet with a central period T_p of 2 seconds. Case of a vertical incident SH wave and with a mean shear-wave velocity for the sedimentary deposit of 800 m/s.
Figure 3.20. Sismogrammes synthétiques à différentes positions le long des profils de Vétroz et Bramois. L'ondelette incidente est une ondelette de Ricker avec une période centrale Tp de 2 secondes. Cas d'une onde incidente verticale de type SH et une vitesse moyenne de l'onde cisaillante pour le dépôt sédimentaire de 800 m/s.

3.3.4 Comparison between 1D and 2D modeling

Comparison between the 1D and 2D cases for the spatial distribution of the maximum amplification and associated frequencies along the Vétroz profile is displayed in figure 3.21. The parameters used for the calculation are identical as those described in table 3.15 (§ 3.3.3).

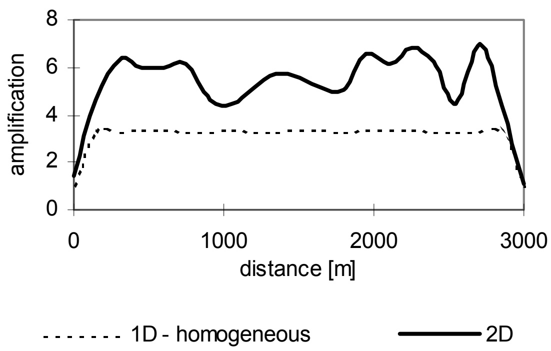

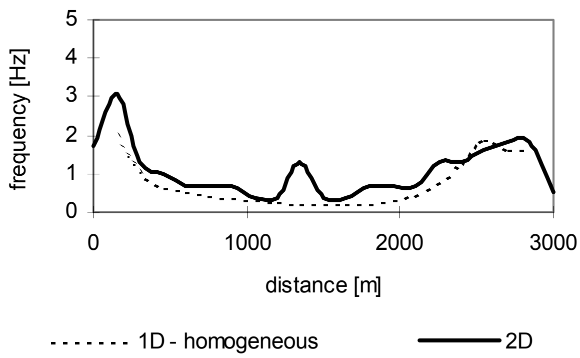

Figure 3.21. Comparison between 1D and 2D modeling for the spatial distribution of the maximum amplification and associated frequencies along the Vétroz profile. Case of a SH wave with vertical incidence.
Figure 3.21. Comparaison entre la modélisation 1D et 2D en ce qui concerne la répartition spatiale de l'amplification maximale et les fréquences associées pour le profil de Vétroz. Cas d'une onde SH à incidence verticale.

It can be seen in figure 3.21 that the pattern of the amplification resulting from the 2D modeling varies with the location along the profile. For the 1D case, the amplification value is almost constant except on the border. Moreover the 2D amplification values are at least two times higher than the 1D ones. Regarding the frequencies, the general trend is quite similar for the 1D and 2D modeling, low frequency in the center part and increasing values towards the edges. The 2D modeling seems to give slightly higher values.

A comparison between the 1D and 2D case is also shown in figure 3.22 but considering the amplification functions at different locations on the profile. Three interesting elements can be pointed out :

- in the center part of the valley the maximal amplification occurs at the fundamental frequency in the 1D as well as in the 2D case;
- the presence of a shoulder induces a seismic response having a quite similar trend as the 1D case. This is due to the fact that this shoulder is deep and marked enough to generate its own response and the geometry is near a 1D case, i.e. a plane layer;
- in the main part of the sedimentary valley, the fundamental resonant frequency is higher and exhibits a stronger amplification in the 2D case than in the 1D case. This has also been observed by other authors (e.g. Bard & Bouchon, 1985; Riepl, 1997).

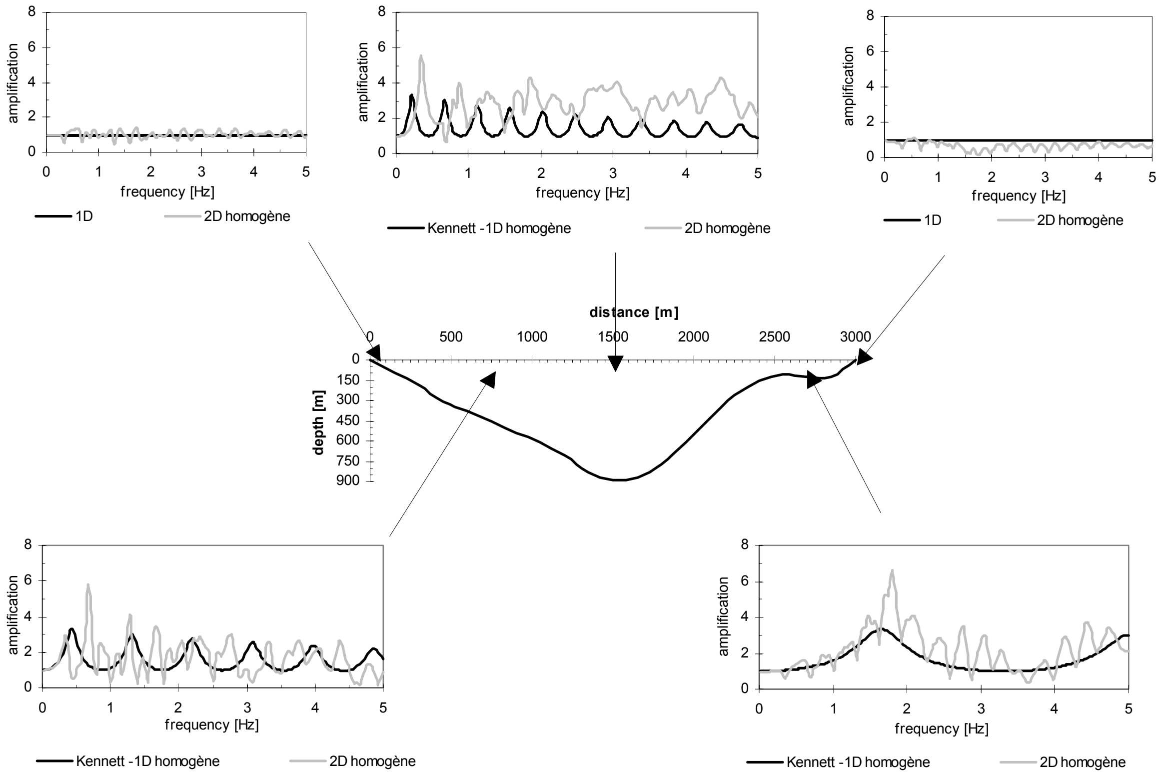

Figure 3.22. Amplification functions at different location along the Vétroz profile. Case of a vertical incident SH wave.
Figure 3.22. Fonctions d'amplification pour différentes stations le long du profil de Vétroz. Cas d'une onde incidente verticale de type SH.

3.3.5 Sensitivity analysis on the 2D response to physical parameters

3.3.5.1 Shear-wave velocity

As the shear-wave velocity value is one of the lesser known parameters, modeling was made using different mean velocities for the sedimentary filling going from 400 m/s to 800 m/s. It seems difficult to assume a mean shear-wave velocity below 400 m/s as the shear-wave profile on Vétroz already shows a higher value at a depth of 176 m (Burri, 1995). Moreover the use of a value of 400 m/s results in a Poisson's ratio of 0.48 which characterizes a very soft material that is likely not the case for the entire Quaternary deposit.

Numerical simulations using different shear-wave velocities are displayed in figure 3.23. The result shows the following features :

- a shear-wave velocity increase in the sedimentary deposit induces an important decrease on the amplification value and an increase in frequency. This is due to the diminution of the velocity contrast between the sedimentary deposit and the bedrock;
- regarding the frequency, the trend is to find low values in the center part of the valley and higher frequency toward the edges;
- the thicker the deposit (Vétroz), the lower are the frequency values.

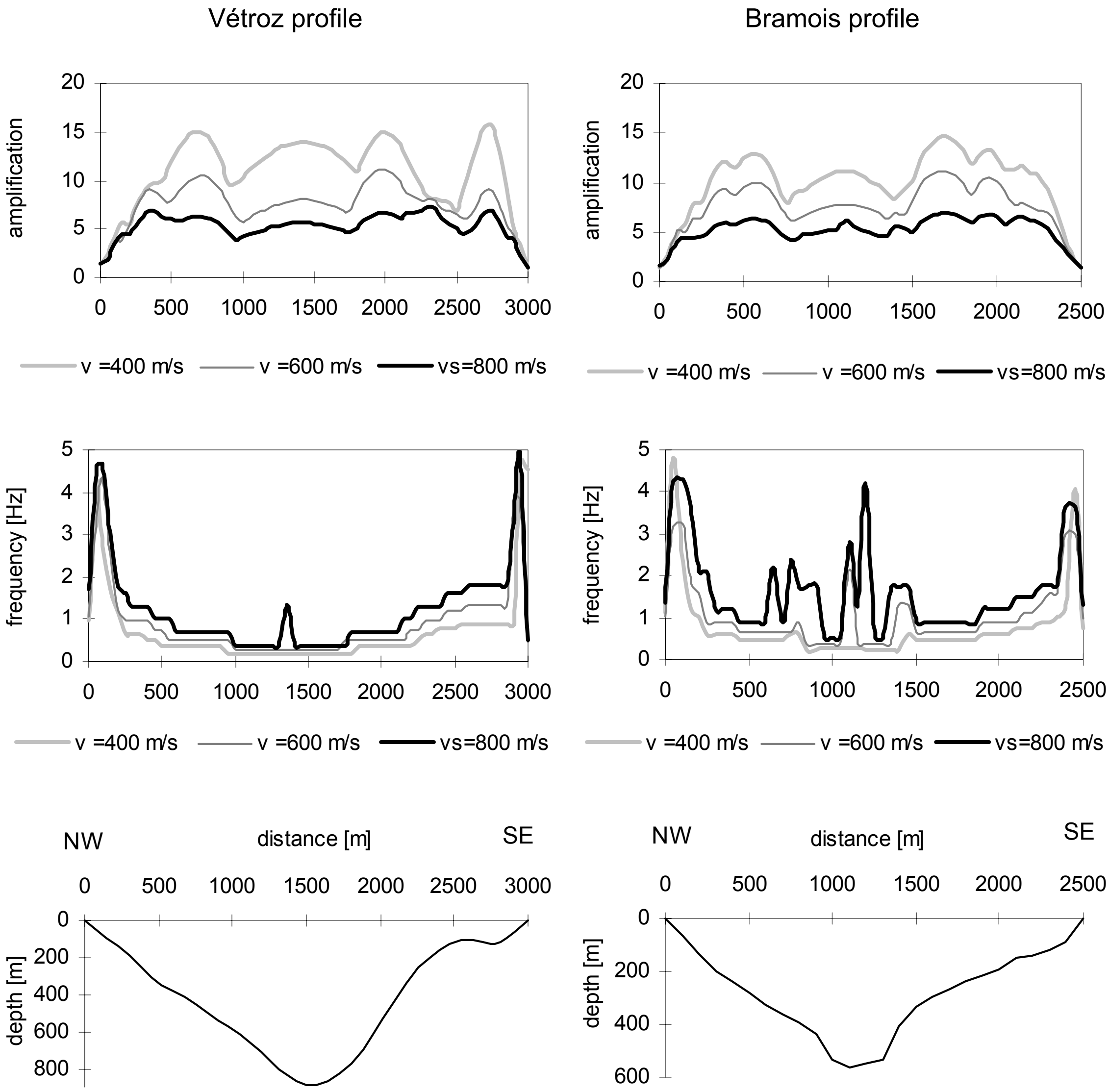

Figure 3.23. Spatial distribution of the maximum amplification and its associated frequency for the Vétroz and Bramois profiles. For a sedimentary filling characterized by a shear-wave velocity of 400 m/s, 600 m/s and 800 m/s. Case of a vertical incident SH wave.
Figure 3.23. Distribution spatiale de l'amplification maximale et de la fréquence associée le long des profils de Vétroz et Bramois. Pour un remplissage sédimentaire caractérisé par des vitesses d'onde cisaillante égales à 400 m/s, 600 m/s et 800 m/s. Cas d'une onde SH à incidence verticale.

It can be seen that some heterogeneities occur in the center part of the Vétroz and Bramois profiles (see also figures 3.28, 3.29). The analysis of individual spectral curves shows that these higher frequency values are harmonics of the fundamental frequency. In most cases, the amplification value of the fundamental frequency and the harmonic are close. The presence of harmonics instead of the fundamental frequency is due to the selection method of the amplification values, based on the maximum value.

It can also be noticed that frequency values on the edges do not exceed 5 Hz. This is due to the fact that the considered frequency range was between 0 and 5 Hz, the upper limitation imposed by the computing capability according to the chosen parameters. Modeling using a more extended frequency range would probably show that values on the rims can exceed 5 Hz.

The main conclusion of the figure 3.23 is that the spatial distribution of the maximum amplification follows a general trend, independently from the shear-wave velocity choice, i.e. higher amplification near the edges and then in the deepest part of the profiles.

Regarding the fundamental frequency, the value is sensitive to the shear-wave velocity contrast as illustrated in figure 3.24. When the shear-wave velocity for the sedimentary deposit decrease, the shear-wave velocity contrast increases, then the fundamental frequency value decreases whereas the amplification logically increases.

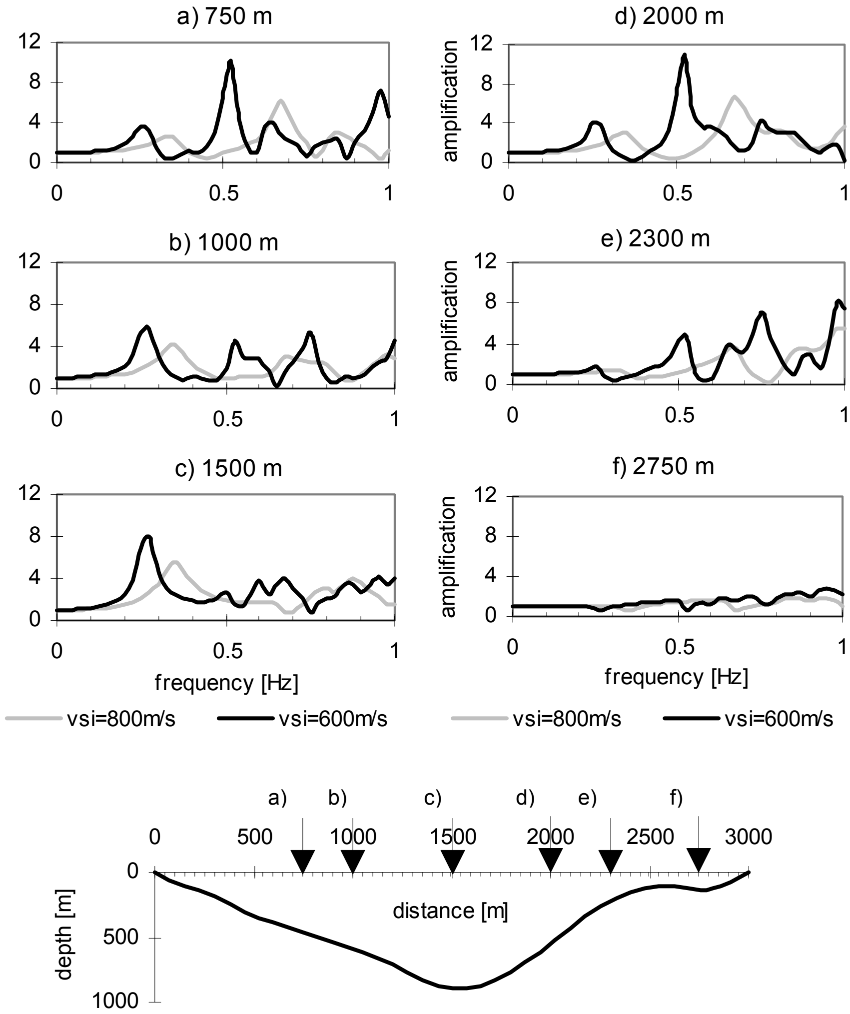

Figure 3.24. Effect of the shear-wave velocity contrast on the fundamental frequency and the amplification value. Case of a vertical incident SH wave for the Vétroz profile.
Figure 3.24. Effet du contraste des vitesses cisaillantes sur la valeur de la fréquence fondamentale et sur l'amplification. Cas du profil de Vétroz pour une onde SH à incidence verticale.

The synthetic seismograms for several stations along the Vétroz and Bramois profiles are displayed (figure 3.25) for two values of shear-wave velocity, 600 m/s and 800 m/s. The results show that in the case of 600 m/s amplitude and duration of the signal are more accentuated, especially for stations located at the vertical of the valley slopes. And this is more marked in the case of the Vétroz profile. The increase in amplitude and duration results from the increase in the shear-wave velocity ratio. Indeed it increases from 2.75 to 3.67. And the difference between

Bramois and Vétroz is likely due to the fact that in the case of the Vétroz profile, slopes are steeper (figure 3.19).

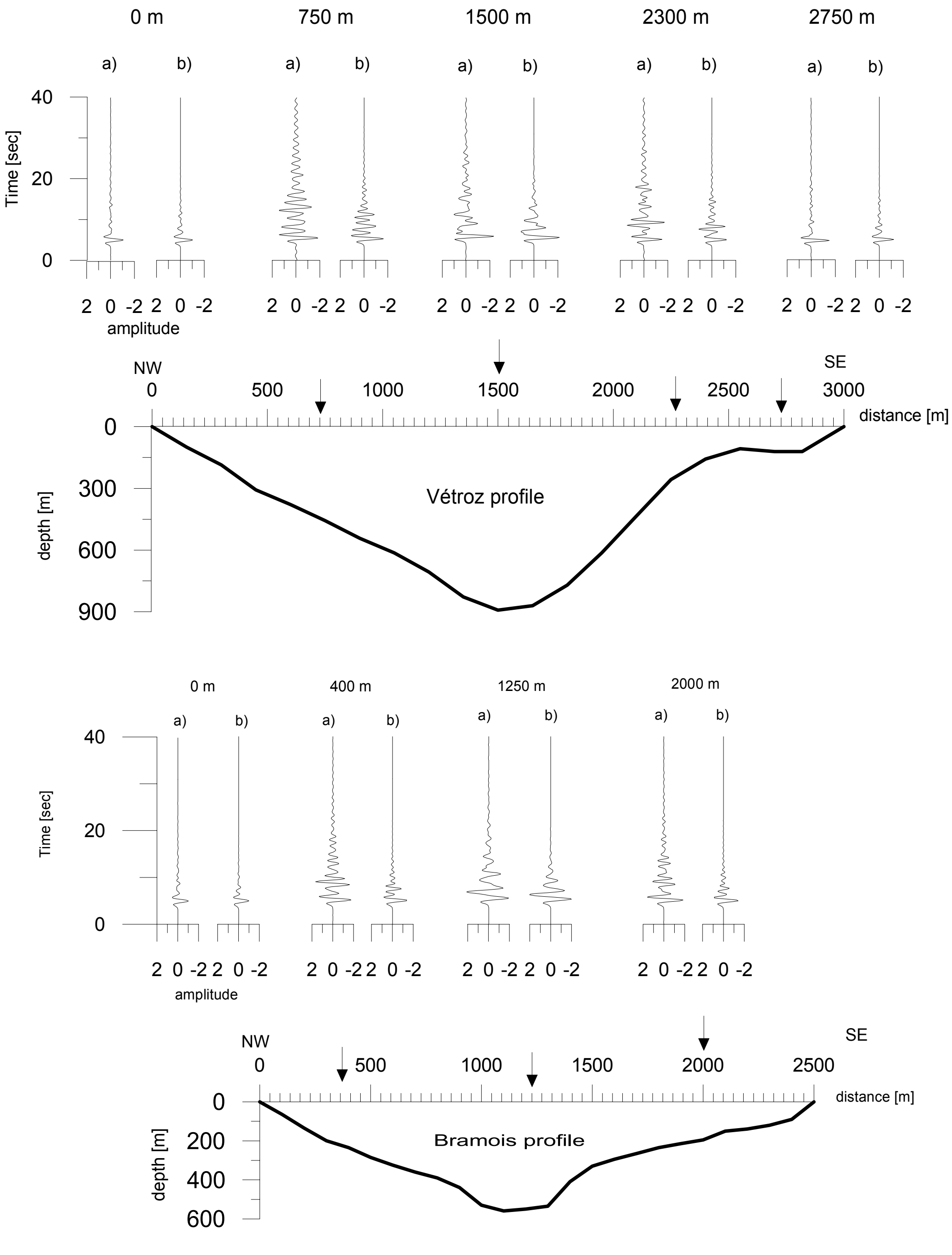

Figure 3.25. Synthetic seismograms for the Vétroz and Bramois profiles. The incident signal is a Ricker wavelet with a characteristic period Tp=2s. Case of a vertical incident SH wave. a) case of a mean Vs = 600 m/s for the sedimentary deposit b) case of a mean Vs = 800 m/s for the sedimentary deposit.
Figure 3.25. Sismogrammes synthétiques pour les profils de Vétroz et Bramois. Le signal incident est une ondelette de Ricker avec une période caractéristique Tp=2sec. Cas d'une onde SH à incidence verticale. a) cas d'une vitesse moyenne Vs = 600 m/s pour le remplissage sédimentaire. b) cas d'une vitesse moyenne Vs = 800 m/s pour le remplissage sédimentaire.

3.3.5.2 Density and incidence angle

The sensitivity of the maximum amplification and the fundamental resonant frequency with respect to density and incidence angle has been tested for a shear-wave velocity of the sedimentary filling of 800 m/s. The tested parameters for Vétroz as well as Bramois are indicated in table 3.26.

		Vp [m/s]	**Vs [m/s]**	**Poisson's ratio**	**ρ [kg/m³]**	**incidence angle**	**Q**
Reference	sedimentary filling	2050	800	0.41	2100	0	50
	bedrock	4000	2200	0.28	2670		100
variation 1	sedimentary filling	2050	800	0.41	**1900**	0	50
=di	bedrock	4000	2200	0.28	2670	0	100
variation 2	sedimentary filling	2050	800	0.41	2100	0	50
=de	bedrock	4000	2200	0.28	**2500**	0	100
variation 3	sedimentary filling	2050	800	0.41	2100	**30**	50
=angle 30	bedrock	4000	2200	0.28	2670		100
variation 4	sedimentary filling	2050	800	0.41	2100	**60**	50
=angle 60	bedrock	4000	2200	0.28	2670		100

Table 3.26. Variation of physical parameters in order to test the sensitivity of the 2D modeling.
Tableau 3.26. Variations des paramètres physiques pour tester la sensibilité du modèle 2D.

Density values were chosen to be consistent with the value range given to characterize the Quaternary sedimentary deposit (see Appendix B). The influence of density variation on the maximum amplification and associated frequencies are displayed in figure 3.27. The following observations can be pointed out :

- the modification of the density value influences the impedance contrast between the sedimentary deposit and the bedrock. Therefore a decrease of density value in the sedimentary deposit increases the impedance contrast, thus inducing an increase of maximum amplification values whereas a decrease of density value in the bedrock diminishes the impedance contrast, provoking then a decrease of the amplification values;
- frequencies seem to be insensitive to the impedance contrast variation due to the density modification. This is likely due to the fact that the variation induced is too small to produce a visible modification of the frequency content.

Regarding the incident angle of the incident wave on the sedimentary structure, the value depends on the earthquake source location (at depth and at the distance from the observation point) and on the subsurface velocity gradient. Considering that in the Valais region, the most active source up to now is located on the Northern flank of the Rhône valley (Wildhorn area) with various source depths until a maximum value of 15 km, an incident angle with a limit value of 60° seems reasonable whereas the value of 30° is used for comparison.

The main result, observed in figure 3.28, is that amplification values of stations located at the vertical of the edges decreases and that a modification of the amplification values occurs on the edges, especially in the case of an incidence angle of 60°.

Regarding the frequency content, as already noticed, some heterogeneities are present in the center part of the Vétroz and Bramois profiles due to the presence of harmonics, whereas the frequency curve behavior at the edges is controlled by the limited frequency range under study (§ 3.3.5.1)

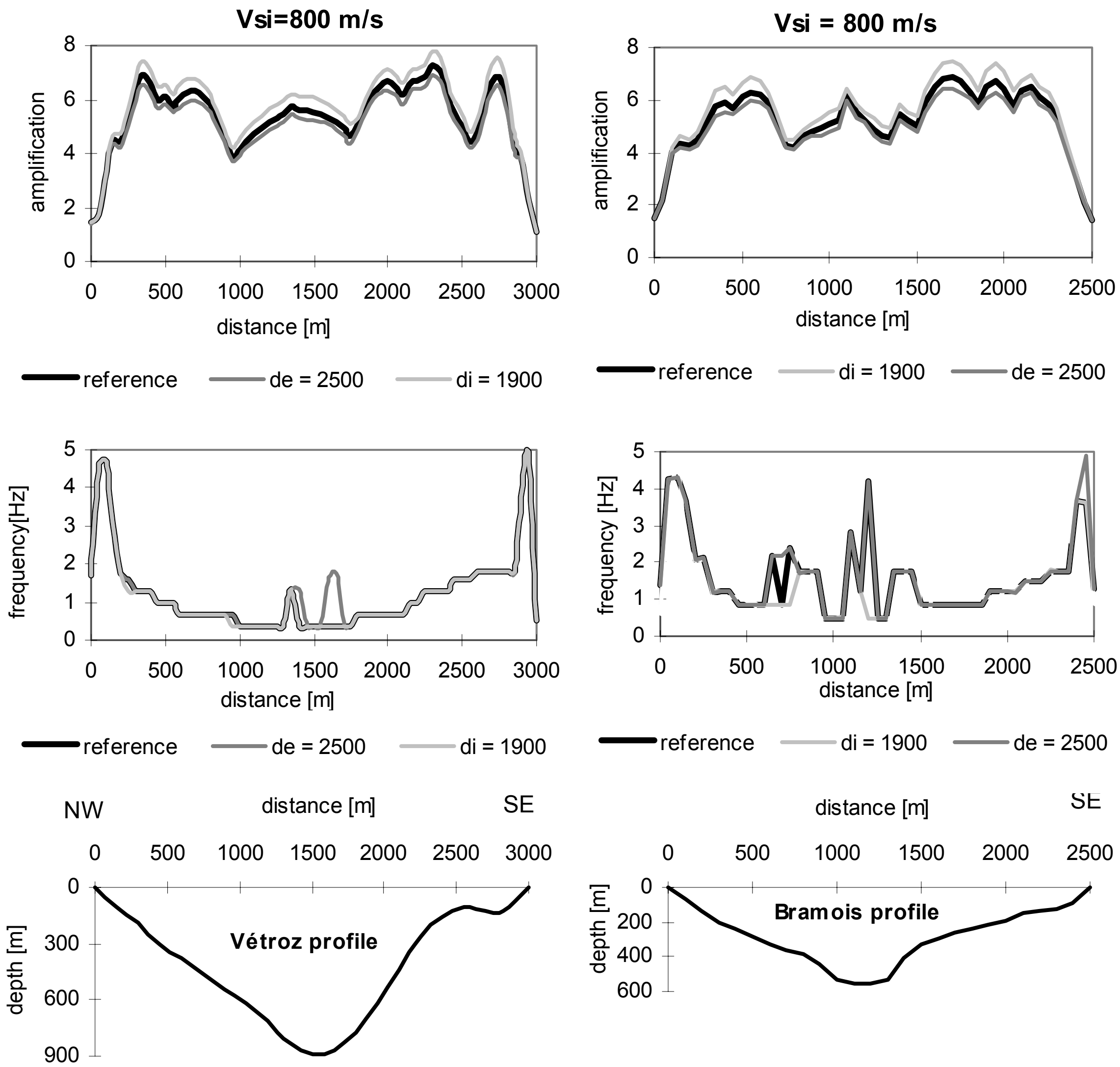

Figure 3.27. Variation of density in order to test the sensitivity of the 2D modeling. Case of the Vétroz and Bramois profiles using a shear-wave velocity for the sedimentary filling of 800 m/s.
Figure 3.27. Variation de la masse volumique afin de tester la sensibilité du modèle 2D. Cas de Vétroz et de Bramois pour une vitesse d'onde S du remplissage sédimentaire de 800 m/s.

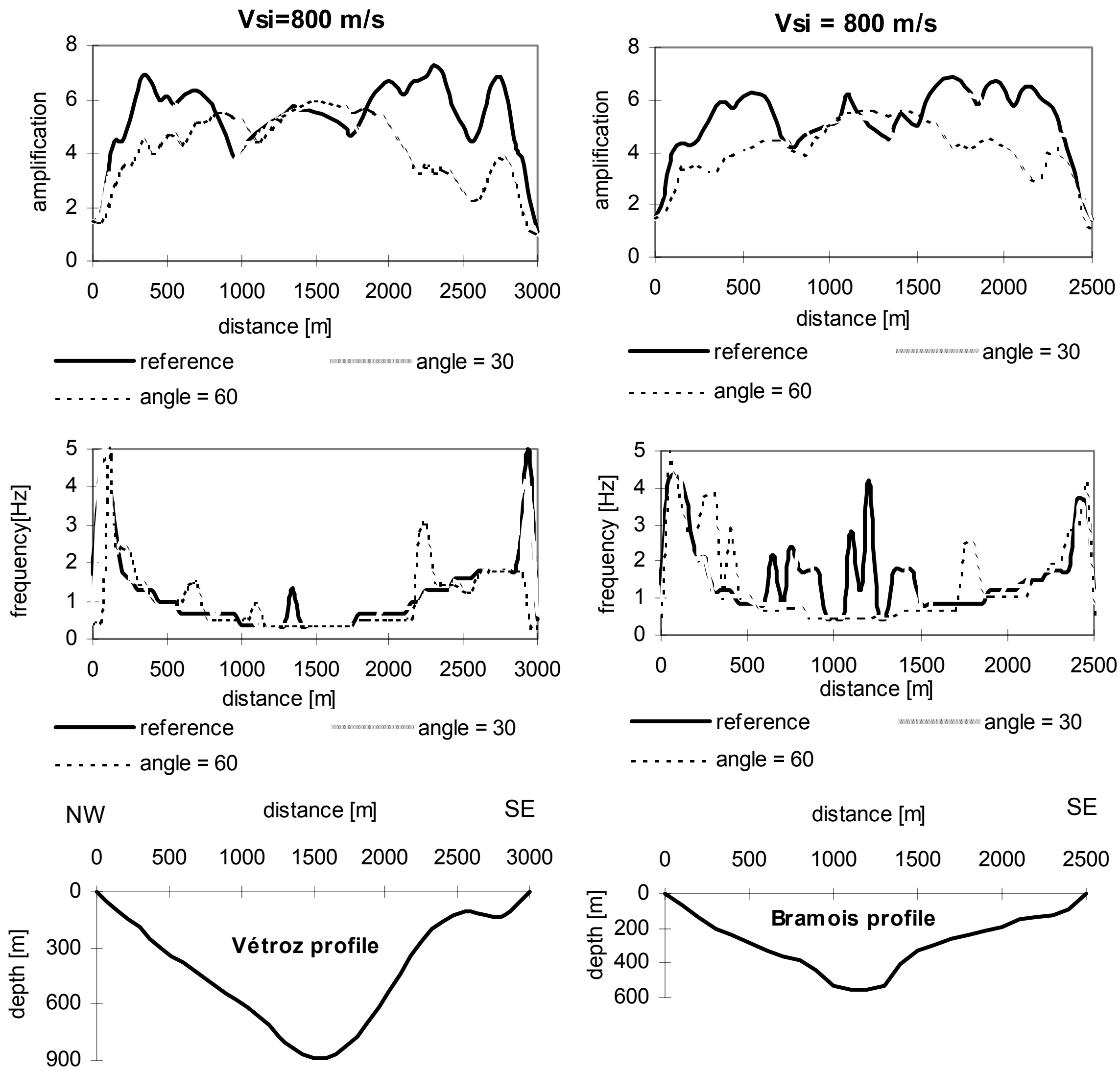

Figure 3.28. Variation of incidence angle in order to test the sensitivity of the 2D modeling. Case of the Vétroz and Bramois profiles using a shear-wave velocity for the sedimentary filling of 800 m/s.
Figure 3.28. Variation de l'angle d'incidence afin de tester la sensibilité du modèle 2D. Cas de Vétroz et de Bramois pour une vitesse d'onde S du remplissage sédimentaire de 800 m/s.

Looking at the fundamental resonant frequency (figure 3.29), the interesting feature is the unchanged position regardless the impedance contrast and the incidence angle as pointed out by Bard & Bouchon (1985). However the curve at the fundamental frequency takes different shape between stations located on the left side (e.g. stations a, b) and the right side of the valley (e.g. station c, d). This is due to the asymmetric geometry of the valley which induces differences on the seismic response, especially when oblique incidence angles of wave are used.

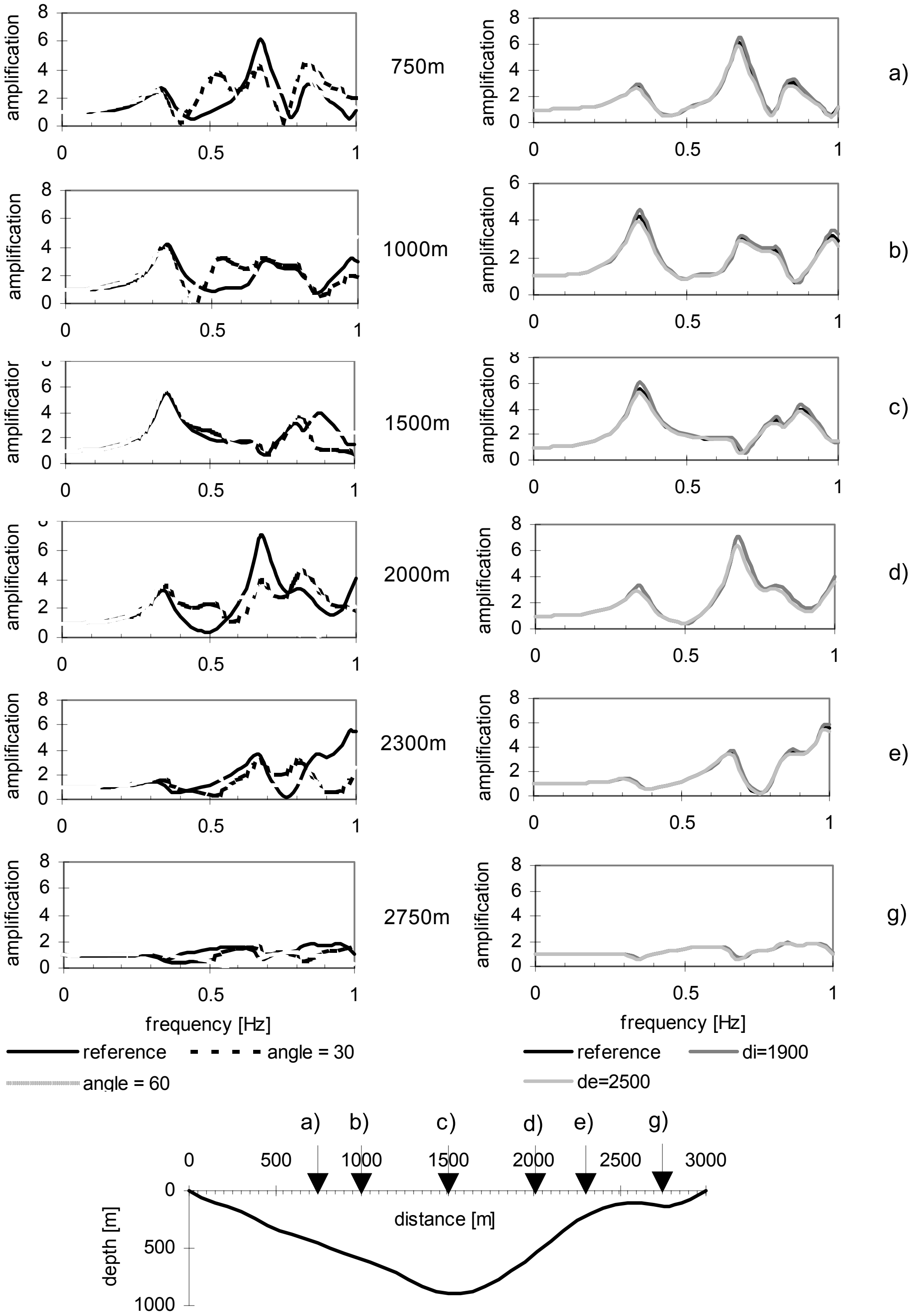

Figure 3.29. Effects of incidence angle (left side) and density (right side) in the SH case. The results are expressed in terms of spectral amplification functions for several stations. The display is limited to 1 Hz in order to have a better resolution on the fundamental frequency position.

Figure 3.29. Effets de l'angle d'incidence (à gauche) et de la masse volumique (à droite) pour une onde SH. Les résultats sont exprimés en terme de fonctions d'amplification spectrale pour différentes stations. La limite d'affichage en fréquence est de 1 Hz afin d'avoir une meilleure vision de la position de la fréquence fondamentale.

3.3.5.3 Uncertainty related to the treatment of the seismic reflection data

The 2D modeling is based on profiles obtained by high-resolution reflection acquisition. The treatment of seismic reflection data follows a multiple step processing. Among them, the migration of data and the choice of stacking velocities are the procedures having the more influence on the final result. Migration consists on correcting the data so that they correspond to the associated position of reflection or diffraction points at depth. It is an important step especially in case of non horizontal layers. Stacking velocities are velocities chosen to allow the seismic traces to be combined as good as possible (Sheriff & Geldart, 1995). These velocities might not correspond exactly to the real velocity of the layer but they are in the same range.

The Vétroz profile has been the subject of three subsequent treatments. The first interpretation of the geometry of the basement was done on the migrated section using the stacking velocity for the depth conversion (Pugin & Marchant, 1992). The second interpretation, which has been used in this part of the work, was based on seismic modeling. The procedure is to compare the interpretation resulting from the processed, stacked and migrated seismic data with a model obtained with simulation of shot records. Then the values of depth and velocity are modified until the best-fit between the model and the field processed data (Pugin et al. 1997) is obtained. The third interpretation is based on a new migration of the seismic profile data (Pugin, personal communication).

The three subsurface geometry of the valley and the associated simulated seismic response are shown in figure 3.30. The modeling parameters are the same as those described in table 3.15.

The following features can be extracted :

- a slight modification on the geometry of the shoulder on the right side of the Vétroz profile modifies the amplification pattern. If the shoulder is accentuated enough (2nd interpretation versus 3rd interpretation) it will induce a distinct amplification pattern;
- the slope gradient attenuation on the right side modifies the amplification pattern, inducing a “large band” effect;
- the displacement of the deepest part to the left (see 3rd interpretation) provokes a shift in amplification and frequency value distribution.

These results show the importance of the basic information in seismic response analysis and zonation. It also demonstrates the sensitivity of the maximum amplification distribution and its associated frequency on the subsurface geometry.

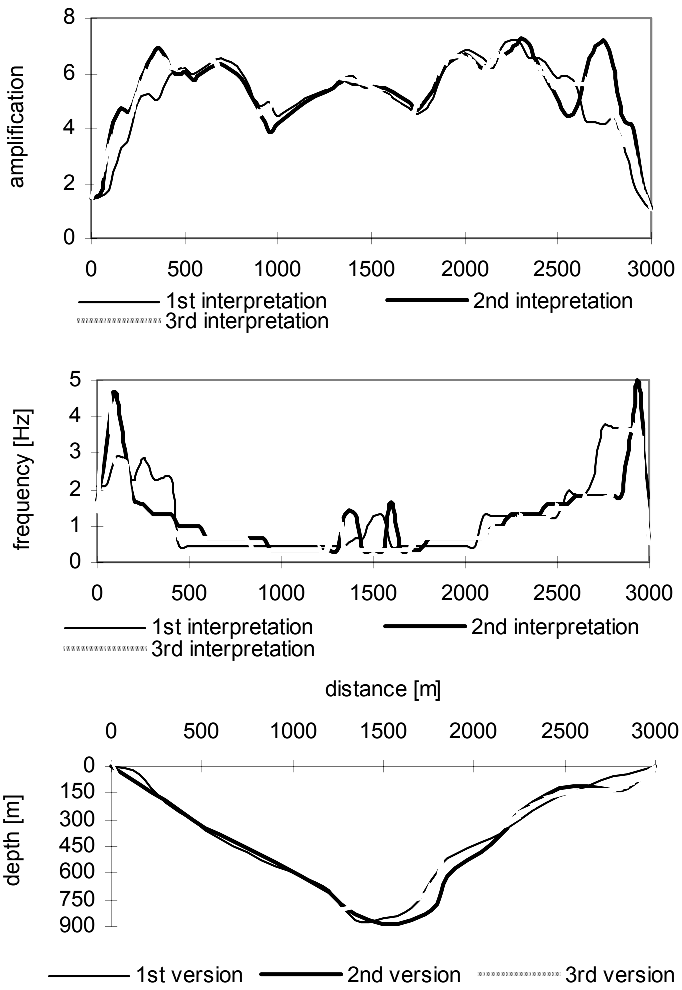

Figure 3.30. 2D modeling comparison between the three basement geometry interpretations of the Vétroz profile.
Figure 3.30. Comparaison des simulations numériques 2D entre les trois interprétations de la géométrie du soubassement du profil de Vétroz.

3.4 An attempt to evaluate the effect of surficial layers

Local seismic response is not only influenced by the subsurface geometry but also by the presence of surficial layers characterized by varying physical properties. As this 2D modeling program does only take into account homogeneous layers, an indirect way has been used to by-pass this difficulty. The procedure consists to combine a 2D transfer function with the one obtained using a 1D model as it allows to take into account several layers. This operation is possible when working in the frequency domain. The result is only an approximation, but gives an idea on the possible influence of surficial layers on seismic response. The procedure is the following (Bard & Chávez-García, 1993; Fäh, personal communication) :

1. taking the station located in the central part of the valley as this station is considered to be the least affected by lateral heterogeneities,
2. computing the 2D transfer function to obtain the response of the homogeneous model and the 1D transfer function for the surficial layers overlaying a half-space having the characteristics of the homogeneous model,
3. multiplying the resulting 1D and 2D transfer functions.

This procedure has only been applied on the Vétroz profile as superficial borehole data (S1, S2, S3; Bureau d'études géologiques SA, 1994) were available in proximity of the center part of this profile. These boreholes gave information on the lithology and thickness of surficial layers up to 15m.

In this procedure, the surficial layers are simplified into two specific layer, one which is dominated by silt and the second one by sandy-silty gravel. The seismic velocities were attributed based on the work of Burri (1995).

As the impedance contrast is an important factor, two shear-wave velocities have been used for the "deep" layer, 400 m/s and 800 m/s. Moreover as the borehole logs show that the thickness of the surficial layers is varying, this element has also been tested.

The parameters used in this application are described in table 3.31. The 2D modeling parameters remain unchanged. Graphs are displayed in figures 3.32 and 3.33.

The following points can be noticed :

- Surficial layers have an impact essentially on the amplification value at higher frequencies (> 1.5Hz). The impact is more important when the impedance contrast is higher between the surficial layers and the underlying one.
- The thicker is the low-velocity layer (130 m/s), the higher is the amplification value, going from 15 to 20 in the case of Vs=800 m/s.

2D modeling parameters

	Vp [m/s]	**Vs [m/s]**	**ρ [kg/m^3]**	**Q**
Sedimentary deposit	2050	400 / 800	2100	50
bedrock	4000	2200	2670	100

1D modeling parameters

thickness [m]		**Vp [m/s]**	**Vs [m/s]**	**ρ [kg/m^3]**	**Q**
2.4 (a)	4.85 (b)	300	130	1300	15
16.4 (a)	10.15(b)	1200	250	1800	15
half space		2050	400 / 800	2100	50

Table 3.31. Parameters applied for the 1D and 2D modeling.
Tableau 3.31. Paramètres employés pour la modélisation 1D et 2D.

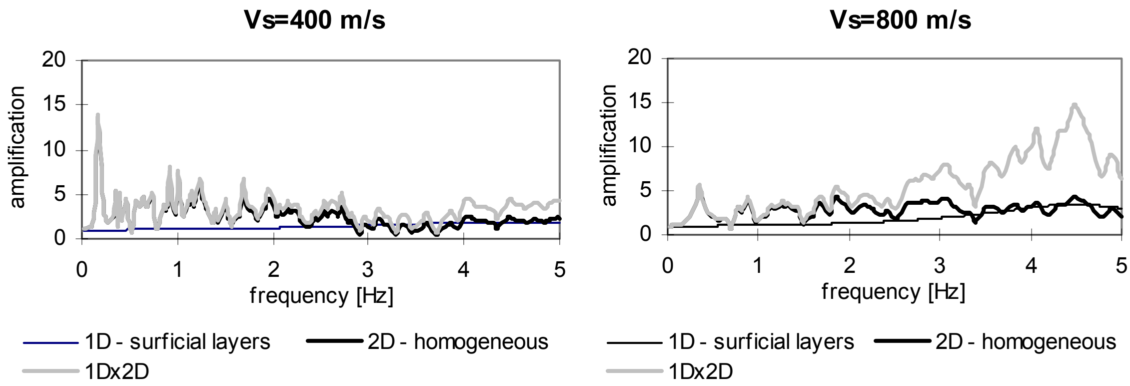

Figure 3.32. Influence of surficial layers on the amplification curve, case (a).
Figure 3.32. Influence des couches superficielles sur la courbe d'amplification, cas (a).

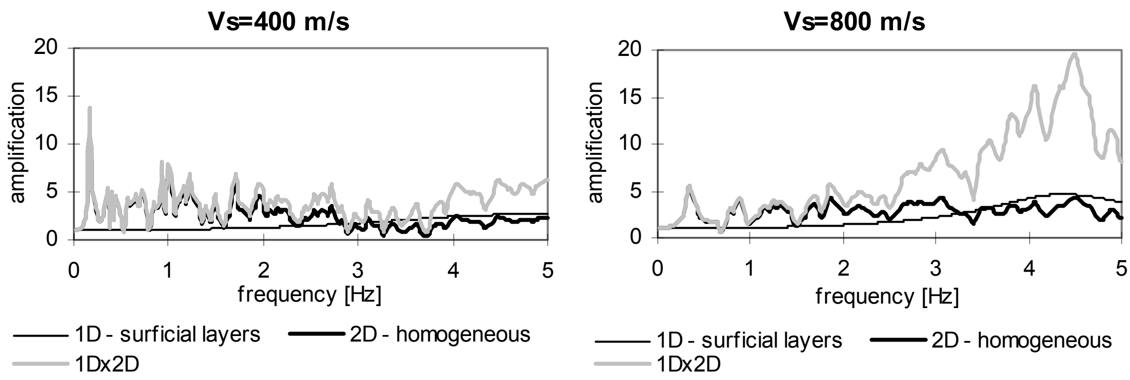

Figure 3.33. Influence of surficial layers on the amplification curve, case (b).
Figure 3.33. Influence des couches superficielles sur la courbe d'amplification, cas (b).

3.5 Conclusions

The presence of unconsolidated material overlaying a harder rock induces an amplification phenomenon. In order to take into account the role of the subsurface geometry on the amplification distribution, the valley response has been studied under a two dimensional point of view using two profiles, Vétroz and Bramois, submitted to a horizontally plane polarized shear wave (SH).

The 2D numerical simulation is based on a homogeneous medium which is a simplification of the natural environment. However it allows to consider the influence of the irregular (non-plane) geometry of the interface between the sedimentary deposit and the basement on site effects, especially on the local variation of soil amplification.

The comparison of the 1D and 2D numerical simulation shows that the finite lateral extension exerts an influence on the maximum amplification pattern and its level as well as on the frequency, showing higher values in the 2D case.

2D modeling has shown that the controlling factors of the maximum amplification distribution across the valley are :

- the asymmetry of the valley characterized by gentle and steeper slopes,
- the slope gradient, which depends on the bedrock variation over the distance,
- the presence of a shoulder on the edge which generates its own seismic response, if the structure is sufficiently accentuated,
- the incident wave angle.

The level of the maximum amplification is related to the seismic impedance contrast between the sedimentary filling and the surrounding rock. A modification of the density in a reasonable range does not imply a strong influence on the amplification level as the shear-wave velocity does.

Concerning the frequency, the major features are :

- the fundamental resonant frequency does not change its position over the entire profiles, whatever the incidence angle. This is the result of a 2D resonance phenomenon which occurs because the two profiles are characterized by a shape ratio and a velocity contrast high enough to provoke this phenomenon,
- the frequency value of the maximum amplification depends on the shear-wave velocity contrast, the value increases when the shear-wave velocity of the sedimentary deposit increases, therefore diminishing the velocity contrast and on the maximum thickness of the deposit, the frequency value increasing when the thickness decreases.

2D modeling can be considered as being an efficient investigation tool for seismic response analysis in elongated alpine valleys characterized by thick and young Quaternary deposit, irregular geometry, deep slopes and a strong impedance contrast.

4 MICROZONATION OF THE SION AREA

4.1 Introduction

In chapter 3, it has been demonstrated for the Vétroz and Bramois profiles that the maximum relative amplification varied with the subsurface geometry and that it was possible to distinguish different zones. Based on these results, an attempt has been made to use 2D modeling for microzonation purpose. This approach is applied in the Sion area.

The study area is about 10 km^2. This zone was divided into 15 regularly spaced profiles and modeling was processed on each of these profiles. The resulting maps are compared with those obtained by the H/V ratio technique. In parallel, a temporary seismic strong motion network has been installed with stations located on specific points in order to record seismic events.

All relevant data have been geographically referenced and integrated into a Geographical information system (GIS).

4.2 Geology

4.2.1 Quaternary deposit

The Sion area is located between the two previously analyzed profiles (chapter 3). It can reasonably be estimated that the deposits in the area are continuous and therefore also present in the area under study.

The interpretation of the Bramois seismic profile, the closest profile to the Sion area shows a Quaternary sedimentary deposit in the Rhône valley composed, after Besson et al. 1993, by (from top to bottom) :

- 30 m of post-lacustrine deposit (gravel, sand, silt),
- 150 m of deltaic deposit (sandy gravel and silt alternance),
- 150 m of glaciolacustrine deposit (gravel, sand, silt),
- 90 m of meltout and reworked till (boulders and fine particles),
- 140 m of subglacial deposit (gravel).

The interpretation of the Vétroz profile gives similar units (Pugin & Marchant, 1992; Marchant & Stampfli, 1993).

Regarding the post-lacustrine deposit in the Sion area, 110 indexed boreholes (Ornstein, 1995) describe the type of deposit and its origin. The depth does not exceed 60 m. The surficial deposit is therefore composed of :

- alluvial fans fed by the Sionne and the Borgne river, characterized by sand;
- alluvium from the Rhône and the Borgne river, mainly composed of sandy gravel with stones and boulders;
- flooding deposits, represented by sandy silts.

In engineering geology several tests can be performed to characterize the soil conditions. One of those tests is the *standard penetration test* (SPT). It consists of driving a sampler into the soil at the bottom of a borehole with a hammer by repeated blows. This hammer is released from a height of 76 cm. The number N of blows necessary to achieve the last 30 cm of penetration indicates the penetration resistance of the sediment (Kramer, 1996). The higher the N value, the more resistant is the sediment and therefore suitable for infrastructures.

In the Sion area SPT measurements were made on 34 of the 110 boreholes. Their location is given in figure 4.7. N values in regard with their depth of acquisition and type of deposit were extracted from the borehole database developed at the National Road Office (state 1997). The distribution of the SPT measurements in function of the lithology and the N values is given by histograms in figure 4.1. It can be noticed that most of the SPT are measured in gravel and sandy gravel (64 data) and that N values are mostly comprised between 10 and 50 blows per 30 cm, but that high values (> 50) are also observed.

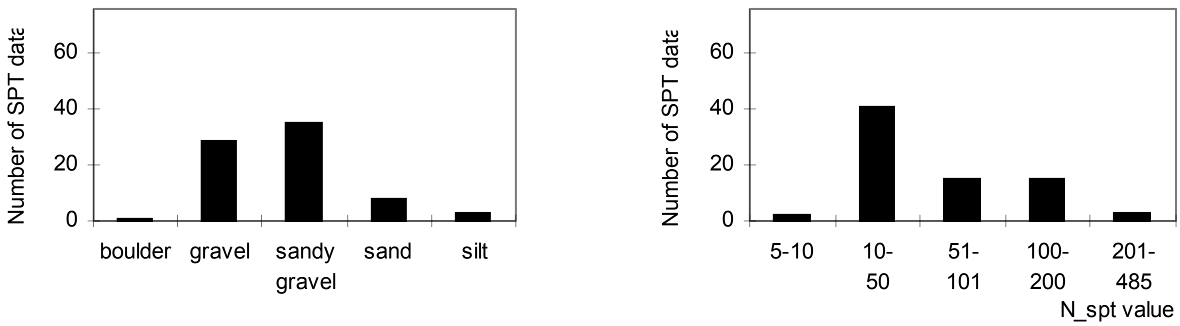

Figure 4.1. Distribution of the SPT data as a function of lithology and N-value range.
Figure 4.1. Répartition des données SPT en fonction de la lithologie et d'intervalle de N.

Some authors (e.g. Ohta & Goto, 1978; Imai & Tonouchi, 1982) have developed empirical relationships that correlate SPT measurements, done in near surface materials similar to those in the Sion area, and the shear-wave velocity. Ohta & Goto (1978) have defined an equation that correlates the shear-wave velocity to the *N* parameter and its depth of acquisition *H* as follows :

$$Vs = 61.62 * N^{0.254} H^{0.222} \quad (1)$$

with a correlation coefficient = 0.82.

The distribution of N values as a function of acquisition depth in the Sion area is shown on figure 4.2. As values higher than 50 are generally considered as not relevant (Imai & Tonouchi, 1982; Injectobohr, written communication), only N values between 5 and 50 have been used in equation (1). The purpose of this investigation is to estimate the distribution of the shear wave with depth. Therefore a fitting curve as a function of depth (figure 4.3) is defined from the shear-wave values derived from equation (1). The resulting equation is as follows :

$$Vs = 125.13*H^{0.27} \quad (2)$$

for N data between 5 and 50 (43 values), with a correlation coefficient = 0.71.

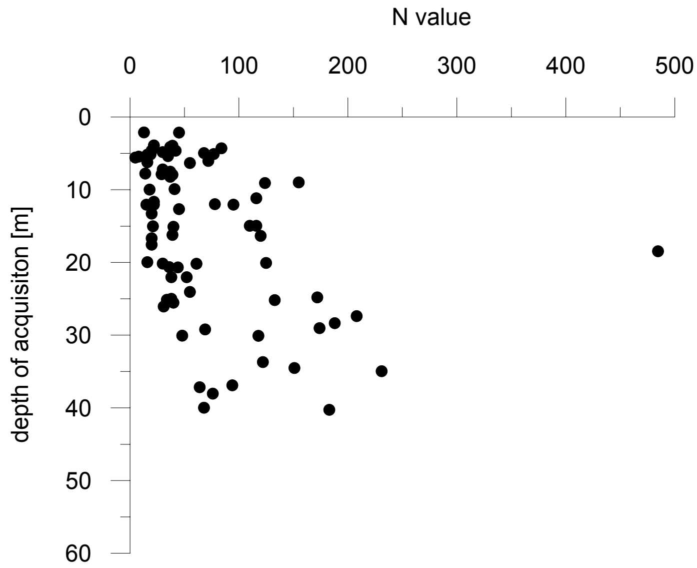

Figure 4.2. N-value distribution in function of depth of acquisition.
Figure 4.2. Distribution des valeurs N en fonction de leur profondeur d'acquisition.

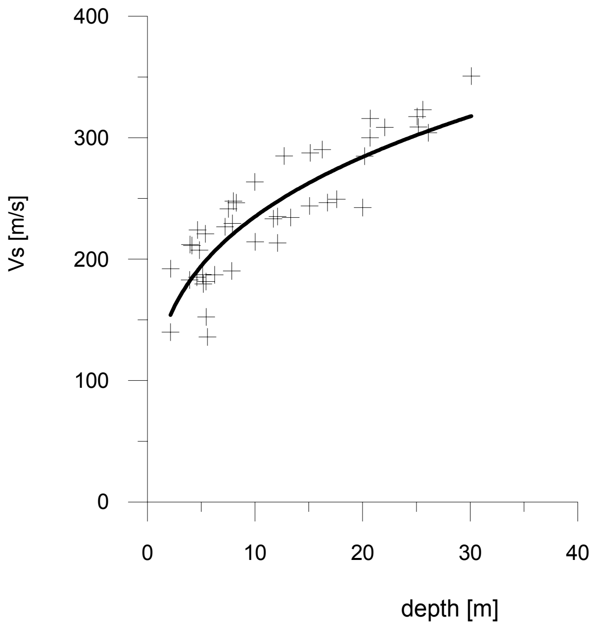

Figure 4.3. Shear-wave velocity values derived from the SPT measurements. The solid line represents the fitting curve.
Figure 4.3. Valeurs d'onde S dérivées des mesures SPT. La ligne solide indique la courbe d'ajustement.

Shear-wave velocity values obtained in the 1994 seismic campaign (Burri, 1995) and those derived from SPT (equation 2) are in the same range (table 4.4). But the comparison shows that values derived from SPT measurements are generally higher. Whatever the data, no relation between shear-wave velocity and depth can be found for the entire depth of the Quaternary deposit in the Sion area. Indeed extrapolation based on SPT measurements cannot be done to more than 80 meter depth as no information is available at higher depth. The seismic campaign does not deliver values at higher depth than 176 m, on the other side.

Shear-wave velocity with seismic refraction[(a)] and reflection[(b)]		**value derived from SPT measurements**
depth [m]	**velocity [m/s]**	**velocity [m/s]**
2.3[a]	130[a]	157
2.6[a]	160[a]	163
8.5[a]	250[a]	225
16[a]	270[a]	267
32.5[b]	260[b]	325
49[b]	280[b]	363
71[b]	340[b]	402
176[b]	420[b]	/

Table 4.4. Comparison between shear-wave velocities obtained by seismic refraction and reflection and derived from SPT measurements.
Tableau 4.4. Comparaison entre les vitesses d'onde S obtenues par sismique réfraction et réflexion et celles dérivés des mesures SPT.

4.2.2 Surface and subsurface topography

The surface topography of the Rhône valley is often disturbed by lateral alluvial fans, especially in the central and upper part of the valley (Sion - Brig). These alluvial fans can either spread out partially or entirely on the valley.

The relief of the Sion area with its two alluvial fans, the Sionne and the Borgne one is displayed in figure 4.5. The data come from the Digital elevation model (DEM25) of the Swiss federal office of topography. This model is characterized by a grid of 25m by 25m.

It can be seen in figure 4.5 that the Sionne alluvial fan shows a more accentuated morphology in comparison with the Borgne one. This element can be better appreciated on figure 4.6 which shows two elevation profiles, the p6 being taken in the area influenced by the Sionne fan structure and the p14 in the zone of the Borgne fan.

An ideal case would be to consider the lateral morphology as it is in the 2D modeling. But the program used does not allow to take such configuration into consideration. Therefore an alternative solution has been introduced as described in the § 4.3.

Regarding the subsurface topography, the information has been obtained using the work of Besson et al. (1993). These authors have derived contour level of the bedrock altitude from the available seismic profiles between Martigny and Bramois, producing an analog map at a scale of 1:50'000. This map was then digitized and rasterized with a resolution of 25m by 25m, giving a digital elevation model for the bedrock.

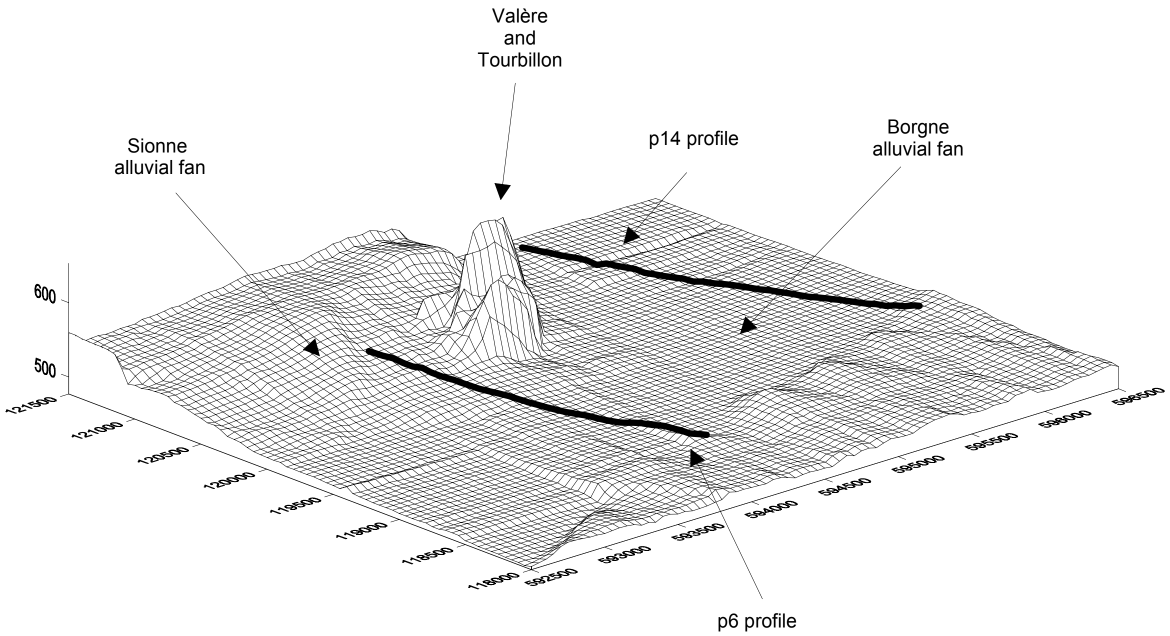

Figure 4.5. Surface topography of the Sion area derived from the DEM25 (OFT, 1993). The vertical scale is exaggerated by a factor of 4.
Figure 4.5. Topographie de la région de Sion dérivée du MNT25 (OFT, 1993). L'échelle verticale est exagérée d'un facteur de 4.

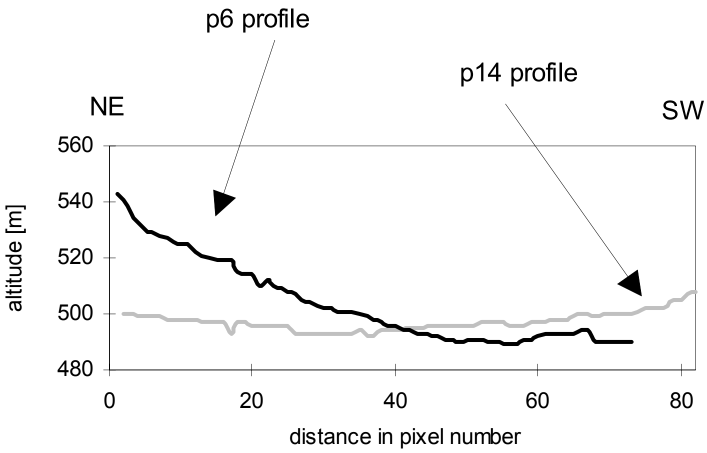

Figure 4.6. Elevation values derived from the DEM25 (OFT, 1993) for the 2D modeling p6 and p14 profiles.
Figure 4.6. Données d'altitude obtenues du MNT25 (OFT, 1993) pour les profils de modélisation 2D p6 et p14.

The deposit thickness (figure 4.7) was obtained from the difference between the surface altitude from the digital elevation model (DEM25; OFT, 1993) and the bedrock altitude. The maximum thickness is about 600 m.

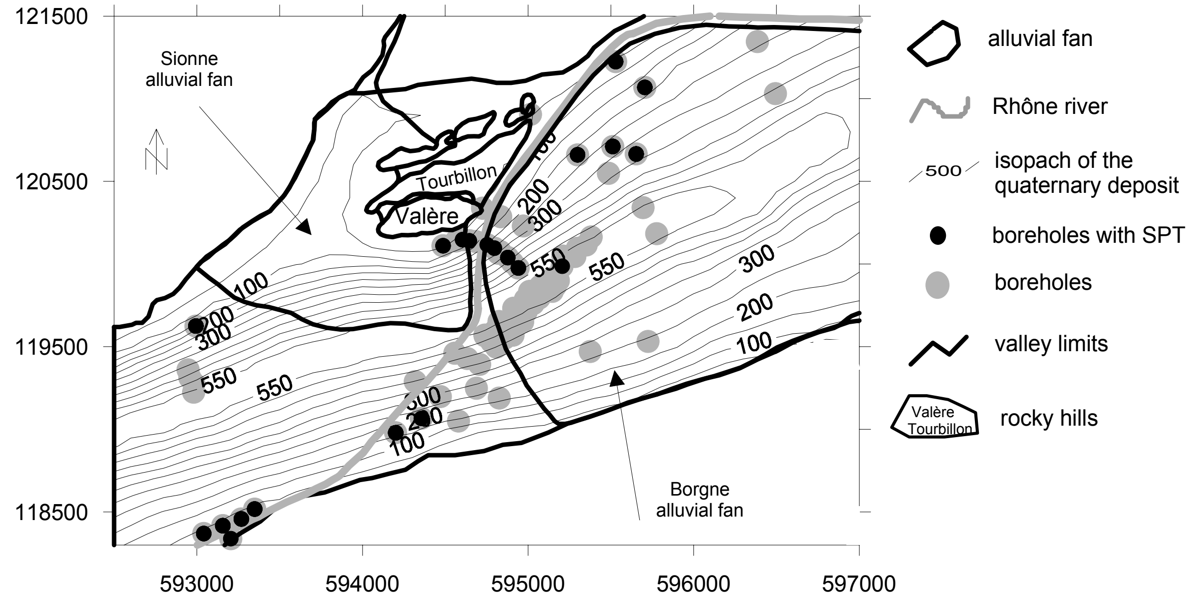

Figure 4.7. Isopachs of the Quaternary deposit and the main geological features (alluvial fans, hills).
Figure 4.7. Isopaches du dépôt Quaternaire et des principales structures géologiques.

4.3 2D simulation

In order to apply the 2D modeling for zoning purposes, the chosen area was divided into 15 profiles (figure 4.8) perpendicular to the valley axis. The distance between each profile is 250 m and the observation points at the surface are positioned every 50 m.

These profiles were first drawn on an analog map, then digitized. The data on the Quaternary thickness layer were extracted using the module PROFILE of IDRISI. This module requires a vector line and the raster image from which the data will be extracted. Then it does a distance calculation between the two extremities of the vector line to determine the number of pixels that will be processed. The distance calculation is based on the following formula :

$$D^2 = (\max X - \min X)^2 + (\max Y - \min Y)^2$$

The number of pixels will depend on the resolution of the raster image.

The result gives the data value and its location along the profile. This procedure was applied for the 15 profiles.

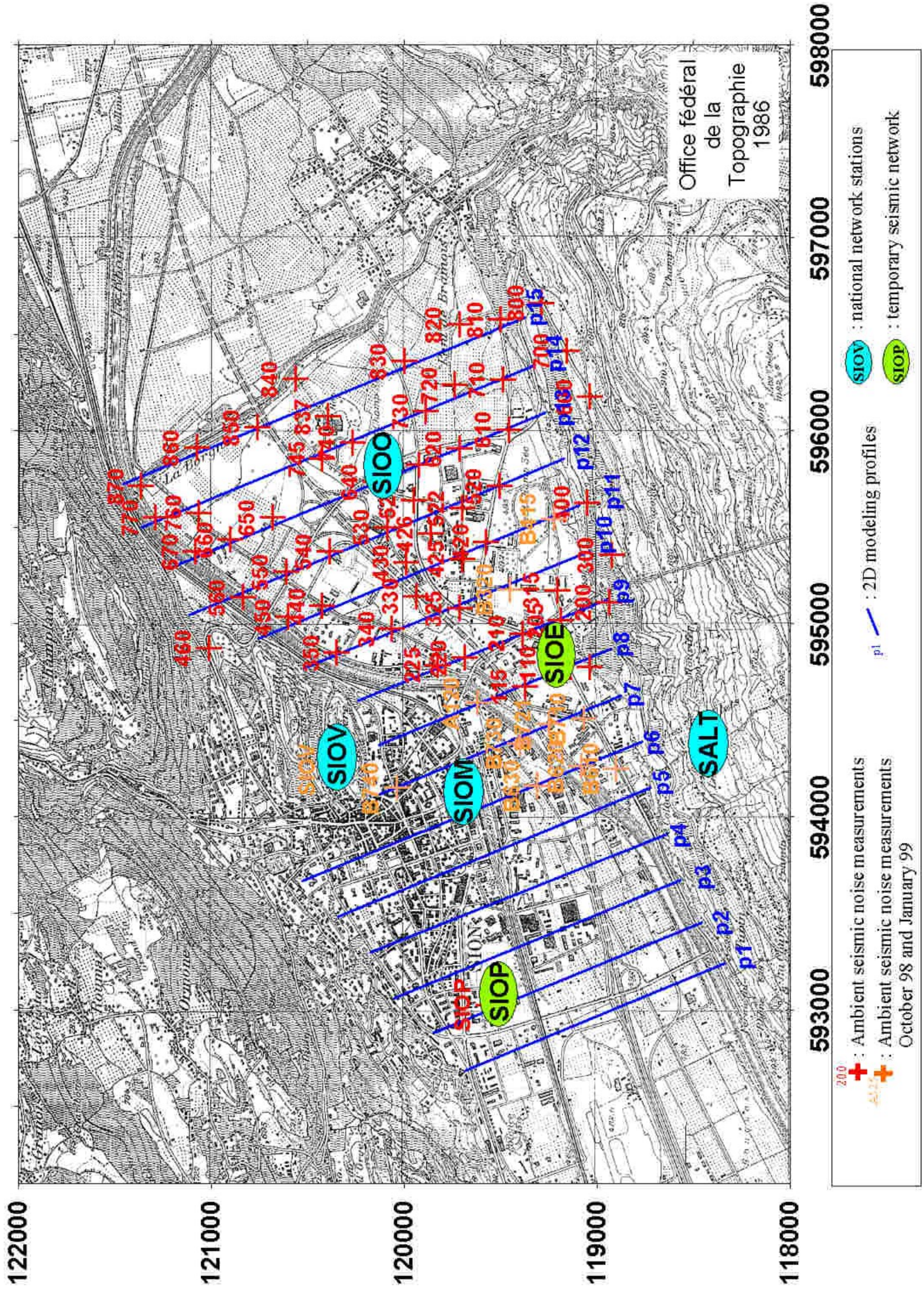

Figure 4.8. Location of the different methodologies applied in the Sion area

4.3.1 Profile characteristics

As it has already been mentioned, the alluvial fan, especially the Sionne one, on which the town of Sion is mostly built, must be considered explicitly. This element cannot be integrated as it is into the modeling program, since only flat surfaces can be considered. Moreover this deposit is not totally distributed on the valley but also partly recovers the valley flanks. It was therefore necessary to :

1. determine a reference altitude in order to get the valley-flank boundary,
2. correct the profiles in order to partly consider the sediments of the alluvial fan. That will reinforce the thickness of the deposit on the concerned side as shown by figure 4.9. The profiles concerned by this correction are the p4, p5 and p6 (figure 4.8).

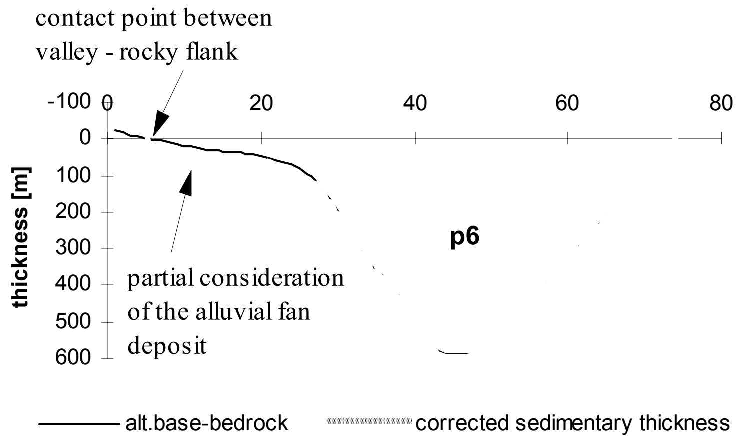

Figure 4.9. Presentation of the alluvial fan accounted for into the 2D modeling. Example of the p6 profile.
Figure 4.9. Présentation de la prise en compte du cône de déjection dans la modélisation 2D. Exemple du profil p6.

Before modeling, all the profiles have been resampled to obtain an information on thickness each 100 m.

Table4.1. It can be noticed some geometrical variations, which modify the symmetry, and the presence (e.g. profile 6) or absence of a flat shoulder (e.g. profile 15). These two elements will have an influence on the seismic response as it has already been demonstrated on the Vétroz profile and will be confirmed in this case.

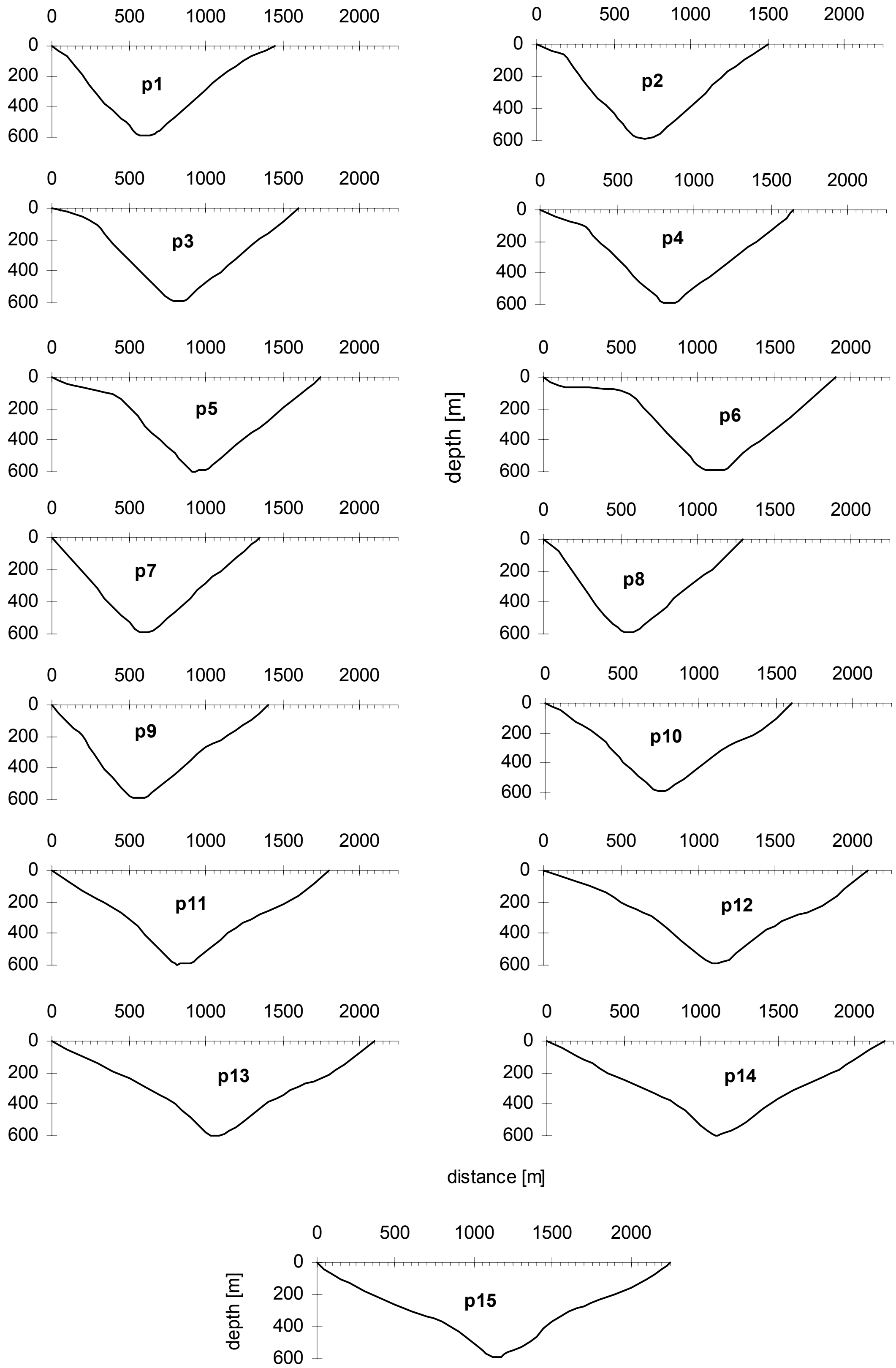

Figure 4.10. The subsurface geometry of the Quaternary deposit for the 15 profiles submitted to 2D modeling from downstream to upstream.

Figure 4.10. Géométrie de la subsurface du dépôt sédimentaire quaternaire pour les 15 profiles destinés à la modélisation 2D, de l'aval vers l'amont.

The length and maximum depth of these profiles, which are key parameters for the estimation of the shape ratio, are summarized in table 4.11. It can be seen that the depth does not vary significantly.

Profile	**1**	**2**	**3**	**4**	**5**	**6**	**7**	**8**	**9**	**10**	**11**	**12**	**13**	**14**	**15**
Length [**km**]	1.45	1.5	1.6	1.65	1.75	1.9	1.35	1.3	1.4	1.6	1.8	2.1	2.1	2.2	2.25
Depth [**m**]	587	586	587	592	594	593	594	589	591	591	592	592	595	595	589

Table 4.11. Geometrical parameters of the 15 profiles.
Tableau 4.11. Paramètres géométriques des 15 profils.

4.3.2 Physical properties

As the geological interpretation of the high resolution seismic reflection profiles Vétroz and Bramois does not show major differences in lithology and as the depth in the Sion area is not varying significantly, the mean physical properties for each profile can be assumed to be identical. Parameter values are summarized in table 4.12

	Vp [**m/s**]	**Vs** [**m/s**]	**Poisson's ratio**	ρ [**kg/m³**]	**Q**
filling	2050	800	0.41	2100	50
bedrock	5000	3000	0.22	2670	100

Table 4.12. Physical parameters used for the 15 profiles.
Tableau 4.12. Paramètres physiques des 15 profils.

P velocities and densities values represent average values compiled from different work done in the Rhône valley (see Appendix B). The P wave velocity for the bedrock is increased up to 5000 m/s as values equal to 5000 m/s or even higher have been found for the bedrock (Maurer, 1993; Pugin, personnal communication). The S wave velocity is obtained using the Vp/Vs ratio found by Maurer (1993) in the Wildhorn area on the basis of microearthquakes. This ratio is equal to 1.67 for the first kilometer which gives a Poisson's ratio equal to 0.22. This indicates a relatively hard bedrock. Usually this value is assumed to be equal to 0.25 for an ideal rock.

For the sedimentary filling, the mean value of 800 m/s is preserved as this value is in the range of velocity used to characterize quaternary deposit in an Alpine context (see chapter 3, § 3.3.3). Neither SPT data nor shear-wave values obtained from seismic profiles allowed to determine the shear-wave velocity evolution with depth on the entire depth of the sedimentary filling (see § 4.2.1).

4.3.3 Results

This modeling approach focused on shear waves as they are primarily responsible for damages on the built environment. Therefore each profile was submitted to a vertically incident plane wave of SH (horizontally polarized shear wave) and SV (vertically polarized shear wave) types in the profile plane (azimuth = 0).

The total length considered in the simulation is three times the length of the irregularity and the wavelength is divided into 5 segments.

Concerning the frequency, it is usually considered in engineering seismology that the frequency range of interest goes up to 10-15 Hz. In the simulation, the upper limit has been fixed to 5 Hz. The reason is the limitation of the computer capacity in regard with the chosen parameters (e.g. simulation point each 50m, three times the length of the profile, 5 segments per wavelength). However this frequency range (0-5Hz) covers the fundamental resonance frequency of structures such as bridges, pipelines, tanks and for buildings with 2 floors and higher, based on the rule of thumb (Hays, written communication) :

$$T_b = \frac{N}{10} = \frac{1}{f_0}$$

with T_b being the period of the building ($_b$), N the number of stories and f_0 the fundamental frequency.

The results are expressed in terms of amplification curves. For an incident SH wave, the amplification is obtained by dividing the displacement amplitude at the surface by the response of the bedrock in absence of sedimentary filling, i.e. by a factor of 2.

In the case of a SV incident wave, the seismic response observed on the surface is given on the x and z axis as this type of wave is converted into P waves (z component) and generate Rayleigh wave when interacting with surficial deposit. Therefore the response of the bedrock in absence of sedimentary filling is varying with the incidence angle and differently for the x and z component. When the SV wave is vertically incident to the structure, the amplitude is equal to 2 for the x component and 0 for the z component as this component is not triggered in the presence of a flat structure (without sedimentary filling).

The amplification factor will be obtained by the ratio between the total amplitude vector on surface and on bedrock, as follows :

$$A = \frac{\sqrt{Ux_s^2 + Uz_s^2}}{\sqrt{Ux_b^2 + Uz_b^2}}$$

with $Ux_{s,b}$ being the movement amplitude on the x axis for the structure (s) and the bedrock (b) and $Uz_{s,b}$ being the movement amplitude on the z axis for the structure (s) and the bedrock (b).

The comparison between the amplification functions of the 1D case and the 2D modeling (with a SH and SV incident waves) at different locations on the p6 profile are displayed in figure 4.13. The parameters used are described in table 4.10. One can noticed that this profile displays the same geometrical feature as the Vétroz profile (chapter 3), i.e. the presence of a shoulder, but on the opposite site. Except this shoulder, the seismic response pattern is representative for the others 14 profiles in the Sion area.

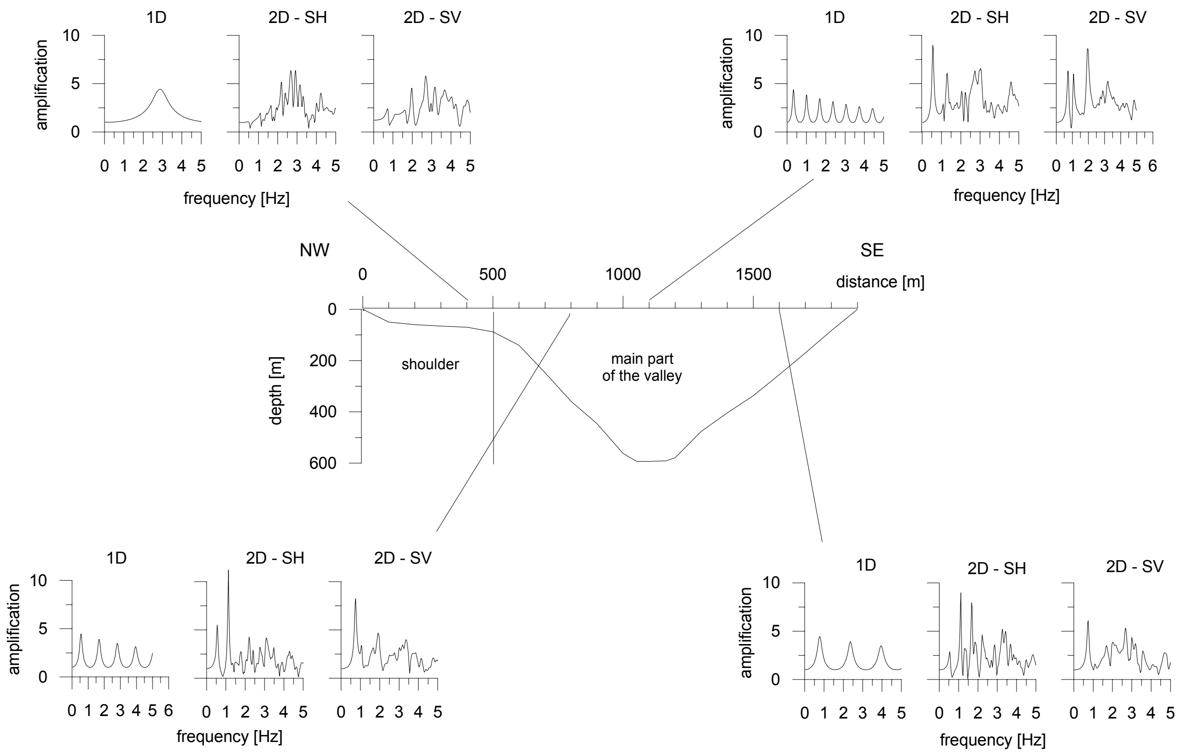

Figure 4.13. Amplification functions for 1D and 2D modeling of the p6 profile. The 2D fundamental frequency stays unchanged whatever the observation point location along the profile. The shoulder is an exception.
Figure 4.13. Fonctions d'amplification pour la modélisation 1D et 2D du profil p6. La fréquence fondamentale de résonance reste identique quelque soit la position de la station d'observation le long du profil. L'épaulement fait exception.

The main remark concerns the stability of the lowest resonant frequency, not only for the SH case but also for the SV case. As described in chapter 3, this stability is dependent on the shape ratio and the velocity contrast. If these parameters are high enough, the valley can develop a 2D resonance. In this case, the velocity contrast ($Vs_{bedrock}/Vs_{sed}$) is equal to 3.75 and the shape ratio varies between 0.57 to 0.93 as shown in table 4.14. One can notice that the 2D intrinsic lowest resonance frequency value differs depending on the incident wave, being higher in the case of a SV wave. It also varies for each profile in function of the shape ratio. The lower the shape ratio, the lower is the fundamental frequency.

profile	**1**	**2**	**3**	**4**	**5**	**6**	**7**	**8**	**9**	**10**	**11**	**12**	**13**	**14**	**15**
shape ratio	0.93	0.80	0.77	0.76	0.75	0.74	0.84	0.86	0.83	0.79	0.70	0.65	0.62	0.58	0.57
f_0 [Hz] 2D - SH	0.60	0.575	0.575	0.575	0.575	0.55	0.60	0.60	0.60	0.575	0.55	0.525	0.525	0.525	0.50
f_0 [Hz] 2D - SV	0.80	0.775	0.775	0.75	0.75	0.75	0.80	0.825	0.80	0.75	0.70	0.675	0.65	0.65	0.625

Table 4.14. Relation between shape ratio and 2D fundamental frequency for SH and SV cases.
Tableau 4.14. Relation entre rapport de forme et la fréquence fondamentale 2D pour les cas d'une onde SH et SV.

It must be pointed out that a 1D model only gives one value for the fundamental resonance of a sedimentary structure submitted to a vertical incident shear wave. Therefore, knowing that the fundamental resonance of the soil can vary depending on the incoming wave, then the considered axis is of prime interest in analyzing the seismic response of infrastructure.

4.3.4 Microzonation based on 2D modeling

The maximum relative amplification factor and its corresponding frequency, which also represents the predominant frequency of the sedimentary filling at which the amplification is maximum, have been shown to be a more representative parameters of the seismic response in function of the location throughout the valley. As buildings have their own resonant frequency, and as damages are increasing when the building enters in resonance with the soil, it is important to know the predominant resonant frequency of the soil in order to further investigate the building.

In this work the maximum relative amplification and its corresponding frequency will be used as zoning parameters. Using the information given by the 15 profiles at regular intervals, zonation maps for the SH and the SV cases will be obtained.

For each site spectrum, on each profile, the maximum amplification value and its associated frequency have been extracted and georeferenced (see appendix C). Then using SURFER software a linear kriging interpolation was applied on amplification and frequency data separately. For every grid node, all the data points were used. But as the kriging interpolation is using distance weighting factors, the more distant points are carrying little weight comparing to the closest points. It therefore allows to emphasize the local variation. Moreover a preferred direction was incorporated in order to reinforce the weight of the data along the valley axis. The result is given through regular interpolated grid with a cell size of 25m.

This grid is then exported into the GIS software IDRISI to allow the classification on a raster. Before this, it was necessary to discard external false interpolated values. These false values are generated by the interpolation on the edges where data are missing. The correction is done through a masking procedure in order to establish an appropriate map. The procedure consists on applying a mask on the interpolated data, where the mask is a binary image with the value 1 attributed to the area of interest and 0 on the rest of the image. The multiplication of both images (the mask and the interpolated data) produces a map without the false values. Then the interpolated amplification values have been linearly classified in 6 classes for the SH case (table 4.15). For the incident SV wave, only the first 5 classes are present, because the maximum amplification reaches 9.

Class	Amplification range
1	1-2
2	2-4
3	4-6
4	6-8
5	8-10
6	10-12

Table 4.15. Classification of the maximum amplification values.
Tableau 4.15. Catégories de classification pour les amplifications maximales.

The frequency values for the SH and SV cases were classified in 5 non-linear classes (table 4.16) with the objective to mainly display the zones containing the lowest resonant frequency. The lowest resonant frequency is 0.5 for the SH case, and 0.625 for the SV case (see table 4.16). Therefore for better comparison between frequency zone distribution, the classification is based on the SH case.

Class	Frequency range for SH	Frequency range for SV

1	0.1-0.6(inclusive)	/
2	>0.6-1	>0.6-1
3	1-2	1-2
4	2-3	2-3
5	3-5	3-5

Table 4.16. Categories of classification for frequencies corresponding to maximum amplification.
Tableau 4.16. Catégories de classification pour les fréquences associées aux amplifications maximales.

Two maps are produced (figure 4.17 and figure 4.18) for each incident wave type (SH and SV) showing the capability of areas to amplify the ground motion to a certain level at specific frequency. In order to appreciate the Sion environment, maps have been superimposed on an aerial photography taken in 1992.

These maps display the frequencies at which the level of amplification is maximum based on the specified parameters. Both frequency maps show the same tendency, i.e. low frequency in the center of the valley and higher frequency toward the edges. This is coincident with the evolution of the deposit thickness, low frequency values corresponding to the deepest part of the Quaternary sedimentary filling in the middle of the valley and higher values to the thinner part at the rims. However it has to be noticed that the resulting maps are only available for the frequency range 0-5Hz. On the rims, maximum amplification can occur at higher frequency than 5 Hz.

The presence of a higher frequency content zone in the center part of the valley, on the SV map (figure 4.18), is related to the capture of harmonics as already observed in the case of a SH wave for the Vétroz and Bramois profiles (chapter 3, § 3.3.5.1). It can be mentioned that characterizing the sedimentary layer with a lower quality factor (i.e. higher attenuation capability) than the value used in the present case, may sufficiently reduce the amplification of the harmonics so that the fundamental frequency would be the predominant one. As a result, the higher frequency zone would disappear. Therefore further investigation on the attenuation behavior of the Quaternary deposit in the Rhône valley is of prime interest.

As already noticed the fundamental frequency value shifts toward higher value in the case of SV. This has a direct implication on building behavior as both components are inducing amplification at different frequency.

It can be argued that the microzonation map resulting from the SH case represents the upper boundary of the soil amplification capability, except for the frequency band between 0.6 - 1Hz, in which no specific investigation has been done on the level of amplification in case of an incident SH wave.

4.3.4.1 Correlation between maximum relative amplification distribution and thickness as well as slope gradient variations

Regarding the maximum amplification distribution, it may be interesting to compare it with the Quaternary thickness (figure 4.19a) and slope gradient variations of the bedrock. In order to do so the slope gradient image (figure 4.19b) is calculated using the SURFACE module of IDRISI. It is based on the formula (Collet, 1992) :

$$\text{slope gradient} = \sqrt{GC^2 + GL^2}$$

with *GC* = slope gradient in column and *GL* = slope gradient in line.

In the software IDRISI,

GC = DFDX / (n*p*r)
GL = DFDY / (n*p*r)

with *DFDX, DFDY* = derivative in x, in y, *n* = number of pixels ponderated, *p* = ponderation value, *r* = resolution of the image. The derivatives are obtained through a 3x3 high pass filter window. The denominator is equal to 50 (2 pixels ponderated, with a ponderation value equal to 1 and a resolution equal to 25 m). Then the slope gradient in degree is obtained using the arc-tangent function.

The comparison itself is done by using the module CROSSTAB of IDRISI. This module gives the opportunity to cross the information contained in two images and to obtain a cross-tabulation table giving all the available combinations between the categories of both maps and indicating the importance of each combination as well as the strength of the association through the Cramer's V statistic test (Ott, Larson & Mendenhall, 1987). This test is based on the assumption that parameters are dependent and it gives an estimation of the strength of the relationship. The dependency is calculated using the chi-square test before applying the Cramer's V test. A value of zero in the Cramer's V test means no association and a value of 1 a perfect association. Results for the association amplification - thickness, amplification - slope gradient for both types of waves are given in table 4.20. They show that the association is stronger for the SV case, whatever the parameter considered, and stronger for the thickness whatever the type of wave.

Association	**SH - wave**	**SV - wave**
Amplification - thickness	0.64	0.69
Amplification - slope gradient	0.45	0.49

Table 4.20. Association test between maximum amplification - thickness and maximum amplification - slope gradient for SH and SV incident waves.
Tableau 4.20. Test d'association entre l'amplification maximum - épaisseur et amplification maximum - gradient de pente pour les ondes incidentes SH et SV.

Charts based on the results of the cross-tabulation for the SH and SV amplification case versus the slope gradient of the bedrock and the thickness of the Quaternary deposit are shown in figure 4.21. The distribution is given in number of picture elements (pixels), the elementary cell of a raster image. For each class of amplification, the number of pixels is distributed according to the slope or thickness categories present in this class.

Therefore these charts give two main indications, i.e. the dominant amplification over the entire area and the predominant thickness or slope class for each category of amplification. Concerning the dominant amplification over the valley, it can be seen that the value is between 6-10 for the SH case and 4-8 for the SV case. Then for each class of amplification according to the specific wave, the dominant category of thickness of the Quaternary deposit and the slope gradient can be extracted. The result is summarized in tables 4.22 and 4.23. Regarding the SH case, the higher class of the maximum amplification occurs for a thickness between 500 and 600 m and for a slope between 20-30 ° whereas for the SV case, it corresponds to a thickness varying between 300-400 m and for a slope between 40-50°.

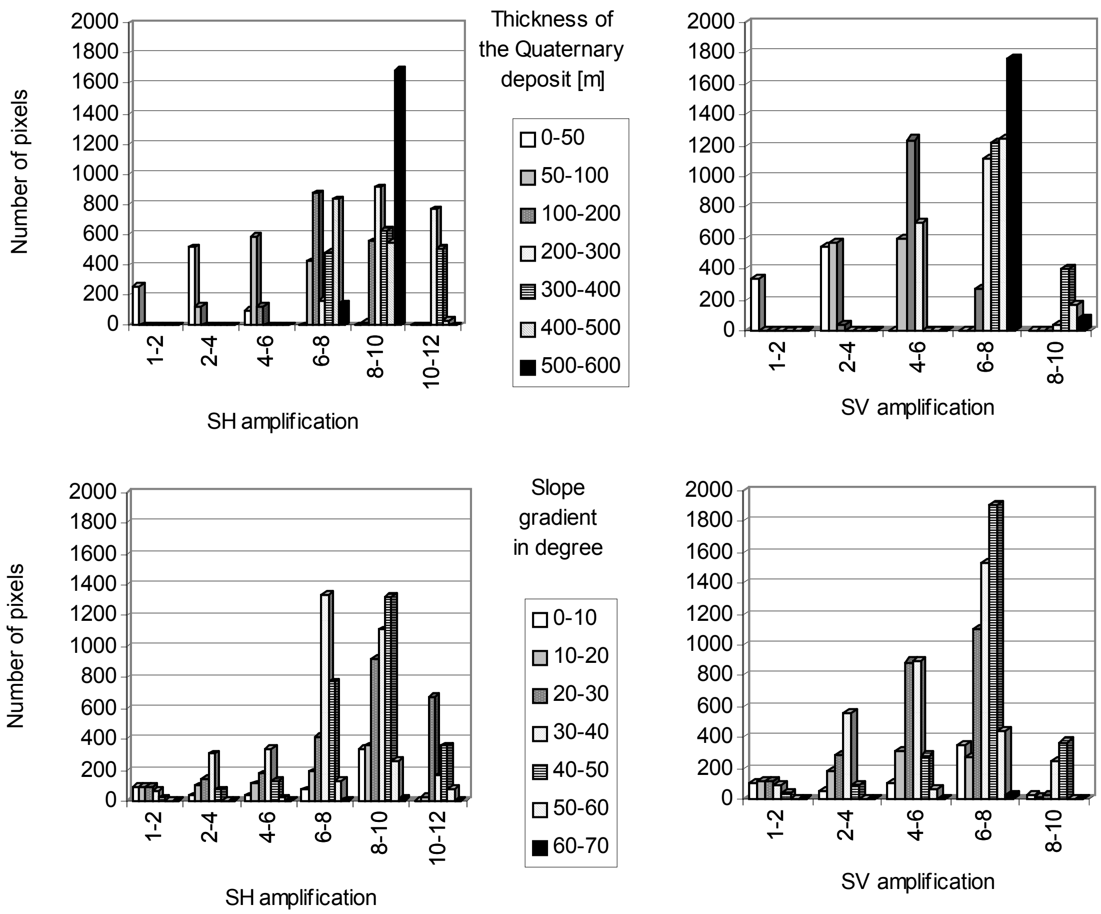

Figure 4.21. Graphical illustration of the cross-tabulation between the maximum amplification (for a vertical incident SH and SV wave) and thickness of the Quaternary deposit, and the maximum amplification versus slope gradient of the bedrock.
Figure 4.21. Illustration graphique de la table de contingence entre l'amplification maximale (pour les deux cas d'onde vertical incidente - SH et SV) et l'épaisseur du dépôt quaternaire et entre l'amplification maximale et le gradient de pente du substratum rocheux.

Maximum	Slope gradient	Thickness of the

amplification	of the bedrock [°]	Quaternary deposit [m]
1-2	0-10	0-50
2-4	30-40	0-50
4-6	30-40	50-100
6-8	30-40	100-200
8-10	40-50	500-600
10-12	20-30	200-300

Table 4.22. Predominant classes of slope gradient of the bedrock and thickness of the Quaternary deposit for each category of maximum amplification - SH case.
Tableau 4.22. Classes dominantes du gradient de pente du soubassement rocheux et d'épaisseur du dépôt Quaternaire pour chaque catégorie d'amplification maximale - case de l'onde SH.

Maximum amplification	Slope gradient [°]	Thickness of the Quaternary deposit [m]
1-2	10-20/20-30	0-50
2-4	30-40	50-100
4-6	20-30/30-40	100-200
6-8	40-50	500-600
8-10	40-50	300-400

Table 4.23. Predominant classes of slope gradient of the bedrock and thickness of the Quaternary deposit for each category of maximum amplification - SV case.
Tableau 4.23. Classes dominantes de gradient de pente du soubassement rocheux et d'épaisseur du dépôt Quaternaire pour chaque catégorie d'amplification maximale - case de l'onde SV.

4.3.4.2 Sensitivity analysis on the 2D response to physical parameters

Zonation maps have been established using the maximal amplification value for each observation point and its associated frequency and assuming a vertical incident wave. Some sensitivity tests have already been done on the Vétroz and Bramois profile on these two parameters. However, in the Sion case, profiles are showing various shapes, some being almost perfectly symmetric whereas some others being asymmetric and they have also been submitted to an incident SV wave. Therefore complementary tests have been processed on three representative profiles, p6, p8 and p14 (figure 4.8). They may allow to demonstrate the influence of the type of incident wave, incidence angle and physical properties on the maximum amplification and its associated frequency.

Effect of the incidence angle on the maximum amplification and its frequency

The angle of incidence at the base of the alluvium is depending on the seismic source depth and on the characteristics of the layers across which the waves will propagate. The Valais region is characterized by numerous faults having a potential of seismic activity. Therefore the Sion area can be affected by numerous sources having different azimuths with different incidence angles.

Two values of incidence, 30 and 60°, were tested approaching from both sides of the structure. Hence in figures 4.24 to 4.26 the sign (+) means that the wave is coming from the left side (azimuth 0°) of the profile whereas the sign (-) means that the wave is coming from the right side (azimuth 180°).

In the SH wave case, amplification factors were obtained dividing all amplitudes by a factor of two as discussed in chapter 3. Regarding the SV case, amplitudes are different depending on the incidence angle and the concerned component. For an incidence angle of 30°, the amplitude is equal to 1.61 on the x component and to 1.07 on the z component, whereas for an incidence angle of 60°, the amplitude on the x component is equal to 0.52 and to 1.12 on the z component.

The comparison between the seismic response obtained from vertical and oblique incident waves are represented on figures 4.24 to 4.27 considering both types of waves, SH and SV. The amplification pattern is shown on figures 4.24 and 4.25 and the frequency content is shown on figures 4.26 and 4.27.

In a 1D case, as the angle of incidence increases, the amplification decreases. In the 2D modeling, the relationship between those two elements is dependent on the subsurface topography, particularly on the presence of asymmetry, and on the type of incident wave. This is specifically visible on the p8 profile. Looking at the SH case, an oblique incident wave produces higher amplification on the edge than for a vertical incidence. This is especially accentuated for an angle of incidence of 30° arriving from the left side (North side). This phenomenon is likely due to the presence of a steep slope edge in the North. This element can be considered as a strong reflector of waves bouncing the energy back into the valley and thereby participating to the generation and propagation of surface waves (Papageorgiou & Kim, 1991). Considering the SV case, amplification values are mostly lower for an incident wave at 30° than a vertically one, but when the angle rises up to 60°, the pattern shows an interesting tendency (figure 4.25). Looking for example at the response given by a wave incident from the left side, the amplification is increasing until the center part of the valley is reached and then the amplification is inverted starting to decrease. Another point is that for a symmetric or almost symmetric profile like the p14 profile, both sides are acting like a mirror, one side giving the reverse response of the other side (figures 4.24 and 4.25).

Regarding the frequency content, and in the case of a SH wave, the variation between vertical and oblique incidence is rather sensitive on the edge showing a lateral shift depending from which side the incident wave is approaching (figure 4.26 and 4.27). In the center part of the valley, values remain unchanged. In opposite, for the SV case, the frequency content is more heterogeneous, showing higher values over the whole profile for a wave incident with an angle of 60°.

As observed for the Vétroz and Bramois profiles (chapter 3, § 3.3.5), some saturation still occurs on the edges regarding the frequency content, not only for the SH case, but also for the SV case. This is due to the fact that the upper frequency was set up to 5 Hz, a boundary imposed by the computing capability limitation in regard to the chosen parameters.

SH case SV case

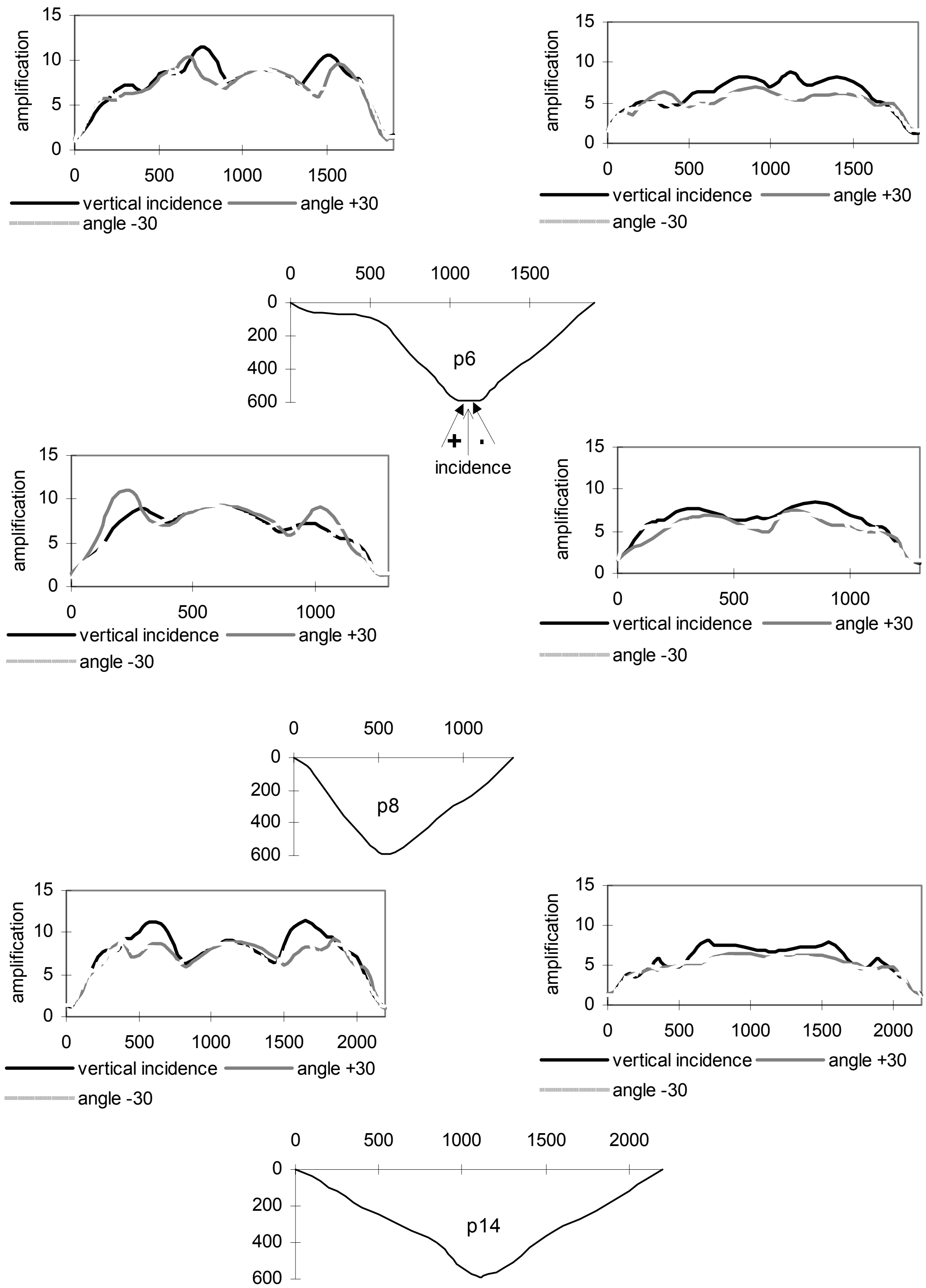

Figure 4.24. Influence of the incidence angle on the maximum amplification value for a SH and SV incident wave for three characteristic profiles in the Sion area. The incident wave is coming with an angle of 30°.
Figure 4.24. Influence de l'angle d'incidence sur l'amplification maximum pour une onde de type SH et SV pour trois profils caractéristiques de la région de Sion. L'onde incidente a un angle de 30°.

SH case SV case

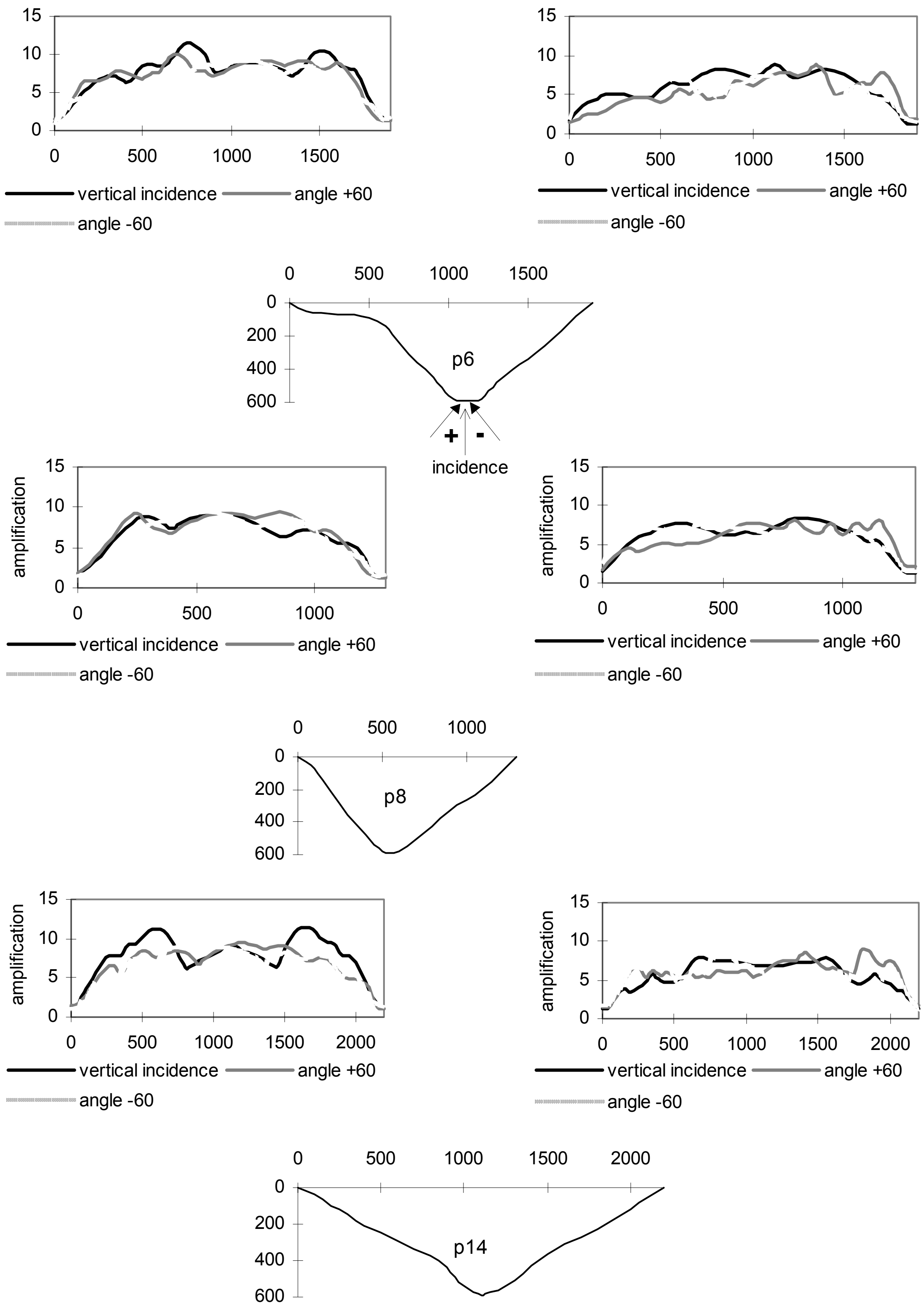

Figure 4.25. Influence of the incidence angle on the maximum amplification value for a SH and SV incident wave for three characteristic profiles in the Sion area. The incident wave is coming with an angle of 60°.
Figure 4.25. Influence de l'angle d'incidence sur l'amplification maximale pour une onde de type SH et SV pour trois profils caractéristiques de la région de Sion. L'onde incidente a un angle de 60°.

SH case SV case

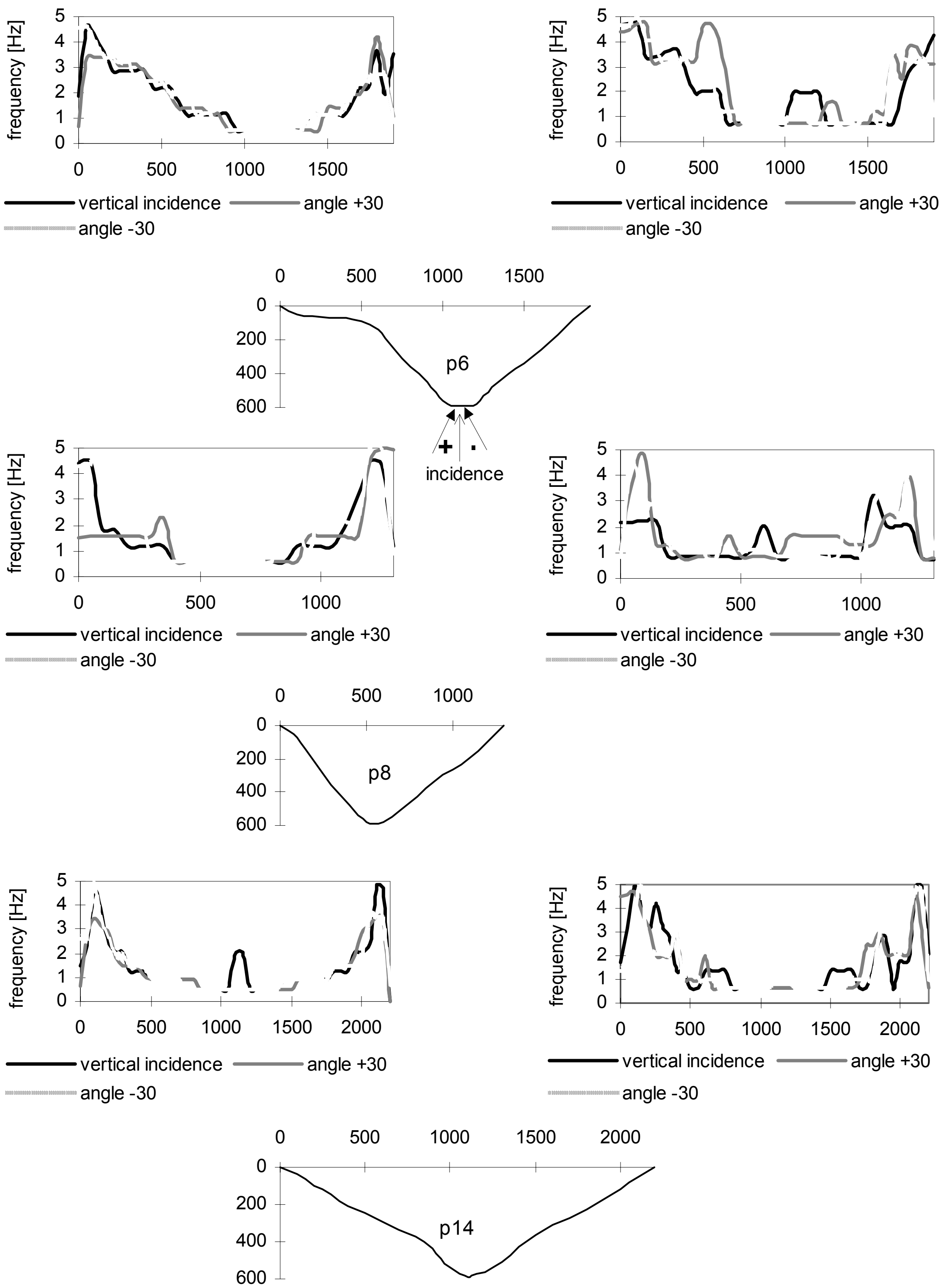

Figure 4.26. Influence of the incidence angle on the frequency corresponding to the maximum amplification value for a SH and SV incident wave for three characteristic profiles in the Sion area. The incident wave is coming with an angle of 30°.
Figure 4.26. Influence de l'angle d'incidence sur la fréquence de l'amplification maximale pour une onde de type SH et SV pour trois profils caractéristiques de la région de Sion. L'onde incidente a un angle de 30°.

SH case SV case

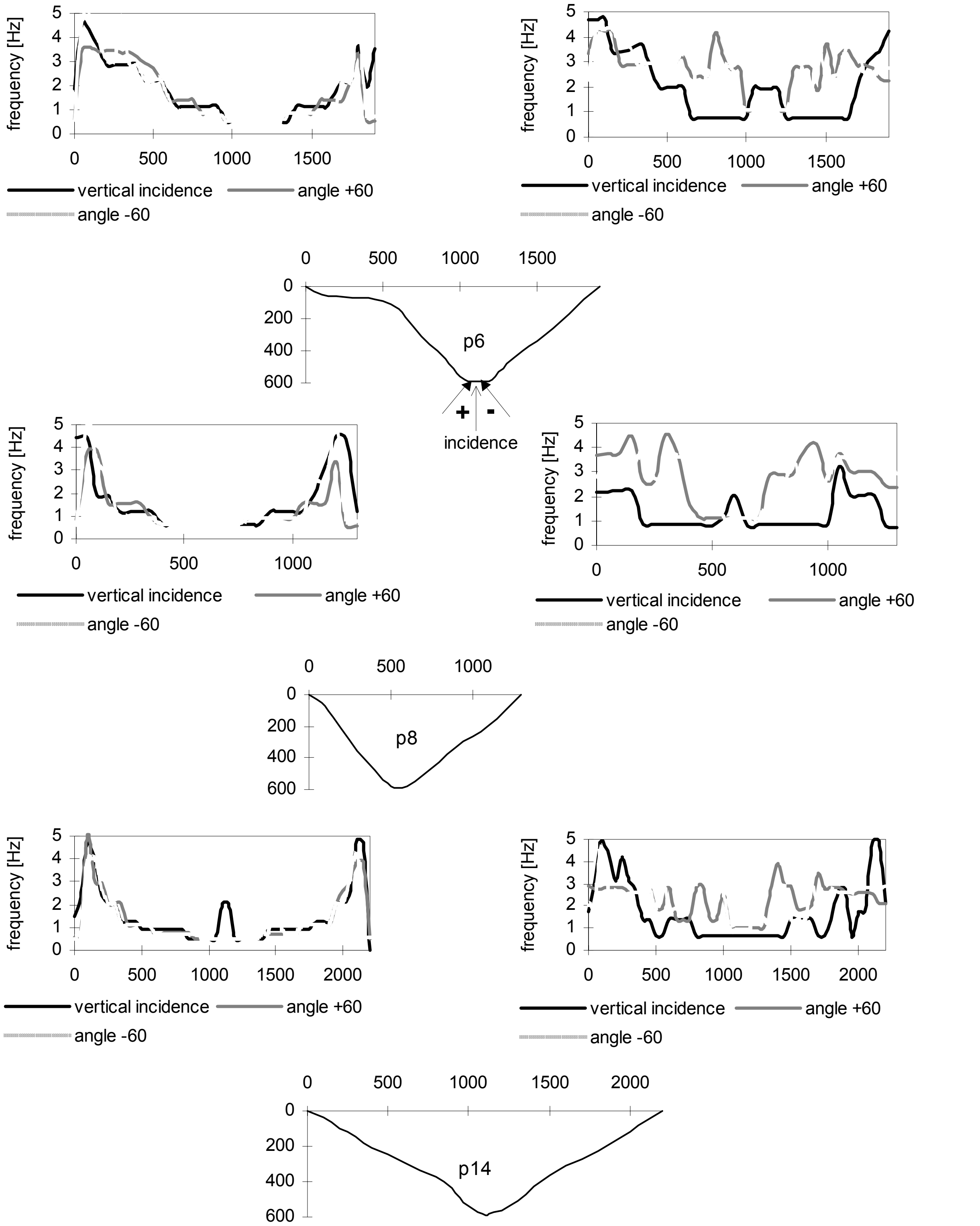

Figure 4.27. Influence of the incidence angle on the frequency corresponding to the maximum amplification value for a SH and SV incident wave for three characteristic profiles in the Sion area. The incident wave is coming with an angle of 60°.
Figure 4.27. Influence de l'angle d'incidence sur la fréquence de l'amplification maximale pour une onde de type SH et SV pour trois profils caractéristiques de la région de Sion. L'onde incidente a un angle de 60°.

Effect of the Poisson's ratio on the maximum amplification and its frequency

Poisson's ratio can potentially influence the seismic response of a structure submitted to a SV wave as this type of wave can be converted into P waves and generate Rayleigh waves. Therefore in order to test the impact of this parameter, the P wave velocity was modified, in one hand for the bedrock and in the other hand for the sedimentary filling. For the bedrock, one considered the case where the Vp/Vs ratio = 1.73, meaning a Poisson's ratio equal to 0.25, the standard value. For the sedimentary filling, the value was chosen to be equal to 0.42, which corresponds to a Vp/Vs ratio = 2.68.

Results are only displayed (figure 4.28) for the p6 profile as the two others p8 and p14 show the same tendency. It can be seen that keeping the P wave velocity within a reasonable range, it does not influence the maximum amplification and its associated frequency very much.

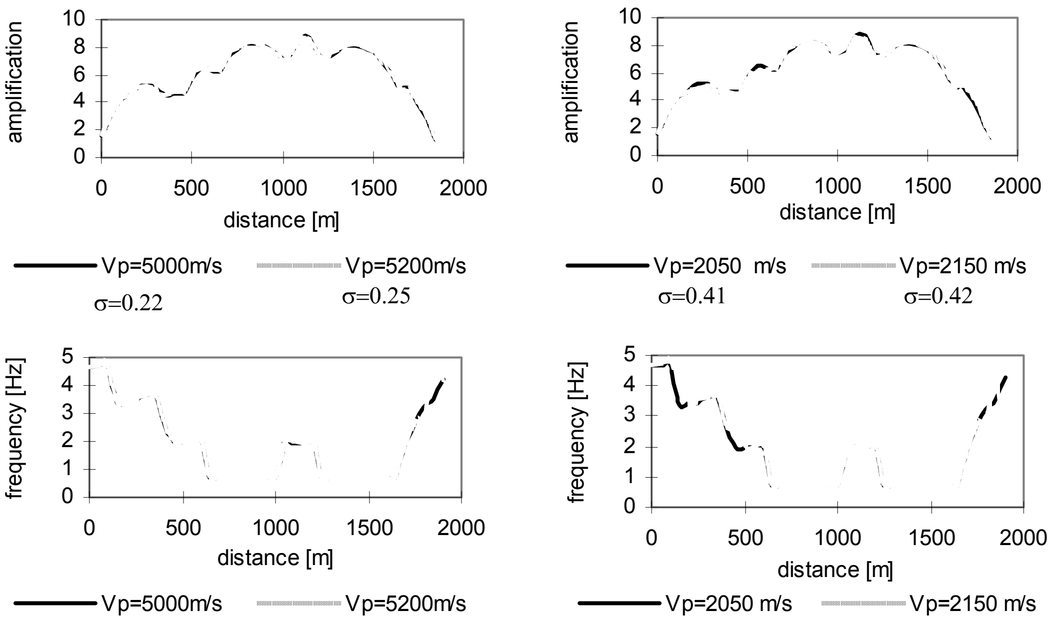

Figure 4.28. Impact of the Poisson's ratio on the maximum amplification and its associated frequency for the p6 profile. Modification of the Poisson's ratio for the bedrock (left side) and for the sedimentary filling (right side). SV wave case.
Figure 4.28. Influence du coefficient de Poisson sur la valeur de l'amplification maximale et la fréquence associée pour le profil p6. Modification du coefficient pour le soubassement rocheux (à gauche) et pour le remplissage sédimentaire (à droite). Cas d'une onde SV.

Effect of the Q factor on the maximum amplification and its frequency

When the Q factor is reduced, i.e. the soil is characterized by a stronger seismic attenuation capacity, the maximum amplification value decreases over the entire profile (figure 4.29). Regarding the frequency content, the modification are minor.

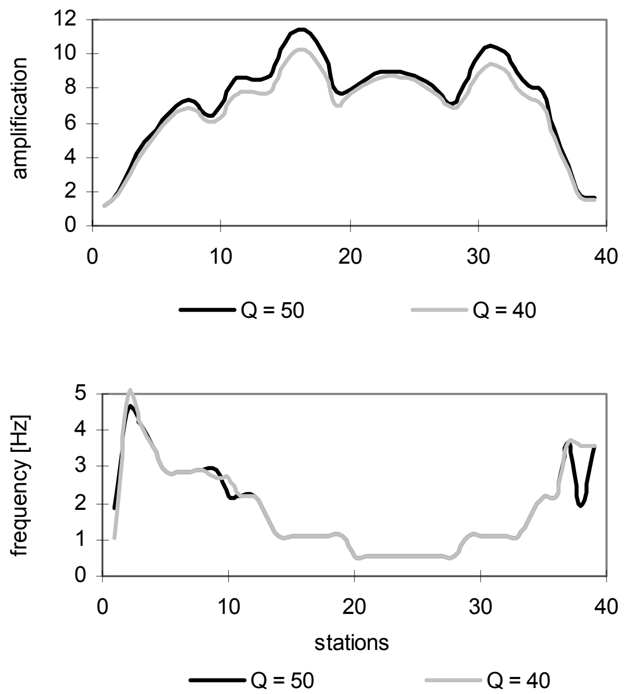

Figure 4.29. The effect of the Q factor on the maximum relative amplification value and on the corresponding frequency for the p6 profile. SH wave case.
Figure 4.29. Effet du facteur Q sur l'amplification maximale relative et les fréquences correspondantes pour le profil p6. Cas d'une onde SH.

4.4 Ambient seismic noise measurements

2D modeling is a predictive approach. Therefore in-situ measurements are useful to compare results. But in area with moderate to low seismicity it may require a long time before having a strong motion database representative enough to characterize the site response. Thus alternative approaches have to be applied.

In the Sion area, microtremors have been analyzed using the ratio of the horizontal to vertical component (H/V). The purpose is to test this technique in an Alpine valley characterized by thick unconsolidated sedimentary deposit and to compare the result with the 2D modeling and the earthquake measurement.

4.4.1 Field measurements

Ambient seismic noise measurements were acquired during three campaigns. The first acquisition has been done by Gonzenbach (1997b) in May 97, then followed in October 98 and January 99 by two small campaigns (Rosset & Frischknecht, unpublished) in order to verify some points and acquire new data. Measurement points were chosen as close as possible from the 2D modeling profiles. The majority of the 64 points were measured on the valley floor as displayed by the figure 4.8. Sites were chosen as to be as quiet as possible, avoiding the close vicinity of heavy traffic. The measurements were done during the day.

The microtremor data were recorded using a three component 1Hz portable digital Lenhartz MARSlite seismometer (figure 4.30). At each site, around 5 minutes of ground ambient noise were

GPS antenna

recorded with a sampling rate of 16ms. The figure 4.31 shows an example of ambient seismic noise recorded at the location of the SIOO station, one of the temporary station.

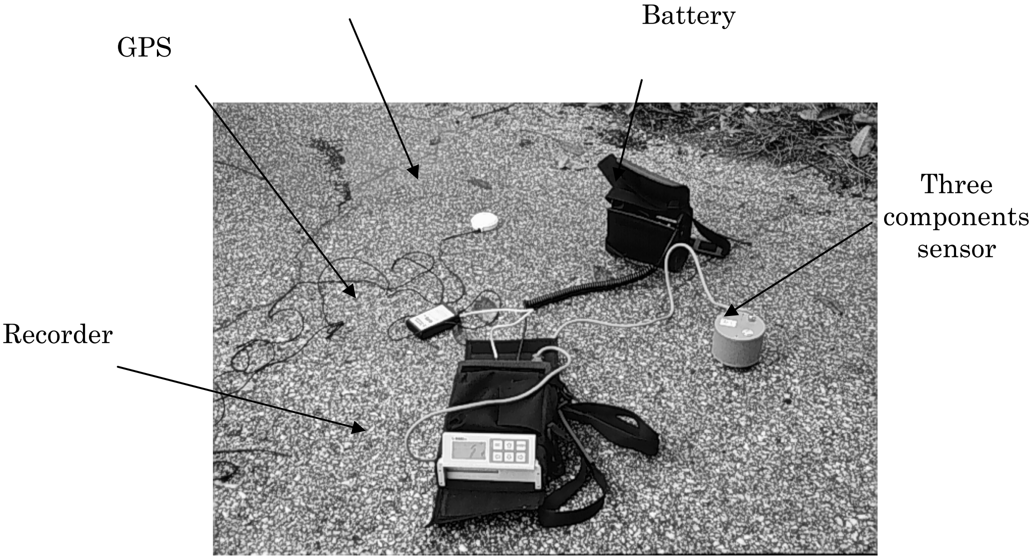

Figure 4.30. The acquisition unit of the ambient seismic noise. A portable digital Lenhartz MARSlite seismoter with a three component 1Hz sensor.
Figure 4.30. L'unité d'acquisition du bruit de fond. Un sismomètre digital portable Lenhartz MARSlite avec un capteur à trois composantes ayant une fréquence propre de 1Hz.

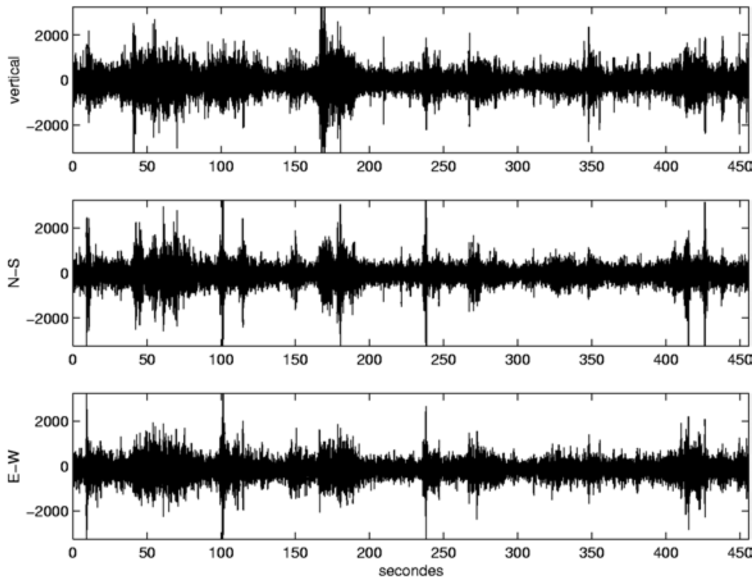

Figure 4.31. Example of raw signal of ambient seismic noise recorded at the SIOO site.
Figure 4.31. Example d'un signal de bruit de fond brut enregistré sur le site de la station SIOO.

Two H/V ratios obtained on ambient seismic noise and measured at the same time and place, but using two types of seismometer, a 1Hz and a 0.2 Hz are displayed on figures 4.32 and 4.33 respectively. Except the influence of the data treatment which was different, it can be seen that the general shape of the spectrum is really similar and the predominant frequency occurs at the same value. Discrepancies only occur for the amplification level due to a loss of energy below 1Hz for the 1Hz seismometer and also to the data treatment (e.g. filtering).

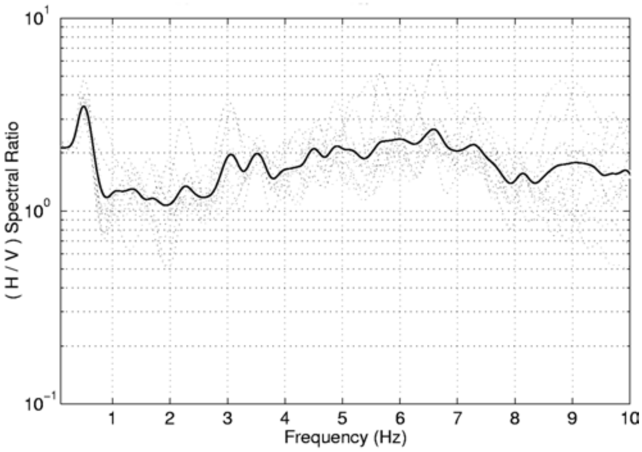

Figure 4.32. H/V spectral ratio obtained at the SIOO site using a 1Hz seismometer.
Figure 4.32. Rapport spectral H/V obtenu sur le site de SIOO en utilisant un sismomètre avec une fréquence naturelle de 1Hz.

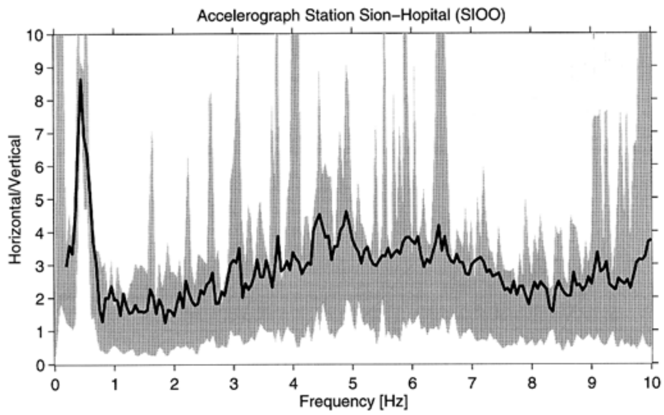

Figure 4.33. H/V spectral ratio obtained at the SIOO site using a 0.2Hz seismometer (SED, unpublished).
Figure 4.33. Rapport spectral H/V obtenu sur le site de SIOO en utilisant un sismomètre ayant une fréquence propre de 0.2Hz (SED, non publié).

4.4.2 Data processing

The signal processing is divided into the following steps (Gonzenbach, 1997a,b; Frischknecht et al. 1998). Each component is submitted to the same processing, using the same parameters :

- selection of the signal portion to analyze,
- segmentation of the selected signal into non-overlapping 33s time-windows,
- detrend and taper signal windows in order to minimize distortion of the spectrum due to the finite nature of the time series,
- Fast Fourier Transform on each window to obtain the signal in frequency domain,

- non destructive smoothing on each spectrum,
- computation of the spectral ratio using the formula $\frac{H}{V} = \frac{\sqrt{S_{NS}^2 + S_{EW}^2}}{S_V}$ for each window,
- average of all H/V ratios from all windows,
- identification of the predominant frequency and its amplification value in three predefined frequency band (0-1Hz, 1-10Hz, 10-20Hz).

No instrument correction was applied. All the described operations were processed using SPECTRATIO[4].

4.4.3 Results

As microtremor data were acquired as close as possible to the 2D profiles, the results of the microtremor data treatment will be displayed in comparison with the 2D modeling, for the SH case as well as for the SV case. One will focus on data measured on the valley. The data on the valley flank will not be plotted. Some others must also be discarded as they do not present an identifiable frequency peak (more or less flat transfer function, e.g. point 710, figure 4.34).

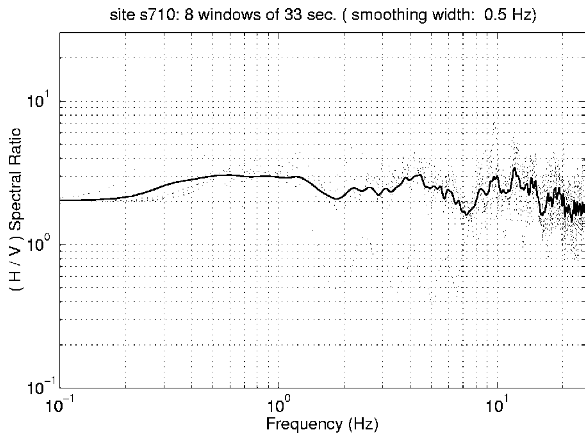

Figure 4.34. H/V ratio on microtremors for the station 710 which exhibits a relatively flat transfer function.
Figure 4.34. Rapport H/V sur bruit de fond pour la station 710 qui présente une fonction de transfert relativement plate.

6 profiles are displayed on figure 4.35. The data plotted are the frequency value at which the maximum amplification occurs, for the 2D modeling as well as for the H/V ratio on microtremors. In the latter case, the value is picked on the mean H/V spectral ratio. These data are only joined by a dotted line to underline the tendency as measurement points are not as numerous as the 2D modeling, and might show a different behavior in between.

It can be observed that both approaches exhibit the same tendency, i.e. low frequency in the center part of the profile, which corresponds to the thickest part of the sedimentary deposit. The value is generally lower for the H/V ratio.

[4] © Gonzenbach, 1997 - CERG

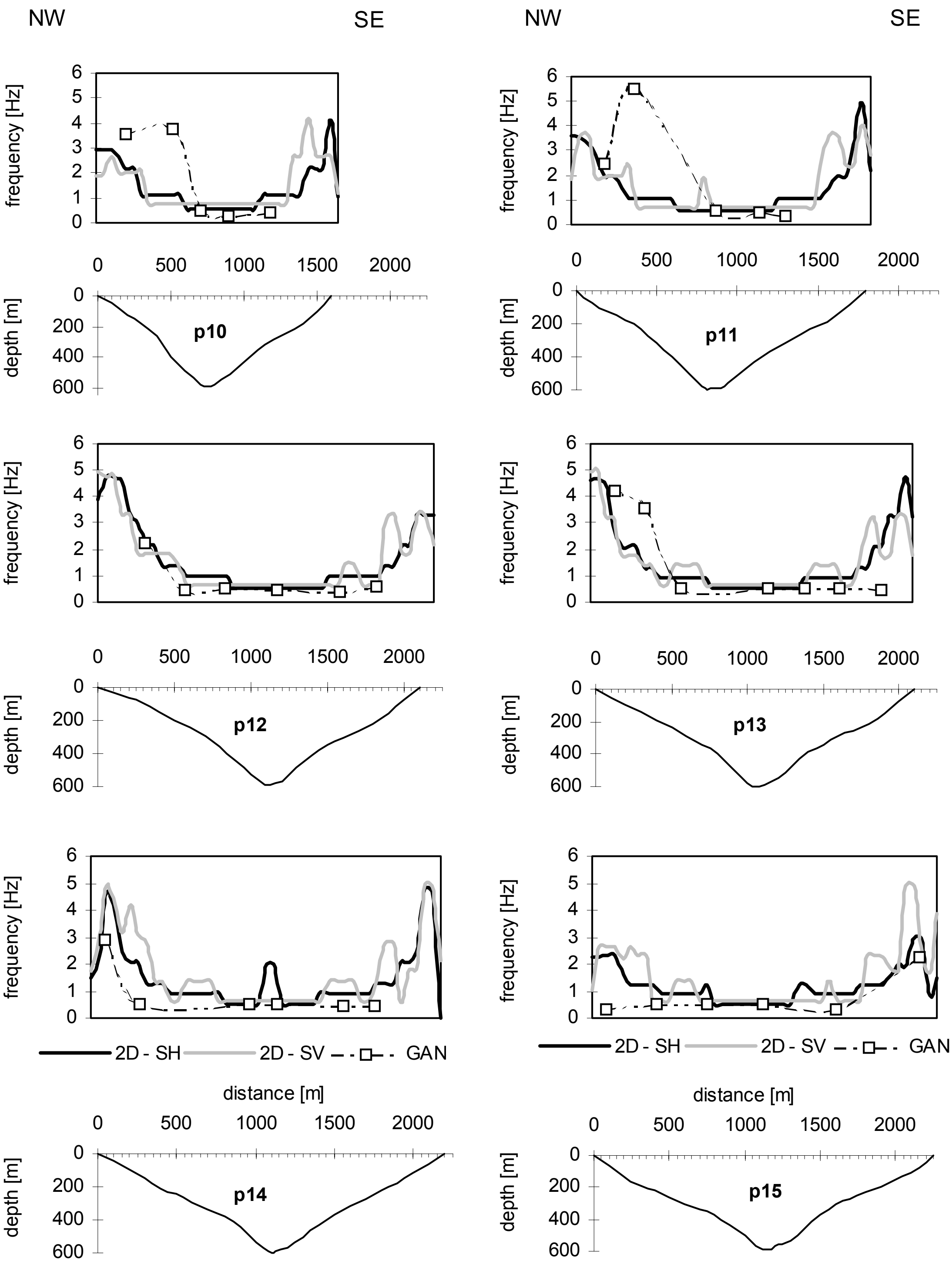

Figure 4.35. Comparison between 2D modeling and microtremors for the frequency of the maximum amplification on 6 main profiles.
Figure 4.35. Comparaison entre la modélisation 2D et le bruit de fond de la fréquence de l'amplification maximale pour 6 profiles principaux.

Regarding at the edges, the H/V ratio presents different behaviors, as :

- higher frequencies toward the edges as predicted by 2D modeling, e.g. p12 profile;

- lower frequencies than predicted by 2D modeling, e.g. p15 profile;
- higher frequencies than predicted by the 2D modeling, e.g. p10 profile.

Causes of these various behaviors might be due to :

- perturbation during the ambient seismic noise acquisition which induces especially high frequency component (industrial activities, power station);
- difference in lithology (especially in terms of velocity contrast) which might influence the ambient seismic noise measurement;
- the deepening of the valley is not as regular as supposed between the two high seismic resolution profiles.

As shown by Le Brun (1997) in the Grésivaudan valley, frequency values obtained from the H/V ratio on ambient seismic noise can be used to obtain the thickness of the sedimentary deposit. Indeed as the H/V ratio is considered to deliver reliable information on the fundamental frequency of the soil deposit (e.g. Lermo & Chávez-García, 1994) and is based on the 1D assumption, the thickness of the Quaternary deposit can be retrieved from the following formula :

$$f_0 = \frac{V_s}{4H}$$

with V_s being the mean shear-wave velocity in m/s and H the thickness of the deposit in meter.

The *Vs* parameter is set to 800 m/s as used in 2D modeling. Isopachs of the Quaternary deposit can then be drawn from the thickness values by a linear kriging interpolation. The resulting map for the Sion area is shown on figure 4.36. Comparing this image with the thickness map obtained from the interpolation between seismic profiles (figure 4.8), several observations can be done. First of all, the maximum thickness value is in the same range. Secondly, if one excepts bordering zones subject to inadequate interpolation due to the lack of data, the deposit geometry is not as regular as in figure 4.7. The higher frequency zone on the H/V frequency map (figure 4.39) converted in thickness shows a rapid thickness variation. On the opposite the low frequency anomaly exhibits a less accentuated thickness evolution.

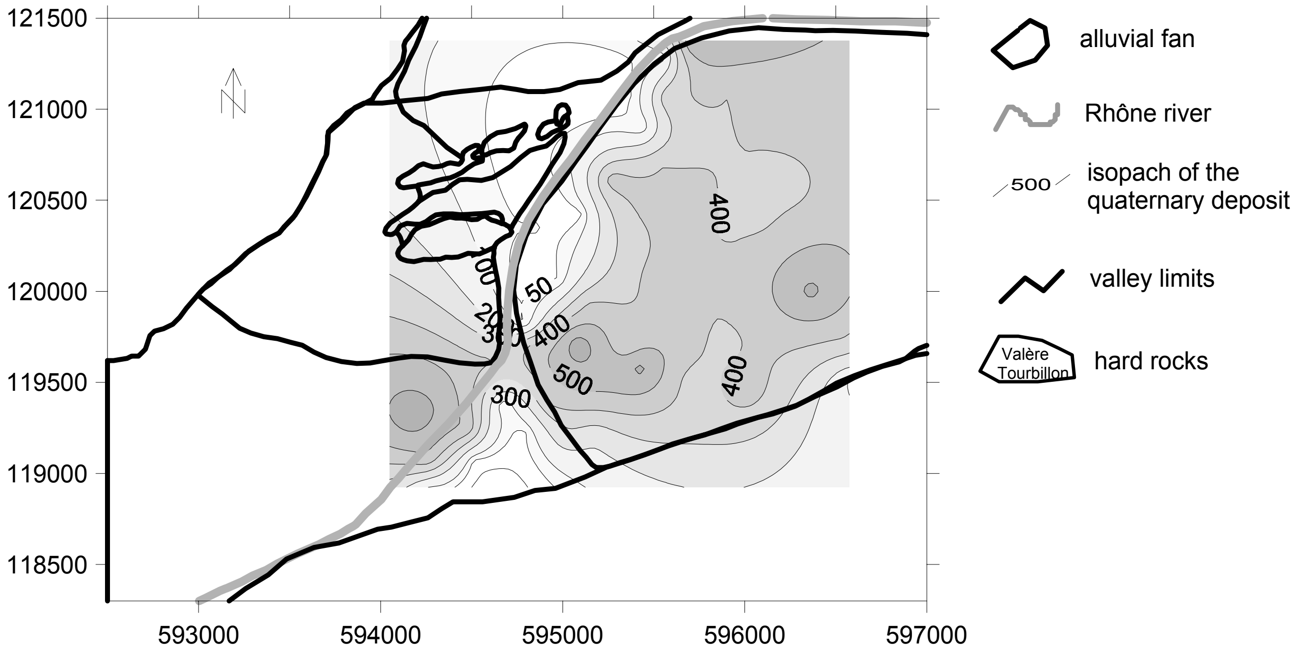

Figure 4.36. Quaternary isopachs based on the interpolation of frequency values obtained with the H/V ratio on microtremors.
Figure 4.36. Isopaches du Quaternaire basés sur l'interpolation des valeurs fréquentielles obtenues par le rapport H/V sur bruit de fond.

Regarding the amplitude of the H/V ratio which is assumed by Nakamura (1989) to be representative of the amplification level, figure 4.37 shows the comparison with the 2D modeling. One can notice that values from the H/V ratio are generally lower than predicted by the 2D modeling. However in some cases (e.g. p14 profile) values can be higher. This is likely due to wind or a very near source of noise as the amplitude is very sensitive to the source-receiver distance as theoretically demonstrated by Lachet & Bard (1994). In any case assuming that the profiles represent the existing subsurface geometry, the amplitude of the H/V ratio does not show any link with thickness variation.

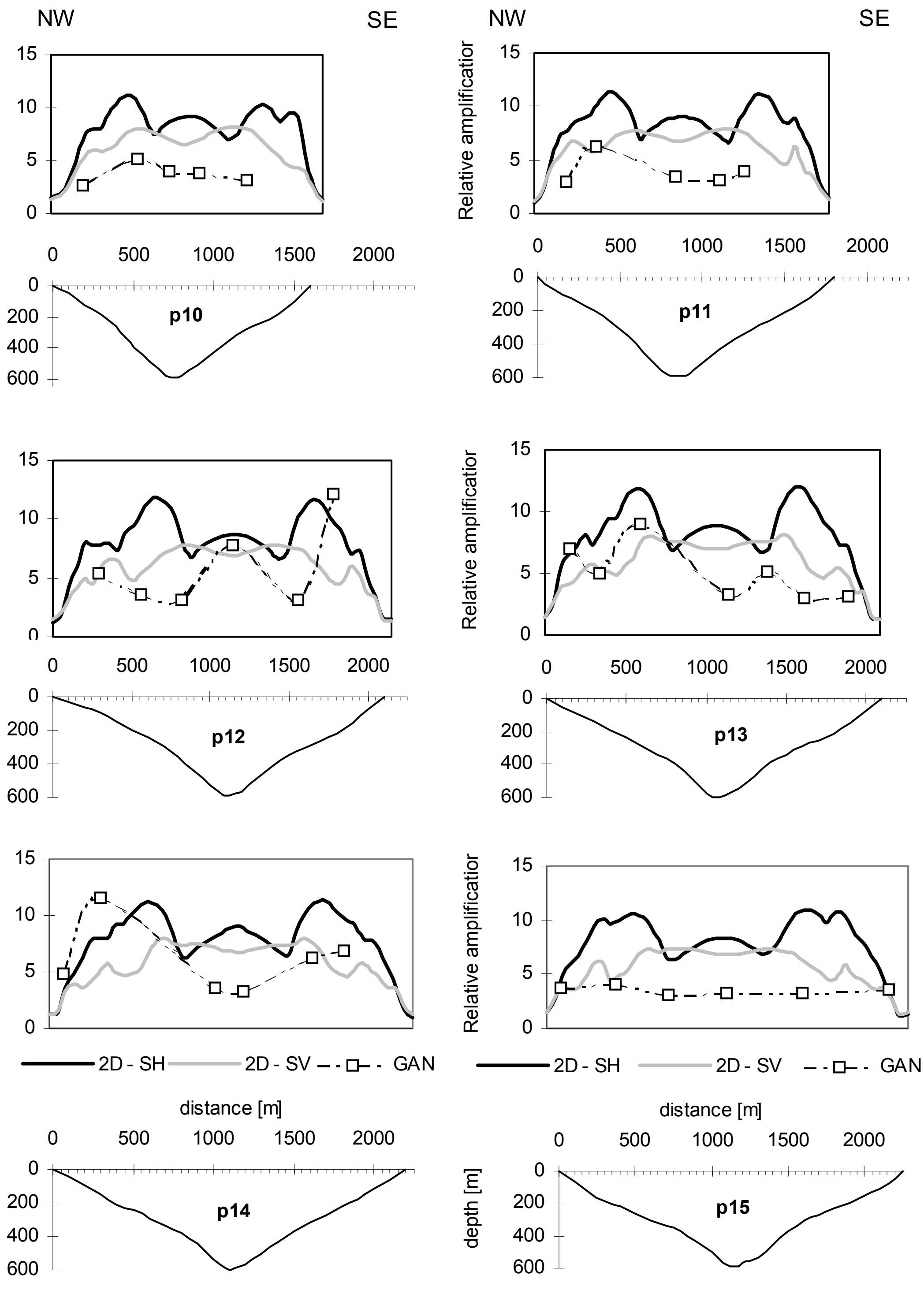

Figure 4.37. Comparison between 2D modeling and microtremors for the maximum amplification on 6 main profiles.

Figure 4.37. Comparaison entre la modélisation 2D et le bruit de fond de l'amplification maximale pour 6 profiles principaux.

4.4.4 Microzonation based on microtremors

The H/V ratio technique is considered to give a reliable indication of the dominant frequency of a sedimentary structure (Lachet & Bard, 1994; Lermo & Chávez-García, 1994). Therefore the measurement points were used to draw a map of the dominant frequency of the valley. As one is interested in the valley response itself and as the values located on the valley flank can interfere in the interpolation, only the values located on the valley floor were used. Moreover some other values were discarded as they were isolated (e.g. point B740).

The interpolation was produced by using a linear kriging algorithm (SURFER software). The result is a regular grid with a cell size of 25m x 25m. A mask was applied with the IDRISI software in order to remove the zones of inadequate interpolation due to the absence of data.

The frequency range goes from 0.31 to 5.52 Hz. The values were classified in 5 non-linear categories as described in table 4.38 in order to focus on the lowest frequency content. The final map is shown on figure 4.39. In order to appreciate the distribution of the frequency values versus the thickness of the deposit, the isopachs are overlaid on the figure. As already observed on the transverse profiles most of the valley is dominated by a low resonant frequency with some places exhibiting higher frequency values.

Classe	**Frequency range**
1	0.3-0.5
2	0.5-0.6 (inclusive)
3	>0.6-1
4	1-2
5	2-3
6	3-6

Table 4.38 Categories of classification for frequencies corresponding to maximum amplification.
Tableau 4.38. Catégories de classification pour les fréquences associées aux amplifications maximales.

In terms of amplification, it has been also noticed from the transverse profiles that no clear tendency of distribution occurs. As a result, one will display only the measured points overlaid on Quaternary isopachs (figure 4.40). The minimum level is 3 and the maximum is 17. Values higher than 10 should be considered with some precaution, as they are isolated points and might have then be influenced by very local sources of noise and/or geologic conditions. Most of the values are ranged between 3 to 5 which is up to a factor of 4 less than the 2D amplification.

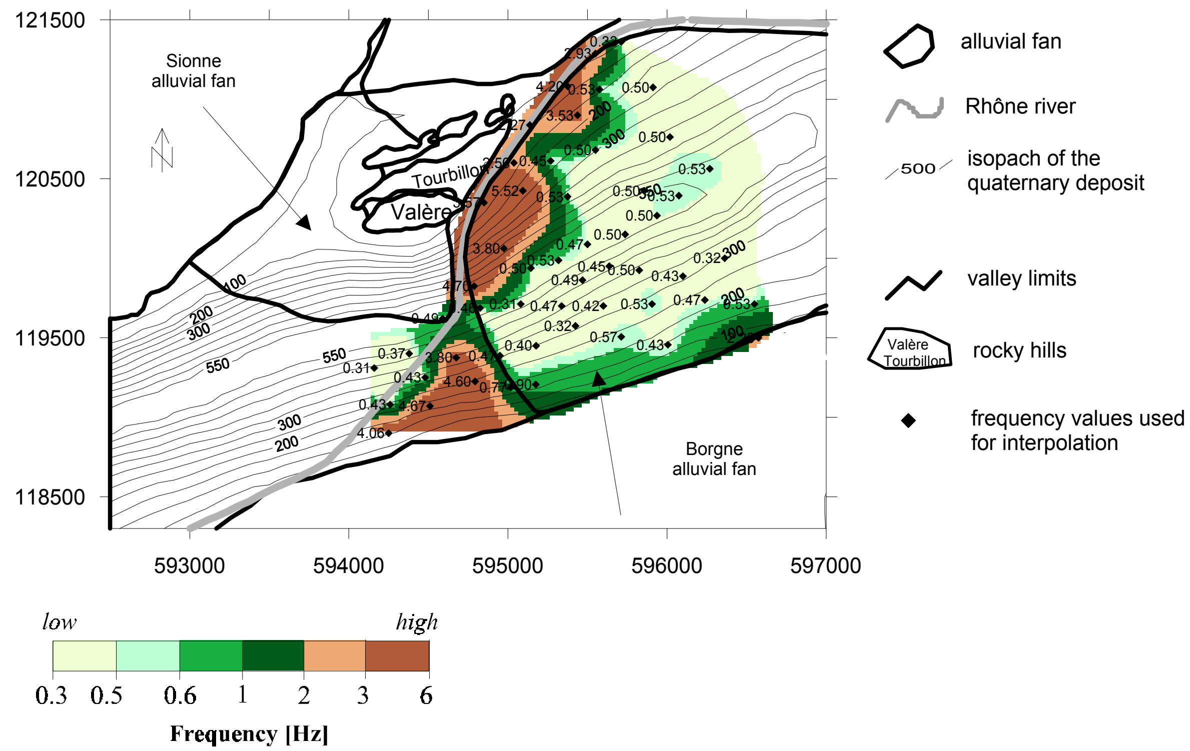

Figure 4.39. The predominant frequency map obtained by the Nakamura's technique on microtremors for the Sion area with the isopachs of the Quaternary deposit.
Figure 4.39. Carte des fréquences dominantes obtenues par la méthode de Nakamura sur le bruit sismique pour la région de Sion avec les isopachs du dépôt Quaternaire.

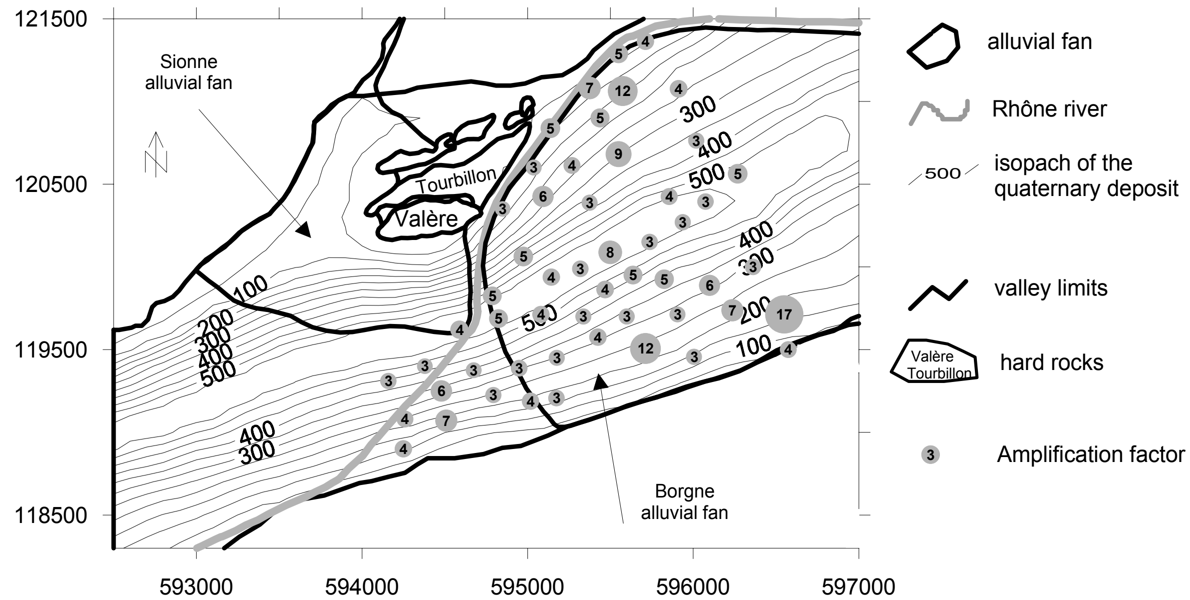

Figure 4.40. Maximum amplification values obtained by the Nakamura technique on mictrotremors for the Sion area overlaid on Quaternary thickness curves.
Figure 4.40. Valeurs d'amplification maximale obtenues par la méthode de Nakamura sur le bruit sismique pour la région de Sion superposés sur les courbes d'épaisseur du dépôt Quaternaire.

4.5 Temporary strong motion network

Initially three accelerometers with three components of the Swiss Seismological Service (SED) were installed in the Sion area, two on rocks and one on soil. Later it was decided to increase the number of stations on soil. Therefore in May 1997, three temporary stations of the Center of Geological Risk Studies (CERG) were installed. Sites were selected in order to represent different types of geometrical configuration, as it was shown by the modeling profiles.

The main instrument parameters for all the stations in the Sion area are described in table 4.41. The position of all the stations is indicated on figure 4.8 and the main site characteristics are described in table 4.41.

	SIOO	SIOM*	SIOE	SIOP	SIOV*	SALT*
Instrument type	SMACH SM2	SMACH SM2	SMACH SM2	SMACH SM2	SMACH SM2	SMACH SM2
Natural frequency	10 Hz	10 Hz	10 Hz	10 Hz	10 Hz	10 Hz
Damping	67 %	67 %	67 %	67 %	67 %	67 %
Full scale amplitude	0.5 g	0.5 g	0.5 g	0.5 g	0.5 g	0.5 g
Sampling rate samples/sec	256	128	128	128	128	128
Cut-off frequency band	0.2 - 30 Hz	0.2 - 30 Hz	0.2 - 30 Hz	0.2 - 30 Hz	0.2 - 30 Hz	0.2 - 30 Hz
Pre-event time	12 sec	12 sec	12 sec	12 sec	12 sec	12 sec
Post-event time	20 sec	10 sec	20 sec	20 sec	10 sec	10 sec
Trigger level • X, Y, Z	0.003 g[5]	0.003** g	0.003 g	0.003 g	0.003 g	0.003 g

* Smit, 1996, ** Smit, written communication

Table 4.41. Main instrumental parameters for the 6 accelerometers present in the Sion area.
Tableau 4.41. Paramètres instrumentaux principaux des 6 accéléromètres présents dans la région de Sion.

For stations SIOO, SIOP and SIOE, a borehole log was available in proximity. As the lithology can vary very rapidly in a Quaternary context, these boreholes are only given as an indication on the very surficial subsurface composition (table 4.42).

The SALT and SIOV stations are considered to be located on rock (Smit, 1996).

Name	Geology	Thickness

[5] g = earth gravity (9.80665 m/s_2 or 980.665 cm/s_2)

		of the sedimentary deposit
SIOO (Sion-Ophtalmology)	Rhône alluvium in the center part of the valley where the deposit is considered to be the thicker	573 m
SIOP (Sion-Police)	Rhône alluvium on the edge of the valley, right side	277 m
SIOE (Sion-Environment)	Rhône alluvium on the edge of the valley, left side	242 m
SIOM (Sion-Mayennets)	Sionne alluvium on Rhône alluvium	446 m
SALT* (Salins-Turin)	1-10m of till on Schist and coal from the Houillère zone	/
SIOV* (Sion-Valère)	Triassic quartzite	/

* Smit (SED)

Table 4.42. Main geological characteristics of the sites where the accelerometers are located in the Sion area.
Tableau 4.42. Caractéristiques géologiques principales des sites de localisation des accéléromètres de la région de Sion.

stations	boreholes	lithology	Depth to the water table
SIOO	RN10 (1988) - 12 m	soil (50 cm) gray silt (1m80) sandy - silty gravel (9m70)	> 5m (on borehole log)
SIOE	RN39 (1989) - 12 m	mix elements (70 cm) gray silt (1m60) silty gravel (2m10) sandy gravel (7m60)	> 3m (from piezometers)
SIOP	S1 (1995) - 30 m	alternation gravel - sand with intercalations of silt	> 2m (from piezometers)

Table 4.43. Surficial subsurface lithologies in proximity of SIOO, SIOE, and SIOP accelerometers.
Tableau 4.43. Dépôts superficiels situés à proximité des accéléromètres SIOO, SIOE, et SIOP.

On the 7 of May 1998, an earthquake of M_L=3.1 (weak motion) occurred in the Grand Dixence area at a focal depth of about 6 km (SED, database). It was located in the South flank of the Rhône valley at the Swiss meter coordinates 596400/108143. The epicentral distance from the earthquake site to the recorders varies around 10 to 12 km. All the stations in the Sion area, except the one located on the Valère Hill (SIOV), have been triggered. It should be mentioned that the station SIOV is not located on the top of the hill but between the Valère and Tourbillon Hills. This might explain the fact that this station was not triggered by the earthquake.

Maximum acceleration values in cm/s^2 for each station and each component are given in table 4.44. It can be seen that the highest values occur at the SIOP and SIOE stations located at the valley edges. It can also be noticed on figures 4.45 to 4.47 that these stations display signals having the highest amplitude and the largest duration no matter which component. All acceleration time histories displayed on figures 4.45 to 4.47 were corrected as instrumental data exhibited a drift from zero. The correction was done by removing the mean.

Stations	NS component	EW component	V component

	[cm/s²]	**[cm/s²]**	**[cm/s²]**
SIOO	4.8	4.5	3.5
SIOM	4.8	6.0	3.8
SIOP	10.9	10.8	12.4
SIOE	6.0	9.3	6.1
SALT	4.0	4.4	4.8

Table 4.44. Maximum acceleration values for each component of strong motion stations.
Tableau 4.44. Valeurs d'accélération maximum pour chaque composante des stations accélérométriques.

The EW component of all signals in function of the closest 2D profile (figure 4.48) confirm that stations located on the vertical of hidden valley flanks exhibit higher amplitudes and the longer signal durations; the stronger signal occurring at the vertical of the steeper slope (station SIOP-Y). These observations are in agreement with the 2D modeling results.

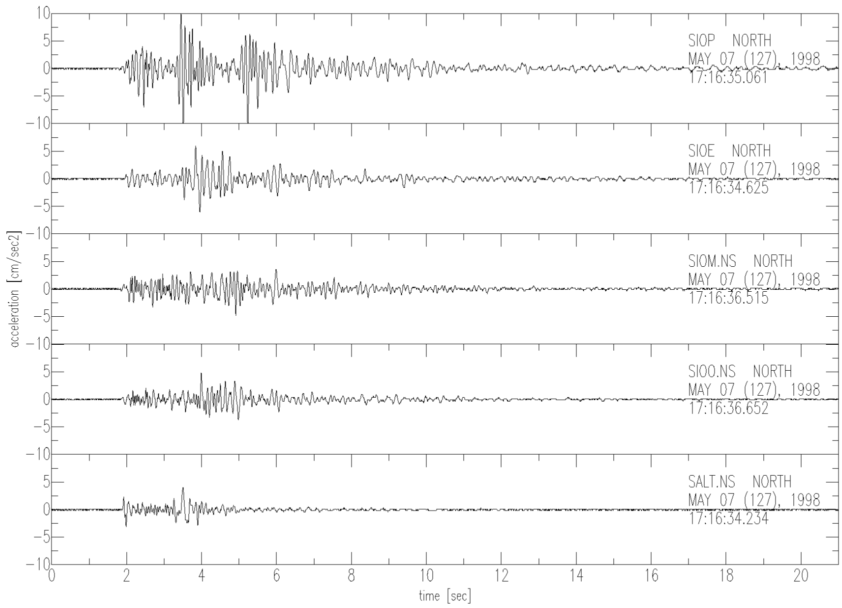

Figure 4.45. Acceleration time histories of the Grande Dixence earthquake. NS horizontal component (Smit, 1998; Wagner et al. 2000).
Figure 4.45. Accélérogrammes du tremblement de terre de la Grande Dixence. Composante horizontale NS (Smit, 1998; Wagner et al. 2000).

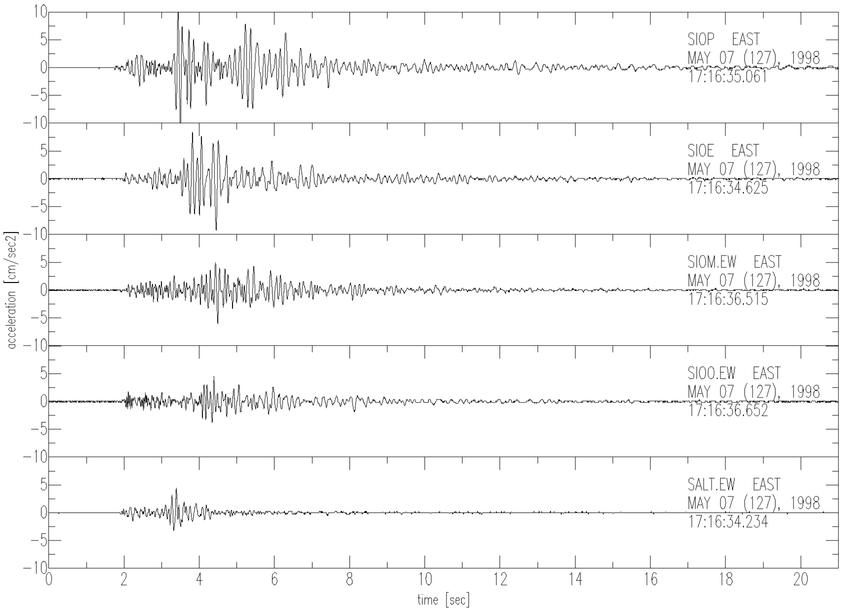

Figure 4.46. Acceleration time histories of the Grande Dixence earthquake. EW horizontal component (Smit, 1998; Wagner et al. 2000).
Figure 4.46. Accélérogrammes du tremblement de terre de la Grande Dixence. Composante horizontale EW (Smit, 1998; Wagner et al. 2000).

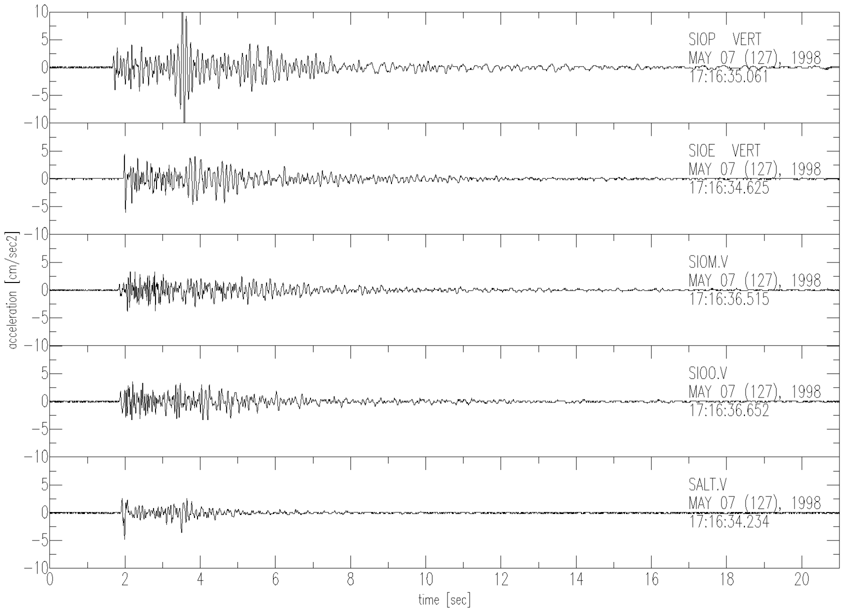

Figure 4.47. Acceleration time histories of the Grande Dixence earthquake. Vertical component (Smit, 1998; Wagner et al. 2000).
Figure 4.47. Accélérogrammes du tremblement de terre de la Grande Dixence. Composante verticale (Smit, 1998; Wagner et al. 2000).

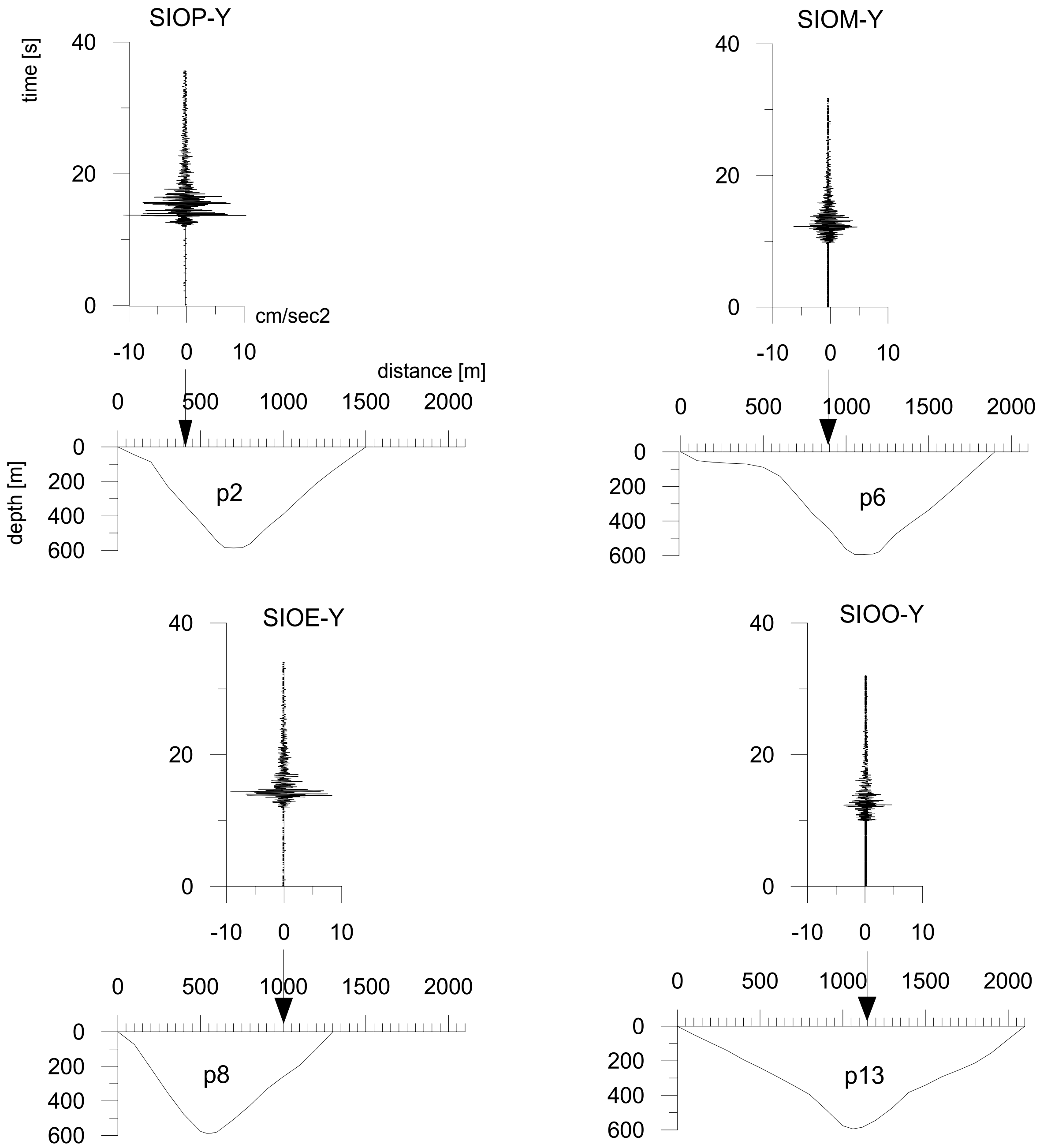

Figure 4.48. Accelerometers location according to the subsurface geometry of the Rhône valley.
Figure 4.48. Localisation des accéléromètres en fonction des profils de subsurface de la vallée du Rhône.

4.5.1 Signal analysis

Depending on the location of the recorders, signals may be disturbed by local noise (industrial activities, traffic, etc). Consequently in order to determine the reliable frequency range, a signal-to-noise ratio has to be evaluated for each record. A window of three seconds was chosen for this purpose before the event and on the signal itself, containing both P and S waves. The useful frequency band is then chosen based on a threshold criterion, which usually varies between two and three. Following Borcherdt & Gibbs (1976), one has used a signal-to-noise ratio higher than 2. Examples of signal-to-noise ratio are given in figures 4.49 and 4.50 for the NS horizontal component of the SALT and SIOO stations.

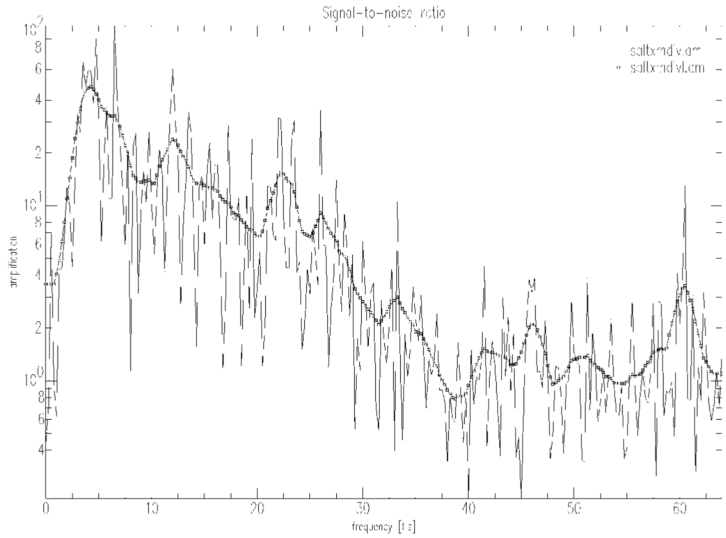

Figure 4.49. Signal-to-noise ratio for the station SALT on the NS horizontal component. The single line represents the raw ratio whereas the line with squares represents the smoothed ratio.
Figure 4.49. Rapport du signal sur bruit pour la composante horizontale NS de la station SALT. La ligne représente le rapport brut, la ligne de carrés représente le rapport adouci.

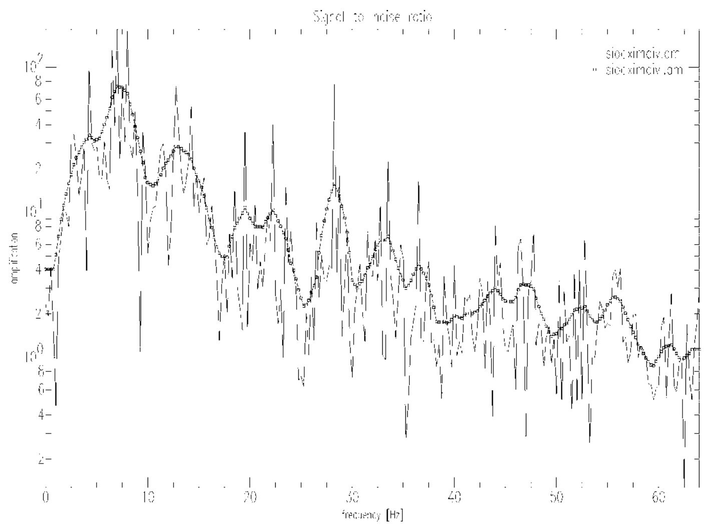

Figure 4.50. Signal-to-noise ratio for the station SIOO on the NS horizontal component. The single line represents the raw ratio whereas the line with squares represents the smoothed ratio.
Figure 4.50. Rapport du signal sur bruit pour la composante horizontale NS de la station SIOO. La ligne représente le rapport brut, la ligne de carrés représente le rapport adouci.

Based on the threshold of a value higher than 2, the frequency band for the SALT station is going up to 30 Hz which is the limit of the useful frequency range of the SMACH SM2, whereas it goes up to 25 Hz for the SIOO station.

Considering all the stations, an upper cutoff for the frequency band is set to 15 Hz. Consequently all acceleration time histories were filtered with a low-pass filter.

After removing the noise, the SIOO station was resampled in order to have a sampling rate conforming to the other stations (see table 4.41). Then the following questions to resolve remained :

- the part of the chosen window on the time series (the entire signal, the S wave part only, etc),
- the length of the window.

Entire signal can be used in order to avoid the difficulty to separate the different wave motion in the signal as it is affected by scattering effects (Theodulidis et al., 1996) or to obtain a better resolution to determine the low frequency amplification factors (e.g. Steidl et al., 1995). However the objective of this part is to compare the result not only with the ambient seismic noise but also with the 2D modeling which has been done on the basis of incident shear waves. Therefore the window is chosen to start at the beginning of the S wave and ending where the signal is still twice the background noise in order to integrate the later arrivals, thus giving a better stability and frequency resolution (Seekins et al. 1996). The selection was done based on the SIOE station, as it is one of the stations displaying the longer signal. The window length is therefore 11.5 seconds and is taken for all stations.

Once the signal portion is selected, the signal can be analyzed with the following procedure :

- tapering signal window in order to minimize distortion of the spectrum due to the finite nature of the time series using a cosine window (5% of the total window length),
- Fast Fourier Transform to obtain the signal in frequency domain,
- window selection to only keep the interesting frequency range,
- applying twice a moving window based on an average smoothing algorithm with a halfwidth of 3 (a 7x7 window filter) on each spectrum,
- spectral ratio between smoothed amplitude spectrum to obtain the spectral amplification.

The most widely used method to obtain the spectral amplification is the standard spectral ratio technique. This technique (see chapter 2) is based on a ratio using data recorded on the sedimentary filling to those from a site on bedrock chosen as a reference. The general assumption to use a station on bedrock as a reference station is to consider that its seismic response is representative for the input motion at the base of the sedimentary filling (Lermo & Chávez-García, 1994; Steidl et al. 1996). However Steidl et al. (1996) show that sites on rock can generate their own response depending on the quality of the rock, whether it is weathered, fracturated or not. Consequently to consider a site suitable to be used as a reference site, it should exhibit a relatively flat transfer function with an amplitude around one (Field & Jacob, 1995; Steidl et al. 1996). A way to test this is to use the H/V ratio on ambient seismic noise and/or on seismic ground motion. If the H/V ratio is flat for the reference station in the frequency range of interest, this station can be considered as reliable (e.g. Lermo & Chávez-García, 1994).

The H/V ratio is calculated using the following formula :

$$S(f) = \frac{\sqrt{NS_s^2(f) + EW_s^2(f)}}{V_s(f)}$$

It can be seen on figure 4.51 that the level of amplification at the SALT station, chosen as a reference site, is not around 1 over the frequency range of interest. It can be therefore considered that this station is not free from site effects.

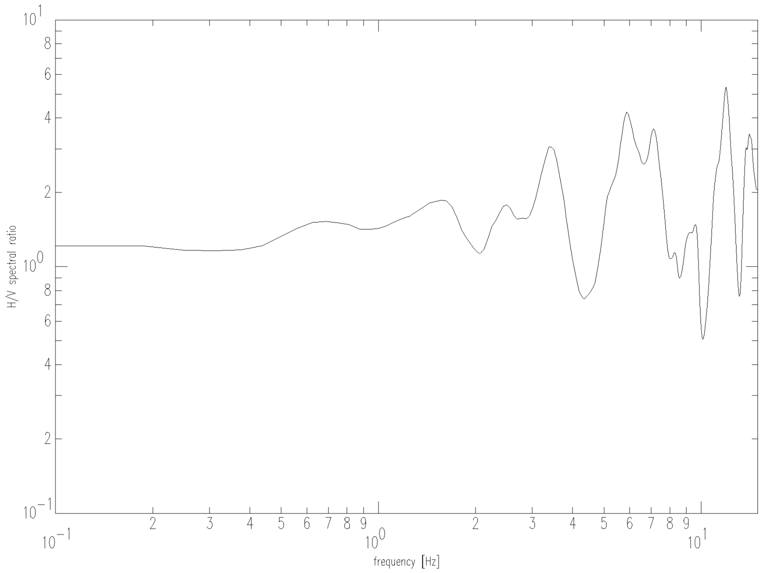

Figure 4.51. H/V spectral ratio on seismic weak ground motion obtained at the SALT site (“rock” site).
Figure 4.51. Rapport spectral H/V sur le mouvement sismique faible pour le site SALT (site au “rocher”).

This fact has a direct effect on the calculation of the standard spectral ratio. Comparing this ratio to the H/V ratio on the weak motion for the SIOO station points out discrepancies. Usually the comparison of both techniques agrees at least on the position of the lower frequency (e.g. Lermo & Chávez-García, 1993), which is not the case on figure 4.52. This is due to the reference site own response.

Consequently it can be said that the SALT station is not suitable to evaluate the seismic response induced by the sedimentary filling using the standard spectral ratio. Therefore the H/V ratio technique to estimate the soil response has to be applied.

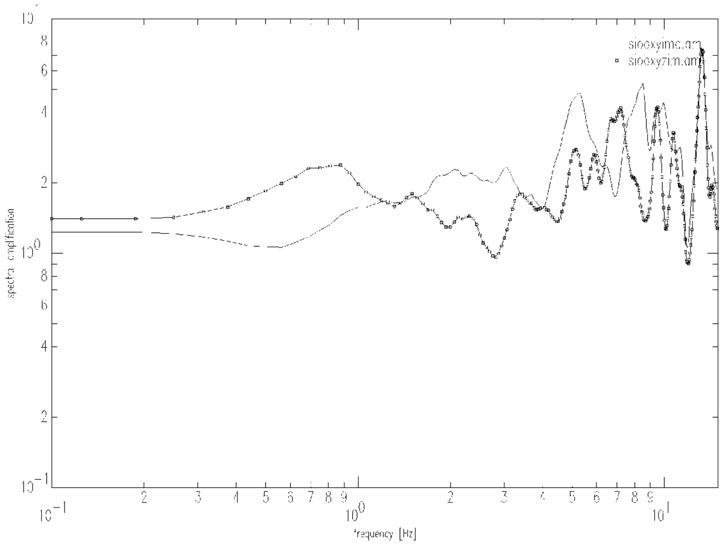

Figure 4.52. Comparison between the standard spectral ratio on weak motion (solid line) and the H/V ratio on weak motion (squared line) for the SIOO station.
Figure 4.52. Comparaison entre le rapport spectral standard sur le mouvement faible (ligne solide) et le rapport H/V sur le mouvement faible (ligne à carrés) pour la station SIOO.

4.5.2 Comparison between ambient seismic noise and weak motion

Ambient seismic noise and weak ground motion are compared based on the same analysis approach, i.e. the H/V ratio technique using the sum of the horizontal components (see § 4.5.1). The comparison (figure 4.53) is only made for the SIOE, SIOO and SIOP stations as ambient seismic noise measurements were available only for these stations.

Main characteristics of the H/V ratios (fundamental frequency, level of amplification, predominant peak and level of amplification) are summarized in table 4.54. Even if a single event is obviously not enough to draw any definitive conclusion, preliminary observations can still be made, such as :

- for the stations observed, H/V ratio on seismic ground motion displays the predominant frequency in the range [3-15 Hz];
- in the center of the valley (SIOO station), characterized by the thickest deposit, the fundamental resonant frequency is below 1 Hz, at 0.5 Hz from the H/V ratio on ambient seismic noise and around 0.8-0.9 Hz from the H/V ratio on weak motion;
- on the edges, stations show a different behavior. On the northern edge, for the SIOP station, H/V ratio on ambient seismic noise as well as on weak motion shows a fundamental frequency around 0.8-0.9 Hz. On the southern edge, for the SIOE station, the fundamental frequency is rather difficult to identify. The predominant peak is located between 4-5 Hz as showed by the H/V ratio on ambient seismic noise as well as on weak motion.

H/V Spectral Ratio on ground ambient noise **H/V Spectral Ratio on weak ground motion**

SIOE station (left edge of the valley)

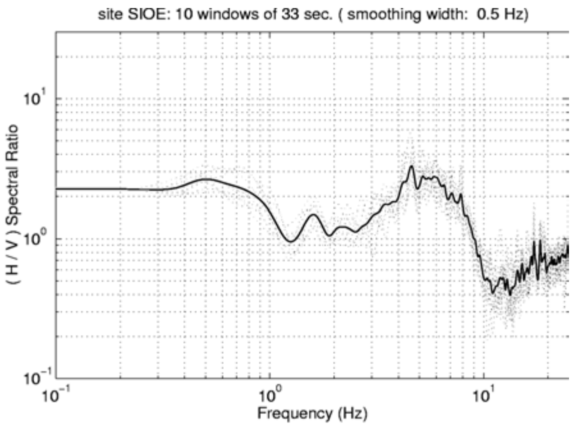

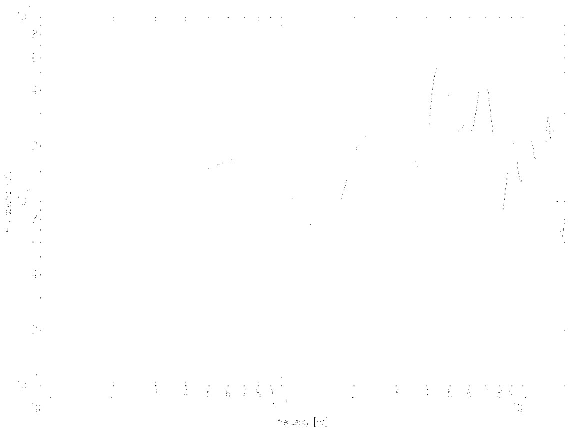

SIOO station (center part of the valley)

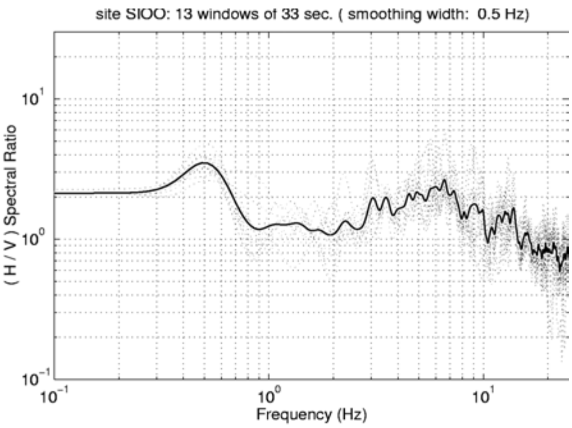

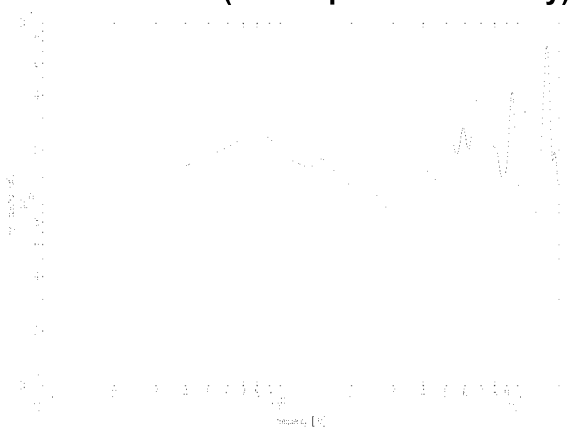

SIOP station (right edge of the valley)

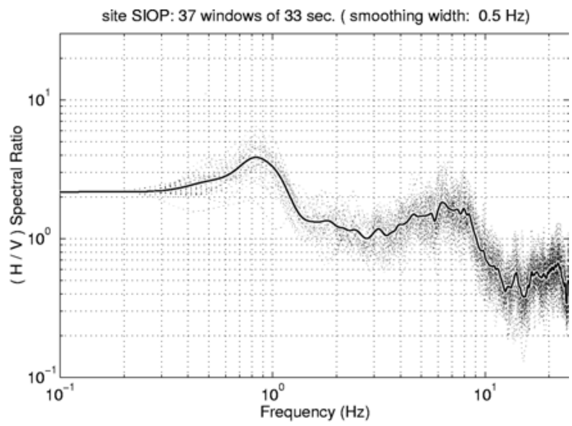

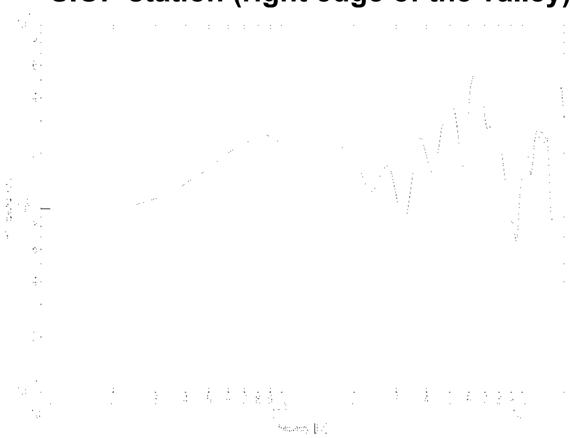

Figure 4.53. Comparison of H/V ratio technique on ambient seismic noise (left side - frequency interval 0.1-30Hz) and weak ground motion (right side - frequency interval 0.1-15Hz) for the stations SIOE, SIOO and SIOP.

Figure 4.53. Comparaison de la technique du rapport H/V appliquée sur le bruit ambient (à gauche - interval de fréquence 0.1-30Hz) et sur un tremblement de terre (à droite - interval de fréquence 0.1-15Hz) pour les stations SIOE, SIOO et SIOP.

SIOE	SIOO	SIOP

	ambient noise	weak motion	ambient noise	weak motion	ambient noise	weak motion
fundamental frequency [Hz] amplification level	/ /	/ /	0.5 >3	0.8-0.9 >2	0.8-0.9 <4	0.8-0.9 <3
predominant peak frequency [Hz] amplification level	4-5 >3	4-5 >5	0.5 >3	~14 >7	0.8-0.9 <4	6-7 >6

Tableau 4.54. Main characteristics recapitulative of in-situ measurements (ambient seismic noise and weak motion) for three stations located on the Rhône valley.
Tableau 4.54. Récapitulation des charactéristiques principales des mesures in-situ (bruit de fond et séisme faible) pour trois stations localisées dans la vallée du Rhône.

The result for the SIOE station raises some questions if this response is compared with the one of SIOP. Indeed both stations are normally characterized with a sediment thickness superior than 200 m but they behave differently in the H/V ratio for ambient noise. Several reasons can be put foreward, either the thickness is not as great as it is supposed to be under the SIOE station or the method to calculate the H/V ratio attenuates the peak. The latter hypothesis seems to be confirmed by the result obtained using the H/V ratio on each component (figure 4.55) where it can be seen that the SIOE exhibits a peak at low frequency on the NS component.

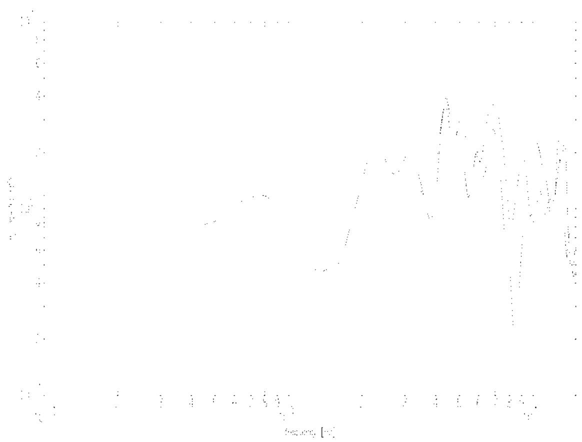

Figure 4.55. H/V ratios for the NS component (solid line) and the EW component (dotted line) for the SIOE station.
Figure 4.55. Rapports H/V pour la composante NS (ligne solide) et pour la composante EW (ligne pointillée) pour la station SIOE.

Another observation is that H/V ratio on weak motion as well as on microtremors exhibits two peaks. But for the H/V ratio on microtremors the predominant peak is rather located in the low frequency range whereas the situation is reverse for the H/V ratio on weak motion. As H/V data on microtremors are more numerous, it has been noticed in Sion and in Grenoble (Le Brun, 1997) that the presence of a double peak is depending on the location. In Sion, it has also been observed that the amplitude is varying with the location. An explanation of the occurrence of a second peak in higher frequency might be related with the presence of a water table. The Sion area is characterized by a water table of varying depth. This influences the thickness of the non-saturated sedimentary layer and also modifies the Poisson's ratio, as P wave velocity is sensitive to the water content. Thickness and Poisson's ratio have an impact on the frequency content and amplitude. Further investigation has to be done to verify this hypothesis.

Considering the level of amplification for the predominant peak, the value is always abound 1.5 times higher for the weak motion than for the ambient noise, whatever the station is.

4.5.2.1 Comparison between 2D modeling and weak motion

As the 2D modeling was processed using incident SH and SV waves, amplification functions are available on both horizontal components. Up to now an amplification function has been identified based on both horizontal components to characterized the seismic response under a SV wave. In this part, only the amplification function obtained on the X component will be considered. It is obtained in the same manner as that for the SH case, i.e. by dividing the displacement amplitude at the surface by the response of the bedrock without of the sedimentary filling (§ 4.3.3). The weak motion will be analyzed using a H/V ratio based on a single component, i.e. the EW component and the NS component following the formula :

$$S(f) = \frac{H_s(f)}{V_s(f)}$$

H_s being either the NS component or the EW component on soil and $V_s(f)$ being the vertical component on soil.

Before comparison, all acceleration time series, after the drift correction and the low-pass filtering, were submitted to a rotation to 338°. Indeed, as the 2D modeling was applied along profiles having a angle of 22° counterclockwise from the North, it is necessary to rotate signals in order to be in the same axis definition. Then the acceleration time series were treated as described in § 4.5.1.

The 2D amplification function was resampled in order to have a frequency sampling rate identical to the seismic record and was smoothed twice with a 5x5 filter.

Comparison between weak motion and 2D modeling for the SIOE, SIOM, SIOO and SIOP stations is given in figure 4.56 for the EW rotated component (parallel to the main valley axis - Y component in the 2D modeling). As 2D modeling was limited in the calculation to 5 Hz, the comparison is displayed up to this frequency. The same comparison for the NS rotated component (perpendicular to the main valley axis) is given in figure 4.57.

One interesting feature to observe is the good agreement of the fundamental frequency position between the seismic response predicted by the 2D modeling on the X component and the H/V ratio on the NS rotated component of weak motion for the SIOO, SIOE and SIOP stations. On the EW rotated component, it can be noticed that the fundamental frequency shifts toward higher value in the case of the weak motion for the SIOO and SIOP station.

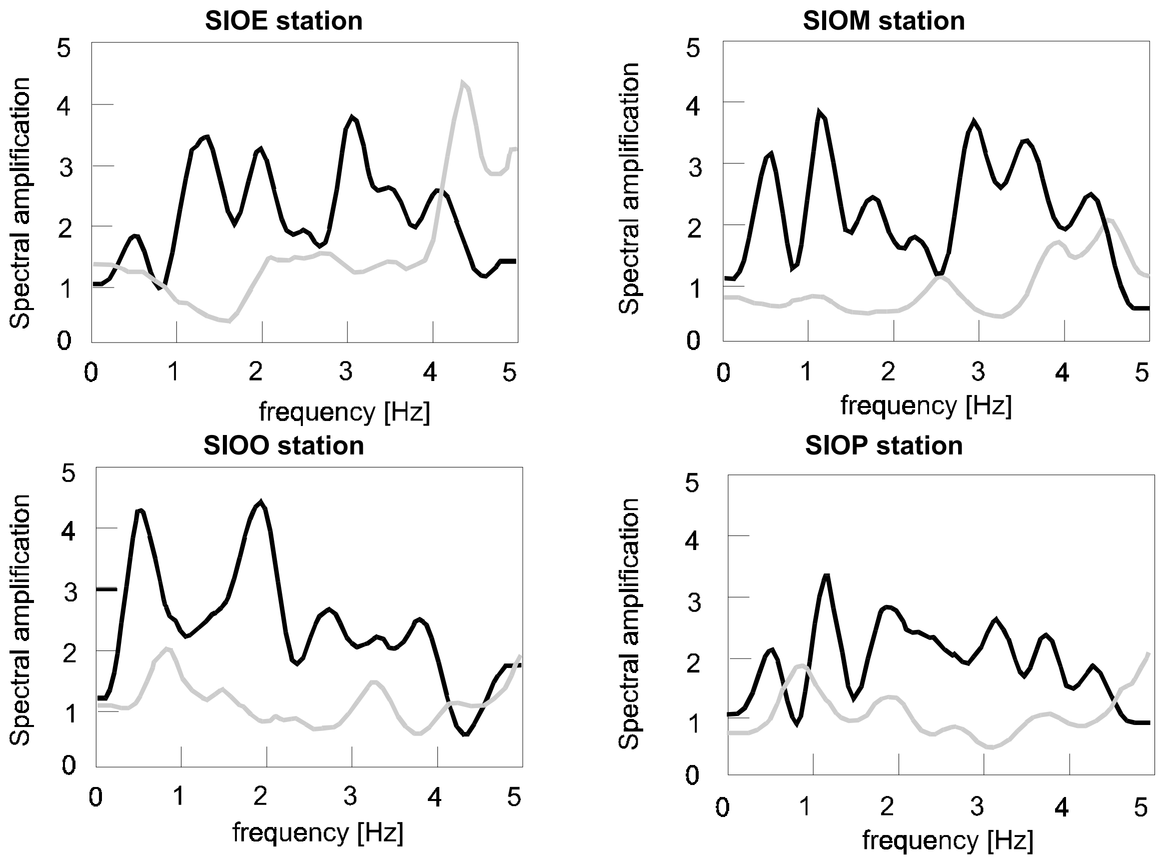

Figure 4.56. Comparison of amplification function between the rotated EW component of the weak motion (gray line) and 2D modeling - SH wave - Y component (black line) for stations SIOE, SIOM, SIOO and SIOP, located on the Rhône valley. Frequency range 0.1-5Hz.

Figure 4.56. Comparaison des fonctions d'amplification entre la composante EW modifiée du tremblement de terre (trait gris)) et la modélisation 2D - onde SH - composante Y (trait noir) pour les stations SIOE, SIOM, SIOO et SIOP, situées dans la vallée du Rhône. Interval de fréquence 0.1-5Hz.

Then considering the two stations exhibiting a low frequency peak on weak motion for both components, i.e. SIOO and SIOP stations, the following points can be noticed :

- for both stations, the difference on the fundamental frequency value between the NS and EW rotated components of the weak motion is not as high as predicted by the 2D modeling. In contrast, the SIOP station exhibits a remarkably stable fundamental frequency on both components;
- for both stations, the value of the fundamental frequency observed on the EW rotated component is higher for the weak motion than predicted by the 2D modeling;
- on the SIOO station, the small shift toward lower frequency for the NS rotated component in comparison with the EW rotated component, which is in contradiction with the 2D modeling predicting the reverse case.

The amplification level is different between 2D modeling and weak motion. 2D modeling systematically exhibits higher values for the fundamental frequency. A possible explanation is that weak motion does not contain enough energy to excite the very low frequencies up to a certain level. Indeed it has been shown (e.g. Aki, 1967) that the amplitude spectrum density is dependent on the earthquake magnitude. The higher the magnitude, the higher will be the amplitude at low frequency.

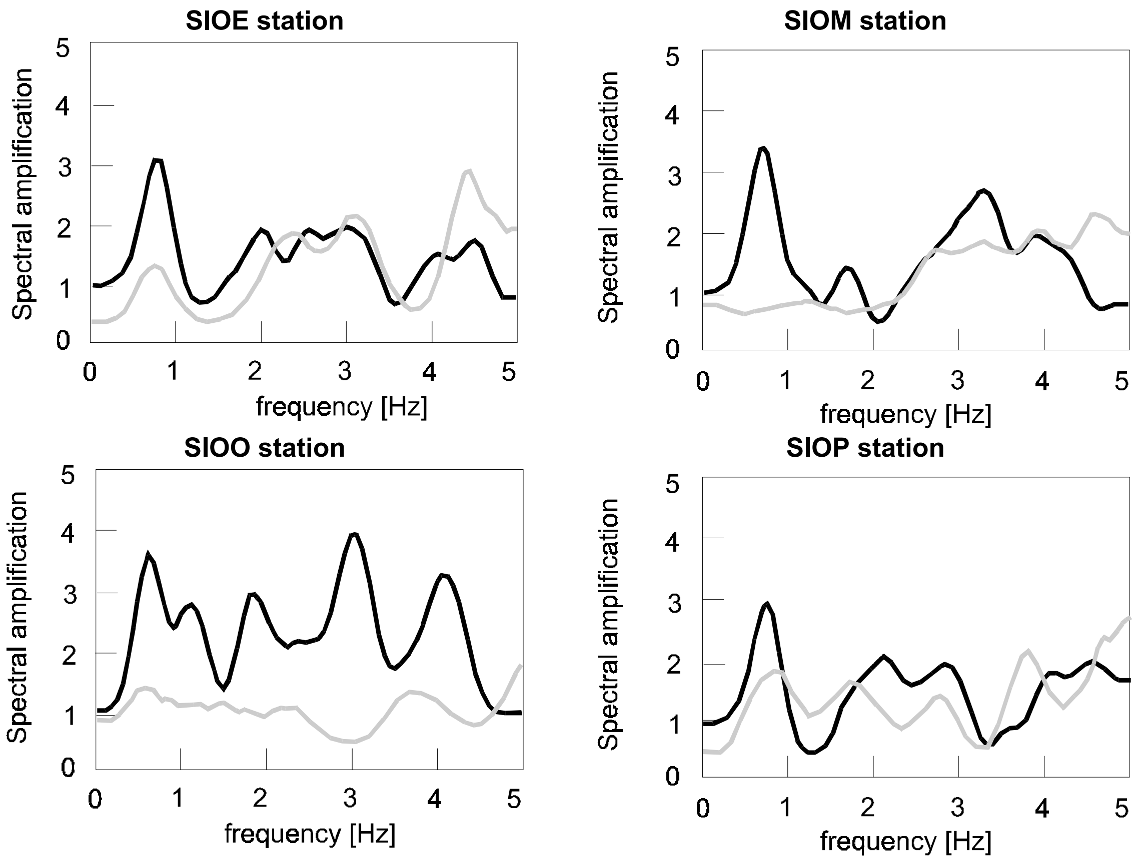

Figure 4.57. Comparison of amplification function between the rotated NS component of the weak motion (gray line) and 2D modeling - SV wave - X component (black line) for stations SIOE, SIOM, SIOO and SIOP, located on the Rhône valley. Frequency range 0.1-5Hz.
Figure 4.57. Comparaison des fonctions d'amplification entre la composante EW modifiée du tremblement de terre (trait gris) et la modélisation 2D - onde SV - composante X (trait noir) pour les stations SIOE, SIOM, SIOO et SIOP, situées dans la vallée du Rhône. Interval de fréquence 0.1-5Hz.

4.6 Conclusions

In the Sion area, 15 transverse profiles have been treated with 2D modeling. Based on the maximum amplification factor and its associated frequency, maps have been worked out. It could be shown that zone delineation are modified by the incidence angle of the seismic waves, especially in case of a non-vertical incident shear wave on a strongly asymmetric profile.

As modeling is always based on hypothesis and simplification at different level, other techniques have to be used in order to cross-check the results. Therefore microtremor measurements were recorded on sites as close as possible to the 2D modeling and a frequency map was also established based on the results obtained from the H/V ratio. It partly confirmed the results obtained from the 2D modeling, especially in the center part of the valley, characterized by the deeper sedimentary deposit. Both approaches agree on the fact that in this part of the valley induces a frequency resonance below 1 Hz. But 2D modeling predicts a higher value. Toward the edges, they show the same behavior, i.e. increasing frequency, but they disagree on the pattern. The 2D modeling predicts an increase of the frequency value from the center to the edge, whereas the H/V ratio technique produces zones on the edge either with higher frequency or lower frequency than predicted. This might be due by a change in physical properties of the sediments (velocity) or in thickness that is not shown by maps drawn from the high-resolution seismic profiles and thus not considered in the 2D modeling.

Considering sites where the stations of a temporary seismic network are located, weak motion data were analyzed using the H/V ratio technique, as the reference site showed to be subject to site effects. The comparison between H/V ratio on weak motion and on microtremors shows that the SIOO station (in the center of the valley) exhibits a fundamental frequency higher for the H/V on weak motion. It may be due to the fact that microtremors just have enough energy to excite the sedimentary layer beneath the measurement point whereas H/V on seismic motion can be contaminated with laterally propagating waves modifying the frequency content. On the valley edges, SIOP and SIOE show a different behavior. Both H/V ratios agree for the SIOP. For the SIOE, the fundamental frequency is not well marked. In all cases, the H/V ratio on weak motion and on microtremors shows a double peak. The occurrence of a second peak in higher frequency, which depends on the location, might be related to the presence of a water table, this element being at varying depth and modifying the Poisson’s ratio.

The comparison between weak motion and 2D modeling on single components shows a good agreement for the NS rotated component, but disagrees on the behavior on the EW rotated component. Moreover the SIOP station shows an unchanged position of the fundamental frequency on both components. A more representative database is therefore required to further investigate the reasons of discrepancies. Some of the remaining questions concern the stability of the fundamental frequency, the shift of its value toward higher frequencies, the sensitivity of the valley seismic response on the azimuth, incidence angle of incoming waves.

In conclusion 2D modeling predicts the general trend of the valley, showing that linear amplification is varying throughout the valley. Such results have a direct implication for infrastructure as areas are exhibiting different seismic behavior. Moreover the seismic response can be modified by very local geologic conditions. Therefore seismic zonation maps are an useful step in delineating tendency, but at specific sites, local detailed investigations (e.g. boreholes, geophysical and geotechnical measurements) are required.

5 MICROZONATION OF THE SUSTEN - BRIG AREA

Why was this data gathered?
What was collected?
Who collected it?
How was it collected?
How current is it?
Where is this data at?
Bureau of Land Management, Denver, 1995

5.1 Introduction

The Susten - Brig area is localized in the upper part of the Rhône valley, where the Quaternary sedimentary deposit becomes thinner. It is also the region where two of the strongest earthquakes in the Valais region occurred, i.e. 1755 Brig and 1855 Visp.

In this area the influence of local soil conditions will be analyzed based on a qualitative rating scheme allowing to consider the role of the surficial deposits, depth to the water table and also the thickness and the slope gradient of the sedimentary deposit as the results obtained in the Sion area showed that these two latter elements are among the controlling factors of the amplification distribution across the valley. A geographical information system is employed to facilitate the acquisition, handling and manipulation of all these data.

The study focuses on the zone limited by the following Swiss coordinates in meters :

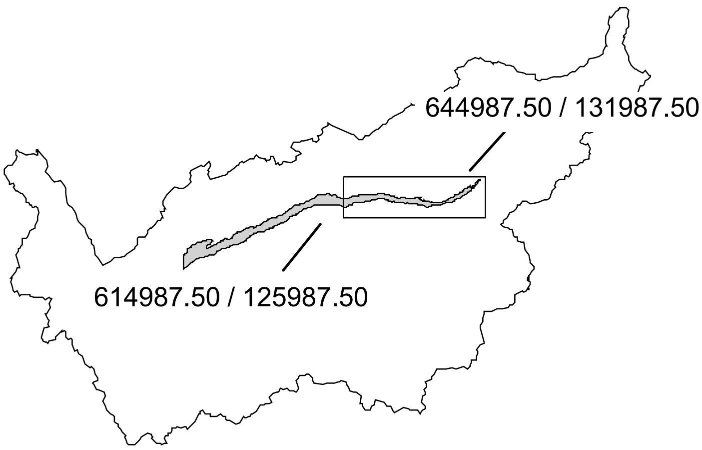

Figure 5.1. Localisation and coordinates of the Susten-Brig area in the canton of Valais.
Figure 5.1. Localisation et coordonnées de la zone Susten-Brig dans le canton du Valais.

For a better readability, all the final cartographic maps show the coordinates rounded to nearest kilometer, respectively 645 km/132 km and 615km/126 km. Moreover each thematic map is overlaid on the shaded relief obtained on the basis of the digital elevation model of the Swiss Federal Office of Topography.

All the analogue data were first digitized with Arc/Info, then rasterized and integrated into the IDRISI geographical information system. Spatial analysis requests each integrated layer inside the database to be conformed in terms of the number of rows and columns, the coordinates and the resolution. Therefore the concerned study area is composed of 240 rows and 1200 columns. The resolution is set to 25 m.

The analogue maps on the surface geology, depth to the ground water table and thickness of the Quaternary deposit were drawn at 1:10'000 scale on the basis of a field campaign carried out in May-June 1996 (Vaudan, 1996) for the SISVAL project (Wagner et al. 2000).

5.2 GIS database

5.2.1 Introduction

In this part of the work, one will indicate the most important parameters that characterize the various layers that have been created and combined. Therefore the data will be described by defining the purpose and the date of the data, accuracy of the data, the spatial data representation, the spatial reference system, and the attribute description (e.g. descriptor, ordinal number, etc.).

Accuracy is often confused with precision. Tomlin (1990) gives the following explanation to clarify these terms :

Whereas the precision is the degree of refinement with which a measurement can be expressed, accuracy is the degree to which such a measurement conforms to that which it represents.

There are at least two levels of accuracy, positional and attribute accuracy.

The positional uncertainty of coordinate data for vector data is usually estimated by the root mean square error (RMS error) during the digitalization. It is based on the differences between the coordinates on the analog map and the coordinates after transformation and the mean error is expressed in the same unit as the cartographic data. The formula is the following :

$$\text{RMS error} = \sqrt{\frac{\sum (X_i - X_t)^2}{n}}$$

X_i being the real coordinates and X_t the transformed coordinates; n is the number of measurements.

As an example, based on a map at a scale 1:10'000 (in centimeter) which has been digitized with a RMS error equal to 0.001 (or 1mm), the positional accuracy is then not better than 10 m.

The attribute accuracy is more difficult to define as numerous processes can intervene from the field information to the integration into a GIS modifying the quality of data. Therefore an attribute accuracy would rather be defined on a qualitative scheme.

5.2.2 Surficial geologic map

5.2.2.1 Introduction

Standard geologic maps usually depict the Quaternary deposit as a single unit. However earthquakes have shown that the distribution of damages is not only depending on the quality of the construction but is also strongly related to the variation within the Quaternary deposits. Physical properties such as seismic velocity or density of materials are related to the type of deposit (alluvial fan, alluvial plain, fluvial terrace, etc), its composition (gravel, sand, silt, clay) and its age (Holocene, Pleistocene). Therefore identifying the different types of deposit is a preliminary and necessary step.

Numerous geotechnical investigation, mainly in United States and Japan, are carefully analyzing the first 30 meters for seismic zonation purpose, as these meters are considered to have the most critical impact on the amplification (Hays, 1980).

5.2.2.2 Description

The mapping, based on field observations, boreholes log and geotechnical reports allowed to draw a surface geologic map with 11 characteristic units, such as :

- Flooding deposit,
- Flooding deposit on old alluvial fan,
- Rhône gravel,
- Young alluvial fan (active or recently active fan),
- Old alluvial fan (inactive fan),
- Debris,
- Dump,
- Artificial filling up,
- Old loops of river filled,
- Ancient marshes,
- Sandy lens,

These units were all deposited during the Holocene period (less than 10,000 years old). Deposits like old loops of river or ancient marshes are related with the Rhône river history and were mapped as active in 1860 by the Swiss Federal Railways. The flooding deposit on old alluvial fan is located in Brig and is the result of the Saltina river floodings which occurred in 1993 (Kunz & Rey, 1995). Dump and artificial filling up are the result of the human activities in the last 40 years.

Looking up to the first 30-40 meters, the Rhône alluvium deposit can be divided into the units described in table 5.2 (Vaudan, 1996).

The flooding deposit is mainly characterized by silt. As the thickness of this material is varying, showed by the boreholes data, and as this element is a factor influencing the soil behavior during an earthquake, distinction was made as followed :

- flooding deposit (silt) on Rhône gravel > 1m thick
- flooding deposit (silt) on Rhône gravel < 1 m thick

Units	Depth [m]	Lithology	N value range SPT
Superior flooding deposit a)	0 - 5	sandy silt	2 - 29
Superior Rhône gravel	5 - 10	sandy, silty gravel	2 - 87
Inferior flooding deposit	10 - 25	fine sand, silt	5 - 39
Inferior Rhône gravel b)	25 - 30	sandy, silty gravel	14 - 85

a) up to 20 m at certain places
b) up to 40 m at certain places

Table 5.2. Geotechnical characteristics of the Rhône alluvium.
Tableau 5.2. Caractéristiques géotechniques des alluvions du Rhône.

The characteristics of the digitized map are described In table 5.3. The resulting raster map is displayed in figure 5.4a. It shows that the dominating deposit is the flooding deposit on the Rhône gravel with a thickness superior than 1m.

Identification	Created on	30.12.96
	Corrected on	31.01.97
Spatial data organization	spatial data representation	Vector object : polygon
Data quality	RMS error positional accuracy	0.001-0.002 10-20 m
	lineage	analogue map 1:10’000
Reference system	Spatial reference system Xmin - Xmax Ymin - Ymax	Swiss Coordinates in meter 616’000 - 644’000 126’000 - 130’000

Table 5.3. Main characteristics of the vector file established from the analog map on surficial geology.
Tableau 5.3. Caractéristiques principales du fichier vecteur obtenu à partir de la carte analogique de la géologie de surface.

Susten-Brig area

a) Surficial geologic map

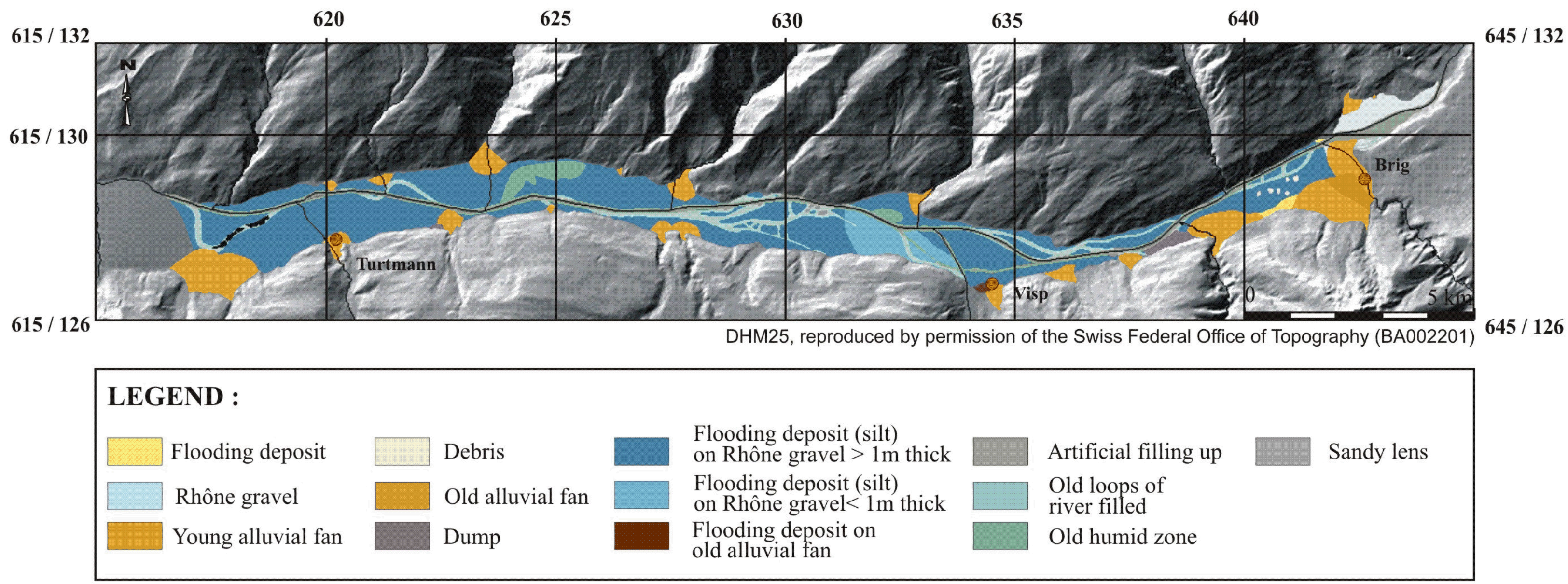

b) Depth to the ground water table

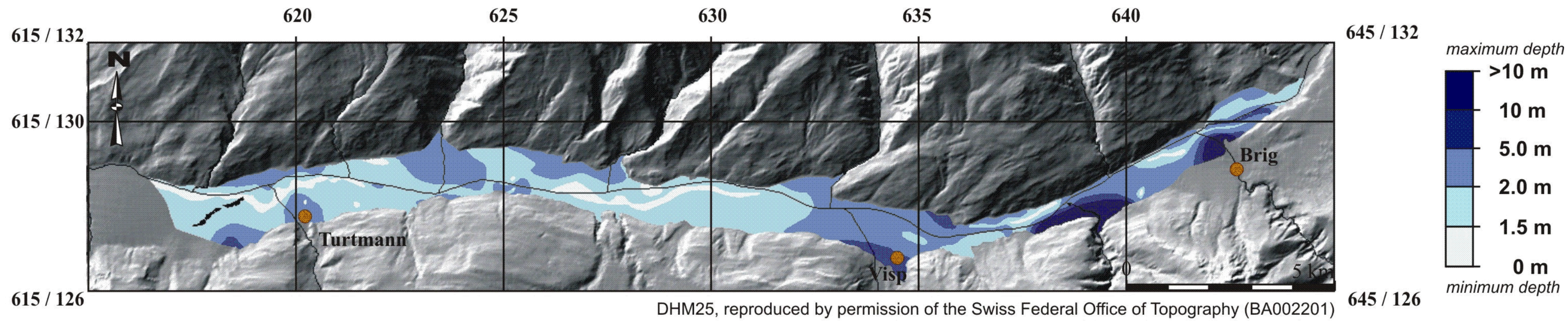

Figure 5.4. a) Surficial geologic map
b) Depth to the water table

5.2.3 Depth to the ground water table

5.2.3.1 Introduction

Gutenberg (1957) mentioned that ground shaking was stronger at places where the ground water table was close to the surface and that his defined average ratio of duration was affected by the variation of the depth to the water table.

The fact is that the depth to the ground water table implies the existence of a non-saturated layer with variable thickness depending on the variation of the ground water table. This layer, called low velocity layer in seismic exploration, has specific characteristics, such as (Sheriff & Geldart, 1995) :

- high capacity of seismic energy absorption,
- large effects on traveltimes due to the low velocity and rapid change in velocity,
- due to the low velocity, wavelengths are shortened therefore much smaller features can produce significant scattering and noise,
- the marked change at the base of the layer bends the seismic rays, thus the travel through the layer is almost vertical whatever the direction of travel beneath the layer.

Therefore this layer represents a strong discontinuity especially for P wave velocity as this kind of wave is sensitive to the water content. Moreover considering an incident SV wave, the converted P wave at the free surface can be trapped in this layer and induce high-frequency resonance which has only been observed on vertical component (Aki, 1988).

Another effect that can be provoked by the presence of a shallow ground water table at a site is the ground failure induced by liquefaction. The susceptibility of this phenomenon decreases as the depth to the water table increases (Kramer, 1996). But it also depends on geologic criteria (soil type, age of deposit, density) and earthquake characteristics (magnitude, duration and amplitude).

In the Rhône valley water escape structures in the alluvium were reported during the 1755 and 1855 earthquakes in Brig and Visp. Such structures are generally considered as an indicator of high excess pore pressure generation which is an element to induce ground failure if this excess is large enough (Kramer, 1996). However the liquefaction phenomenon can occur without inducing ground displacement and ground failure large enough to cause damage to buildings and other structures (Bertero et al. 1997). Therefore a careful investigation on liquefaction susceptibility and opportunity (which depends on the frequency of earthquake occurrence and the intensity of seismic ground motion; Bertero et al. 1997) is required to define the potential of liquefaction of an area and to which extent it will occur, this is a study on its own not included in this work.

Estimation of the influence of the water table on seismic intensities (table 5.5) was initially given by Medvedev (1965) and Evernden & Thomson (1985). In Switzerland, 320 macroseismic observations show that the presence of a shallow water table (0 to 5 m below the ground surface) can increase the seismic intensity up to 1.5 MSK unit (Beer, 1997).

Medvedev (1965)		**Evernden & Thomson (1985)**	
depth to the ground water table [m]	Intensity increment	depth to the ground water table [m]	Intensity increment
0-1 4 10	1 0.5 0	0-30ft (0-9m) 30ft - 100 ft (0-30m) /	1.5 0.5 /

Table 5.5. Intensity increment in function of the depth to the ground water table.
Tableau 5.5. Augmentation de l'intensité en fonction de la profondeur de la nappe phréatique.

5.2.3.2 Description

Thickness of the non-saturated layer can be considered as equivalent to the depth to water table as the latter term is defined as corresponding to the distance from the surface to free ground water (Rogers et al. 1985).

The basic information is given by piezometers which are densely distributed along the traffic lines in the Rhône valley. Regular campaigns are done during the year to obtain the information on the water table level. It is then possible to have its minimal and maximal position over a year. The thickness of the non-saturated layer is obtained based on the difference between the surface elevation and the altitude of the water table. In the present case, the reference altitude corresponds to the maximum altitude of the water table, i.e. the position at which the water table is the closest to the ground surface.

On the analogue map, the thickness of the non-saturated layer is drawn by isopachs. Each isopach has an attribute value between 1 meter to more than 10 meters.

The table 5.6 describes the resulting vector file.

Identification	Created on	15.01.97
	Corrected on	30.12.98
Spatial data organization	spatial data representation	Vector object : polygon
Data quality	RMS error positional accuracy	0.001-0.002 10-20 m
	attribute precision	1 m
	lineage	analogue map 1:10'000
Reference system	Spatial reference system Xmin - Xmax Ymin - Ymax	Swiss Coordinates in meter 615000 - 645000 126000 - 131000

Table 5.6. Main characteristics of the vector file established from the analog map on depth to the water table.
Tableau 5.6. Caractéristiques principales du fichier vecteur obtenu à partir de la carte analogique de la profondeur de la nappe phréatique.

The valley boundary, which includes the alluvial fan limits, was used to close all the isopachs before rasterization. The resulting raster image is displayed in figure 5.4b classified in five categories. It can be noticed that the ground water table mostly lies between 0 to 5 meters under the surface and that the maximum depth to the water table (> 10 m) occurs where alluvial fans take place.

5.2.4 Thickness of the Quaternary deposit

5.2.4.1 Introduction

The Quaternary alluvial deposit increases the amplitude of the seismic waves several times more than the rock. The thickness of such deposit is one of the significant parameters controlling the ground motion, especially for the resonant frequency at which the maximum amplification will occur. Usually this frequency will decrease as the thickness of the deposit increases (Gutenberg, 1957; Rogers et al. 1985).

In terms of intensity, based on macroseismic observations through Switzerland (Beer, 1997), the general tendency is that the presence of an unconsolidated deposit layer increases the seismic intensity whatever the thickness. The mean intensity increment varies between 0.2 up to 1.2 MSK unit. The maximum increment occurs for thickness ranges 0-5m and 50-100m for which the MSK seismic intensity increment can go up to 1 MSK unit.

5.2.4.2 Description

The Turtmann high-resolution reflection seismic profile (PNR20) and the one deep borehole in Brigerbad (Service des routes nationales, Bianchetti, 1988) are the only source of information about the thickness of the Quaternary sedimentary deposit in this part of the Rhône valley. Therefore as a preliminary approach the thickness was determined based on a geometrical technique. Using several profiles across the valley, the flanks of the valley were extrapolated until they cross, based on the assumption that they follow the same slope gradient under the surface. Thus the isopachs were drawn between the profiles (Vaudan, personal communication) each 100 m up to a maximum value of 400 m. The analogue map was drawn at a 1:10'000 scale. The digitalization of the map was processed with ARC/INFO giving the vector file of which the characteristics are described in table 5.7. The contour of the valley including the alluvial fans was added to represent the zero isopleth, without closing the extremities in order to avoid a too important distortion during the interpolation procedure.

Before interpolation, the vector file was transformed in a raster image, and then transferred to the Ilwis software. This software had at that time a more efficient interpolator than the IDRISI software. Then the resulting image has been smoothed by a 3x3 window and corrected from deviant values which appeared at the open ends. This operation was processed by overlaying a mask on the raster image.

Identification	Created on	30.12.96
	Corrected on	05.02.97
Spatial data organization	spatial data representation	Vector object : isoline
Data quality	RMS error positional accuracy	0.001-0.002 10-20 m
	attribute precision	100 m
	lineage	analogue map 1:10'000
Reference system	Spatial reference system Xmin - Xmax Ymin - Ymax	Swiss Coordinates in meter 615000 - 645000 127000 - 130000

Table 5.7. Main characteristics of the vector file established from the analog map on thickness of the Quaternary deposits.
Tableau 5.7. Caractéristiques principales du fichier vecteur obtenu à partir de la carte analogique de l'épaisseur des dépôts quaternaires.

Finally the image was classified in 5 categories of thickness and the resulting image is displayed in figure 5.a. The distribution of the categories over the study area in terms of number of pixels for each category, indicated in figure 5.9, shows that the dominant category is for 0-50m, followed by the 100-200m one.

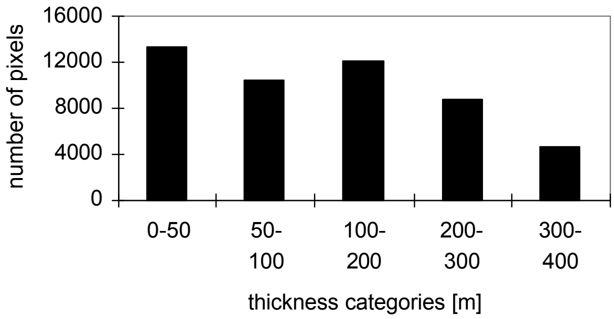

Figure 5.9. Distribution of thickness categories in number of pixels.
Figure 5.9. Distribution des catégories d'épaisseur en nombre de pixels.

Susten - Brig area

a) Thickness of the Quaternary sedimentary deposit

b) Slope gradient of the bedrock

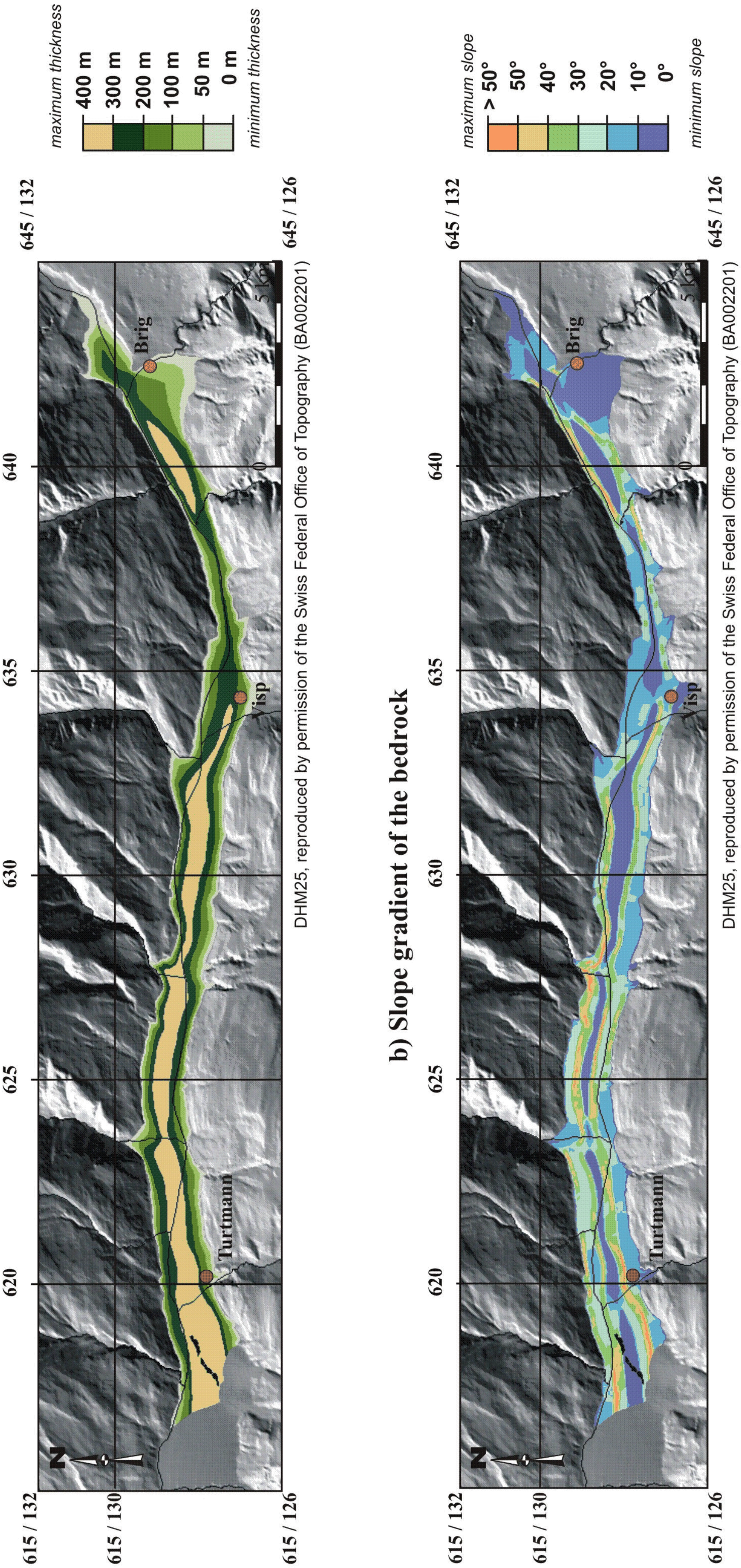

Figure 5.8 a) Thickness of the Quaternary sedimentary deposit
b) Slope gradient of the bedrock

5.3 Qualitative seismic amplification map

A microzonation map integrating the influence of the local site conditions is already existing for the Susten-Brig area (Wagner et al. 2000). This map (figure 5.15b) is expressed in terms of MSK seismic intensity correction factors. Correction factors have been estimated for the various surficial geologic units, the depth to the water table and the thickness of the sedimentary deposit. However it does not consider the slope gradient, a parameter which also controls the amplification distribution across the valley as demonstrated in the Sion area.

In order to capture the effect of this element on the distribution of the amplification in the Susten-Brig area, and as no corresponding MSK intensity correction factors are available, a qualitative rating scheme is developed and applied. The rating scheme has for purpose to assign various values to qualify the influence of a specific parameter on the ground motion. In this case the value 1 has been chosen to indicate the lower influence on the ground motion and the value 5 the stronger influence. Due to the available data the rated parameters are the surficial geologic deposit, the depth to the ground water, the thickness and the slope gradient of the Quaternary deposit. For the first two parameters, the rating scheme is based on the intensity increment that has been estimated in the SISVAL project (Wagner et al. 2000), 5 being attributed to the maximal intensity increment.

For the thickness of the Quaternary deposit and the slope gradient of the bedrock, the rating scheme is based on 2D modeling results obtained in the Sion area (§ 4.3.4.1). For each class in each parameter, the maximum relative amplification is given in function of the type of shear wave (SV and SH) at vertical incidence (table 5.10).

Thickness [m]	SH amplification	SV amplification
0-50	1-2	2-4
50-100	4-6	2-4
100-200	6-8	4-6
200-300	10-12	6-8
300-400	8-10	8-10
400-500	8-10	6-8
500-600	8-10	6-8

Slope gradient [°]	SH amplification	SV amplification
0-10	1-2	6-8
10-20	8-10	4-6
20-30	10-12	4-6
30-40	6-8	4-6
40-50	8-10	6-8
≥50	8-10	6-8

Table 5.10. Distribution of the SH and SV amplification for each category of the Quaternary thickness and the slope gradient of the bedrock in the Sion area.
Tableau 5.10. Distribution des amplifications SH et SV pour chaque catégorie d'épaisseur du Quaternaire et du gradient de pente du soubassement rocheux dans la zone de Sion.

The slope gradient of the bedrock in the Susten-Brig area has been calculated using the module SURFACE of IDRISI. Values are varying between 0.1-85°. In order to attribute qualitative factors, the image is classified in 6 classes as described in table 5.11. The resulting map is presented in figure 5.8b. The histogram of the slope gradient categories distribution over the study area in terms of the number of pixels (figure 5.12) shows that the dominant slope gradient class is the category 0-10°, in the center part of the valley.

Values	Classes
0-10	1
10-20	2
20-30	3
30-40	4
40-50	5
≥50	6

Table 5.11. Classification of the slope gradient in the Susten-Brig area.
Tableau 5.11. Classification appliquée aux valeurs de gradient de pente dans la zone de Susten-Brig.

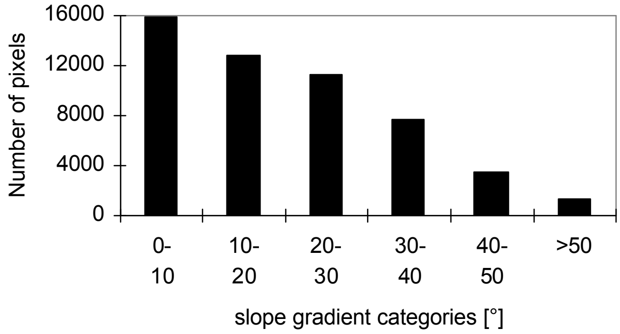

Figure 5.12. Distribution of the slope gradient categories in number of pixels.
Figure 5.12. Distribution des catégories de gradient de pente en nombre de pixels.

Table5.3. The final qualitative seismic amplification map is displayed in figure 5.15a.

It can be seen that the pattern of zones displaying the highest qualitative amplification is mostly controlled by thick deposit and/or by the slope gradient categories characterized by the highest qualitative value (40-50, 20-30, 30-40).

Comparison between the qualitative amplification map (figure 5.15a) and the seismic intensity correction map (figure 5.15b) shows that in the latter case, the amplification distribution is more sensitive to the type of deposit and depth to the water table. Indeed the MSK intensity factor can decrease up to 1 unit MSK when the depth to the water table is increasing from the class 1.5-2.0 to the category 2.0-5.0.

Geologic and geotechnical factors	Rating scheme
Surficial geologic deposits	
• Rhône gravel + old alluvial fan + flooding deposit on old alluvial fan	**1**
• Recent and silty alluvial fan + debris	**2**
• Flooding deposit + Flooding deposit on Rhône gravel ≤ 1 m thick) + old loops + old humid zone + sandy lens	**3**
• Flooding deposit on Rhône gravel > 1 m thick + Artificial filling up + Dump	**4**
Depth to the water table [**m**]	
0-1.5	**5**
1.6-2.0	**4**
2.1-5.0	**3**
5.1-10.0	**2**
>10	**1**
Thickness of the Quaternary deposit [**m**]	
0-50	**1**
50-100	**2**
100-200	**3**
200-300	**5**
300-400	**4**
Slope gradient of the bedrock (in degree)	
0-10	**1**
10-20	**2**
20-30	**4**
30-40	**3**
40-50	**5**
>50	**5**

Table 5.13. Rating scheme applied in the Susten-Brig area for the qualitative seismic amplification map based on the local geologic conditions.
Tableau 5.13. Catégorisation appliquée dans la région de Susten-Brig pour la carte d'amplification sismique qualitative basée sur les conditions géologiques locales.

Class of amplification factor	Descriptor of amplification level
3 - 6	very low
6 - 9	low
9- 12	medium
12- 15	high
15 - 19	very high

Figure 5.14. Corresponding scale between qualitative amplification factors and descriptors.
Figure 5.14. Echelle de correspondance entre les facteurs qualitatifs d'amplification et les descriptions du niveau de l'amplification.

Susten-Brig area

a) Qualitative seismic amplification map

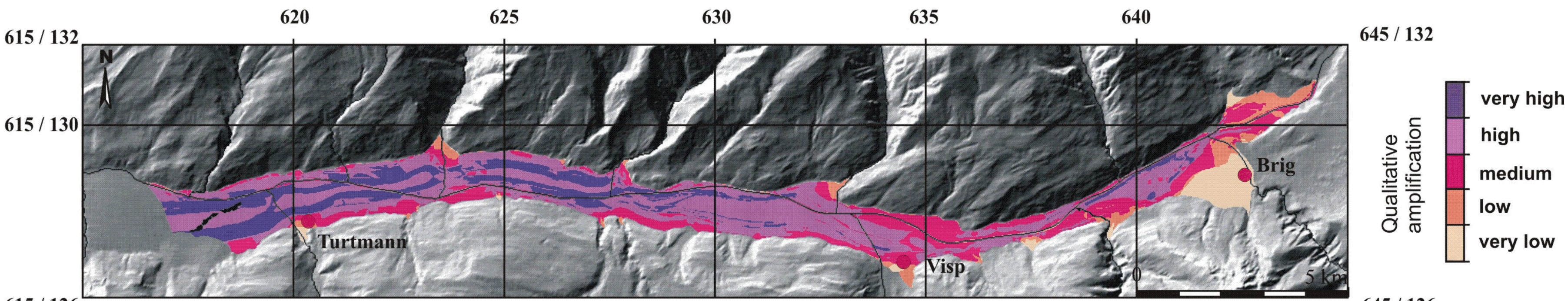

DHM25, reproduced by permission of the Swiss Federal Office of Topography (BA002201)

b) MSK seismic intensity correction map

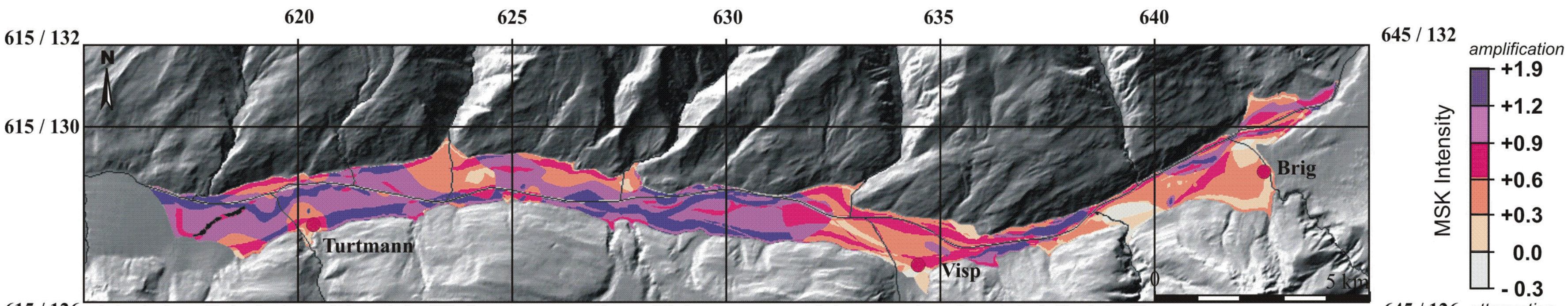

DHM25, reproduced by permission of the Swiss Federal Office of Topography (BA002201)

Figure 5.15. a) Qualitative seismic amplification map
b) MSK seismic intensity correction map

5.4 Conclusion

Both seismic microzonation approaches confirm that the upper part of the Rhône valley has the capability to amplify the ground motion, and it is due to its specific conditions, i.e. thick young Quaternary sediments, steep slopes, shallow water table and rapid lateral variations of surficial geologic deposits.

Comparison of results demonstrates the role of parameters that play a major role in amplification but at different level. Indeed the geometry of the valley, which is characterized by its slope gradient and thickness variation, mostly controls the amplification at a larger scale whereas the surficial deposits and the ground water table will modify the seismic response at a very local scale.

6 DISCUSSION ON MICROZONATION MAPS

Several methodologies, from a qualitative rating scheme to numerical modeling, have been employed in this research in order to characterize the influence of the local geologic conditions on the ground motion. Each technique carries intrinsic advantages and limitations of utilization as summarized in the table 6.1.

Among these methodologies, three have been applied for microzonation purpose, i.e. the rating scheme based on the seismic intensity, the H/V ratio on microtremors and the 2D modeling. The question that may arise and which is of prime importance for the utilization of microzonation maps is related to the uncertainty level associated with the results.

6.1 Uncertainties

It was not the purpose of this research to track uncertainties through all the data and to quantify them. This task is complex as the establishment of maps include all steps from data acquisition to integration into a GIS and to their treatment. Nevertheless it is necessary to be conscious that uncertainties are always present. In microzonation procedure, uncertainties are of three major types, i.e. spatial uncertainty, model uncertainty and parameter uncertainty.

6.1.1 Spatial uncertainty

Spatial uncertainty is related to positional errors, various data scales and parameter variations defining the boundary characteristics.

Positional errors can originate from source documents (positional errors during compilation or production) and analog to digital conversion. Regarding the scale, the only limit which can be postulated is that the positional accuracy in both study areas is not better than 25 m, based on the resolution of the grid image.

All microzonation maps produced in this work display boundaries. In most cases these boundaries are not hard boundaries as initial maps exhibit continuous variation of parameters (e.g. slope gradient, thickness of sediments, amplification level). Boundaries result from classification of data, a procedure applied for cartographic representation purpose.

6.1.2 Model uncertainty

Model uncertainty is caused by the simplification of the nature complexity (e.g. geological context, seismic solicitation) or connected with the lack of knowledge on processes.

Simplification is usually considered to be acceptable when results are close to the reality. On opposite a more complex model will require a greater number of data and even more detailed, which are usually not available.

Method of investigation	Parameters	Main advantages	Main limitations
Qualitative rating scheme	• Qualitative factors	• rating the factors which are believed to influence the seismic response of a specific site (thickness of the quaternary deposit, lithology, slope, depth to the water table, etc)	• has to be improved by new macroseismic data
Seismic intensity anomalies	• correction factors based on intensity MSK anomalies	• the amplification or attenuation factors are expressed in terms of seismic intensity, allowing to test the influence on the regional seismic hazard	• the anomaly values depend on the attenuation law definition
Standard spectral ratio on weak or strong motion	• fundamental resonant frequency and superior resonant peak frequencies • amplification factor • based on 1D assumption	• based of seismic events • not dependent on the regional seismic hazard	• request a site on rock as a reference site • request a consequent number of stations to illustrate all the local soil conditions available in an Alpine valley
H/V ratio on ambient seismic noise	• predominant frequency • amplification factor • based on 1D assumption	• fast data acquisition • not dependent on the regional seismic hazard	• underestimation of the amplification factor • application limits not well defined -theory has to be improved
1D modeling	• fundamental resonant frequency and superior peak frequencies • amplification factor	• multiple layers • not dependent on the regional seismic hazard	• good knowledge of geotechnical data requested • vertical column of soil only → do not consider the lateral effects which can be induced by the edges →underestimate the amplification
2D modeling	• predominant frequency • amplification factor	• consideration of the subsurface geometry which induce specific effects (duration, amplification, etc) • analysis of the main physical parameters which control the site effects (shape ratio, shear-wave velocity, Poisson's coefficient, etc.) • not dependent on the regional seismic hazard.	• computation requests (time, memory) • homogenous model (1 layer + half space) • the used model does not allow to consider the valley flanks on surface (could be integrated) • difficulty to obtain shear-wave velocity data, bulk density.

Table 6.1. Advantages and limitations of site effect analysis methods used in the Rhône valley.
Tableau 6.1. Avantages et limites des méthodes d'analyse des effets de site employées dans la vallée du Rhône.

Due to the very limited amount of strong motion data, the near field influence and the nonlinearity of soil response are phenomena that have not been brought into evidence in the Rhône valley yet. Distinction between near field and far field is done as at proximity of the epicenter (near field), source directivity and radiation pattern can have a stronger influence on the ground motion than the local soil conditions. The near field extension is depending on the magnitude of the earthquake as described by Krinitzsky & Chang (1988). The higher the magnitude, the higher is the near field extension. In their study, Krinitzsky & Chang (1988) showed that a 5.0 magnitude earthquake has a maximal extension of 5 km whereas a 6.0 magnitude earthquake will see its near-field extension multiply by a factor of five. Of course such results should be demonstrated in the Rhône valley environment.

Regarding the soil behavior, it is usually considered that it follows a linear behavior law, i.e. amplification factor based on weak motion should be extrapolated in case of strong motion. However nonlinearity of soil response, i.e. mainly a deamplification phenomenon, has been observed in laboratory and also in some strong motion events. Indeed strong motion events such as the 1985 Michoacan (M_w[1]=8.0) and 1989 Loma Prieta (M_w=7.1) earthquakes showed that weak motion amplification factor overestimated the strong motion one and that the deamplification was accompanied by changes in resonant frequencies, the values being shifted toward lower values (Beresnev & Wen, 1996). Up to now, the threshold acceleration beyond which nonlinearity will occur is not well defined. Moreover the level of nonlinearity depends on the physical properties of the soil. It may be considerable for soft clays and sands and negligible for stiffer materials (Beresnev & Wen, 1996).

In case of nonlinearity existence in the Rhône valley, the obtained microzonation maps in the Sion area and Susten-Brig area might be considered as a conservative case.

6.1.3 Parameter uncertainty

Parameter uncertainties or errors occur at all steps involved in the production of microzonation maps and they are propagating throughout. Uncertainties on parameter are related with the accuracy and precision of the input data and will influence the level of amplification and frequency. In the Sion area, the sensitivity study on the major parameters involved in the modeling allows to test the influence of parameter variations and in a way to constrain the uncertainties. In the Susten-Brig area, the chosen parameter is a qualitative factor, therefore uncertainty cannot be easily defined.

In both cases, only new geophysical, geologic and geotechnical data acquisition will allow to reduce the level of uncertainties.

6.2 Utility of microzonation maps

Establishment of microzonation maps through various independent techniques as it was done in this work helps to constrain the uncertainty. Indeed, the comparison of results shows similarities as well as discrepancies. Similarities tend to reduce uncertainties, whereas further investigation is required to understand the reasons of discrepancies.

The maps in this study are drawn based on the present knowledge and the available data and techniques. They can therefore be changed at any time as data are acquired and new methods are developed. Nevertheless such maps are an useful tool. They display areas in function of their capability to alter the ground motion. They cannot obviously be used immediately in a building

[1] Moment magnitude

code, but they can be useful in defining steps to improve such codes. These maps also contribute to raise awareness among policy maker, land-use planers and politicians on the capacity of Alpine valleys to amplify the seismic ground motion. They can serve as guidance for a preventive management.

7 CONCLUSIONS AND PERSPECTIVES

Local geologic conditions can strongly modify the impact of an earthquake. Therefore the purpose of this research was to analyze the seismic behavior of the Rhône valley as it is a deep and embanked Alpine valley characterized by thick and young Quaternary deposits, steep slopes, rapid lateral variation of surficial deposits and the presence of a shallow water table. Two zones have been investigated : the Sion and the Susten-Brig areas.

In the Sion area, the effect of the Rhône valley has been studied in the frequency domain using 2D modeling, H/V ratio on ambient seismic noise and on seismic ground motion. This part of the valley is characterized by a sedimentary filling having a maximum thickness up to 595 m and a strong seismic impedance contrast equal to 4.7.

The 2D results can be summarized as follows :

- The 2D modeling approach allowed to study the influence of the irregular interface between sedimentary deposit and surrounding rocks on the seismic response. The calculation was done in the frequency range up to 5Hz using a homogenous model with a viscoelastic behavior law. It has been stated that the fundamental resonant frequency stays unchanged whatever the position across the profile. This is an indication that the valley is susceptible to induce a resonance which involves the entire deposit as a whole. This phenomenon depends on the shape ratio, defined in function of the maximum thickness of the sedimentary deposit and its width, and on the velocity contrast between the sedimentary layer and the basement. These two parameters as well as the global thickness of the deposit, the type of incident wave and incidence angle also influence the value of this fundamental resonant frequency.

- The maximum amplification and its associated frequency are the parameters used to delineate zones capable of amplifying the seismic ground motion. The level of maximum amplification depends strongly on seismic velocity contrast. The position of amplification occurrence depends on the incidence wave and angle related to the geometry of the subsurface (irregularity and asymmetry).

- The maximum amplification occurs at the fundamental resonant frequency in the central part of the valley, which corresponds to the deepest part of the valley, and at higher frequency modes toward the edges.

Establishing zonation maps was another objective of this research. Predictive maps have been elaborated for the Sion area using 2D modeling and H/V ratio on ambient seismic noise results. Both methods agree on the fact that the fundamental resonant frequency is below 1 Hz and occurs in the part of the valley corresponding to the thickest part. And the frequency value is increasing toward the edges. But comparing the frequency maps obtained by 2D modeling and H/V ratio on microtremors, some discrepancies occur, the H/V ratio technique showing zones with higher or lower frequencies than predicted by the 2D modeling. Causes of this difference are likely to be related to very local geologic variation that are not be considered in the 2D modeling.

Sensitivity analysis on the 2D response according to various parameters (e.g. incidence angle of the wave, Poisson's ratio, seismic impedance, etc.) allows to constrain the uncertainties. These tests show that the critical parameter is the incidence angle related to a strong asymmetry of the valley geometry as it can modify the spatial distribution of maximum amplification and associated frequency in comparison with a vertical incidence. Other parameters, comprised in a plausible value range, only slightly modify the level of maximum amplification and the associated frequency without displacing the zones of maximum seismic response.

Seismic stations were installed at specific places on the valley floor in complement of the national network. Due to the trigger level, only one event was recorded; it is thus not a representative sampling for soil response characterization. However it allowed some preliminary observations. In the time domain records displaying longer duration and higher amplitude were found on site at the vertical of the valley slopes, as predicted by 2D modeling. In the frequency domain, 2D amplification function and H/V ratio on ground motion agree on the fundamental frequency in the center part of the valley, show a shift for stations located on the edges and disagree on the level of amplification. Regarding the comparison between the H/V ratio on weak ground motion and on ambient noise, it showed a good agreement on the predominant frequency for stations located on the edges, a shift toward higher frequency for the H/V on weak motion and the amplification obtained on ambient noise was lower of a factor around 1.5. Moreover both ratios exhibit two peaks, one in low frequency and one in high frequency and more or less accentuated depending on the location. This occurrence might be related to the presence in this area of a water table close to the surface.

In the upper part of the Rhône valley, in the Susten-Brig area, the capability of the Rhône valley to amplify the soil response has been evaluated based on a qualitative approach allowing not only to integrate geotechnical data but also to incorporate the information obtained in the Sion area. It has been compared with the seismic intensity anomaly approach applied in a previous work. Microzonation maps showed that in the case of the latter approach, the major factor controlling of the amplification phenomenon is the depth to the water table and thickness of the deposit, whereas for the qualitative approach, the soil response is mainly controlled by the steep slopes. Such results point out the spatial impact depending on the considered parameter. Indeed parameters such as slope gradient and thickness of the quaternary deposit are likely to have an impact on a larger scale than the surficial deposits and the depth to the water table, which are elements showing a great variability on a very local scale.

All these results, in the Sion area as well as in the Susten-Brig area, demonstrate the complexity of the amplification phenomena in Alpine valleys and expose some possible future lines of investigations, such as :

- the application domain of the H/V ratio on ambient seismic noise in Alpine valleys. This method is an interesting option in a moderate seismically active zone due to its rapidity of signal acquisition and treatment as well as its low cost. However it is necessary to further investigate the noise content and to better correlate measurements with the known geology and hydrogeology as well as geotechnical and geophysical parameters in order to develop a better understanding on the information given by the H/V ratio;

- the reduction of uncertainty. The use of various techniques in seismic response analysis and comparison of results allows uncertainties related to the chosen methodology to be reduced. Therefore microzonation maps are already an useful tool for preventive planning. However new knowledge on physical processes (e.g. near-field, non-linearity), new data acquisition (e.g. shear-wave velocity as a function of depth, quality factor), development of new model (e.g. integration of surficial layers) will allow to better constrain uncertainties and thus enhancing the microzonation map.

- the integration of the signal duration as a key parameter. In this work, the notions of qualitative amplification factor as well as predominant frequency and associated amplification are used. But also the signal duration has an impact on the resistance of built environment and is controlled by the local geologic conditions;

- the characterization of the seismic response in Alpine valleys in order to be used in building code procedures.

Finally this work points out that embanked and deep Alpine valleys, such as the Rhône valley, have a high capability to amplify the soil ground motion. The set of microzonation maps produced in this research could help in developing an improved building code and serve for guidance in a preventive land-use planning.

BIBLIOGRAPHY

Aki K. (1967) : Scaling law of seismic spectrum — Journal of Geophysical Research, vol. 72, N°4, 1217-1231

— (1988) : Local site effects on strong ground motion *in* Proceedings of the ASCE Conference on earthquake engineering and soil dynamics II, Rolla, Missouri, 103-155

Aki K. & Richards P.G. (1980) : Quantitative seismology : theory and methods — ed. W.H. Freeman, San Francisco, 932 p.

Balling N. & Banda E. (1992) : Europe's lithosphere - recent activity. In : A continent revealed : The European Geotraverse (D. Blundell, R. Freeman, and St. Mueller, eds), Cambridge University Press, 111-135

Bard P.-Y. (1994) : Effects of surface geology on ground motion: recent and remaining issues, 19 p. — Xth European conference on Earthquake Engineering, Vienne, August 28-September 2, 19 p.

Bard P.-Y. & Bouchon M. (1980a) : The seismic response of sediment-filled valleys. Part I. The case of incident SH waves — Bull. of the Seism. Soc. of America., vol.70, N°4, 1263-1286

— (1980b) The seismic response of sediment-filled valleys. Part II. The case of incident P and SV waves — Bull. of the Seism. Soc. of America., vol.70, N°5, 1921-1941

— (1985) : The two-dimensional resonance of sediment-filled valleys — Bull. of the Seism. Soc. of America, vol. 75, N°2, 519-541

Bard P.-Y., Bouchon M., Campillo M & Gariel J.-C. (1992) : Numerical simulation of strong ground motion using the discrete wavenumber method : a review of main results — Recent advances in Earthquake Engineering and structural dynamics, 23-64

Bard P.-Y & Chávez-García F. J. (1993) : On the decoupling of surficial sediments from surrounding geology at Mexico City — Bull. of the Seism. Soc. of America, vol. 83, N°6, 1979-1991

Beer Ch. (1997) : Erdbebengefährdung in Abhängigkeit des geologischen Untergrundes — Beiträge Geologie der Schweiz - Geotechnische Serie N°92, 66 p.

Beresnev I.A. & Wen K.-L. (1996) : Nonlinear soil response — A Reality ? — Bull. of the Seism. Soc. of Am., vol. 86, 1964-1978

Bernauer I. & Geiger A. (1986) : Lokale Schwerefeldbestimmung und gravimetrische Modellrechnungen im Satelliten (GPS)-Testnetz “Turtmann” (Wallis) — Geodätische-geophysikalische Arbeiten in der Schweiz 38. Schweizerische Geodätische Kommission, 106

Bertero V., Frohmberg K, Gath, E. Greene M., Hays W., Power M., & Youd T. L. (1997) : Earthquake basics. Liquefaction : what it is and what to do about it, — Earthquake Engineering Research Institute. Internet address : http://www.eeri.org/EQ_Basics/LIQ/LIQUEFAC.html, 8 p.

Besson O., Marchant R., Pugin A. & Rouiller J.-D. (1993) : Campagne de sismique-réflexion dans la vallée du Rhône entre Sion et St-Maurice : perspectives d'exploitation géothermique des dépôts torrentiels sous-glaciaires — Bull. du Centre d'hydrogéologie de l'Université de Neuchâtel, 12, 39-58

Borcherdt, R. D. (1970) : Effects of local geology on ground motion near San Francisco Bay — Bull. of the Seism. Soc. of America, 60, 1, 29-61

Borcherdt R. D. & Gibbs J. F. (1976) : Effects of local geological conditions in the San Francisco Bay region on ground motions and the intensities of the 1906 earthquake — Bull. of the Seism. Soc. of America, vol. 66, N°2,467-500

Bouchon M. & Barker J.S. (1996) : Seismic response of a hill : the example of Tarzana, California — Bull. of the Seism. Soc. of America, vol. 86, N°1A, 66-72

Bullen K.E. & Bolt B. A. (1993) : An Introduction to the theory of seismology, ed. Cambridge University Press, 4th edition, 499 p.

Burri J.-P. (1995) : Détermination par sismique des vitesses des ondes S et P dans la région de Vétroz — Rapport "Géologie-Géophysique, Genève" pour le project IDNDR-SISVAL, 38 p.

Collet C. (1992) : Systèmes d'information géographique en mode image — Collection gérer l'environnement, ed. Presses polytechniques et universitaires romandes, 186 p.

Cornell C.A. (1968) : Engineering Seismic Risk Analysis. Bull. Seism. Soc. of America, vol. 58, 1583-1606

Cotton F., Berge C., Lemeille F., Pitarka A., Lebrun B. & Vallon M. (1998) : 3D simulation of earthquakes and seismic hazard in the Grenoble's basin (western Alps) — Proceedings of the Eleventh European Conference on Earthquake Engineering, Paris, 6-11 septembre, 10 p.

Dao H. (1998) : L'accès aux données géoréférées à l'Université de Genève, séminaire Centre universitaire d 'écologie humaine (CUEH)

Dravinski M., Ding G. & Wen K.L. (1996) : Analysis of spectral ratios for estimating ground motion in deep basins — Bull. of the Seism. Soc. of America, vol. 86, N°3, 646-654

Duval A.-M., Méneroud J.-P., Vidal S. & Bard P.-Y. (1996) : Une nouvelle méthode d'évaluation de la réponse des sols aux séismes par enregistrement du bruit de fond — Bull. des Laboratoires des Ponts et Chaussées, 203, 75-90

Evernden J.F. & Thomson J.M. (1984) : Predicting Seismic Intensities — in J.I. Ziony (ed.) : Evaluating Earthquake Hazards in the Los Angeles Region, Prof. Pap. U.S. geol. Survey 1360, Washington D.C., 151-202

Fäh D. (1985) : Seismische Mikrozonierung in der Schweiz. Diploma Thesis, ETH Zürich, 126 p.

Fäh D., Rüttener E., Noack T. & Kruspan P. (1997) : Microzonation of the city of Basel — Journal of Seismology 1, ed. Luwer Academic Publishers, 87-102

Fäh D., Suhadolc P., Mueller St. & Panza G.F. (1994) : A hybrid method for the estimation of ground motion in sedimentary basins : Quantitative modeling for Mexico City — Bull. of the Seism. Soc. of Am., vol. 84, N°2, 383-399

Field E. H. & Jacob K. H. (1995) : A comparison and test of various site-response estimation techniques, including three that are not reference-site dependent — Bull. of the Seism. Soc. of Am., vol. 85, N° 4, 1127-1143

Finckh P. & Klingelé E., (1991) : Seismic reflection profiling in the Swiss Rhone valley, part 2 : gravimetric and geological interpretation of the Roche-Vouvry line — Eclogae geol. Helv. 84/3, 359-368

Finger W. & Weidmann M. (1987) : Quelques données géologiques nouvelles sur la vallée du Rhône entre Sierre et le Léman — Bull. Murithienne 105; 27-40

Finn W. D. L. (1991) : Geotechnical engineering aspects of microzonation *in* Proceedings of the fourth International Conference on seismic zonation, August 25-29, Stanford, California, USA, vol. 1, 199-259

Frischknecht C. (1997) : Bewertung des geologischen Untergrundes der Rhonetal - Region Sion auf die seisimiche Erschütterungsfähigkeit. In Mayer-Rosa D., Rüttener E., Fäh D., Schindler C., Beer Ch., Wagner J.J., Frischknecht C. Erdebebengefährdung und Mikrozonierung in der Schweiz. Beitrag zur Erforschung des Erdbebenrisikos in Abhängigkeit vom geologischen Untergrund — Schlussbericht NFP31, ed. vdf, ETH Zürich, 90 p.

Gariel J.-C., (1990) : programme de simulation 1D basé sur la méthode de Kennett (1983) — code numérique mis à disposition par le Laboratoire de géophysique interne et de tectonophysique en 1994

Geiger A, Kahle H.G., Gubler E. (1986) : Recent crustal movements in the Alpine mediterranean region analyzed in the Swiss Alps — Tectonophysics 130, 289-298

Gonzenbach M. (1997)a : Etude des effets de site par enregistrement du bruit de fond sismique, 1er rapport de travail — Ecole Polytechnique Fédérale de Lausanne et Centre des risques géologiques, Université de Genève, *inédit*, 47 p.

— (1997)b : Etude des effets de site par enregistrement du bruit de fond sismique, application de la méthode du rapport H/V (2ème rapport de travail) — Ecole Polytechnique Fédérale de Lausanne et Centre des risques géologiques, Université de Genève, *inédit*, 59 p.

Gonet O. (1965) : Etude gravimétrique de la plaine du Rhône; région St-Maurice - Lac Léman. Matériaux pour la Géologie de la Suisse, Géophysique N°6, Commission Géotechnique Suisse, 50

Grünthal G. (1998) : European Macroseismic Scale 1998, — cahiers du Centre européen de géodynamique et de séismologie, Luxembourg, 99 p.

Gutenberg B. (1957) : Effects of ground on earthquake motion — Bull. Seism. Soc. America, 47, 221-250

Hartzell S., Harmsen S., Frankel A., Carver D., Cranswick E., Meremonte M., & Michael J. (1998) : First-generation site-response maps for the Los Angeles Region based on Earthquake ground motion — Bull. Seismol. Soc. Am., vol. 88, N°2, 463-473

Haskell N.A. (1953) : The dispersion of surface waves in multilayered media — Bull. Seismol. Soc. America, vol. 43, 17-34

Hays W.W. (1980) : Procedures for estimating earthquake ground motion — Professional Paper 1115, United States Geological Survey, Reston, VA, 77 p.

Imai T. & Tonouchi K. (1982) : Correlation of N value with S-wave velocity and shear modulus — Proceedings of the second european symposium on penetration testing, Amsterdam 24-27 May, vol. 1, 67-72

Jongmans D. (1991) : L'influence des structures géologiques sur l'amplification des ondes sismiques, mesures in situ et modélisation — thèse, Université de Liège, inédit, 236 p.

Jongmans D. & Campillo M. (1993) : The determination of soil attenuation by geophysical prospecting and the validity of measured Q values for numerical simulations — Soil Dynamics and Earthquake Engineering, 12, 149-157

Kahle H.G., Geiger E., Bürki B., Gubler E., Marti U., Wirth B., Rothacher M., Gurtner W., Beutler G., Bauersima I., & Pfiffner O.A. : (1997) : Recent crustal movements, geoid and density distribution : contribution from intergrated satellite and terrestrial measurements — Results of NRP20, Deep structure of the Swiss Alps, ed. Birkhaüser Verlag, Basel, 251-259

Kennett B.L.N. (1983) : Seismic wave propagation in stratified media, ed. Cambridge University Press, 342 p.

King J.L. & Tucker B.E. (1984) : Observed variations of earthquake motion across a sediment-filled valley — Bull. Seism. Soc. of America, vol. 74, N° 1, 137-151

Kramer S.L. (1996) : Geotechnical earthquake engineering — ed. Prentice Hall, Upper Saddle River, New Jersey, 653 p.

Krinitzsky E. L. & Chang F. K. (1988) : Intensity-Related Earthquake Ground Motions — Bulletin of the Association of Engineering Geologists, vol. XXV, N°4, 425-435

Kudo K. (1995) : Practical estimates of site response. State-of-art report — Proceedings of the fifth international Conference on seismic zonation, October 17-19, vol. III, 1878-1907

Kunz P. & Rey J.-M. (1995) : Intempéries du 23 septembre 1994 dans le Haut-Valais (massif du Simplon) : répétition de l'événement de 1993 un an après, — Bull. Murithienne 113, 3-19

Lachet C. (1996) : Observation des séismes en milieux urbains : Méthodes simples d'étude des effets de site et de simulation des mouvements forts — Thèse, Observatoire de Grenoble et Laboratoire de géophysique et tectonophysique, Université Joseph Fourier Grenoble I, *inédit,* 245 p.

Lachet C. & Bard P.-Y. (1994) : Numerical and theoretical investigations on the possibilities and limitations of the Nakamura's technique — Journal of Physics of the Earth, vol. 42, 377-397

Le Brun B. (1997) : Les effets de site : étude expérimentale et simulation de trois configurations, — Thèse, Observatoire de Grenoble et Laboratoire de géophysique interne et tectonophysique, Université Joseph Fourier Grenoble I,*inédit,* 208 p.

Lermo J. & Chávez-García F.J. (1993) : Site effect evaluation using spectral ratios with only one station. — Bull. of the Seism. Soc. of America, vol. 83, N° 5, 1574-1594

— (1994) : Are microtremors useful in site response evaluation ? — Bull. Seism. Soc. Am., 83, 1350-1364

L'illustré (1946) : Quand la terre tremble — revue hebdomadaire suisse, N°5, 31 janvier 1946

Malagnini L., Tricarico P., Rovelli A., Hermann R.B., Opice S., Biella G. & de Franco R. (1996) : Explosion, earthquake and ambient noise recordings in a Pliocene sediment-filled valley : inferences on seismic response properties by reference- and non-reference-site techniques — Bull. of the Seism. Soc. of Am., vol 86, N°3, 670-682

Marchant R. & Stampfli G. (1993) : Interprétation des profils sismiques de Geothermoval dans la région de Sion — rapp. du Laboratoire d'interprétation de sismique réflexion, Université de Lausanne, *inédit*,

Mariétan I. (1945-46) : Le tremblement de terre du 25 janvier 1946 — bull. de la Murith., fasc. LXIII, 70-87

Matthews B. (1995) : The IBM / SP at the University of Geneva — internet address : http://sp.unige.ch

Maurer H.-R. (1993) : Seismotectonics and upper crustal structure in the western swiss Alps — dissertation ETHZ N° 10268, 159 p.

Maurer H.-R., Burkhard M., Deichmann N. & Green A.G. (1997) : Active tectonism in the central Alps : contrasting regimes north and south of the Rhone Valley — Terra Nova, vol. 9, 91-94

Mayer-Rosa D., Rüttener E., Fäh D., Schindler C., Beer Ch., Wagner J.J. & Frischknecht C. (1997) : Erdebebengefährdung und Mikrozonierung in der Schweiz. Beitrag zur Erforschung des Erdbebenrisikos in Abhängigkeit vom geologischen Untergrund — Schlussbericht NFP31, ed. vdf, ETH Zürich, 90 p.

Medvedev S.V. (1965) : Engineering seismology — ed. Oldbourne press, 112p.

Milstead J. & Feldman S. (1999) : Metadata : Cataloging by any other name —

internet address : http://www.onlineinc.com/onlinemag/OL1999/milstead1.html, 8 p.

Montandon F. (1942-43) : Les séismes de forte intensité en Suisse — extrait : Rev. Etudes Calamités, fasc. 18-19 et 20-21, 1-104

— (1946) : Les trois récents séismes du Valais Central — Revue pour l'étude des Calamités, tome IX, fasc. 24, 50-66

Montandon F. **& Staub W**. (1946) : Sur la cause des tremblements de terre du Haut-Valais — Globe LXXXV, Genève, *tiré à part*, 21 p.

Nakamura Y. (1989) : A method for dynamic characteristics estimation of subsurface using microtremor on the ground surface — Quaterly Report of Railway Technical Research Institute, vol. 30, N°1, 25-33

Office fédéral de statistique (1999) : Population — Annuaire statistique de la Suisse 1999, éd. Verlag NZZ, 1999, 15-61

Ohta Y. & Goto N. (1978) : Empirical shear wave velocity equations in terms of characteristic soil indexes — Earthquake Engineering and structural dynamics, vol. 6, 167-187

Olsen K. B., Pechmann J. C. & Schuster G. T. (1995) : Simulation of 3D elastic wave propagation in the Salt Lake Basin — Bull. of the Seism. Soc. of America, vol. 85, N°6, 1688-1710

Ornstein P. (1995) : inventaire des forages réalisés dans la zone Conthey-Granges, fichier informatique

Ott L., Larson R.F. & Mendenhall W. (1987) : Statistics : a tool for the social sciences. 4th ed., — ed. PWS Publishers, Boston, 576 p.

Papageorgiou A.S. & Kim J. (1991) : Study of the propagation and amplification of seismic waves in Caracas valley wih reference to the 29 July 1967 earthquake : sh waves — Bull. Seism. Soc. Am., 81, 2214-2233

Pavoni N., Maurer H. R., Roth Ph. & Deichmann N. (1997) : Seismicity and seismotectonics of the Swiss Alps — Results of NRP20, Deep structure of the Swiss Alps, ed. Birkhaüser Verlag, Basel, 241-250

Pedersen H. A. (1994) : Etude de la diffraction tridimensionnelle des ondes sismiques dans des structures à géométrie bidimensionnelle. Développement théorique et applications — Thèse de l'Université Joseph Fourier-Grenoble I, *inédit*, 182 p.

Pedersen H.A., Sánchez-Sesma F.J & Campillo M. (1994) : Three-dimensional scattering by two-dimensional topographies — Bull. of the Seism. Soc. of Am., vol 84, N°4, 1169-1183

Pedersen H.A., Campillo M. & Sánchez-Sesma F.J. (1995) : Azimuth dependent wave amplification by alluvial valleys **—** Soil Dynamics and Earthquake Engineering, 14, 289-300.

Pessina V., Groaz O. & Veronese L. (1997) : Microzonazione e scenario di danneggiamento sismico a scala locale per un'area di moderata pericolosità — Ingegneria sismica, Anno XIV, N°1, 20-30

Pfiffner O.A., Heitzmann P., Lehner P., Frei W. & Felber M. (1997) : Incision and backfilling of Alpine valley : Pliocene, Pleistocene and Holocene Processes —Results of NRP20 (National Research Program 20), Deep structure of the Swiss Alps, ed. Birkhaüser Verlag, Basel, 265-276

Pugin A., Marchant R., Besson O. & Stampfli G. (1997) : Seismic modeling of lines Martigny and Vetroz, *in* Incision and backfilling of alpine valleys : Pliocene, Pleistocene and Holocene processes — Results of NRP20 Deep structure of the Swiss Alps, ed. Birkhaüser Verlag, Basel, 272-276

Pugin A. & Marchant R. (1992) : Interprétation des profils sismiques de Geothermoval (Vallée du Rhône, de St Maurice à Bramois) — rapp. du Laboratoire d'interprétation de sismique réflexion, Université de Lausanne, 14 p., 9 planches, inédit

Ricker N. (1940) : The form and nature of seismic waves and the structure of seismograms — Geophysics, vol. V, N°1-4, 348-366

— (1945) : The computation of output distrubances from amplifiers fro true wavelet inputs — Geophysics, 10, 207-220

Riepl J. (1997) : Effets de site : Evaluation expérimentale et modélisations multidimensionnelles : Application au site test EURO-SEISTEST (Grece), Thèse de Doctorat, Universite Joseph Fourier, Grenoble 1, *inédit*

Riepl J. & Bard (1998) : 3D amplification patterns inside a sedimentary basin and their relation with the interface geometry — Proceedings of the Eleventh European Conference on Earthquake Engineering, Paris, 6-11 septembre, 11 p.

Riepl-Thomas J. & Cotton F. (1999) : Les effets de site. Importance, compréhension et estimation — Cahier Technique n°17, AFPS (Assoc. franç. du génie parasismique), 41-61

Roeder D. (1992) : Sardinia Channel and Atlas in Tunisia : Extension and compression *in* A continent revealed : The European Geotraverse (D. Blundell, R. Freeman, and St. Mueller, eds) — Cambridge University Press, 199-202

Roësset J. M. (1977) : Soil amplification of earthquakes *in* Numerical methods in geotechnical engineering — eds Desai and Christian, McGraw-Hill, New-York, 639-682

Rogers A.M., Tinsley J.C. & Borcherdt R.D. (1985) : Predicting relative ground response *in* Evaluation earthquake hazards in the Los Angeles Region - An earth science perspective — US Geological Survey prof. Paper 1360, 221-247

Rösli U. (1990) : Vereinfachte Geotechnische Karte der Schweiz, Erfassung auf ARC/INFO — Bundesamt für Wasserwirtsch., Bern

Rüttener E. (1995) : Earthquake Hazard Evaluation for Switzerland — Matériaux pour la Géologie de la Suisse, Geophysique Nr. 29, Commission Suisse de Géophysique, Studentendruckerei Zürich. 106 p.

Sägesser R. & Mayer-Rosa D. (1978) : Erdbebengefährdung in der Schweiz — Schweizerische Bauzeitung, 78/7, Zürich, 1 p.

Sánchez-Sesma F.J., Ramos-Martínez J. & Campillo M. (1993) : An indirect boundary element method applied to simulate the seismic response of alluvial valleys for incidence of P, S and Rayleigh waves — Earthquake engineering and structural dynamics 22, 279-295

Schindler C., Beer Ch., Mayer-Rosa D., Rüttener E., Wagner J.-J., Jaquet J.-M. & Frischknecht C. (1996) : Integrierte Auswertung von seismischen und bodenspezifischen Parameter : Gefährdungskarten im Kanton Obwalden **—** Landeshydrologie und -geologie, Geologische Berichte, Nr 19, Bundesamt für Umwelt, Wald und Landschaft, Bern, 29 Anhangen, 61 p.

Schön J. H. (1996) : Handbook of geophysical exploration. Seismic exploration. Physical properties of rocks : fundamentals and principles of petrophysics, eds. Helbig K. & Treitel S., Pergamon, Elsevier Science Ltd, Oxford, vol 18, 583 p.

Schweizerische Erdbebendienst - SED (1995) : Catalogue des tremblements de terre historiques suisses 1346-1995.

— (1998) : The National strong motion network
internet address :http://seismo.ethz.ch/networks/strong_motion/sm_net.htm

Seekins L. C., Wennerberg L., Margheriti L. & Liu H.-P. (1996) : Site Amplification at five locations in San Francisco, California : A comparison of S waves, codas, and microtremors — Bull. of the Seism. Soc. of America, vol 86, N°3, 627-635

Shah H.C., Mortgat C.P., Kiremidjian A. & Zsutty T.C. (1975) : A Study of Seismic Risk for Nicaragua, Technical Rep. 11, John A. Blume Earthquake Engineering Center, Stanford University, 187 p.

Sheriff R. E. & Geldart L. P. (1995) : Exploration seismology, Cambridge University Press, New-York, 592 p.

Smit P. (1996) : Datenerfassung und Bestimmung der Abminderung der Bodenbewegung bei Erdbeben in der Schweiz; Publikationsserie des Schweizerischen Erdbebendienstes Eidgenössische Technische Hochschule, Zürich, N°108, ed. Druck and Verlag AG, 261 p.

— (1998) : Strong motion bulletin October 1996-May 1998; Publication series of the Swiss Seismological Service, Federal Institute of Technology, Zürich, Swizerland; N°111

Sponheuer W. (1960) : Methoden zur Herdtiefenbestimmung in der Makroseismik — Freiberger Forschungshefte, C88, Akademie-Verglag, Berlin, 116 p.

Spudich P. Hellweg M. & Lee H.W. (1996) : Directional topographic site response at Tarzana observed in aftershocks of the 1994 Northridge, California, Earthquake: Implications for mainshock motions — Bull. of Seism. Soc. of America, vol. 86, N° 1B, S193-S208

Steidl J. H., Bonilla F. & Tumarkin A. G. (1995) : Seismic hazard in the San Fernando Basin, Los Angeles, CA : A site effects study using weak-motion and strong-motion data — Proceedings of the fifth international Conference on seismic zonation, October 17-19, vol. II, 1149-1156

Steidl J.H., Tumarkin A. G. & Archuleta R. J. (1996) : What is a reference site — Bull. of Seism. Soc. of Am. Vol. 86, N° 6, 1733-1748

Technical Committee for Earthquake Geotechnical Engineering - TC4 (1993) : Manual for zonation on seismic geotechnical hazards — ed. The Japanese Society of Soil Mechanics and Foundation Engineering, 149 p.

Theodulidis N. & Bard P.Y. (1995) : Horizontal to vertical spectral ratio and geological conditions : an analysis of strong motion data from Greece and Taiwan (SMART-1) — Soil Dynamics and Earthquake Engineering 14, 177-197

Theodulidis N., Bard P.Y., Archuleta R. & Bouchon M. (1996) : Horizontal-to-vertical spectral ratio and geological conditions : the case of Garner Valley downhole array in Southern California — Bull.Seism. Soc. Am., 86, 306-319

Thomson W.T. (1950) : Transmission of elastic waves through a stratified solid — Journal of applied Physics, 21, 89-93

Tomlin C. D. (1990) : Geographic Information Systems and Cartographic Modeling — ed. Prentice Hall, Englewood Cliffs, New Jersey, 249 p.

Vaudan J. (1996) : SISVAL : Région Susten-Brig, Rapport sur les cartes de base, *inédit,* 5p. + 9 annexes

Volger G. H. O. (1858) : Untersuchungen über das Phänomen der Erdbeben in der Schweiz. Dritter Theil : Die Erdbeben im Wallis, 524 p.

Wagner J.-J. (1970) : Elaboration d'une carte d'anomalie de Bouguer. Etude de la vallée du Rhône de St-Maurice à Saxon (Suisse) — Thèse, ed. Blanc-Wittwer S.A. Genève, *inédit*, 91 p.

Wagner J.-J., Frischknecht C., Rosset, Ph., Sartori M., Schindler C., Beer C., Mayer-Rosa D., Rüttener E., Smit P. (2000) : Contribution au zonage sismique dans la vallée du Rhône, entre Sion et Brig, canton du Valais, Suisse — projet SISVAL-IDNDR, Landeshydrologie und -geologie, Geologische Bericht, *en impression,* 104p.

Wanner E. & Grütter M. (1950) : Etudes sur les répliques du tremblement de terre du Valais, de 1946 à 1950 — bull. de la Murith., fasc. LXVII, éd. Société valaisanne des sciences naturelles, 25-42

Wenk Th., Lacave C. & Peter K. (1998) : The Adana-Ceyhan earthquake of June 27, 1998 — SGB, Schweizer Gesellschaft für Erdbebeningenieurwesen und Baudynamik, 47 p.

Yegian M.K., Ghahraman V.G. & Gazetas G. (1994) : Seismological, soil, and valley effects in Kirovakan, 1988 Armenia Earthquake — Journal of Geotechnical Engineering, vol. 120, N°2, 349-365

Appendix A

Rossi - Forel Intensity scale 1883*	MSK Intensity scale 1964	EMS scale 1998	Definition** of the EMS-98	Description of typical observed effects** (abstracted) of the EMS-98	Magnitude*
	I	I	**Not felt**	Not felt.	
I	II	II	**Scarcely felt**	Felt only by very few individual people at rest in houses.	2
II III	III	III	**Weak**	Felt indoors by a few people. People at rest feel a swaying or light trembling	3
IV	IV	IV	**Largely observed**	Felt indoors by many people, outdoors by very few. A few people are awakened. Windows, doors and dishes rattle	
V VI	V	V	**Strong**	Felt indoors by most, outdoors by few. Many sleeping people awake. A few are frightened. Buildings tremble throughout. Hanging objects swing considerably. Small objects are shifted. Doors and windows swing open or shut.	4
VII	VI	VI	**Slightly damaging**	Many people are frightened and run outdoors. Some objects fall. Many houses suffer slight non-structural damage like hair-line cracks and fall of small pieces of plaster.	5
VIII	VII	VII	**Damaging**	Most people are frightened and run outdoors. Furniture is shifted and objects fall from shelves in large numbers. Many well built ordinary buildings suffer moderate damage; small cracks in walls, fall of plaster, parts of chimneys fall down; older buildings may show large cracks in walls and failure of fill-in walls.	
	VIII	VIII	**Heavily damaging**	Many people find it difficult to stand. Many houses have large cracks in walls. A few well built ordinary buildings show serious failure of walls, while weak older structures may collapse.	
IX	IX	IX	**Destructive**	General panic. Many weak constructions collapse. Even well built ordinary buildings show very heavy damage; serious failure of walls and partial structural failure.	6
	X	X	**Very destructive**	Many ordinary well built buildings collapse.	7
X	XI	XI	**Devastating**	Most ordinary well built buildings collapse, even some with good earthquake resistant design are destroyed.	
	XII	XII	**Completely devastating**	Almost all buildings are destroyed.	8

* Smit (1996)
** Grünthal (1998)

c.frischknecht

Compilation of the main geophysical parameters measured in the Rhône valley

Author	Place	Methodology	Density [g/cm^3]		P velocity [km/s]		S velocity [km/s]	
			rocks	sediments	rocks	sediments	rocks	sediments
Gonet (1965)	from St-Maurice to the Leman	gravimetric study	2.40 - 2.67	1.9 - 2.0				
Wagner (1970)	from St-Maurice to Saxon	measurements on sample gravimetric modeling	2.67 (mean value)	2.2 (mean value)				
Bernauer &Geiger (1986)	Turtmann	gravimetric modeling	2.71 (mean value)	1.95-2.28 2.1 (mean value)				
Finck & Klingelé (1991)	Roche-Vouvry line	gravimetric study	2.67	1.30 - 2.30				
Klingelé (1997)	Rawil	gravimetric study - 3D modeling	2.70 - 2.72	2.0 (mean value)				
Finger & Weidmann (1987)	between Sierre and the Leman lake	seismic modeling			5.0	0.5 - 1.7		
Finckh & Frei (1991)	Vouvry line	seismic reflection (stacking velocity)				1.9 - 2.0		
Pugin & Marchant (1992)	from St-Maurice to Bramois	seismic reflection (stacking velocity)				on Martigny profile 1.6 - 2.5		
Marchant & Stampfli (1993)	Sion area	seismic reflection (stacking and internal velocity)				1.66 - 2.64		
Burri (1995)* *see details in chapter 3	Vétroz	• seismic refraction • seismic reflection (stacking velocity)			• 4.0	• 0.3 - 2.0 • 1.2 - 2.8	• 0.456	• 0.13 - 0.27 • 0.26 - 0.42
Pugin et al. (1997)	Vétroz	seismic modeling			5.0	1.65 - 2.4		

Compilation of the main geophysical parameters measured in the Rhône valley

data for a vertical incident SH wave					*data for a vertical incident SV wave*			
coordx	**coordy**	**Amax**	**frequency**		**coordx**	**coordy**	**Amax**	**frequency**
592685.43	119681.27	1.69	3.925	**p1 profile**	592685.43	119681.27	1.78	2.100
592704.64	119635.11	4.30	4.700		592704.64	119635.11	3.45	2.150
592723.86	119588.95	6.41	3.025		592723.86	119588.95	5.38	2.175
592743.07	119542.79	7.33	2.450		592743.07	119542.79	6.15	2.200
592762.29	119496.63	7.78	1.200		592762.29	119496.63	6.34	0.800
592781.50	119450.47	9.36	1.200		592781.50	119450.47	7.22	0.800
592800.72	119404.31	10.02	1.200		592800.72	119404.31	7.75	0.800
592819.93	119358.15	9.62	1.200		592819.93	119358.15	7.90	0.800
592839.15	119311.99	8.31	1.200		592839.15	119311.99	7.70	0.800
592858.36	119265.83	8.11	0.600		592858.36	119265.83	7.24	0.800
592877.58	119219.66	8.76	0.600		592877.58	119219.66	6.68	0.800
592896.79	119173.50	9.17	0.600		592896.79	119173.50	6.23	0.800
592916.01	119127.34	9.34	0.600		592916.01	119127.34	6.17	2.175
592935.22	119081.18	9.26	0.600		592935.22	119081.18	6.42	0.800
592954.44	119035.02	8.92	0.600		592954.44	119035.02	7.02	0.800
592973.65	118988.86	8.36	0.600		592973.65	118988.86	7.69	0.800
592992.87	118942.70	7.61	0.600		592992.87	118942.70	8.25	0.800
593012.08	118896.54	6.72	0.600		593012.08	118896.54	8.56	0.800
593031.30	118850.38	7.90	1.200		593031.30	118850.38	8.54	0.800
593050.51	118804.22	8.65	1.200		593050.51	118804.22	8.19	0.800
593069.73	118758.06	8.58	1.200		593069.73	118758.06	7.53	0.800
593088.94	118711.90	7.75	1.200		593088.94	118711.90	6.63	0.800
593108.15	118665.74	6.34	1.200		593108.15	118665.74	5.80	3.150
593127.37	118619.58	5.44	2.450		593127.37	118619.58	5.30	2.000
593146.58	118573.42	7.15	3.025		593146.58	118573.42	5.10	2.000
593165.80	118527.26	6.67	3.000		593165.80	118527.26	3.87	2.000
593185.01	118481.10	4.88	4.150		593185.01	118481.10	2.77	4.625
593204.23	118434.94	2.22	4.125		593204.23	118434.94	2.08	4.550
593223.44	118388.78	1.21	4.050		593223.44	118388.78	1.19	0.725
593242.66	118342.62	1.37	1.900		593242.66	118342.62	1.23	4.500
592879.76	119849.88	1.49	4.325	**p2 profile**	592879.76	119849.88	1.37	2.025
592898.77	119803.63	3.11	4.375		592898.77	119803.63	2.37	4.050
592917.78	119757.39	5.60	4.400		592917.78	119757.39	3.62	4.050
592936.78	119711.14	6.45	2.950		592936.78	119711.14	4.63	2.100
592955.79	119664.90	7.78	2.975		592955.79	119664.90	6.26	2.125
592974.80	119618.65	7.41	2.400		592974.80	119618.65	6.66	2.125
592993.81	119572.40	8.23	1.175		592993.81	119572.40	6.53	0.775
593012.81	119526.16	9.69	1.175		593012.81	119526.16	7.32	0.775
593031.82	119479.91	10.19	1.175		593031.82	119479.91	7.80	0.775
593050.83	119433.66	9.66	1.175		593050.83	119433.66	7.94	0.775
593069.84	119387.42	8.22	1.175		593069.84	119387.42	7.77	0.775
593088.84	119341.17	8.04	0.575		593088.84	119341.17	7.36	0.775
593107.85	119294.93	8.66	0.575		593107.85	119294.93	6.83	0.775
593126.86	119248.68	9.07	0.575		593126.86	119248.68	6.38	0.775
593145.87	119202.43	9.26	0.575		593145.87	119202.43	6.95	2.100
593164.87	119156.19	9.22	0.575		593164.87	119156.19	7.02	2.100
593183.88	119109.94	8.96	0.575		593183.88	119109.94	6.80	0.775
593202.89	119063.69	8.48	0.575		593202.89	119063.69	7.39	0.775
593221.90	119017.45	7.83	0.575		593221.90	119017.45	7.93	0.775

Compilation of the main geophysical parameters measured in the Rhône valley

593240.90	118971.20	7.02	0.575		593240.90	118971.20	8.28	0.775
593259.91	118924.96	8.13	1.175		593259.91	118924.96	8.35	0.775

data for a vertical incident SH wave					***data for a vertical incident SV wave***			
coordx	**coordy**	**Amax**	**frequency**		**coordx**	**coordy**	**Amax**	**frequency**
593278.92	118878.71	9.10	1.175		593278.92	118878.71	8.11	0.775
593297.93	118832.46	9.24	1.175		593297.93	118832.46	7.57	0.775
593316.93	118786.22	8.53	1.175		593316.93	118786.22	6.78	0.775
593335.94	118739.97	7.13	1.175		593335.94	118739.97	6.18	3.100
593354.95	118693.72	5.98	1.775		593354.95	118693.72	5.01	2.000
593373.96	118647.48	6.31	2.950		593373.96	118647.48	4.60	1.975
593392.96	118601.23	6.23	3.525		593392.96	118601.23	3.53	1.975
593411.97	118554.99	3.41	4.550		593411.97	118554.99	2.76	4.050
593430.98	118508.74	1.60	4.500		593430.98	118508.74	1.34	4.500
593449.99	118462.49	1.47	2.850		593449.99	118462.49	1.22	1.150
593060.35	120049.94	1.39	2.200	**p3 profile**	593060.35	120049.94	1.27	1.125
593079.44	120003.73	1.51	2.200		593079.44	120003.73	1.29	1.125
593098.54	119957.52	1.79	4.150		593098.54	119957.52	1.39	1.975
593117.63	119911.31	3.40	5.000		593117.63	119911.31	2.26	3.975
593136.73	119865.10	5.57	4.525		593136.73	119865.10	3.23	3.975
593155.82	119818.89	6.84	3.425		593155.82	119818.89	4.16	2.050
593174.91	119772.68	7.55	2.900		593174.91	119772.68	5.73	2.075
593194.01	119726.47	7.90	2.325		593194.01	119726.47	6.45	2.100
593213.10	119680.25	8.54	1.150		593213.10	119680.25	5.96	0.775
593232.19	119634.04	10.21	1.150		593232.19	119634.04	6.90	0.775
593251.29	119587.83	10.96	1.150		593251.29	119587.83	7.57	0.775
593270.38	119541.62	10.59	1.150		593270.38	119541.62	7.93	0.775
593289.48	119495.41	9.15	1.150		593289.48	119495.41	7.95	0.775
593308.57	119449.20	7.58	0.575		593308.57	119449.20	7.68	0.775
593327.66	119402.99	8.32	0.575		593327.66	119402.99	7.20	0.775
593346.76	119356.78	8.89	0.575		593346.76	119356.78	6.65	0.775
593365.85	119310.57	9.25	0.575		593365.85	119310.57	6.68	2.050
593384.95	119264.36	9.38	0.575		593384.95	119264.36	7.48	2.000
593404.04	119218.15	9.28	0.575		593404.04	119218.15	7.44	2.000
593423.13	119171.94	8.96	0.575		593423.13	119171.94	6.74	0.750
593442.23	119125.73	8.44	0.575		593442.23	119125.73	7.32	0.775
593461.32	119079.52	7.75	0.575		593461.32	119079.52	7.82	0.775
593480.41	119033.31	6.91	0.575		593480.41	119033.31	8.12	0.775
593499.51	118987.09	8.89	1.150		593499.51	118987.09	8.13	0.775
593518.60	118940.88	10.18	1.150		593518.60	118940.88	7.83	0.775
593537.70	118894.67	10.50	1.150		593537.70	118894.67	7.25	0.775
593556.79	118848.46	9.82	1.150		593556.79	118848.46	6.42	0.775
593575.88	118802.25	8.33	1.150		593575.88	118802.25	5.47	0.750
593594.98	118756.04	6.92	1.750		593594.98	118756.04	4.95	2.000
593614.07	118709.83	5.97	3.450		593614.07	118709.83	4.26	1.975
593633.17	118663.62	5.51	3.425		593633.17	118663.62	3.22	4.150
593652.26	118617.41	2.34	4.500		593652.26	118617.41	1.96	3.875
593671.35	118571.20	1.45	2.825		593671.35	118571.20	1.21	1.150
593297.42	120175.09	1.60	2.925	**p4 profile**	593297.42	120175.09	1.30	1.925
593315.92	120128.64	2.64	3.450		593315.92	120128.64	2.37	3.625
593334.43	120082.19	5.36	3.475		593334.43	120082.19	3.49	3.625
593352.93	120035.74	6.78	3.500		593352.93	120035.74	3.75	3.650

Compilation of the main geophysical parameters measured in the Rhône valley

593371.43	119989.29	7.02	3.250		593371.43	119989.29	4.21	2.025
593389.94	119942.84	6.52	2.750		593389.94	119942.84	5.46	2.025
593408.44	119896.39	6.78	1.675		593408.44	119896.39	6.28	2.050
593426.94	119849.94	8.32	1.125		593426.94	119849.94	5.97	2.050

data for a vertical incident SH wave					***data for a vertical incident SV wave***			
coordx	**coordy**	**Amax**	**frequency**		**coordx**	**coordy**	**Amax**	**frequency**
593445.45	119803.49	10.37	1.125		593445.45	119803.49	6.37	0.750
593463.95	119757.04	11.64	1.125		593463.95	119757.04	7.11	0.750
593482.46	119710.59	11.80	1.125		593482.46	119710.59	7.59	0.750
593500.96	119664.14	10.80	1.125		593500.96	119664.14	7.80	0.750
593519.46	119617.69	8.79	1.125		593519.46	119617.69	7.73	0.750
593537.97	119571.24	7.49	0.575		593537.97	119571.24	7.43	0.750
593556.47	119524.79	8.15	0.575		593556.47	119524.79	6.99	0.750
593574.97	119478.34	8.64	0.575		593574.97	119478.34	6.55	0.750
593593.48	119431.89	8.92	0.575		593593.48	119431.89	6.75	2.025
593611.98	119385.44	8.99	0.575		593611.98	119385.44	6.95	1.950
593630.48	119338.99	8.84	0.575		593630.48	119338.99	6.71	1.950
593648.99	119292.54	8.49	0.575		593648.99	119292.54	6.88	0.750
593667.49	119246.09	7.95	0.575		593667.49	119246.09	7.36	0.750
593685.99	119199.64	7.28	0.550		593685.99	119199.64	7.76	0.750
593704.50	119153.19	7.17	1.125		593704.50	119153.19	7.97	0.750
593723.00	119106.74	9.43	1.125		593723.00	119106.74	7.93	0.750
593741.51	119060.29	10.88	1.125		593741.51	119060.29	7.64	0.750
593760.01	119013.84	11.33	1.125		593760.01	119013.84	7.10	0.750
593778.51	118967.39	10.74	1.125		593778.51	118967.39	6.35	0.750
593797.02	118920.94	9.30	1.125		593797.02	118920.94	5.74	2.675
593815.52	118874.49	7.82	1.675		593815.52	118874.49	4.94	3.150
593834.02	118828.03	6.94	2.175		593834.02	118828.03	4.77	3.650
593852.53	118781.58	5.55	3.275		593852.53	118781.58	4.24	2.725
593871.03	118735.13	3.77	3.700		593871.03	118735.13	3.20	2.700
593889.53	118688.68	1.22	1.950		593889.53	118688.68	1.28	0.700
593908.04	118642.23	1.37	1.075		593908.04	118642.23	1.22	1.125
593484.58	120343.44	1.10	1.075	**p5 profile**	593484.58	120343.44	1.33	4.875
593503.59	120297.20	1.54	2.825		593503.59	120297.20	2.26	4.875
593522.61	120250.95	3.83	4.450		593522.61	120250.95	3.30	4.400
593541.62	120204.71	5.20	4.025		593541.62	120204.71	4.39	3.575
593560.63	120158.46	5.91	3.175		593560.63	120158.46	5.10	3.575
593579.65	120112.22	6.89	3.175		593579.65	120112.22	4.72	3.600
593598.66	120065.98	7.88	2.700		593598.66	120065.98	4.44	2.700
593617.67	120019.73	8.09	2.200		593617.67	120019.73	5.51	2.025
593636.69	119973.49	8.49	2.225		593636.69	119973.49	6.49	2.025
593655.70	119927.24	8.09	1.700		593655.70	119927.24	6.53	2.025
593674.71	119881.00	8.58	1.700		593674.71	119881.00	6.10	0.750
593693.72	119834.76	9.98	1.125		593693.72	119834.76	7.00	0.750
593712.74	119788.51	10.61	1.125		593712.74	119788.51	7.67	0.750
593731.75	119742.27	10.24	1.125		593731.75	119742.27	8.07	0.750
593750.76	119696.03	9.29	1.150		593750.76	119696.03	8.17	0.750
593769.78	119649.78	7.52	1.150		593769.78	119649.78	8.00	0.750
593788.79	119603.54	7.99	0.575		593788.79	119603.54	7.64	0.750
593807.80	119557.29	8.61	0.575		593807.80	119557.29	7.16	0.750
593826.82	119511.05	9.04	0.575		593826.82	119511.05	7.72	2.000

Compilation of the main geophysical parameters measured in the Rhône valley

593845.83	119464.81	9.25	0.575		593845.83	119464.81	8.82	2.000
593864.84	119418.56	9.25	0.575		593864.84	119418.56	8.84	2.000
593883.86	119372.32	9.02	0.575		593883.86	119372.32	7.81	2.000
593902.87	119326.07	8.59	0.575		593902.87	119326.07	7.26	0.750
593921.88	119279.83	7.97	0.575		593921.88	119279.83	7.72	0.750
593940.90	119233.59	7.20	0.575		593940.90	119233.59	8.05	0.750

data for a vertical incident SH wave					***data for a vertical incident SV wave***			
coordx	**coordy**	**Amax**	**frequency**		**coordx**	**coordy**	**Amax**	**frequency**
593959.91	119187.34	7.90	1.150		593959.91	119187.34	8.17	0.750
593978.92	119141.10	9.25	1.125		593978.92	119141.10	8.03	0.750
593997.94	119094.85	10.22	1.125		593997.94	119094.85	7.64	0.750
594016.95	119048.61	10.19	1.125		594016.95	119048.61	7.00	0.750
594035.96	119002.37	9.25	1.125		594035.96	119002.37	6.15	0.750
594054.98	118956.12	8.24	1.700		594054.98	118956.12	5.16	0.750
594073.99	118909.88	8.63	2.200		594073.99	118909.88	4.88	2.000
594093.00	118863.63	7.35	2.200		594093.00	118863.63	4.97	4.900
594112.01	118817.39	4.26	2.175		594112.01	118817.39	3.25	2.725
594131.03	118771.15	2.18	2.575		594131.03	118771.15	1.93	4.900
594150.04	118724.90	1.38	1.100		594150.04	118724.90	1.24	4.350
593669.74	120527.85	1.18	1.875	**p6 profile**	593669.74	120527.85	1.63	4.675
593688.63	120481.56	2.00	4.625		593688.63	120481.56	3.23	4.700
593707.52	120435.26	3.39	4.200		593707.52	120435.26	4.10	4.725
593726.41	120388.97	4.86	3.575		593726.41	120388.97	4.44	3.375
593745.30	120342.67	5.60	2.875		593745.30	120342.67	5.07	3.400
593764.19	120296.38	6.68	2.875		593764.19	120296.38	5.16	3.450
593783.08	120250.08	7.27	2.875		593783.08	120250.08	5.05	3.650
593801.97	120203.79	7.23	2.900		593801.97	120203.79	4.56	3.650
593820.85	120157.49	6.39	2.900		593820.85	120157.49	4.64	2.700
593839.74	120111.20	6.95	2.200		593839.74	120111.20	4.68	1.975
593858.63	120064.90	8.46	2.200		593858.63	120064.90	5.71	2.000
593877.52	120018.61	8.66	2.225		593877.52	120018.61	6.47	2.000
593896.41	119972.31	8.45	1.675		593896.41	119972.31	6.31	2.000
593915.30	119926.02	8.94	1.125		593915.30	119926.02	6.28	0.750
593934.19	119879.73	10.61	1.125		593934.19	119879.73	7.20	0.750
593953.08	119833.43	11.44	1.125		593953.08	119833.43	7.86	0.750
593971.97	119787.14	11.19	1.125		593971.97	119787.14	8.22	0.750
593990.86	119740.84	9.89	1.125		593990.86	119740.84	8.28	0.750
594009.75	119694.55	7.78	1.125		594009.75	119694.55	8.06	0.750
594028.64	119648.25	7.90	0.550		594028.64	119648.25	7.62	0.750
594047.53	119601.96	8.45	0.550		594047.53	119601.96	7.08	0.750
594066.42	119555.66	8.81	0.550		594066.42	119555.66	7.60	1.975
594085.31	119509.37	8.99	0.550		594085.31	119509.37	8.64	1.950
594104.20	119463.07	8.97	0.550		594104.20	119463.07	8.63	1.950
594123.08	119416.78	8.75	0.550		594123.08	119416.78	7.46	1.950
594141.97	119370.48	8.36	0.550		594141.97	119370.48	7.20	0.750
594160.86	119324.19	7.80	0.550		594160.86	119324.19	7.70	0.750
594179.75	119277.90	7.11	0.550		594179.75	119277.90	8.06	0.750
594198.64	119231.60	8.30	1.125		594198.64	119231.60	8.18	0.750
594217.53	119185.31	9.86	1.125		594217.53	119185.31	8.04	0.750
594236.42	119139.01	10.52	1.125		594236.42	119139.01	7.63	0.750
594255.31	119092.72	10.17	1.125		594255.31	119092.72	6.96	0.750

Compilation of the main geophysical parameters measured in the Rhône valley

594274.20	119046.42	8.97	1.125		594274.20	119046.42	6.10	0.750
594293.09	119000.13	8.20	1.675		594293.09	119000.13	5.08	0.750
594311.98	118953.83	7.75	2.200		594311.98	118953.83	4.89	1.950
594330.87	118907.54	5.61	2.200		594330.87	118907.54	3.96	2.750
594349.76	118861.24	3.54	3.700		594349.76	118861.24	2.80	3.200
594368.65	118814.95	1.73	1.950		594368.65	118814.95	1.36	3.525
594387.54	118768.65	1.59	3.550		594387.54	118768.65	1.22	4.250
594116.34	120127.37	1.21	4.400	**p7 profile**	594116.34	120127.37	1.40	2.075
data for a vertical incident SH wave					***data for a vertical incident SV wave***			
coordx	**coordy**	**Amax**	**frequency**		**coordx**	**coordy**	**Amax**	**frequency**
594135.32	120081.11	2.77	2.400		594135.32	120081.11	3.18	2.125
594154.30	120034.85	5.54	2.400		594154.30	120034.85	5.29	2.150
594173.27	119988.59	7.02	2.425		594173.27	119988.59	6.24	2.175
594192.25	119942.34	7.97	1.175		594192.25	119942.34	6.03	0.800
594211.23	119896.08	9.28	1.175		594211.23	119896.08	6.98	0.800
594230.21	119849.82	9.66	1.175		594230.21	119849.82	7.61	0.800
594249.18	119803.56	9.03	1.175		594249.18	119803.56	7.89	0.800
594268.16	119757.30	7.61	1.200		594268.16	119757.30	7.81	0.800
594287.14	119711.04	7.62	0.600		594287.14	119711.04	7.43	0.800
594306.12	119664.79	8.31	0.600		594306.12	119664.79	6.87	0.800
594325.10	119618.53	8.80	0.600		594325.10	119618.53	6.32	0.800
594344.07	119572.27	9.05	0.600		594344.07	119572.27	7.00	2.025
594363.05	119526.01	9.06	0.600		594363.05	119526.01	7.56	2.025
594382.03	119479.75	8.83	0.600		594382.03	119479.75	6.68	2.025
594401.01	119433.49	8.36	0.600		594401.01	119433.49	7.17	0.800
594419.99	119387.24	7.70	0.600		594419.99	119387.24	7.78	0.800
594438.96	119340.98	6.88	0.600		594438.96	119340.98	8.19	0.800
594457.94	119294.72	7.32	1.175		594457.94	119294.72	8.30	0.800
594476.92	119248.46	8.56	1.175		594476.92	119248.46	8.08	0.800
594495.90	119202.20	8.97	1.175		594495.90	119202.20	7.55	0.800
594514.87	119155.94	8.49	1.175		594514.87	119155.94	6.73	0.800
594533.85	119109.68	7.27	1.175		594533.85	119109.68	5.72	0.800
594552.83	119063.43	6.38	1.800		594552.83	119063.43	5.45	2.050
594571.81	119017.17	5.01	3.025		594571.81	119017.17	4.76	2.025
594590.79	118970.91	4.39	3.000		594590.79	118970.91	3.31	4.275
594609.76	118924.65	2.03	4.175		594609.76	118924.65	1.74	4.250
594628.74	118878.39	1.45	2.900		594628.74	118878.39	1.23	0.725
594371.79	120132.73	1.56	4.425	**p8 profile**	594371.79	120132.73	1.56	2.150
594390.95	120086.55	2.61	4.450		594390.95	120086.55	2.92	2.200
594410.11	120040.36	3.98	1.875		594410.11	120040.36	4.96	2.225
594429.27	119994.18	5.68	1.875		594429.27	119994.18	6.06	2.250
594448.43	119948.00	7.32	1.200		594448.43	119948.00	6.36	0.825
594467.59	119901.82	8.54	1.200		594467.59	119901.82	7.23	0.825
594486.75	119855.63	8.86	1.200		594486.75	119855.63	7.69	0.825
594505.92	119809.45	8.23	1.200		594505.92	119809.45	7.72	0.825
594525.08	119763.27	7.44	0.600		594525.08	119763.27	7.39	0.825
594544.24	119717.08	8.23	0.600		594544.24	119717.08	6.81	0.825
594563.40	119670.90	8.80	0.600		594563.40	119670.90	6.22	0.800
594582.56	119624.72	9.14	0.600		594582.56	119624.72	6.24	1.150
594601.72	119578.53	9.22	0.600		594601.72	119578.53	6.63	2.025
594620.88	119532.35	9.05	0.600		594620.88	119532.35	6.46	0.800

Compilation of the main geophysical parameters measured in the Rhône valley

594640.04	119486.17	8.65	0.600		594640.04	119486.17	7.10	0.825
594659.20	119439.99	8.04	0.600		594659.20	119439.99	7.80	0.825
594678.36	119393.80	7.26	0.600		594678.36	119393.80	8.27	0.825
594697.52	119347.62	6.35	0.600		594697.52	119347.62	8.43	0.825
594716.68	119301.44	6.61	1.200		594716.68	119301.44	8.23	0.825
594735.84	119255.25	7.26	1.200		594735.84	119255.25	7.68	0.825
594755.01	119209.07	7.18	1.200		594755.01	119209.07	6.86	0.825
594774.17	119162.89	6.40	1.200		594774.17	119162.89	6.47	3.250
594793.33	119116.71	5.46	1.925		594793.33	119116.71	5.45	2.025
594812.49	119070.52	5.28	3.175		594812.49	119070.52	5.36	2.025

data for a vertical incident SH wave					***data for a vertical incident SV wave***			
coordx	**coordy**	**Amax**	**frequency**		**coordx**	**coordy**	**Amax**	**frequency**
594831.65	119024.34	4.11	4.475		594831.65	119024.34	3.50	2.025
594850.81	118978.16	1.57	4.350		594850.81	118978.16	1.50	0.775
594869.97	118931.97	1.44	1.175		594869.97	118931.97	1.24	0.750
594598.98	120239.46	1.18	2.100	**p9 profile**	594598.98	120239.46	1.32	0.750
594617.83	120193.15	2.42	4.950		594617.83	120193.15	2.31	2.150
594636.68	120146.84	5.47	2.975		594636.68	120146.84	4.48	2.200
594655.53	120100.53	6.34	2.975		594655.53	120100.53	5.84	2.200
594674.38	120054.22	8.40	1.175		594674.38	120054.22	5.97	2.225
594693.23	120007.91	10.28	1.175		594693.23	120007.91	6.73	0.800
594712.08	119961.60	11.23	1.175		594712.08	119961.60	7.44	0.800
594730.93	119915.29	11.03	1.175		594730.93	119915.29	7.79	0.800
594749.78	119868.97	9.68	1.175		594749.78	119868.97	7.77	0.800
594768.63	119822.66	7.59	0.600		594768.63	119822.66	7.45	0.800
594787.48	119776.35	8.32	0.600		594787.48	119776.35	6.96	0.800
594806.33	119730.04	8.84	0.600		594806.33	119730.04	6.49	0.800
594825.18	119683.73	9.13	0.600		594825.18	119683.73	6.26	0.800
594844.03	119637.42	9.17	0.600		594844.03	119637.42	6.42	0.800
594862.88	119591.11	8.97	0.600		594862.88	119591.11	6.89	0.800
594881.73	119544.80	8.53	0.600		594881.73	119544.80	7.54	0.800
594900.58	119498.49	7.91	0.600		594900.58	119498.49	8.14	0.800
594919.43	119452.18	7.13	0.600		594919.43	119452.18	8.54	0.800
594938.28	119405.87	6.28	1.175		594938.28	119405.87	8.65	0.800
594957.13	119359.56	8.27	1.175		594957.13	119359.56	8.45	0.800
594975.98	119313.25	9.55	1.175		594975.98	119313.25	7.94	0.800
594994.83	119266.94	9.94	1.175		594994.83	119266.94	7.19	0.800
595013.68	119220.63	9.42	1.175		595013.68	119220.63	6.27	0.800
595032.53	119174.31	8.14	1.175		595032.53	119174.31	5.26	0.775
595051.38	119128.00	6.37	1.175		595051.38	119128.00	4.80	1.975
595070.23	119081.69	5.78	2.975		595070.23	119081.69	4.66	1.950
595089.08	119035.38	4.71	2.975		595089.08	119035.38	3.60	1.950
595107.93	118989.07	2.44	4.625		595107.93	118989.07	1.68	3.950
595126.78	118942.76	1.42	1.150		595126.78	118942.76	1.21	1.300
594766.75	120522.88	1.58	2.900	**p10 profile**	594766.75	120522.88	1.34	1.900
594785.71	120476.61	1.82	2.925		594785.71	120476.61	1.61	1.925
594804.66	120430.34	3.21	2.950		594804.66	120430.34	2.67	2.650
594823.62	120384.08	4.85	2.675		594823.62	120384.08	3.99	2.025
594842.57	120337.81	7.33	2.150		594842.57	120337.81	5.41	2.050
594861.53	120291.54	8.08	2.150		594861.53	120291.54	6.06	2.050
594880.48	120245.27	8.20	1.100		594880.48	120245.27	5.87	2.075

Compilation of the main geophysical parameters measured in the Rhône valley

594899.44	120199.01	9.85	1.100		594899.44	120199.01	6.17	0.750
594918.39	120152.74	10.86	1.100		594918.39	120152.74	7.00	0.750
594937.35	120106.47	11.20	1.125		594937.35	120106.47	7.60	0.750
594956.30	120060.20	10.76	1.125		594956.30	120060.20	7.93	0.750
594975.26	120013.94	9.35	1.125		594975.26	120013.94	7.96	0.750
594994.22	119967.67	7.44	0.575		594994.22	119967.67	7.73	0.750
595013.17	119921.40	8.17	0.575		595013.17	119921.40	7.35	0.750
595032.13	119875.13	8.72	0.575		595032.13	119875.13	6.93	0.750
595051.08	119828.87	9.07	0.575		595051.08	119828.87	6.63	0.750
595070.04	119782.60	9.21	0.575		595070.04	119782.60	6.55	0.750
595088.99	119736.33	9.13	0.575		595088.99	119736.33	6.76	0.750
595107.95	119690.06	8.84	0.575		595107.95	119690.06	7.16	0.750

data for a vertical incident SH wave					***data for a vertical incident SV wave***			
coordx	**coordy**	**Amax**	**frequency**		**coordx**	**coordy**	**Amax**	**frequency**
595126.90	119643.80	8.35	0.575		595126.90	119643.80	7.62	0.750
595145.86	119597.53	7.70	0.575		595145.86	119597.53	8.02	0.750
595164.81	119551.26	6.93	0.575		595164.81	119551.26	8.24	0.750
595183.77	119504.99	7.47	1.125		595183.77	119504.99	8.23	0.750
595202.73	119458.73	9.11	1.125		595202.73	119458.73	7.96	0.750
595221.68	119412.46	10.00	1.100		595221.68	119412.46	7.46	0.750
595240.64	119366.19	10.39	1.100		595240.64	119366.19	6.77	0.750
595259.59	119319.92	9.89	1.100		595259.59	119319.92	5.96	2.675
595278.55	119273.65	8.64	1.100		595278.55	119273.65	5.40	2.625
595297.50	119227.39	9.43	2.150		595297.50	119227.39	4.49	4.175
595316.46	119181.12	9.12	2.150		595316.46	119181.12	4.29	2.700
595335.41	119134.85	5.71	2.150		595335.41	119134.85	4.08	2.675
595354.37	119088.58	2.47	4.125		595354.37	119088.58	2.31	2.650
595373.32	119042.32	1.41	1.075		595373.32	119042.32	1.22	1.200
594921.58	120755.87	1.00	3.600	**p11 profile**	594921.58	120755.87	1.15	1.850
594940.77	120709.70	2.11	3.550		594940.77	120709.70	2.25	3.600
594959.96	120663.53	4.68	3.225		594959.96	120663.53	4.19	3.625
594979.16	120617.36	7.04	2.800		594979.16	120617.36	5.29	1.925
594998.35	120571.19	7.75	1.950		594998.35	120571.19	6.50	1.925
595017.54	120525.02	8.54	1.950		595017.54	120525.02	6.78	1.950
595036.73	120478.85	8.87	1.475		595036.73	120478.85	6.34	1.950
595055.92	120432.68	9.28	1.025		595055.92	120432.68	5.71	2.400
595075.12	120386.51	10.62	1.025		595075.12	120386.51	5.98	0.700
595094.31	120340.34	11.32	1.025		595094.31	120340.34	6.67	0.700
595113.50	120294.17	11.25	1.025		595113.50	120294.17	7.22	0.700
595132.69	120248.00	10.38	1.025		595132.69	120248.00	7.58	0.700
595151.89	120201.83	8.95	1.050		595151.89	120201.83	7.73	0.700
595171.08	120155.66	6.97	0.550		595171.08	120155.66	7.68	0.700
595190.27	120109.49	7.68	0.550		595190.27	120109.49	7.49	0.700
595209.46	120063.32	8.27	0.550		595209.46	120063.32	7.21	0.700
595228.65	120017.15	8.71	0.550		595228.65	120017.15	7.05	1.925
595247.85	119970.98	8.97	0.550		595247.85	119970.98	6.77	0.700
595267.04	119924.81	9.05	0.550		595267.04	119924.81	6.76	0.700
595286.23	119878.64	8.94	0.550		595286.23	119878.64	6.92	0.700
595305.42	119832.47	8.66	0.550		595305.42	119832.47	7.20	0.700
595324.61	119786.30	8.21	0.550		595324.61	119786.30	7.53	0.700
595343.81	119740.13	7.63	0.550		595343.81	119740.13	7.80	0.700

Compilation of the main geophysical parameters measured in the Rhône valley

595363.00	119693.96	6.94	0.550		595363.00	119693.96	7.94	0.700
595382.19	119647.79	6.78	0.550		595382.19	119647.79	7.93	0.700
595401.38	119601.62	8.73	1.050		595401.38	119601.62	7.73	0.700
595420.58	119555.45	10.14	1.025		595420.58	119555.45	7.35	0.700
595439.77	119509.28	10.99	1.025		595439.77	119509.28	6.82	0.700
595458.96	119463.11	11.04	1.025		595458.96	119463.11	6.18	0.700
595478.15	119416.94	10.32	1.025		595478.15	119416.94	5.44	0.700
595497.34	119370.77	9.00	1.025		595497.34	119370.77	4.78	2.400
595516.54	119324.60	8.40	1.475		595516.54	119324.60	4.70	3.625
595535.73	119278.43	8.93	1.950		595535.73	119278.43	6.18	3.625
595554.92	119232.26	7.14	1.950		595554.92	119232.26	4.04	2.425
595574.11	119186.09	5.32	3.225		595574.11	119186.09	3.51	2.425
595593.30	119139.92	2.84	4.950		595593.30	119139.92	2.28	4.050
595612.50	119093.75	1.47	2.175		595612.50	119093.75	1.26	2.825

data for a vertical incident SH wave — *data for a vertical incident SV wave*

coordx	coordy	Amax	frequency		coordx	coordy	Amax	frequency
595046.74	121112.72	1.24	3.900	**p12 profile**	595046.74	121112.72	1.45	4.950
595066.01	121066.58	1.97	4.750		595066.01	121066.58	2.05	4.775
595085.29	121020.45	4.24	4.775		595085.29	121020.45	3.15	4.800
595104.56	120974.31	6.04	4.525		595104.56	120974.31	4.15	3.325
595123.83	120928.18	7.93	3.400		595123.83	120928.18	4.95	3.350
595143.11	120882.04	7.81	3.000		595143.11	120882.04	4.51	1.850
595162.38	120835.90	7.86	2.200		595162.38	120835.90	5.82	1.850
595181.65	120789.77	7.97	2.200		595181.65	120789.77	6.63	1.850
595200.93	120743.63	7.36	1.400		595200.93	120743.63	6.46	1.850
595220.20	120697.50	8.90	1.400		595220.20	120697.50	5.44	1.850
595239.48	120651.36	9.40	1.400		595239.48	120651.36	4.76	1.450
595258.75	120605.22	10.51	0.975		595258.75	120605.22	5.34	0.675
595278.02	120559.09	11.51	0.975		595278.02	120559.09	6.04	0.675
595297.30	120512.95	11.86	0.975		595297.30	120512.95	6.66	0.675
595316.57	120466.82	11.46	0.975		595316.57	120466.82	7.18	0.675
595335.84	120420.68	10.30	0.975		595335.84	120420.68	7.55	0.675
595355.12	120374.54	8.42	0.975		595355.12	120374.54	7.75	0.675
595374.39	120328.41	6.70	0.525		595374.39	120328.41	7.80	0.675
595393.66	120282.27	7.34	0.525		595393.66	120282.27	7.69	0.675
595412.94	120236.14	7.88	0.525		595412.94	120236.14	7.49	0.675
595432.21	120190.00	8.32	0.525		595432.21	120190.00	7.25	0.675
595451.48	120143.86	8.61	0.525		595451.48	120143.86	7.04	0.675
595470.76	120097.73	8.75	0.525		595470.76	120097.73	6.94	0.675
595490.03	120051.59	8.74	0.525		595490.03	120051.59	6.97	0.675
595509.31	120005.46	8.57	0.525		595509.31	120005.46	7.13	0.675
595528.58	119959.32	8.26	0.525		595528.58	119959.32	7.36	0.675
595547.85	119913.18	7.83	0.525		595547.85	119913.18	7.58	0.675
595567.13	119867.05	7.28	0.525		595567.13	119867.05	7.75	0.675
595586.40	119820.91	6.65	0.525		595586.40	119820.91	7.80	0.675
595605.67	119774.78	7.14	0.975		595605.67	119774.78	7.71	0.675
595624.95	119728.64	9.27	0.975		595624.95	119728.64	7.46	0.675
595644.22	119682.50	10.78	0.975		595644.22	119682.50	7.34	1.450
595663.49	119636.37	11.55	0.975		595663.49	119636.37	6.62	1.450
595682.77	119590.23	11.54	0.975		595682.77	119590.23	5.93	0.675
595702.04	119544.10	10.83	0.975		595702.04	119544.10	5.26	0.675

Compilation of the main geophysical parameters measured in the Rhône valley

595721.31	119497.96	9.55	0.975		595721.31	119497.96	4.57	0.675
595740.59	119451.82	8.58	1.400		595740.59	119451.82	4.83	2.950
595759.86	119405.69	7.12	1.400		595759.86	119405.69	6.00	3.350
595779.14	119359.55	7.34	2.200		595779.14	119359.55	5.22	1.850
595798.41	119313.42	5.30	2.200		595798.41	119313.42	3.78	1.850
595817.68	119267.28	3.41	3.350		595817.68	119267.28	3.36	3.350
595836.96	119221.14	1.60	3.325		595836.96	119221.14	1.48	3.300
595856.23	119175.01	1.45	3.300		595856.23	119175.01	1.34	2.200
595287.50	121212.50	1.40	4.600	**p13 profile**	595287.50	121212.50	1.46	4.975
595306.68	121166.32	2.66	4.650		595306.68	121166.32	2.65	5.000
595325.86	121120.15	5.44	4.450		595325.86	121120.15	3.92	3.225
595345.04	121073.97	6.64	2.875		595345.04	121073.97	4.08	3.225
595364.21	121027.80	7.12	2.100		595364.21	121027.80	4.61	1.800
595383.39	120981.62	8.17	2.125		595383.39	120981.62	5.41	1.800
595402.57	120935.45	7.34	2.125		595402.57	120935.45	5.66	1.800
595421.75	120889.27	8.44	1.350		595421.75	120889.27	5.35	1.400

data for a vertical incident SH wave					***data for a vertical incident SV wave***			
coordx	**coordy**	**Amax**	**frequency**		**coordx**	**coordy**	**Amax**	**frequency**
595440.93	120843.09	9.42	1.350		595440.93	120843.09	5.13	1.400
595460.11	120796.92	9.63	0.950		595460.11	120796.92	4.87	0.650
595479.28	120750.74	10.92	0.950		595479.28	120750.74	5.51	0.650
595498.46	120704.57	11.72	0.950		595498.46	120704.57	6.12	1.400
595517.64	120658.39	11.88	0.950		595517.64	120658.39	7.41	1.400
595536.82	120612.22	11.28	0.950		595536.82	120612.22	8.06	1.400
595556.00	120566.04	9.96	0.950		595556.00	120566.04	7.85	1.400
595575.18	120519.87	7.98	0.950		595575.18	120519.87	7.55	0.650
595594.35	120473.69	6.79	0.525		595594.35	120473.69	7.59	0.650
595613.53	120427.51	7.44	0.525		595613.53	120427.51	7.52	0.650
595632.71	120381.34	7.99	0.525		595632.71	120381.34	7.36	0.650
595651.89	120335.16	8.42	0.525		595651.89	120335.16	7.18	0.650
595671.07	120288.99	8.72	0.525		595671.07	120288.99	7.02	0.650
595690.25	120242.81	8.87	0.525		595690.25	120242.81	6.93	0.650
595709.42	120196.64	8.86	0.525		595709.42	120196.64	6.96	0.650
595728.60	120150.46	8.71	0.525		595728.60	120150.46	7.07	0.650
595747.78	120104.28	8.40	0.525		595747.78	120104.28	7.25	0.650
595766.96	120058.11	7.96	0.525		595766.96	120058.11	7.44	0.650
595786.14	120011.93	7.42	0.525		595786.14	120011.93	7.58	0.650
595805.32	119965.76	6.79	0.525		595805.32	119965.76	7.63	0.650
595824.49	119919.58	6.98	0.950		595824.49	119919.58	7.56	0.650
595843.67	119873.41	9.19	0.950		595843.67	119873.41	7.74	1.400
595862.85	119827.23	10.82	0.950		595862.85	119827.23	8.13	1.400
595882.03	119781.05	11.74	0.950		595882.03	119781.05	7.68	1.400
595901.21	119734.88	11.94	0.950		595901.21	119734.88	6.53	1.400
595920.39	119688.70	11.42	0.950		595920.39	119688.70	5.45	0.650
595939.56	119642.53	10.33	0.950		595939.56	119642.53	4.83	0.650
595958.74	119596.35	9.17	1.350		595958.74	119596.35	4.51	1.400
595977.92	119550.18	8.39	1.350		595977.92	119550.18	5.19	2.850
595997.10	119504.00	7.36	2.125		595997.10	119504.00	5.39	3.225
596016.28	119457.83	7.09	2.100		596016.28	119457.83	4.78	1.800
596035.46	119411.65	5.19	3.275		596035.46	119411.65	3.46	1.800
596054.63	119365.47	3.33	3.250		596054.63	119365.47	3.46	3.225

Compilation of the main geophysical parameters measured in the Rhône valley

596073.81	119319.30	1.50	4.750		596073.81	119319.30	1.53	3.200
596092.99	119273.12	1.35	3.225		596092.99	119273.12	1.34	1.750
595499.23	121359.04	1.30	1.475	**p14 profile**	595499.23	121359.04	1.32	1.725
595518.28	121312.81	1.43	2.300		595518.28	121312.81	1.59	3.125
595537.33	121266.58	3.65	4.625		595537.33	121266.58	3.21	4.925
595556.38	121220.36	4.83	3.900		595556.38	121220.36	3.86	4.225
595575.44	121174.13	6.30	2.425		595575.44	121174.13	3.53	3.150
595594.49	121127.90	7.61	2.050		595594.49	121127.90	4.09	4.200
595613.54	121081.67	7.91	2.075		595613.54	121081.67	4.80	3.125
595632.59	121035.44	7.90	1.300		595632.59	121035.44	5.81	2.775
595651.64	120989.22	9.07	1.300		595651.64	120989.22	5.02	1.375
595670.69	120942.99	9.28	1.300		595670.69	120942.99	4.73	1.375
595689.75	120896.76	10.11	0.925		595689.75	120896.76	4.78	0.650
595708.80	120850.53	10.97	0.925		595708.80	120850.53	5.39	0.650
595727.85	120804.30	11.29	0.925		595727.85	120804.30	6.60	1.375
595746.90	120758.07	11.00	0.925		595746.90	120758.07	7.74	1.375
595765.95	120711.85	10.02	0.925		595765.95	120711.85	8.03	1.375
595785.00	120665.62	8.44	0.925		595785.00	120665.62	7.56	1.375

data for a vertical incident SH wave | ***data for a vertical incident SV wave***

coordx	coordy	Amax	frequency		coordx	coordy	Amax	frequency
595804.06	120619.39	6.43	0.950		595804.06	120619.39	7.41	0.650
595823.11	120573.16	6.53	0.525		595823.11	120573.16	7.49	0.650
595842.16	120526.93	7.15	0.525		595842.16	120526.93	7.44	0.650
595861.21	120480.71	7.69	0.525		595861.21	120480.71	7.30	0.650
595880.26	120434.48	8.13	0.525		595880.26	120434.48	7.12	0.650
595899.31	120388.25	8.44	0.525		595899.31	120388.25	6.93	0.650
595918.36	120342.02	8.98	2.025		595918.36	120342.02	6.80	0.650
595937.42	120295.79	9.00	2.025		595937.42	120295.79	6.76	0.650
595956.47	120249.57	8.52	0.525		595956.47	120249.57	6.83	0.650
595975.52	120203.34	8.26	0.525		595975.52	120203.34	6.96	0.650
595994.57	120157.11	7.86	0.525		595994.57	120157.11	7.14	0.650
596013.62	120110.88	7.34	0.525		596013.62	120110.88	7.30	0.650
596032.67	120064.65	6.74	0.525		596032.67	120064.65	7.38	0.650
596051.73	120018.43	6.55	0.950		596051.73	120018.43	7.36	0.650
596070.78	119972.20	8.58	0.925		596070.78	119972.20	7.43	1.375
596089.83	119925.97	10.19	0.925		596089.83	119925.97	8.00	1.375
596108.88	119879.74	11.15	0.925		596108.88	119879.74	7.57	1.375
596127.93	119833.51	11.44	0.925		596127.93	119833.51	6.55	1.375
596146.98	119787.28	11.10	0.925		596146.98	119787.28	5.44	0.650
596166.04	119741.06	10.20	0.925		596166.04	119741.06	4.81	0.650
596185.09	119694.83	9.54	1.300		596185.09	119694.83	4.52	1.375
596204.14	119648.60	9.26	1.300		596204.14	119648.60	5.18	2.775
596223.19	119602.37	8.01	1.300		596223.19	119602.37	5.77	2.775
596242.24	119556.14	7.75	2.075		596242.24	119556.14	4.92	0.600
596261.29	119509.92	7.06	2.050		596261.29	119509.92	4.47	1.775
596280.34	119463.69	5.33	2.425		596280.34	119463.69	3.55	1.775
596299.40	119417.46	3.43	4.825		596299.40	119417.46	3.41	4.950
596318.45	119371.23	1.71	4.700		596318.45	119371.23	2.05	4.900
596337.50	119325.00	1.33	1.550		596337.50	119325.00	1.20	2.100
595722.24	121455.02	1.42	2.250	**p15 profile**	595722.24	121455.02	1.42	1.025
595741.47	121408.87	2.72	2.275		595741.47	121408.87	2.96	2.650

Compilation of the main geophysical parameters measured in the Rhône valley

595760.70	121362.71	4.89	2.300
595779.93	121316.56	6.02	2.325
595799.15	121270.40	6.70	1.600
595818.38	121224.25	8.10	1.250
595837.61	121178.09	9.54	1.250
595856.84	121131.94	10.11	1.250
595876.07	121085.78	9.66	1.250
595895.30	121039.63	9.95	0.900
595914.52	120993.47	10.46	0.900
595933.75	120947.32	10.53	0.925
595952.98	120901.16	10.28	0.925
595972.21	120855.01	9.47	0.925
595991.44	120808.85	8.08	0.925
596010.67	120762.70	6.56	1.250
596029.90	120716.54	6.36	0.500
596049.12	120670.39	6.90	0.500
596068.35	120624.23	7.37	0.500
596087.58	120578.08	7.76	0.500
596106.81	120531.92	8.08	0.525
596126.04	120485.77	8.30	0.525

data for a vertical incident SH wave

coordx	coordy	Amax	frequency
596145.27	120439.61	8.37	0.525
596164.49	120393.46	8.29	0.525
596183.72	120347.30	8.08	0.525
596202.95	120301.15	7.74	0.500
596222.18	120255.00	7.33	0.500
596241.41	120208.84	6.85	1.225
596260.64	120162.69	7.27	1.250
596279.87	120116.53	8.13	0.925
596299.09	120070.38	9.63	0.925
596318.32	120024.22	10.58	0.925
596337.55	119978.07	10.91	0.925
596356.78	119931.91	10.86	0.900
596376.01	119885.76	10.41	0.900
596395.24	119839.60	9.76	1.250
596414.46	119793.45	10.69	1.250
596433.69	119747.29	10.50	1.250
596452.92	119701.14	9.36	1.250
596472.15	119654.98	8.16	1.600
596491.38	119608.83	7.35	1.975
596510.61	119562.67	6.06	1.950
596529.84	119516.52	4.55	3.000
596549.06	119470.36	2.69	3.000
596568.29	119424.21	1.10	0.825
596587.52	119378.05	1.33	1.500

595760.70	121362.71	3.87	2.650
595779.93	121316.56	3.66	2.675
595799.15	121270.40	3.81	2.225
595818.38	121224.25	4.94	2.650
595837.61	121178.09	6.10	2.300
595856.84	121131.94	5.98	2.300
595876.07	121085.78	4.34	0.625
595895.30	121039.63	4.89	0.625
595914.52	120993.47	5.43	0.625
595933.75	120947.32	6.43	1.350
595952.98	120901.16	7.16	1.350
595972.21	120855.01	7.36	1.350
595991.44	120808.85	7.07	0.625
596010.67	120762.70	7.28	0.625
596029.90	120716.54	7.38	0.625
596049.12	120670.39	7.38	0.625
596068.35	120624.23	7.30	0.625
596087.58	120578.08	7.15	0.625
596106.81	120531.92	7.00	0.625
596126.04	120485.77	6.86	0.625

data for a vertical incident SV wave

coordx	coordy	Amax	frequency
596145.27	120439.61	6.78	0.625
596164.49	120393.46	6.79	0.625
596183.72	120347.30	6.88	0.625
596202.95	120301.15	7.02	0.625
596222.18	120255.00	7.15	0.625
596241.41	120208.84	7.26	0.625
596260.64	120162.69	7.27	0.625
596279.87	120116.53	7.19	0.625
596299.09	120070.38	6.99	0.625
596318.32	120024.22	6.84	1.350
596337.55	119978.07	6.24	0.625
596356.78	119931.91	5.74	0.625
596376.01	119885.76	5.19	0.625
596395.24	119839.60	4.62	0.625
596414.46	119793.45	4.60	2.300
596433.69	119747.29	5.90	2.300
596452.92	119701.14	5.13	2.275
596472.15	119654.98	4.52	1.775
596491.38	119608.83	4.08	1.750
596510.61	119562.67	3.59	4.925
596529.84	119516.52	3.68	4.875
596549.06	119470.36	2.60	2.650
596568.29	119424.21	1.31	1.700
596587.52	119378.05	1.39	3.900